Proceedings

FIRST INTERNATIONAL CONFERENCE ON ADVANCED STRUCTURAL STEELS (ICASS 2002)

Date
May 22-24, 2002

Place
Tsukuba International Congress Center
Tsukuba, Japan

Organized by
National Institute for Materials Science (NIMS)

In Conjunction with
The Iron and Steel Institute of Japan
Chinese Society for Metals
Korean Institute of Metals and Materials

FIRST INTERNATIONAL CONFERENCE ON ADVANCED STRUCTURAL STEELS (ICASS 2002)

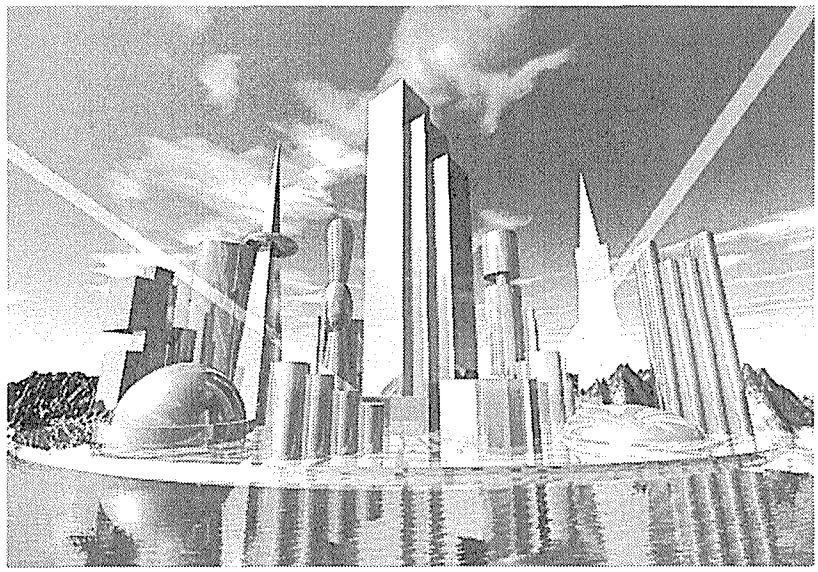

Date

May 22-24, 2002

Place

Tsukuba International Congress Center
Tsukuba, Japan

Organized by

National Institute for Materials Science (NIMS)

In Conjunction with

The Iron and Steel Institute of Japan
Chinese Society for Metals
Korean Institute of Metals and Materials

URL ▶ http://www.nims.go.jp/icass/

Approved by

Architectural Institute of Japan
Japan Association of Corrosion Control
The Japan Institute of Metals
Japan Society of Corrosion Engineering
The Japan Society for Heat Treatment
The Japan Society of Mechanical Engineers
Japanese Society of Steel Construction
The Japan Society for Technology of Plasticity
The Japan Welding Engineering Society
Japan Welding Society
Society of Automotive Engineers of Japan, Inc.
The Surface Finishing Society of Japan
The Society of Materials Science, Japan
The Society of Naval Architects of Japan
Japan Society of Civil Engineers

JSCE-Approved CPD Program

Preface

The first International Conference on Advanced Structural Steels (ICASS) is organized by National Institute for Materials Science (NIMS) in conjunction with The Iron and Steel Institute of Japan (ISIJ), Chinese Society for Metals (CSM) and Korean Institute of Metals and Materials (KIMM). The first ICASS will feature information on the latest scientific and technological developments in advanced structural steels and a summary of the achievements of the five-year project at NIMS in plenary lectures and technical sessions, which will consist of more than 182 presentations. The plenary lectures will report on the current state and future prospects of advanced-steel projects in progress in Japan, China, Korea and Europe. Technical sessions will cover such fields as creating high-strength steels and their applications to power generators, marine structures etc., and nano-scopic analyses and engineering of new materials for joining and welding. The common theme of all sessions is to create more resource-efficient and environmentally-friendly materials.

On behalf of NIMS, ISIJ, CSM and KIMM, we would like to welcome all of our colleagues to Tsukuba International Congress Center, located in the central part of Tsukuba Science City, for the first international conference. We hope that the conference will provide participants with an opportunity to exchange information and to have fruitful discussions on the latest scientific and technical progress in the field of structural steels. ICASS will be held biannually in Japan, China and Korea. We are very pleased to host the first ICASS in Tsukuba and wish ICASS continuous success in future.

Almost simultaneously with ICASS, the 6th Workshop on the Ultra-Steel will also be held by NIMS at the same Congress Center on May 21. All the ICASS participants are welcome to attend the workshop free of charge, especially the poster session, where the latest achievements in Ultra-Steel will be displayed in English and discussion will be made in English. Posters will be exhibited until May 22, the first day of ICASS, in an open-house style. We hope the presenters will also have the opportunity to discuss the latest progress of Ultra-Steels in Japan.

Conference Organizing Committee
Chairperson
Prof. Teruo Kishi
National Institute for Materials Science

Conference Organization

Organizing Committee

Chairperson

Prof. Teruo Kishi *(President, NIMS, Japan)*

Vice-chairpersons

Mr. Mutsumi Ohji *(Former President, The Iron and Steel Institute of Japan)*

Prof. Weng Yuqing *(President, The Chinese Society for Metals, China)*

Mr. Kang Chang Oh *(Chairman, Iron and Steel Committee / Korean Institute of Metals and Materials, Korea)*

International Advisory Committee

Prof. H. K. D. H. Bhadeshia *(Univ. of Cambridge, UK)*

Dr. W. Y. Choo *(POSCO, Korea)*

Dr. S. A. David *(Oak Ridge National Laboratory, USA)*

Dr. R. E. Dolby *(TWI, UK)*

Prof. G. S. Frankel *(Ohio State Univ., USA)*

Prof. J. Hald *(Technical Univ. of Denmark, Denmark)*

Prof. J. W. Morris, Jr. *(Univ. of California, Berkeley, USA)*

Prof. P. Neumann *(Max Planck Institute, Germany)*

Prof. M. O. Speidel *(ETH, Zurich, Switzerland)*

Prof. Z. Tian *(Central Iron Steel Research Institute, China)*

Steering Committee

Dr. A. Sato *(Former Director, NIMS-MEL, Japan)* Chairperson

Dr. S. Aihara *(Nippon Steel, Japan)*

Dr. E. Akiyama *(NIMS, Japan)*

Prof. A. Azushima *(Yokohama National Univ., Japan)*

Dr. T. Hara *(NIMS, Japan)*

Dr. T. Inoue *(NIMS, Japan)*

Ms. E. Katayama *(NIMS, Japan)*

Dr. K. Kimura *(NIMS, Japan)*

Dr. T. Kodama *(NIMS, Japan)*

Dr. S. Kuroda *(NIMS, Japan)*

Prof. K. Maruyama *(Tohoku Univ., Japan)*

Dr. F. Masuyama *(Mitsubishi Heavy Industry, Japan)*

Prof. F. Minami *(Osaka Univ., Japan)*

Dr. K. Miyahara *(NIMS, Japan)*

Dr. K. Nagai *(NIMS, Japan)*

Dr. T. Nishimura *(NIMS, Japan)*

Mr. H. Okada *(NIMS, Japan)*

Prof. T. Sakai *(Electro Communication Univ., Japan)*

Dr. S. Sato *(Kawasaki Steel, Japan)*

Prof. M. Seo *(Hokkaido Univ., Japan)*

Mr. T. Shiraga *(NKBS, Japan)*

Dr. T. Takahashi *(NIMS, Japan)*

Prof. S. Takaki *(Kyushu Univ., Japan)*

Dr. S. Tsukamoto *(NIMS, Japan)*

Dr. K. Tsuzaki *(NIMS, Japan)*

Contents

UGS: Phase Transformation IV

UGS: Severe Plastic Deformation and Related Phenomena I

UGS: Severe Plastic Deformation and Related Phenomena II

UGS: Severe Plastic Deformation and Related Phenomena III

Deformation Behavior at High Strain Rate and the Modeling I

Deformation Behavior at High Strain Rate and the Modeling II

High-Speed Deformation for TRIP Steel

High Strength Steels for Welded Structures I

High Strength Steels for Welded Structures II

Application of High Strength Steels

Microstructure of Welds and Mechanical Properties I

Microstructure of Welds and Mechanical Properties II

Heat Affected Zone of High Strength Steels

Advanced Coal-Fired Power Plants I

Advanced Coal-Fired Power Plants II (Steel Development)

Advanced Coal-Fired Power Plants -III (Steel Development)

Welded Joints of Creep Resistant Steels

Microstructural Aspects of Creep Resistant Ferritic Steels I

Microstructural Aspects of Creep Resistant Ferritic Steels II

Microstructural Aspects of Creep Resistant Ferritic Steels III

Microstructural Aspects of Creep Resistant Ferritic Steels IV

High Temperature Properties of Creep Resistant Steels I

High Temperature Properties of Creep Resistant Steels II

Application of Continuous Casting and Hot-Direct Rolling Process for Scrap Steels I

Application of Continuous Casting and Hot-Direct Rolling Process for Scrap Steels II

Application of Continuous Casting and Hot-Direct Rolling Process for Scrap Steels III

Structures Resistant to Hydrogen Embrittlement I

Structures Resistant to Hydrogen Embrittlement II

The State of Hydrogen and Its Effect on Fractures I

The State of Hydrogen and Its Effect on Fractures II

Structures Resistant to Fatigue I

Structures Resistant to Fatigue II

Corrosion Control of Infrastructure I

Corrosion Control of Infrastructure II

Corrosion Control of Infrastructure III

Corrosion Control of Infrastructure IV

New Stainless Steels I

New Stainless Steels II

Surface Modification and Surface Treatment

Novel Methods in Surface Analyses I

Novel Methods in Surface Analyses II

Novel Methods in Surface Analyses III

Plenary Session

(Hall 300)

Microstructure Refinement in Structural Steels

Weng Yuqing

The Chinese Society for Metals

Beijing, China, 100711

The output of steel products in China was 150 million tons in 2001 . Among this, structural steels occupied about 95% of total steel production. In order to reach the goal of "double strength and/or double service life" for the Chinese Governmental R & D project: "Fundamental Research on New generation of iron and steel material in China", the research team was organized at late 1998. The key course is to seek Microstructure refinement (Ultra-fine grain), purified technology for steel making and subsequent casting and uniformity distribution of solute during solidification. The above three technologies should be combined on the basis of modern metallurgical production route and cost-reduction route.

In this paper, the progress of microstructure refinement in structural steels is going to be reported briefly based on our work. Three kinds of structural steels dealt with are:

1. Steels with ferrite (F) and pearlite (P) microstructure, which occupied 70% of the total structural steels, mostly belong to plain-carbon steel and low or micro alloyed steels. Its strength level (σ_s) is about 195~355 MPa as hot-rolled condition. There are three methods applied and developed:

(a) Austenite dynamic recrystallization with larger Z-H (Zener-Hollman parameter), that is higher $\dot{\varepsilon}$, and lower rolling temperature T_d with heavier deformation ratio (ε) combined together. This method is applied in roughing mills. Since higher rolling load is required and γ-DRX could not be applied to $T_d \leqslant 1000℃$ and $\dot{\varepsilon} \leqslant 10s^{-1}$ (if true strain ε=90%) in plain-carbon steels. This is the only pre-refinement method in practice.

(b) Deformation Induced Ferrite Transformation (DIFT) technology. In order to release the free energy increase (ΔG_D) which partly stored in steel during hot rolling or after hot rolling, ΔG_D could be transferred to produce a driving force for $\gamma \rightarrow \alpha$ at certain F+P microstructure. DIFT process has been systematically studied by our team including thermodynamics, kinetics, nucleation and grain growth theory, crystallographic relation with new phase/ matrix, mechanical properties, alloy element effects, weathering resistance and so on. It is believed this is one of the best ways to refine the ferrite microstructure.

(c) Ultra-fine grain produced by ultra-fine (5~10 nm) distribution in plain-carbon steel. On the bases of purified plain-carbon steel ($S \leqslant 0.006\%$, $O < 0.003\%=$, ultra-fine grain steel (α-grain size ranged between 2~5μm which depends on strip thickness) can be obtained in thin-slab casting and continuous rolling rout (CSP). Very fine oxides Fe_2O_3 with spinal structure= and sulfides (MnS) are distributed along α grain boundaries and dislocation lines area. The size of oxides and sulfides is ranged between 5~10 nm. It is this distribution, which causes grain refinement and strengthening of the steel. Yielding strength has been nearly doubled from 195MPa to 330Mpa and elongation keeps higher level.

2. Steel with low carbon bainite (LCB) or Ultra-low carbon bainite (ULCB) microstructure

The microstructure with ultra-fine ferrite and pearlite (UFG F+P) is not only for best mechanical properties in micro-alloyed steels. As being studied in comparison between (UFG F+P) and acicular ferrite (AF) microstructure in ultra-low carbon bainite steels, AF microstructure has better resistance to stress corrosion cracking (SCC) in H_2S environment for pipe line application even UFG f grain size refines to about 1 μm. However, hot deformation has strong effect on microstructure refinement for these LCB or ULCB steels. Investigation of CCT and DCCT diagrams has been carried out. It shows that hot deformation can accelerate transformation, depress the formation of lath ferrite and bainite and refine the island structure, so that promote the formation of acicular ferrite microstructure.

One way to refine the microstructure in LCB or ULCB steels is to develop so called "Relaxing-Precipitation-Control (RPC)" technology. Deformation Induced precipitation (DIP) would occur after final rolling immediately in some LCB or ULCB steels at certain conditions. If certain period (a few seconds to tens seconds) can be kept at final rolling temperature by controlled rolling, dislocation structure will be relaxed to some equilibrium state, due to dislocation redistribution and precipitation process control. Ultra-fine bainite and martensite composite structure would form at middle-temperature and sequent cooling period. These causes mechanical properties increased and yield strength raised to about 800MPa ($\Delta\sigma_s \approx 150$MPa) under lower cost condition.

3. Microstructure refinement in alloy structure steels

With fast-heat treatment (using direct-electric heating technology) for 42CrMo (SCM 440/AISI 4140) steel, the grain size of austenite could be refined down to 1.8μm on average. By this treatment, many mechanical properties can be improved, for example, σ_b could reach to higher than 1400MPa. This is ultra-fine microstructure for austenite, of cause; this implies ultra-fine tempered martensite to be formed.

A carbide-free bainite martensite steel (a low carbon Mn-Si-Cr steel) , has been experimentally investigated. Which is called as CFB/M. Mechanical properties are as following: σ_b 1600MPa, $\sigma_{0.2}$ 1335MPa, δ_5 13.5%, ψ 56.2%, A_k 81J. These are some carbon enriched retained austenite film locating at lath boundaries or even sub-lath boundaries, which improve steel toughness and increase the resistance to hydrogen-induced cracking (HIC).

Up to now, many Chinese steel companies keep eyes on this project, more and more R & D workers from industry intend to join this research. New generation steel will be applied in the not far future.

Properties of Fine Grained Steel Produced by SIDT Process and Improvement of HAZ Properties by Using Thermally Stable TiN Particles

Wung-Yong Choo

Technical Research Laboratories, POSCO, Korea

1.Outline

Two critical problems are existing in production and processing of fine grained steel. One is the requirement of heavy deformation at low temperature and the other is the prevention of grain growth in heat affected zone (HAZ). To solve two critical problems, new rolling technology based on strain induced dynamic transformation (SIDT) has been developed and technology based on thermally stable TiN particle has been also developed to prevent the austenite grain growth in HAZ. Two new technologies and trial production results of plate based on these new technologies were summarized

2. Formation of fine ferrite grain by using SIDT phenomena.

Many researches have been performed to obtain fine grained ferrite by applying heavy deformation in austenite region. Heavy deformation in nonrecrystallization region of austenite is helpful for increasing the ferrite nucleation site and results in the fine ferrite grain by static transformation during cooling process.[1] Instead of static transformation, dynamic transformation could be enhanced by deformation between Ae3 and Ar3 temperature region under certain deformation condition.[2,3] Ferrite grin size obtained by SIDT is very fine and more importantly grain growth rate of SIDT ferrite is much slower than conventional ferrite obtained by static transformation. This slow growth kinetics of SIDT ferrite is understood by pinning effect of fine cementite particles which are formed on the triple point of ferrite grain. Many experimental results showed that preferential nucleation site of SIDT ferrite is austenite grain boundary. Preferential nucleation of SIDT ferrite on grain boundary is very helpful for reducing the critical strain needed for SIDT ferrite formation because energy state of grain boundary is already high and only small addition of deformation energy is enough for the dynamic transformation. This advantage allows obtaining fine ferrite grain under light multipass hot rolling schedule. Fig.1 shows the result of multipass rolling, about 20% SIDT ferrite was obtained in each rolling pass with 20% reduction.

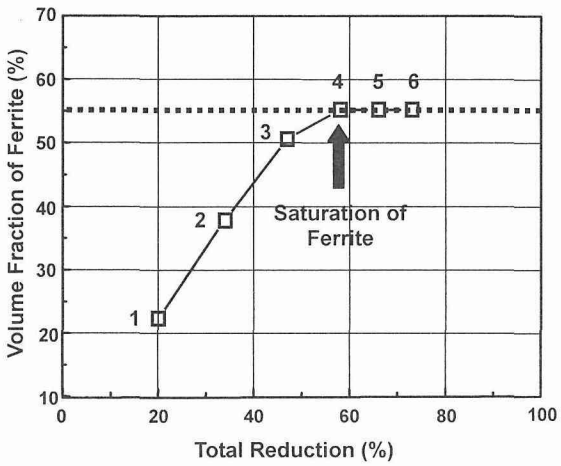

Fig. 1 Formation of SIDT ferrite in multi-pass hot rolling schedule

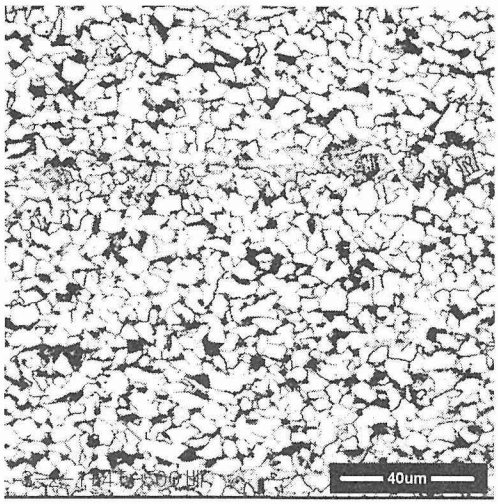

Fig. 2 Typical fine microstructure obtained in trial production

3. Prevention of grain growth in HAZ by stable TiN particles

In conventional Ti bearing steel, it is difficult to retard the austenite grain growth in HAZ during welding because TiN particle is dissolved and pinning effect of TiN particle disappears. To avoid this difficulty, thermal stability of TiN particle is improved by increasing the nitrogen content in steel. Increased thermal stability of TiN particle is helpful for preventing the austenite grain growth by pinning effect. Round robin tests of field produced high nitrogen TiN steel were performed to evaluate the HAZ toughness in various welding conditions. Test results showed that HAZ toughness was significantly improved and width of HAZ was decreased to 1/10 of conventional steel.

4. Results of trial production.

Trial production of fine grained steel was performed by using new two technologies. Chemical composition of trial production was designed to maximize the benefit of thermally stable TiN particles and multipass hot rolling schedule was also designed to enhance the formation of SIDT ferrite. Typical microstructure of trial product is shown in Fig.2, which consists of fine ferrite and pearlite. Depending on the cooling rate after rolling, kinds of second phase varied from pearlite to martensite. Mechanical properties of base metal and HAZ were much improved and showed the benefit of fine grained steel.

References

[1] K.Nagai, Int. Symp. on 'Ultrafine Grained Steel'(ISUGUS 2001), Fukuoka, Japan, Sep. 2001, pp60-67.

[2] W.Y.Choo,K.K.Um,J.S.Lee,D.H.Seo and J.K.Choi, ibid. pp.2-9.

[3] W.Y.Choo, ibid. pp.76-81.

Present Status and Perspectives of European Research in the Field of Advanced Structural Steels

G. Buzzichelli, E. Anelli
Centro Sviluppo Materiali SpA, Roma, Italy

1. Introduction

Steel is a material of major strategic importance, vital to large industrial sectors such as transports and constructions, where continuous innovation on technologies and products is needed. Since its birth with the Roman treatise in 1952, the European Coal and Steel Community (ECSC) has consistently supported R&D on steel in many sectors of industrial research ranging from process/environment to product development and applications.
The ECSC Steel Programme received in these last years an average annual budget allocation of about 55 million Euro by which a 7% of the total R&D financial communitary effort was covered, with particular emphasis paid to the more basic and fundamental aspects of production technologies and steel properties. Close collaboration and information exchange among research laboratories, Universities and industry across the Europe are key points; basic Research in fact is also managed and co-ordinated by national Institutions and governments in the framework of National Research Programmes.

2. Industrial Research

Various projects have been devoted to develop new materials for flat and long steel products for structural applications. The main streamline is High Strength, in order to match the weight lightening requirements that concern the whole class of load bearing structures and/or steel components and one of the most investigated topic is grain refinement. Three principal sectors of application are selected and briefly commented in this summary.

Automotive industry

The present challenges for steels, in general terms, are the improved formability, corrosion protection, better surface, higher strength, lighter gauge and mass reduction. The ambitious goals of the past ULSAB Project of a safer, lighter and stronger car body, to which most European industries participated, were substantially achieved. A subsequent VDEh-Porsche program has shown the possibility of reducing the weight by 20%. Thinner and stronger strips were developed and produced essentially using a fine tuning of the hot rolling and in-line cooling facilities.
The control of recrystallization, precipitation and phase transformation in hot strip mill (HSM) has been successfully exploited in Europe to develop, at an industrial level, low-C microalloyed steels with an average grain size of 2 to 5 μm and yield strength from 400 to 600 MPa, coupled with good toughness, weldability and fatigue resistance.
The key factor is a strict control of microstructure and precipitation during high speed hot rolling on HSM. Innovative solutions in due course will play a vital role to increase homogeneity and reproducibility of strip properties, while reducing the number of steel chemistries. The use of Ultra Fast Cooling (UFC) for example, the introduction of coil-box, UFC after finishing and CSP lines, lubrication and skin cooling, new dedicated routes for thinner hot coils.

Buildings and infrastructures

In the metal construction industry (medium-low rise building), new markets are being developed in the prefabrication and mixed structures for which steel is particularly suitable. However, more attention is being paid to the improvement of physical properties and the overall performance of the building (or parts of it) rather than to the enhancement of material properties, a new possibility for steel application remaining actually the use of light frames.

In the application field of high rise buildings, high strength beams and other structurals are produced by controlled rolling and quench and self tempering (QST) processes; choosing an optimized chemical composition SMAW butt welding is also possible without preheating.
In the field of large infrastructures such as suspended bridges, new and more performant wire cables would be requested since now: one recent example comes from the just approved Messina Bridge in Italy, to be suspended over the 3500 m of the Sicily Strait. However, research is still underway, as in Japan, to develop reliable carbon steel wires with strengths substantially higher than the actual ones (about 2000 MPa).

Pipelines

Steel pipelines will continue to be one of the most efficient ways of energy transportation through the world, especially when the sea borders are far away from the production sites. An interesting trend is towards high productivity long distance lines characterised by medium-large diameters ($\geq$ 20") and very high operating pressures (> 150 bar). An "ultra-steel" is needed, capable to match very high strength level to weldability and fracture resistance. Europe is very active in this research field, now coming to its developmental stage, at least for the X100 solution. The question remains open for higher grades.

3. Perspectives

Recent European Projects are also in progress to ascertain some basic aspects controlling microstructure formation and properties, such as:

1. understand the nature of the UF structure, its effect on a single property (e.g. validity of Hall-Petch relation) and the mechanisms that can be exploited to improve a combination of properties (e.g. strength and ductility/formability) in carbon and stainless steels;
2. establish for flat and long steel products the most promising technologies to form UF structures, starting from powder material or bulk steels, in both single and multi-phase materials, with consistency at a reasonable cost;
3. ascertain the potential for UF medium and high C steel to replace traditional pearlitic and engineering steel;
3. achieve sub-micron grains in austenitic stainless steel by reversion of strain-induced martensite to austenite [1];
4. develop very fine multi-phase metastable structures able to behave favourably during further processing;
5. assess the aptitude of new UF steels to further processing (annealing, welding, etc.).

Another line of research is bound to the exploitation of the newly developed compact cycles, also attractive under the eco-environmental aspect. A number of recent projects are centred on Thin Slab and Strip Casting technologies, which combine casting and rolling into a unified process, leading to compact and flexible systems, intrinsically cost saving. The possibility of using the peculiarities of rapidly solidified structures is also being investigated.
An innovative route aims at developing ultra fine microstructures, with a mixture of phases, including acicular ferrite and bainite, starting from coarse austenite grains in the as solidified structure through the use of Strain-induced Transformation Rolling (SITR) process. The technological approach by CORUS and VAI [2] applied to rolling after casting, can be used to give heavy reductions at low temperature to produce UF grains in flat thin products. Further developments are in progress, such as in-line heat treatments of work-hardened as-cast steel strips [3].

References

[1] Di Schino, A., Salvatori, I., and Kenny, J.M., these proceedings.
[2] Champion, N.J., Evans, P.J., and Underhill, R.P., Thermomechanical processing of steels, IOM communications, London 2000, pp.625-635.
[3] Lindenberg, H.-U., Brückner, G., and Tacke, K.-H., Steel research 72 (2001) No.11-12, pp.490-495.

- Ultrafine Grained Steels: General View
- UGS: Phase Transformation
- UGS: Severe Plastic Deformation and Related Phenomena

(Convention Hall 200)

Achievements in the Super-Metal Project and its Future Prospects

S.Aihara
Ferrous Super Metal Consortium of JRCM

1. Introduction

The Ferrous Super Metal project which started in 1997 has completed its five-year plan in 2002. In the first two years, basic metallurgical concepts for producing ultra-fine grained steel were established, which were successively extended to laboratory-scale hot-rolling mill experiments. Five mm thick ultra-fine grained steel plates having 1μm in grain size were experimentally produced. Also, experiments on phase transformation under high magnetic field showed a possibility that the process window for producing the ultra-fine grained steels could be enlarged. The ultra-fine grained steels achieved 900MPa class strength without increasing alloying elements and showed excellent properties like strength-ductility balance, toughness and fatigue strength. Other properties including laser and friction-stir welded joint strength have been examined for the future applications. Subjects which should be resolved for producing the ultra-fine grained steels on an industrial scale in the future are also discussed.

2. Achievements in the grain-refinement

It is necessary to increase ferrite nucleation sites and suppress grain-growth in a great amount for breaking through the limit of grain-refinement of the conventional TMC process. In this respect, the project pursued several metallurgical processes. Among these, three types of the processes were found promising for obtaining ultra-fine grains of 1 μ m or less: (i) ferrite transformation after heavy deformation at temperature range much lower than the case of the conventional TMCP <Type-I> , (ii) ferrite recrystallization after heavy deformation in ferrite temperature region <Type-II> and (iii) autonomous reverse transformation by deformation heating by heavy deformation in ferrite temperature region <Type-III>, the last case being refinement of martensite prior austenite grain. Five mm thick sample plates having grain size of approximately 1 μ m have been obtained by applying all these process types.

In the process Type-I, so-called "micro-band" dislocation substructure was obtained by heavily deforming super-cooled austenite below 600degC. Ultra-fine ferrite of 1 μ m was formed from the micro-band substructure by strain-induced low-temperature diffusional transformation (SALT). Austenite grain refinement by recrystallization prior to the heavy deformation at low temperature was effective for enlarging a process window of the Type-I. In the process Type-II, ultra-fine grain was obtained by a combination of heavy deformation of ferrite and effective suppression of grain growth by fine second phase like cementite or Ti-carbide. It was found from intensive EBSP analyses of the ferrite recrystallization process that ferrite grain-refinement was realized by the dynamic-continuous recrystallization. Heavy deformation at austenite-ferrite dual phase region also produced ultra-fine grain steel. In the process Type-III, 0.3mass%C-9mass%Ni steel was used for obtaining ultra-fine martensitic microstructure, instead of low-carbon microalloyed steels in the processes Type-I and II. Strain-induced reverse transformation (SRT) took place in a short period due to a narrow dual-phase temperature range in this steel. The short period reverse transformation allowed no sufficient time for grain growth. Also, recrystallization of austenite possibly contributed to the grain-refinement.

3. Ultra grain-refinement with use of magnetic field

The super metal project introduced a superconducting magnet of 12T inside the bore of

100mm in diameter. A characteristic microstructure of partially transformed ferrite grains which were aligned in the magnetic direction was found. The sample partially transformed in the magnetic field was quenched, cold deformed and then annealed. Cold deformation strain for producing a certain level of ferrite grain size was considerably reduced by the application of the magnetic field. Ultra-fine grained steel wire of 1 μ m was obtained by a combination of Ti addition and the magnetic field during partial transformation. It was presumed from FEM analyses that strain was accumulated easily at the interface between aligned ferrite and martensite as compared with conventional equi-axed dual phase microstructure, which might enhance the recrystallization during annealing thereby realizing the ultra-refinement.

4. Properties of the ultra-fine grained steels

In the project, ultra-fine grained steel plates having grain size of approximately 1 μ m with thickness of 5mm and width of 100mm were produced by a large-scale experimental hot rolling mill. Some properties were examined for these steels.

As can be inferred from the Hall-Petch relationship, yield strength increased almost linearly with inverse square root of ferrite grain size. Tensile strength of 900MPa class could be achieved in steels with chemical composition of 500MPa strength class. It was originally anticipated though that elongation might drop in the ultra-fine grained steel developed in the project. However, the steel showed better strength-elongation balance than conventional high strength steels because the developed steel contained fine and hard second phase like martensite. Under repeated loading, fatigue crack initiation of the ultra-fine grained steel was suppressed probably due to difficult strain accumulation in the grain. High value of fatigue limit strength to tensile strength ratio was maintained.

Another interesting property found in the developed steel is tensile elongation at high temperature. The developed steel showed 200% of total elongation at 750deg.C. A process similar to the superplasticity presumably took place. This distinguished property might be applied to e.g. solid-state joining and hot-press forming.

Performance of laser and friction-stir welded joints was also examined and compared with that of the conventional arc welded joints. The heat-affected zone softening might be a problem in the developed steel. However, drop of tensile strength of the laser welded joint was small because of the limited HAZ hardness drop and narrow softened zone. Joint strength of 800MPa class could be maintained.

5. Feasibility studies for industrial scale production

The ultra-grain refinement processes developed in the project require heavy reduction per rolling pass at low temperature, which leads to a large increase in flow stress. A quite high rolling load for applying 50% reduction per pass was predicted. Basic specifications of the rolling mill were studied. A new design of the rolling mills must be necessary. Processes for relaxing the reduction per pass must be pursued metallurgically.

6. Conclusions

The Ferrous Super Metal Project has opened a new field of the ultra-fine grain metallurgy and developed new types of the rolling process. Impact on the design of steel structure must be enormous if the developed processes and steels are realized on an industrial scale. A succeeding project is being planned, in which many subjects will be studied for realizing the ultra-fine grained steels in the future.

Reference: Proceedings, 4th symposium on Super Metal, Dec. 2001, Tokyo, JRCM.

Goal of the Creation and Properties of Nano-Scale Steel

A. Azushima
Faculty of Engineering, Yokohama National University, Japan

1. Introduction

In recent years, ultra-fine grained steels have developed by the new thermo-mechanical control processing (TMCP) and the severe plastic deformation (SPD) processes. The minimum ferrite grain size obtained by the new TMCP is less than 1μm [1]. On the other hand, in the SPD processes such as the equal channel angular pressing (ECAP) [2,3], the high pressure torsion process (HPT) [4] and the accumulative roll bonding (ARB) [5], steels with a sub-micron scaled grain size are developed. Especially in the ball milling process, steels with a nano-scaled grain size are developed [6]. It is reported that the tensile strength of the steels with ultra-fine grain size increases with decreasing square-root of the grain size, following the conventional Hall-Petch relationship [7].

In order to obtain the steels with the nano-scaled grain size, the SPD processes are effective. In this paper, the creation and properties of nano-scale steels produced by the SPD processes are mainly reviewed.

2. Creation of nano-scale steel

The SPD processes of ECAP, ARB and HPT produce steels with sub-micrometer and nano-scaled grain sizes. In the ECAP process, the severe plastic strain can be introduced into steels without changing the cross section area of billets, so that the grain size of steels is refined down to the sub-micrometer order. The author et al. have developed an apparatus of the repetitive side extrusion of an ultra-fine grain size of steels [3]. They have reported that by the repetitive shear deformation of cold side extrusion of ultra low carbon steel with an initial grain size of 150μm at a room temperature, the ultra-fine grained ultra low carbon steel with a sub-micrometer grain size is developed after 10 passes. From the TEM microstructure, it is evident that the ultra-fine grains with a length of 0.5μm and a width of 0.2μm are formed. Since the SAD pattern shows the appearance of rings, it is anticipated that the boundary angles of almost the ultra-fine grains become respectively high.

Saito et al. have reported that in the ARB process of ultra low carbon steel at 773 K, the ultra-fine grained steel with 0.5μm is also developed after 5 cycles of ARB (equivalent strain of 4.0) [5]. Valiev et al. have reported that in the HPT process of Armco-Fe at a room temperature, the microstructure with a mean grain size of about 100nm is formed after 4 rotations [4].

From these results, the grain size produced by the HPT process is generally smaller that the grain size produced by the ECAP and ARB processes. However, the specimens in the form of relatively small disc are only obtained in the HPT process. Compared with these SPD processes of ECAP, ARB and HPT, the ball milling of steel powders is a useful process for charging the severe plastic deformation into the material and producing the nano-scaled grain size. The smallest grain size with about 10nm has been obtained in the ball milling process [7]. In this process, the bulk specimen for structure materials can not obtained.

3. Properties of nano-scale steel

Fig.1 shows the relationship between the nominal stress and the nominal strain of the as-received specimen and specimens of ultra fine low carbon steel after 1, 2, 5 and 10 passes of the ECAP process. The as-received specimen gives a stress-strain curve exhibiting a normal strain hardening, which the specimen after the ECAP processes don't exhibit the strain hardening, and the stress for each specimen increases rapidly with increasing strain and reaches a maximum value at lower strain without uniform elongation. This is due to the plastic deformation instability caused by exceeding the grain refining under a grain size of

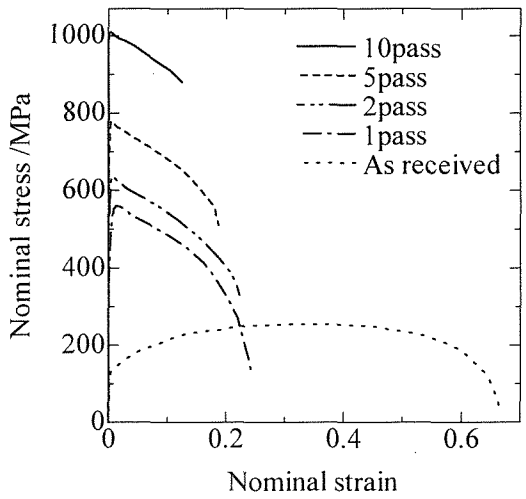

Fig.1. Stress-strain curves of side extruded ultralow-carbon steel specimens

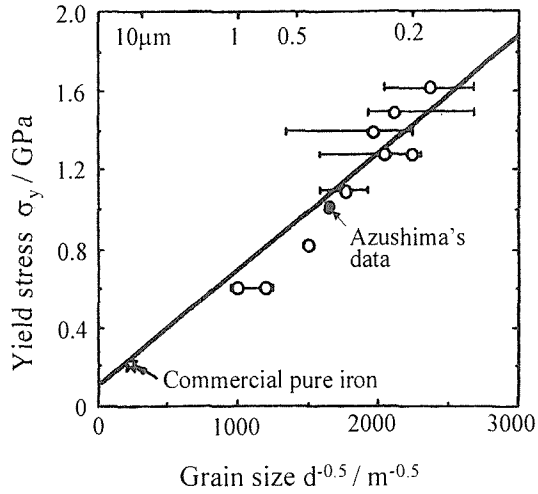

Fig.2. Relationship between yield stress and grain size [7]

1μm. If the uniform elongation is necessary, the grain size over 1μm needs by the heat treatment. The tensile strength increases with increasing pass number of the ECAP. It is over 1000MPa after 10passes and is increased by a factor of 3.0 in comparison with the as-received specimen and the specimen after 10passes.

The experimental data of the as-received specimen after 10 passes are plotted in the Hall-Petch relationship of the yield stress against $d^{-1/2}$ as shown in Fig.2, where d is the measured grain size and the yield stresses are determined from the relationship between the stress and the strain shown in Fig.1. In Fig.1, the experimental data of the ball milling iron powder and the bulk iron with the ultra-fine grained structure obtained by Takaki et al. [7] are plotted. The results obtained by the ECAP process show good agreement with the Hall-Petch relationship obtained.

Concerning with the cold formability of ultra-fine grained ultra low carbon steels, the side extruded specimens with a thickness of 10μm after 1, 2, 5 and 10 passes are rolled up to total reduction in thickness of 95% by multiple passes at room temperature. All specimens after 1,2, 5 and 10 passes can be rolled up to 95%without fracture.

4. Remarks

In this paper, the creation and properties of nano-scale steel produced by the SPD processes are reviewed. In the steels with the single ferrite phase, it is difficult to obtain the steels with the nano-scaled grain size. In order to obtain the nano-scale steels, the use of the steels with two phases such as the ferrite and pearlite will be effective.

References

[1] Hagiwara, H.: Proc. of 3rd Symposium of Super Metal(2000), pp.13-17.
[2] Segal. V.M., Reznikov, V.I., Drobyshevskiy, A.E. and Kopylov, V.I.: Russian Metal 1(1981), pp.99
[3] Azushima, A., Aoki, K and Inoue, T.: Tetsu-To-Hagane 87(2001), pp762-766.
[4] Valiev, R.Z., Islamgaliev, R.K. and Alexandrov, I,V.: Prog. Materials Science 45(2000), pp.103-189.
[5] Saito, Y., Utsunomiya, H. Tsuji, N. and Sakai, T.: Acta Mater. 47(1999), pp579-587.
[6] Umemoto, M., Liu, Z.G., Hao, X.J., Masuyama, K. and Tsuchiya, K.: Mater. Sci. Forum 360-362(2001), pp.167-174.
[7] Takaki, S. and Nakamura, S.: CAMP-ISIJ 12(1999), pp.361-364.

Effects of Processing Parameters of Strain-Induced Dynamic Transformation on the Microstructures and Mechanical Properties of Ultrafine-Grained Low Carbon Steels

J.-K. Choi, D.-H. Seo, J.-S. Lee, K.-K. Um, and W.-Y. Choo
Technical Research Laboratories, POSCO, Pohang P.O.Box 36, 790-785, Korea

1. Introduction

Strain-Induced Dynamic Transformation(SIDT) is very effective for refining the ferrite grains in low carbon steels partly by random crystallographic orientation distribution of ferrite grains formed and partly by early impingement of ferrite grains due to the very high nucleation rate. In the present study, the effects of processing parameters on the threshold(critical) strain for SIDT were quantitatively investigated and the kinetics of dynamic and static transformation in multipass deformation were analyzed. Alloy design concept for increasing SIDT ferrite fraction was introduced. Finally the effect of second phase on the mechanical properties in ultrafine-grained dual phase steel was also examined.

2. Critical strain for strain-induced dynamic transformation

SIDT is a kind of softening process of supercooled and strained austenite and competes with dynamic recrystallization(DRX) during deformation of austenite under Ae3 temperature. Microalloyed low carbon steel specimens were deformed under various processing conditions and the critical amounts of strain for softening of strained austenite were determined from stress-strain curves by utilizing the method proposed by Poliak and Jonas[1].

In Fig. 1, the effects of processing parameters on the critical strain for possible softening mechanisms were plotted. SIDT is the softening mechanism at below Ae3 temperature where the critical strain for SIDT is smaller than that of dynamic recrystallization(DRX), whereas DRX is the softening mechanism at above Ae3 temperature where the opposite is true. This is because the preferential sites for SIDT and DRX are the same and the softening mechanism having the lower critical strain is operated earlier and preoccupies the possible nucleation sites such as grain boundaries and deformation bands, etc..

3. Kinetics and ferrite fraction in SIDT

The kinetics and ferrite fraction in SIDT depend on alloy system and processing parameters such as strain, strain rate, austenite grain size, deformation temperature, etc.. In the present study, it is reported that the actual problems in the realization of heavy deformation to obtain ultrafine-grained structure can be avoided by the successive light deformation with the strain exceeding the critical value for SIDT in each rolling pass, and also the effects of processing parameters on the SIDT kinetics and microstructure are introduced. In addition to these, the increase of Ae3 temperature enhances the SIDT process at the same deformation temperature, which also helps relieve the rolling load problem. As an example, the amounts of SIDT were compared between two alloys containing different Si levels. As can be seen in Fig. 2, the higher Si content steel showed the larger amount of SIDT ferrite. This is because the addition of Si increases Ae3 temperature and in turn accelerates the SIDT process due to both augmented chemical and mechanical driving forces for the phase transformation.

4. Effects of second phase on the mechanical properties in ultrafine dual phase steel

As the ferrite grain becomes fine, the strength of material increases according to Hall-Petch type equation. The problem, however, is that the yield strength increases more rapidly than tensile strength with the decrease in ferrite grain size which results in very poor ductility in ultrafine-grained steel. In order to overcome this problem, dual phase microstructure was adopted. After the formation of SIDT ferrite through hot rolling, the remaining austenite will be transformed to various second phases according to the cooling rate. In Fig. 3, the variations

of tensile and Charpy impact properties of ultrafine dual phase steel were plotted as a function of cooling rate. As the cooling rate is increased, the second phase changed from higher to lower temperature transformation microstructure, and the tensile strength increased maintaining acceptable levels of yield ratio and uniform elongation.

Reference

[1] E. I. Poliak and J. J. Jonas, Acta Mater., 44, p127 (1996).

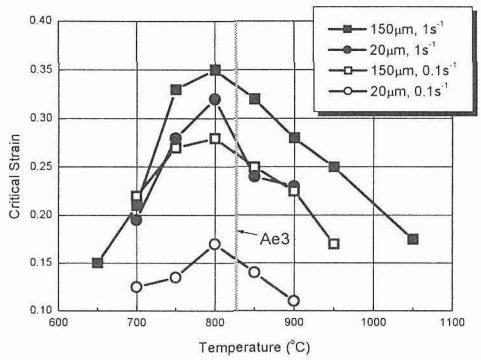

Fig. 1 Effect of processing parameters on the critical strain for softening of strained austenite.

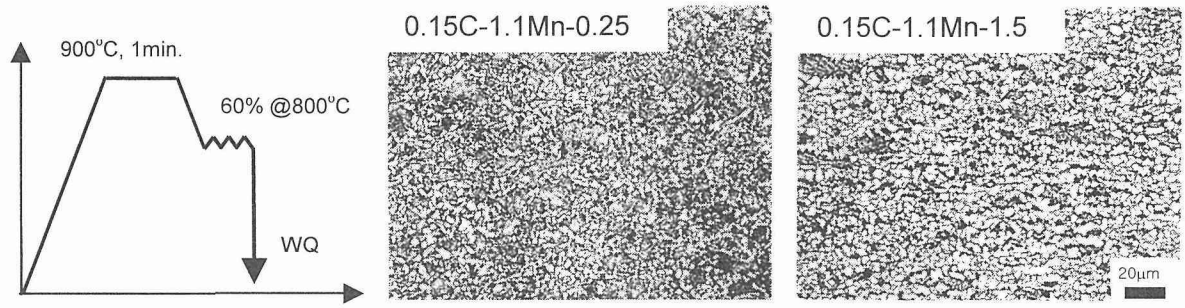

Fig. 2 Effect of Si content on the SIDT fraction in low carbon steel.

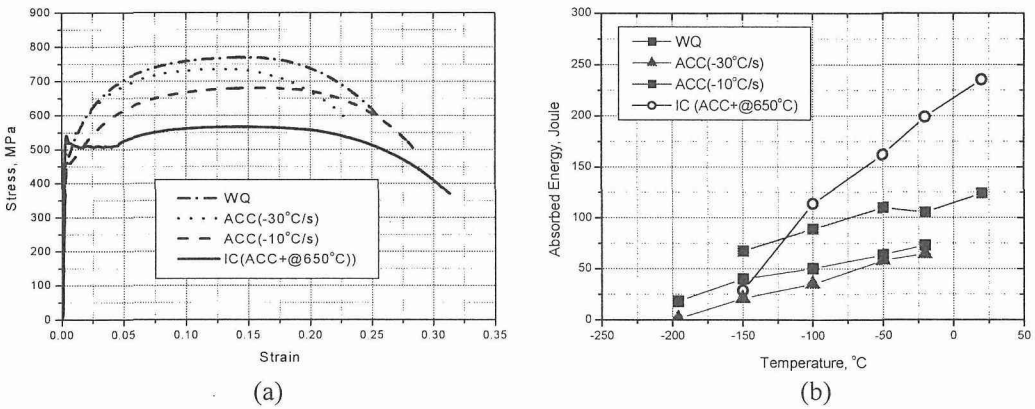

(a) (b)

Fig. 3 Effects of cooling rate on the mechanical properties in ultrafine-grained dual phase steel; (a) tensile test and (b) Charpy impact test.

Ultrafine Grained Steels Through Thermomechanical Processing

G.L. Kelly, H. Beladi and P.D. Hodgson
School of Engineering and Technology, Deakin University, Australia

1. Introduction

Strain-induced transformations (SIT) of austenite to bainite or ferrite can produce ultrafine grained microstructures. The major problem with utilizing SIT on a commercial scale is that the critical strains required are too large to be achieved in a single pass. If multiple passes are to be used to accumulate the strain required for SIT, the effects of softening processes occurring between passes need to be determined.

2. Experimental Methods and Materials

Hot torsion and single pass hot rolling of plain carbon steels at temperatures near the Ar_3 were carried out to determine the critical strains for the transformations. Hot torsion experiments were used to determine the softening kinetics of AISI steel after SIT of $\gamma \rightarrow \alpha$ had been initiated. The changes to the microstructures during softening and after a second deformation were observed.

3. Results and Discussion

The critical reductions in single-pass rolling for SIT to bainite and ferrite increased with increasing carbon content. The critical reduction for the formation of bainite changed from 30 to 40% while that for α formation increased from 50 to 70% as the C content increased from 16 to 35%. Initially the strain-induced ferrite nucleates on planar, intragranular defects [1]. Once deformation stops, the $\gamma \rightarrow \alpha$ transformation continues with coarsening of the strain-induced ferrite and nucleation and growth of other forms of ferrite. The initial ferrite grain size after hot torsion to a strain of 1.5 is 3μm (Fig. 1a), after 10s (72% softening) the grains are elongated in the direction of the original rafts (Fig. 1b). The coarsening continues to 30s when there is very little γ remaining (Fig. 1c).

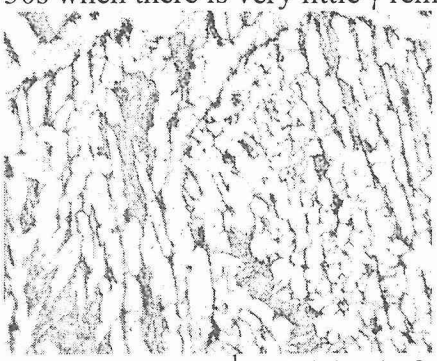

(a) ε =1.5, $\dot{\varepsilon}$ =3s^{-1}, 1 s delay before quench.

(b) ε =1.5, $\dot{\varepsilon}$ =3s^{-1}, 10 s delay before quench.

(c) ε =1.5, $\dot{\varepsilon}$ =3s^{-1}, 30 s delay before quench.

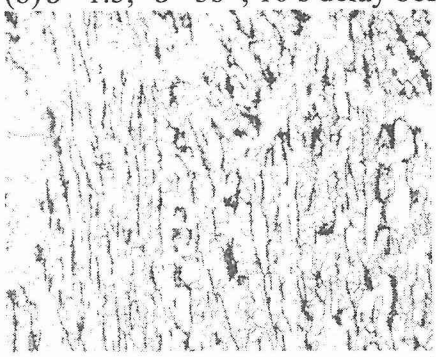

(d) ε_1 =1.5, Δt = 10 s, ε_2 =1.5, $\dot{\varepsilon}$ =3s^{-1},

Fig. 1. (a)-(c) AISI 1010 steel quenched after hot torsion deformation then holding at 760°C. (d) After holding for 10s, applying a second strain of 1.5 then quenching.

Following two strains of 1.5 with an interpass time of 10s, the microstructure is considerably refined (Fig 1d). In contrast to the homogenously dispersed carbides observed after complete transformation to strain-induced ferrite [2], the carbon-enriched areas in this microstructure are very localized. Comparing the microstructures before and after the second strain (Figs 1b and 1d), it is likely that these areas are simply produced by progression of the $\gamma \rightarrow \alpha$ transformation. The final microstructure (Fig. 1d) is formed by warm working of the coarsened ferrite rafts (Fig. 1b), the possible mechanisms are polygonisation and continuous dynamic recrystallisation. Pro-eutectoid ferrite evident after the first strain (Fig. 1b) can no longer be distinguished, it seems likely that this was refined by a similar mechanism to the coarsened strain-induced ferrite.

The microstructures formed during single pass hot rolling are more complex with constituents including ultrafine bainite, ultrafine ferrite, acicular ferrite, proeutectoid ferrite, pearlite and martensite depending on the reduction, rolling temperature and post-rolling thermal treatment.

4. Conclusions

1. Strain-induced ferrite will coarsen during an isothermal hold if the initial transformation is only partially complete due to a lack of pinning.
2. Further deformation of coarsened ferrite results in a refined microstructure, the likely mechanisms are polygonisation or continuous dynamic recrystallisation.
3. Increasing the carbon content increases the critical strain for SIT to both bainite and ferrite.

References

1. Hurley, PJ, Muddle, BC and Hodgson, PD, Microstructure and Microtexture of Ultrafine Ferrite Formed in 0.1%C Steel Using new Strip Rolling Process, Materials Science & Technology, 16(2000), pp.1376-1379
2. Hurley, PJ, Hodgson, PD and Muddle BC, Analysis and Charaterisation of Ultra-fine Ferrite Produced during a New Steel Strip Rolling Process, Scripta Materialia, 40 (1999), pp. 443-438.

Deformation Induced Ferrite Transformation and Grain Refinement in Steels

Han DONG
Central Iron and Steel Research Institute, Beijing 100081, China

1. Introduction

At present, the smallest ferrite grain in plain low carbon steel produced in industrial scale is of 20μm in size, and microalloyed steel strips is of 10μm in size. Nagai et al have obtained grains of 1μm in size in C-Mn steel through heavy deformation at lower temperature. Choo et al applied a new method called dynamic transformation to refine grains of C-Mn steel to about 1μm. It is generally believed that heavy deformation at lower temperature is quite necessary to obtain ultrafine grains in steels. The mechanism for microstructure evolution during heavy deformation at lower temperature are ambiguous: recrystallization of austenite, non-recrystallization of austenite, dynamic transformation, or what we called deformation induced ferrite transformation (DIFT). The principle of DIFT and its applications in grain refinement in steels are presented in this paper.

2. The Principle of Deformation Induced Ferrite Transformation

Austenite to ferrite transformation in steels is one of the typical diffusion transformation which is encountered in a variety of structural steels. For commercial structural steels, the diving force for austenite to ferrite transformation, free energy, is dependent on chemical composition and temperature. For deformed austenite, the accumulative deformation energy could contribute to transformation driving force which results in the promotion to austenite to ferrite transformation if deformation energy could not be released through recrystallization. This kind of transformation is named as deformation induced ferrite transformation (DIFT).

The free energy change ΔG associated with the nucleation process for homogeneous nucleation in steel is

$$\Delta G = -V\Delta G_V + A\gamma + V\Delta G_S \qquad (1)$$

where $V\Delta G_V$ is the volume free energy change. The creation of an area A of interface will give a free energy increase of $A\gamma$. A misfit strain energy per unit volume of the transformed phase is given by ΔG_S. But nucleation in solid steel is almost always heterogeneous. Suitable nucleation sites are non-equilibrium defects such as excess vacancies, dislocations, grain boundaries, stacking faults, inclusions, and free surfaces, all of which increase the free energy of the steel. If the creation of a nucleus results in the destruction of a defect, some free energy ΔG_d will be released thereby reducing the activation energy barrier. The equivalent to Equation 1 for heterogeneous nucleation is

$$\Delta G = -V\Delta G_V + A\gamma + V\Delta G_S - \Delta G_d \qquad (2)$$

The free energy of γ phase is raised through deformation. If it is expressed by change of dislocation density:

$$\Delta G_d = \mu(\rho - \rho_0)\, b^2 V_\gamma \qquad (3)$$

Assume that all of the accumulative energy due to deformation is consumed by the transformation, a CCT diagram can be calculated. The start transformation temperature of one typical CCT of C-Mn steel is shown **Fig.1**, which means that increase of free energy of 40J/mol due to deformation brings about a temperature increase

to 50K approximately. The addition of Nb into steel promotes the accumulation of energy, which results in the promotion of DIFT, **Fig.4**.

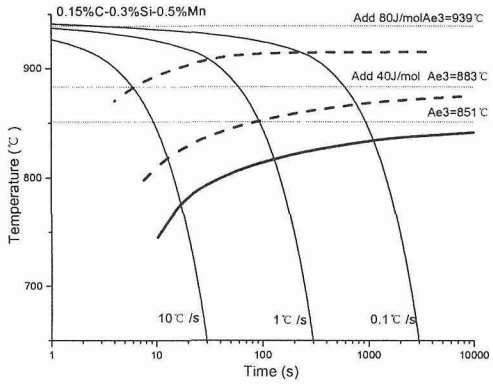

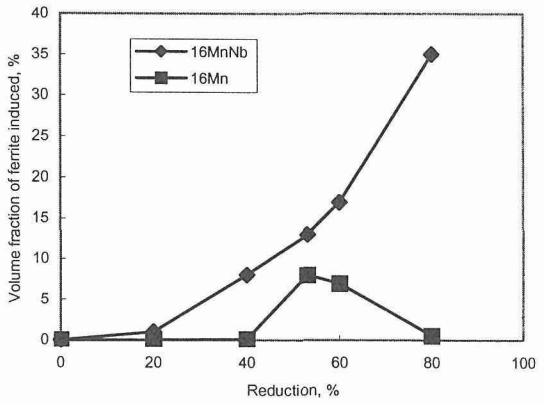

Fig. 1 (left) The start temperature of austenite to ferrite transformation is raised by energy increment induced by deformation.

Fig.2 (right) The addition of Nb promotes DIFT (16Mn and 16MnNb steels deformed at 1073K at strain rate of 5 s^{-1} .)

3. Grain Refinement through DIFT in Steels

Ferrite grain through DIFT is much finer compared with conventional transformed ferrite grain. The accumulative energy in austenite mainly depends upon chemical composition, deforming temperature, strain, strain rate, sample dimensions, and loading manner, etc.. Uniformity dispersion of ultrafine ferrite grains induced by DIFT can be controlled through variables to change accumulative energy. By adopting the theory of DIFT, mean grain size of 4μm in size can be obtained in plain low carbon steel, **Fig.3**, and corresponding mean grain size of 1μm in size can be achieved in microalloyed steel, **Fig.4**. It is proved that DIFT is a very effective method for grain refinement in steels.

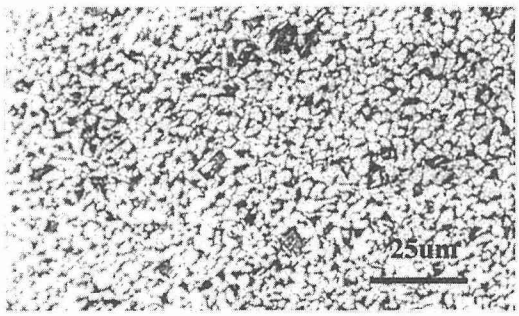

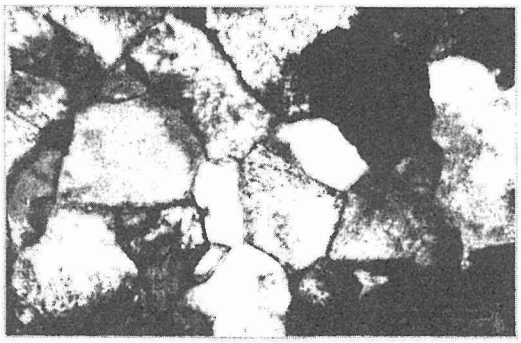

Fig.3 (left) Microstructure of plain low carbon steel (0.18%C-0.21%Si-0.60%Mn) soaked at 1173K, deformed 80% at 1033K and then water cooling to RT.**Fig.4** (right) Microstructure of microalloyed low carbon steel (0.094%C-0.29%Si -1.42%Mn -0.045%Nb -0.008%Ti) soaked at 1473K, deformed 3 passes at 1093K with total reduction of 250% and then water cooling to RT.

DIFT is the γ/α transformation, which happens at higher temperature due to the accumulative energy induced through deformation. DIFT leads to fine grain in plain low carbon steel and ultrafine grain in microalloyed low carbon steel.

Grain refinement in Cu bearing steel through dynamic $\gamma \rightarrow \alpha$ transformation followed by dynamic α recrystallization

Y. Hirai*, K. Hase*, T. Hoshino*, A. Matsuzaki*, K. Amano*,
T. Tsuchiyama** and S. Takaki**
*Technical Research Laboratories, Kawasaki Steel Corp., 1-chome, Mizushima, Kurashiki 712-8511, Japan
**Department of Materials Science and Engineering, Kyushu Univ., 6-10-1 Hakozaki, Fukuoka 812-8581, Japan

1. Introduction

The grain refinement is the most effective way to improve the strength and toughness in steels [1]. Recently many researches to refine the ferrite grains have been carried out [2]-[4]. The heavy deformation of super-cooled austenite is one of the methods to achieve the ultra fine grain structure of the steel [2],[3]. In this study, the effects of a copper addition and the soaking time in an austenite region on the transformation starting temperature (Ar_3 temperature) were investigated in 0.1mass%C-0.2mass%Mn-0.2mass%Si steel. The possibility of grain refinement was also investigated in 2mass%Cu bearing steel.

2. Experimental procedure

0.1mass%C-0.2mass%Si-0.2mass%Mn steel (steel Base) and Cu bearing steel (steel 2Cu) shown in Table 1 was used in this study. These steels were made by vacuum-melting and cast into 10kg ingots. They were hot rolled into plates in 60mm thickness followed by soaking at 1523K for 18ks and air-cooled. The cylindrical specimens of 8mm in diameter and 12mm in length were machined from these plates. The specimens were heated at 1223K for 1ks to 28.8ks and cooled with the cooling rate of 2K/s as shown in Fig.1. Cu segregation to austenite grain boundary was measured by an auger electron multiprobe in the specimen soaked at 1223K for 14.4ks and quenched into water. The specimens were also deformed at the temperature between 873K and 1223K with the reduction of 50% and the strain rate of 1/s, then quenched to room temperature. An optical microscopy, SEM and TEM were used to observe the microstructures. The grain size was measured by an image analysis of the micrographs.

Table 1 Chemical compositions of steels examined(mass%).

Steel	C	Si	Mn	P	S	Cu
Base	0.10	0.22	0.21	0.001	0.001	–
2Cu	0.11	0.22	0.22	0.001	0.001	2.0

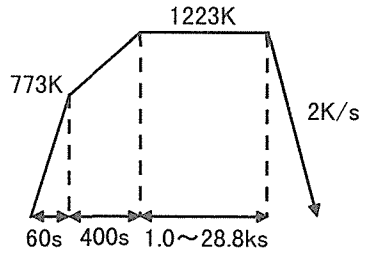

Fig.1 Schematic illustration of heat treatment.

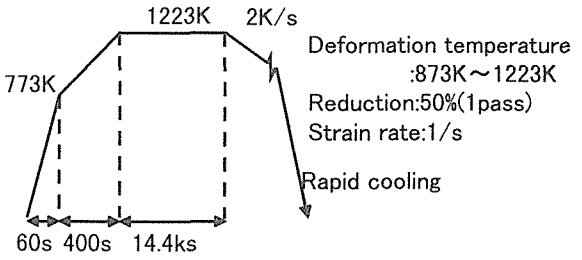

Fig.2 Schematic illustration of compression test.

3. Experimental results and discussion

The effects of soaking time in austenite region on the Ar_3 temperature are shown in Fig.3. The Ar_3 temperature of steel 2Cu remarkably decreased with prolonging the soaking time. On the other hand, the Ar_3 temperature of steel Base was almost constant. The Cu segregation to austenite grain boundaries was observed by an auger analysis. From these results, the

decrease in Ar_3 temperature in steel 2Cu is caused by the segregation of copper to the austenite grain boundaries.

The effect of deformation temperature on deformation stress of steel 2Cu is shown in Fig.4. The deformation stress was remarkably decreased by deforming super-cooled austenite obtained by prolonging the soaking time. The optical microstructure of the specimen whose deformation stress showed minimum value is shown in Fig.5. The ferrite grains were equiaxed and more than 85% ferrite grains consisted of high angle boundaries. The average ferrite grain size was 2.1 μm.

In order to clarify the grain refinement behavior at this temperature, the change in the optical microstructure during the deformation was studied. As a result, it was found that the grain refinement process consists of two stages. In the first stage, the volume fraction of the ferrite formed during the deformation increased with increasing the degree of deformation. In the next stage, the ferrite grains were refined and equiaxed with increasing the degree of deformation. These results show that the grain refinement was achieved by the dynamic $\gamma \rightarrow \alpha$ transformation followed by the dynamic α recrystallization.

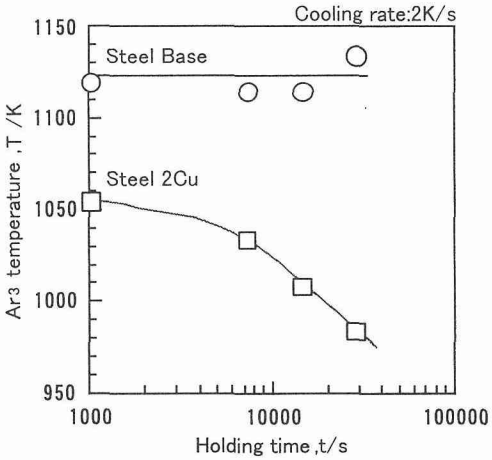

Fig.3 Effect of Cu addition and soaking time in γ region on the Ar_3 temperature.

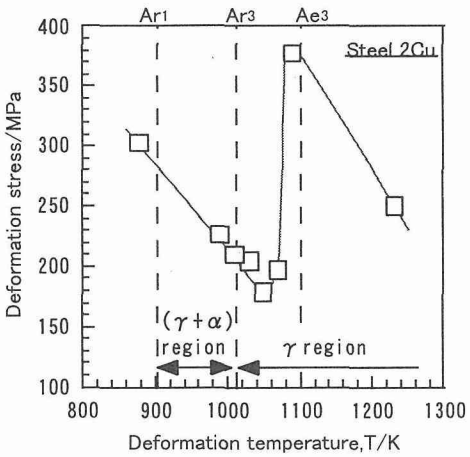

Fig.4 Effect of deformation temperature on deformation stress

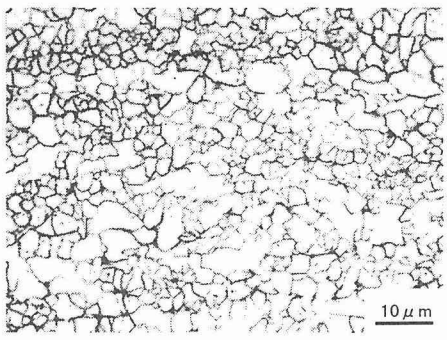

Fig.5 Optical microstructure deformed at 1043K with a reduction of 50% in steel 2Cu.

4. Conclusions

(1)The Ar_3 temperature decreased by prolonging soaking time in γ region because of Cu segregation to γ grain boundaries.

(2)The deformation stress remarkably decreased by deforming super-cooled austenite, due to the dynamic $\gamma \rightarrow \alpha$ transformation followed by the dynamic α recrystallization.

(3)The fine ferrite grain in size of 2.1 μm was obtained by the deformation of super-cooled austenite.

(4)The ferrite grains were refined by the dynamic $\gamma \rightarrow \alpha$ transformation followed by the dynamic α recrystallization in steel 2Cu.

References

[1] S. Takaki : Netsu shori, 40 (2000), 292.
[2] Y. Adachi, T. Tomita, and S. Hinotani : Tetsu-to-Hagane, 85(1999), 620.
[3] W. Y. Choo, J. S. Lee, C. S. Lee, J. K. Choi : CAMP-ISIJ, 13(2000), 1144.
[4] T. Hayashi, S. Torizuka, T. Mitsui, K. Tsuzaki, and K. Nagai : CAMP-ISIJ, 12(1999), 385.

Strain induced dynamic transformation in Nb containing steel

S C Hong, S H Lim, K J Lee, K S Lee
Division of Materials Science & Engineering, Hanyang University, Seoul, Korea

In this study, the amount of dissolved Nb was changed by applying various reheating temperatures and the effect of solute Nb or NbC on strain induced dynamic ferrite transformation was examined. The evolution of the strain induced ferrite grain structure with deformation was investigated by metallography and by measuring the misorientation angle distribution.

Two alloys were prepared by Vacuum Induction Melting. One was based on the 0.14C-1.5Mn-0.7Si (C-Mn steel). The other one was 0.05wt% Nb containing steel (Nb steel). The hot compression test was performed with up to true strain of 1.6 (80% reduction) and constant strain rate of 5/sec with various reheating temperatures by Gleeble 1500. The amount of reduction from 10% to 80% was applied at Ar_3+10℃ respectively and then water quenched immediately to examine the formation of ferrite. The microstructure was observed by OM and TEM and the grain boundary misorientation angle was measured by EBSD.

In the low reheating temperatures such as 900℃, where Nb was mostly precipitated as NbC, the dynamic ferrite grain of Nb steel was finer than that of C-Mn steel, since NbC acted as ferrite nucleation site or strain induced grain growth was inhibited by the precipitates. In case of the higher reheating temperatures such as 1250℃, where most of Nb was dissolved, the ferrite transformation was remarkably reduced and the ferrite morphology was changed as shown in Fig.1.

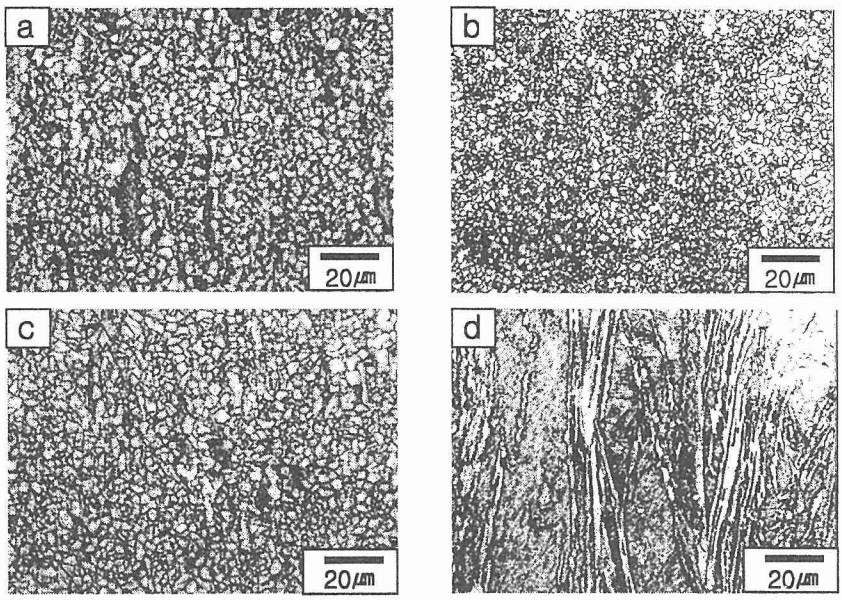

Fig.1 The formation of strain induced ferrite after 80% reduction with reheating temperature

(a) 900℃(C-Mn steel) (b) 900℃(Nb steel)

(c) 1250℃(C-Mn steel) (d) 1250℃(Nb steel)

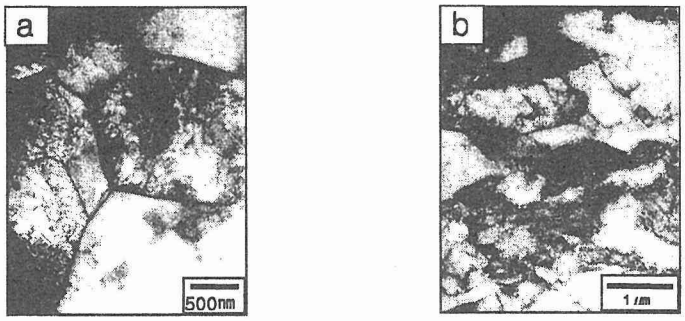

Fig.2 TEM micrographs of Nb steel showing morphology of ferrite grains after 80% reduction with reheating temperature (a) 900℃ (b) 1250℃

By TEM observation of Nb steel, in case of 900℃ reheating, the equiaxed ferrite grains with high angle grain boundary were formed and a large amount of dislocation cells were observed in ferrite grain. When solute Nb was presented after reheating at 1250℃, highly dislocated substructure of ferrite was generated by the deformation, since dynamic recovery was inhibited by solute Nb. As a result, deformed structure with low misorientation angle was exhibited significantly as shown in Fig.2. In this case, the dynamic ferrite volume of Nb steel with amount of reduction was compared with that of C-Mn steel as shown in Fig.3. Over 40% reduction, the ferrite volume of Nb steel was lower than that of C-Mn steel. It was considered that the ferrite transformation during deformation was retarded by both the solute dragging effect of Nb and the consumption of strain energy to precipitation of NbC during deformation. Solute Nb inhibited ferrite grain boundary migration lead to retarding the progress of transformation. The critical driving force (ΔG_v) for nucleation of precipitation was composed of chemical driving force (ΔG_{ch}) and strain induced driving force (ΔG_{st}) [1].

$$\Delta G_v = \Delta G_{ch} + \Delta G_{st}$$

The strain induced driving force was consumed by the precipitation of NbC during the deformation. Thus, the strain induced driving force for strain induced dynamic ferrite transformation was relatively decreased resulting in retardation of the transformation.

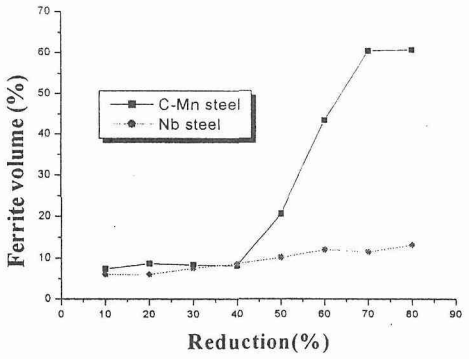

Fig.3 Measured ferrite volume with amount of reduction with reheating temperature of 1250℃

Reference

[1] K.C.Russel, Phase transformation, ASM (1969) pp.219.

Analysis of Microstructure of a microalloyed steel with ultra low carbon content during deformation induced ferrite Transformation

Huoran Hou, Qingyou Liu, Hongju Chen, Xinjun Sun, Han Dong
Central Iron & Steel Research Institute, Beijing, 100081,China

INTRODUCTION

Since reducing the grain size of a material, particularly in the range below 10um, has the potential dual benefits of increasing both the strength and the toughness, the refinement of ferrite grain size has remained a key goal of research into the thermomechanical processing of steels. In recent years, it has been shown that one of the most promising approaches to ferrite grain refinement involves so-called deformation inducing ferrite transformation (DIFT) or strain inducing transformation rolling (SITR) and dynamic recrystallization (DRX) of ferrite [1-5]. This method involves imposing large strain on the steels at the temperature above transformation temperature Ar_3.

However, there have still remained some questions about the process of DIFT and mechanism of the nucleation of induced ferrite. In the present paper, the nucleation of ferrite in a microalloyed steel with ultra low carbon content during the process of DIFT is studied and the microstructures are also observed.

EXPERIMENT

A microalloyed steel with ultra low carbon content was carried to performing the compression test. The chemical composition of the steel is (wt%): 0.003C-1.12Mn-0.22Si-0.011Ti-0.052Nb-0.0036O-< 0.0016P-0.0010S-0.0012N. The transformation temperature (Ar_3) and the equilibrium transformation temperatures (Ae_3) are 1088K and 1151K respectively. The Ar_3 temperatures were measured by using the Formaster-Digital Automatic with the heating or cooling rate of 200K/s. The Ae_3 temperatures were calculated by using the Thermo-Cale software. The hot compression test was conducted in a Gleeble 2000 machine. Reheating conditions were 1423K for 3 min, then cooled down with 5K/s cooling rate to the deformed temperature of 1023K, 1063K, 1093K and 1123K respectively. The specimens were deformed with a single pass with 60% reduction with 15/s strain rate, then quenched immediately. The induced ferrite was observed by optical microscopy, TEM, SEM and EBSD.

RESULTS

The original microstructure of the steel before deformation was austenite. Fig.1 shows the microstructures of the steel deformed at 1023K, 1063K, 1093K and 1123K respectively. Since the specimens were quenched immediately after deformation, it is believed that the ferrite formed during deformation. It can be seen that at the experimental temperature range ferrite were induced in austenite, and the induced ferrite are equiaxed and fine. The induced ferrite nucleated not only at original austenite grain boundaries and deformed bands but also within the austenite grains. Fig.2 shows the TEM morphology of the steel deformed at 1093K. Both the elongated and equiaxed ferrite grains were existed. The dislocation density in the elongated deformed ferrite grains was high, but the dislocation was little in fine equiaxed ferrite grains. Fine cementite particals were precipitated between the original austenite and induced ferrite grain boundaries and along the ferrite grain boundaries. During DIFT process, fine ferrite grains were induced in austenite, so 'carbon rich zone' is formed between the austenite and ferrite grain boundaries and along the ferrite grain boundaries due to the extra carbon during $\gamma \rightarrow \alpha$ transformation. Thus second phase carbides include cementite particles were formed. The fine cementite particles not only inhibit the grain growth but also inhibit the

nucleation of induced ferrite grains. In this way decreasing carbon content can improve induced ferrite formation. Fig.3 shows the EBSD analysis of steel deformed at 1123K. The slight microtexture <001> was formed in the induced ferrite microstructure (Fig.3a). The misorientation of the induced ferrite grains was in general greater than 15° (Fig.3b) .

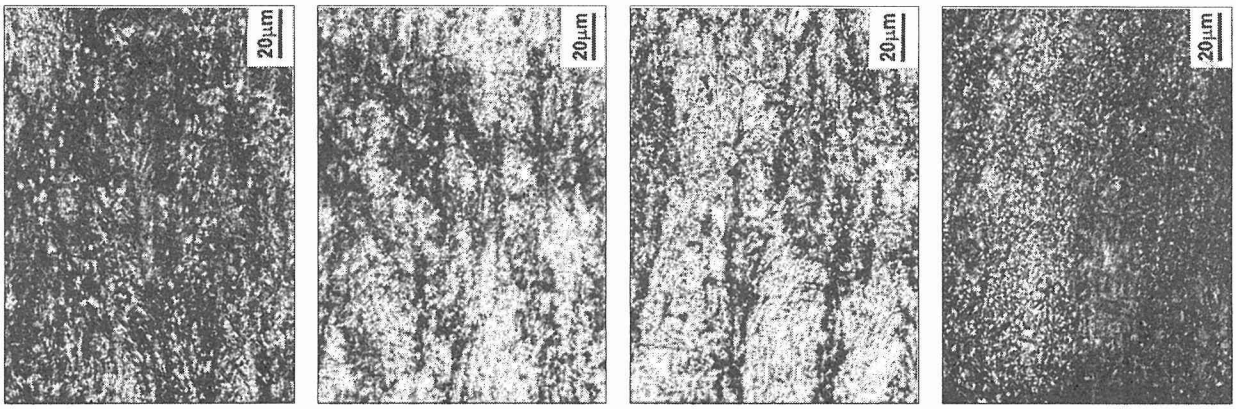

(a) 1023K (b) 1063K (c) 1093K (d) 1123K

Fig.1 microstructures of the steel deformed at 1023K, 1063K, 1093K and 1123K

Conclusions

1. Ferrite can be induced at temperate range 1023K to 1123K during DIFT process. The ferrite grains are formed basically at original austenite grain boundary and deformed bands but also within the austenite grains.
2. The misorientation of the induced ferrite grains is in general greater than 15° . The dislocation density in the elongated deformed ferrite grains is high, but the dislocation is little in fine equiaxed ferrite grains.

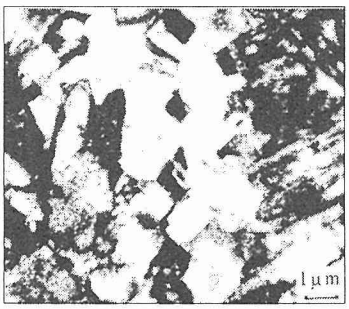

Fig.2 TEM morphology of steel deformed at 1093K

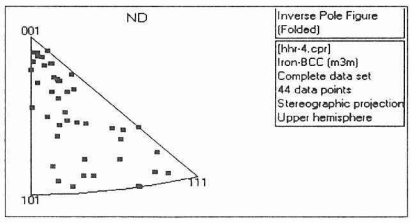

(a) Inverse pole figure

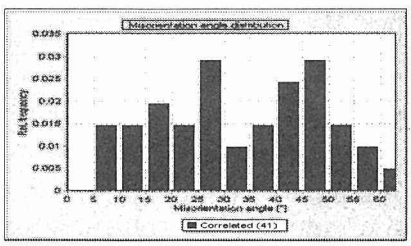

(b) Misorientation (degree)

Fig.3 EBSD analysis of steel deformed at 1123K

References

[1]Matsumura Y. and Yada H., Evaluation of Ultrafine-grained Ferrite in Hot Deformation. Trans. ISIJ, 1987,27, pp.492-497.

[2]W.Y.Choo, J.S.Lee, C.S.Lee and J.K.Choi, Strain induced dynamic transformation of austenite of fine ferrite and it's characteristics. CAMP-ISIJ, 2000,13,pp.1144-1147.

[3]Han Dong, Ultra fine grained steels and properties, International symposium on ultrafine grained steels, Umimonakamichi. Fukuoka, Japan, Sep. 20-22, 2001, pp.18-25.

[4]H.Yada, Y.Matsumura and K.Nakajima, United States Patent. No.4.446, 842 (1984).

[5]P.D. Hodgson, M.R.Hickson and R.K. Gibbs, The producing and mechanical Properties of ultrafine ferrite, Materials Science Forum. Vols.284-286 (1998), pp.63-72.

A FE analysis of ultra-fine grain formation in a simple hot rolling process and experimental verification

C.J.Huang C.L.Mo D.Z.Li Y.Y.Li
Institute of Metal Reserch, Chinese Academy of Sciences, P.R.China

1. Introduction

An interest has arisen recently in the production of steels having an essentially ferritic microstructure and an ultra fine grain size. The basic reason for this interest is to increase strength and improve fracture resistance of steels. A few groups have reported achieving ferrite grains as fine as 1 μm in low carbon steels via simple thermomechanical means [1-5]. One of the most frequently mentioned works among these reports is the hot rolling test done by Hodgson et al. In 1992, Hodgson et al reported having achieved ultra-fine grains by a simple rolling process [8,9]. Hodgson named this novel rolling schedule "strain induced transformation rolling (SITR)". It's very interesting to note that the ultra-fine grains reported in Hodgson's experiments were acquired by a one-pass rolling process with a reduction ratio of only about 30%. It was reported that up to 1/3 of the total section of the rolled specimens was transformed to ultra-fine-grained material.

The simplicity and efficiency of SITR process on grain size reduction made it very appealing. However, the mechanism of grain refinement remains unclear. It is supposed that the two most important factors involving grain refinement in SITR are: (i) High level shear strain due to friction (ii) High level undercooling due to the quenching effect of rolls [9]. This is largely due to the lack of information about the temperature field and strain field inside the specimens during SITR tests. So far it's still impossible to access this kind of information directly.

Fortunately, numerical simulation provides another way to inspect this information. In this paper, a FE simulation is performed to study the temperature and strain distribution within the specimens in SITR processing. The aim of this analysis is to reveal the critical condition at which ultra-fine grains can form.

2. FE analysis

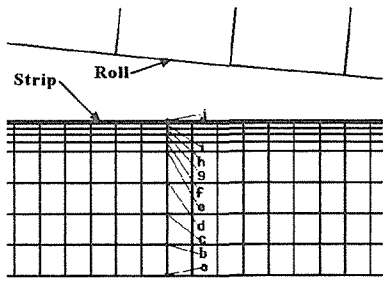

Fig.1

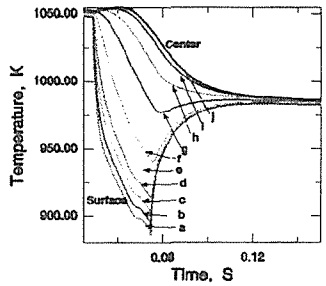

Fig.2(a)

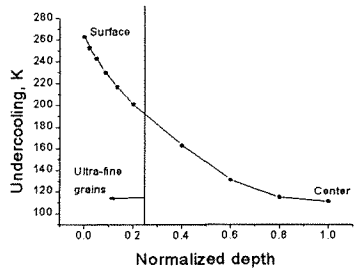

Fig.2(b)

Figure 1 FEM mesh Fig. 2 (a)Temperature history at different depth of the specimen Fig. 2 (b) Undercooling at different depth when deformation just ended

A coupled thermo-mechanical finite element analysis was performed to model the hot rolling experiments (SITR) done by Hodgson et al. Part of the FFM mesh is shown in Fig.1. Fig.2 depicts the temperature-time curves at different depth of the specimen during SITR processing. Curve a to j represents the temperature-time curve at different points of the strip as shown in fig.2. Because cooling rate is very high, it is supposed that $\gamma \rightarrow \alpha$ phase transformation occur at the lowest temperature on the temperature-time curves, which is

supported by Hodgson's microstructure analysis. Then undercooling level of $\gamma \rightarrow \alpha$ transformation during SITR processing can be determined by substrate the lowest temperature in temperature-time curves (curves a-j in figure 2(a)) from the Ae_3 temperature. Undercooling at different depth of the strip is shown in fig.2 (b). It can be seen from fig.2 (b) that undercooling at the surface (about 260K) is much greater than that at the center (about 110K). From fig.2 (b) it can be seen that undercooling level is higher than 190K in areas where ultra-fine grains form.

3. Hot compression test

To verify the effects of undercooling on grain refinement during TMCP, , a set of hot compression experiments were done on thermo-mechanical simulator Gleeble 1500. These experiments differed from other hot compression experiments in that some of the specimens were deformed at very high undercooling. This was realized by cooling the specimens rapidly before deformation. Specimens were deformed immediately after the rapid cooling. Relations between the level of undercooling and grain size were carefully examined. The effects of strain on grain size were also studied in detail. It's found that the critical condition for the formation of ultra-fine grains in hot compression is similar to that in SITR processing.

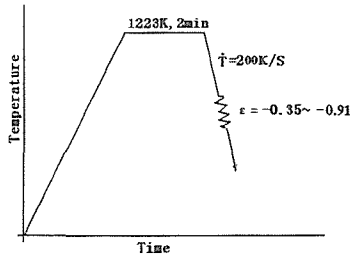

Fig.3 hot compression schedule

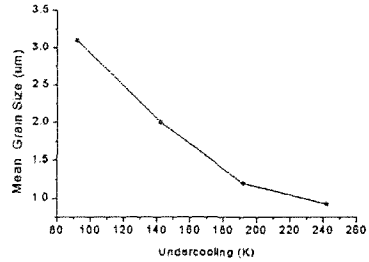

Fig.4 Effects of undercooling on grain size

4. Conclusion

A FE analysis is performed to study the formation of ultra-fine grains during SITR processing. It is found that high level undercooling is the most important feature of SITR processing. Undercooling level was greater than 190K during SITR processing in the surface layer of the specimen, where ultra-fine grains formed A new thermo-mechanical treatment route is designed to verify the effects of undercooling on grain size during TMCP. The required undercooling was about 200K and the required strain was about 0.9 for ultra-fine grain-refinement for the investigated low carbon steel.

References

[1] Hodgson, P.D. Hickson, M.R. and .Gibbs, R.KThe production and mechanical properties of ultrafine ferrite. Mater.Sci.Forum 63-72 (1998), pp.284-286

[2] Priestner, R. and Hodgson, P.D. Ferrite grain coarsening during transformation of thermomechanically processed C-Mn-Nb austenite. Materials Science and Technology. 8 (1992), pp.849-854

[3] Hodgson, P.D. Ultrafine ferrite in low carbon steel. Scripta Mater, 40 (1999) pp.1179-1182

[4] Hurley, P.J. Hodgson, P.D. Muddle, B.C. Analysis and characterization of ultra-fine ferrite produced during a new steel strip rolling process. Script Mater, 40 (1999), 433-436.

[5] Mabuchi, H. Ishikawa, Tadashi. Metallurgical features of steel plates with ultra fine grains in surface layers and their formation mechanism. ISIJ International. 39 (1999), 477-485

Development of Ultra - Fine Grain Steel in Pansteel

Song liqiu Tang li Zuo jun Cheng xingde Zhang kaihua
Material Department of Panzhihua Iron and Steel Research Institute

1 Introduction

In the traditional hot rolling train, the yield strength is about 325MPa, the tensile strength is about 400MPa, and ferrite grain size is about 10 μ m. In order to meet the increasing needs from economic and social developments in the future, the common carbon steel with higher strength and longer life were studied and producted in Panzhihua Iron and Steel company. Without adding alloying element, microstructure refinement is the most efficient way of improving mechanical properties and toughness of low carbon steel. Now grain refining has been studied and grain size can be refined to 1 μ m by various methods in laboratory[1-2]. In the paper, According to the theory of deformation induced transformation and ferrite dynamic recryatallization , the products procedures of 400MPa ultra-fine grain steel were investigated to find an effective way to get ultra-fine grain in common carbon steel in an industrial condition of Panzhihua Iron and Steel company.

2 Experimental procedures

2.1 Test material

The test material was produced from the 120t converter at Panzhihua Iron and Steel Corp, which is cast into 200×1000×5500mm slab by slab caster. The slab is rolled into 3.0×1000 ×5700mm hot plate by the 1450 hot rolling mill. Chemical composition of the material is shown in table 1.

Table 1 Composition of test steel

Steel	C	Si	Mn	P	S
P400	0.11	0.23	0.69	0.021	0.008

2.2 Rolling schedule

P400 hot rolling schedule are show below:

Slab heated → High pressure water dispose of scale → R_1、R_2 Roughing rolling → Hot roll equipment coiling → F_1、F_6 Rolling → Cooling → Coiling (Examine) → Open coil and cut off → Neating → Pack and laid up

The steel was heated at 1200～1230℃, keep for 150 minute and then rolling 6 times. The finishing temperature was 800～830℃, the coiling temperature was 600～630℃.

3 Experimental results and discussion

3.1 Microstructure of P400 steel

Microstructure of P400 steel consisted of ferrite and a little pearlite. The ferrite grain size was about 5～6 μ m.

Suitable temperature range for ultra-fine grains was about higher above Ar_3. P400 hot steel sheets Ar_3 is about 800℃. The finishing temperature of P400 steel was at 800～830℃. Effect of finishing temperature on ferrite grain size was show in figure 1. As seen from figures 1, the ferrite grain size can be refined along with the finishing temperature decrement. The ferrite grain size was about 5～6 μ m when the finishing temperature was about 800～ 830℃.

3.2 The mechanical properties

The result of mechanical properties of P400 steel sheet in transverse, longitudinal and every direction of 45° was listed in table 2. It can be seen that P400 hot rolled plate has little anisotropic property and high total elongation , which is favorable to the formability. Effect of coiling temperature on tensile strength was show in figure 2. The tensile strength was increment along with the coiling temperature decrement.

Table 2. Mechanical property in different directions of HP295 Steel

Direction	σ s, MPa	σ b, MPa	δ 5, %	ψ, %
Horizontal directions	405	510	28	56
Longitudinal directions	400	500	34	65
45° Direction	400	500	31	58
Difference between horizontal and longitudinal	5	10	6	9
Difference between 45° directions and horizontal	5	10	3	2
Difference between 45° directions and longitudinal	0	0	3	7

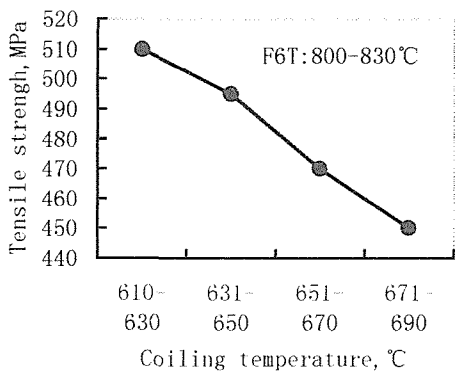

Fig.1 Effect of FT on ferrite grain size

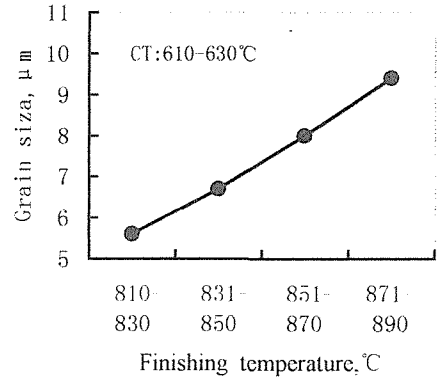

Fig. 2 Effect of CT on tensile strength

4 Conclusion

(1) The ferrite grain of common carbon can be refined in austenite non-recrystallization region. Ultra-fine grain of about 5～6 μ m can be gained in hot rolled steel sheet by multi-pass rolling at finish rolling temperature of 800～830℃ and coiling temperature of about 600～630℃.

(2) The yield strength increase from 235MPa to about 400MPa, the tensile strength increase from 375MPa to about 500MPa. Without significant loss of ductility compared with material produced by conventional processing, the total elongation was more than 28%.

Reference

[1] Mark R.HICKSON, Russell K.GIBBS, Peter D.HODGSON, The Effect of Chemistry on the formation of Ultrafine Ferrite in Steel, ISIJ, 1999, 39(11): 1176-1180.

[2] P.J.HURLEY, B.C.MUDDLE, P.D.HODGSON, Nucleation Site for Ultrafine Ferrite Produced by Deformation of Austenite During Single-Pass Strip Rolling, Metall. and Mater. Trans.A, 2001,32A(6): 1507-1517.

Research on Microstructures Evolution and Precipitation Behavior of Hot Strip of Low Carbon Steel Produced by CSP

KANG Yonglin[1], WANG Kelu[1], YU Hao[1], FU Jie[1], LIU Delu[1],

WANG Zhongbing[2], CHEN Xuewen[2]

1 University of Science and Technology Beijing, Beijing 100083, P.R.China

2 Guangzhou Zhujiang Steel Co. Ltd., Guangzhou 510620, P.R.China

Continuous casting and rolling technics is an original technology in the late 1980's, the great scientific progress in iron and steel field. In comparison with conventional strip hot rolling technology, there are distinct differences in ingot casting, reheat schedule, rolling process, delivery speed on the runout table and so on. Mentioned as above, it is essential to investigate the microstructure evolution, precipitation behavior and properties of hot strip produced by CSP technology..

During the past time, simulators were often used to study on mechanism of microstructure evolution, but the results had much difference with the practice production process due to the capability limitation of instrument. It is known to all, strain and strain rate of latter stands of CSP are too relatively heavy and high to be simulated. Fortunately, we carried out our experiment using the specimens from practice production line in Zhujiang Steel Co. Ltd. The composition of low carbon steel produced by CSP was presented in table 1.

Table 1 Chemical compositions of low carbon steel (wt %)

C	Mn	Si	S	P	Als
0.051	0.39	0.04	0.002	0.026	0.0306

Specimens (Fig. 1) were obtained from the surface layer of subject by suddenly stopping the line during its rolled operation. The microstructures of low carbon steel before, during and after rolling deformation of each stand were observed using optical microscope. At the same time, thin foils of corresponding specimens were investigated using H-800 transmission electronic microscope in order to observe the microstructure evolution and analyze the precipitation behavior induced by strain.

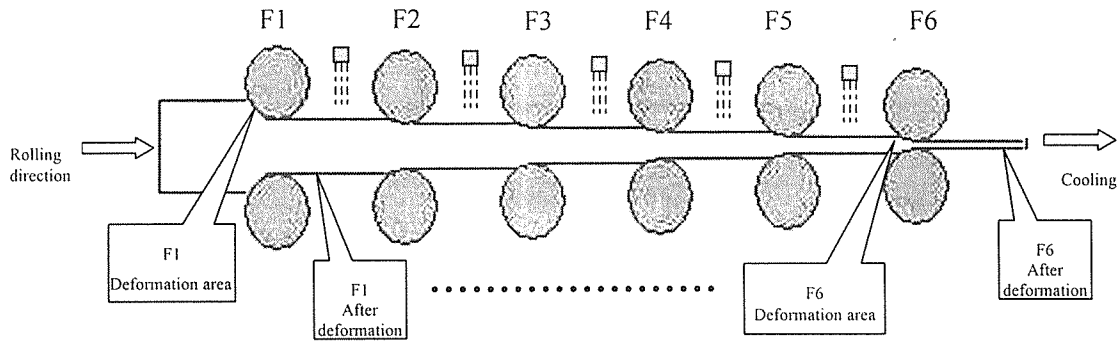

Fig.1 Sketch depicts obtained specimens

Based on rolling schedule, Fig.2 and Fig.3, this paper discussed the mechanism of

microstructure evolution and precipitation strength , and drew out conclusions as below.

(1) With the increasing cumulative strain, the dimension of grain size decreases, moreover, the degree of microstructure refinement is notable in the prior three stands, and further enhances during the latter stands. The average grain size of 2.0mm sheet of finished product is about 4 μ m to 5 μ m. The yield strength and tensile strength are about 350MPa, 425MPa respectively, and elongation rate about 35%.

(2) In the front two stands, because of light cumulative deformation and high temperature, ι few of precipitates, mainly located in grain boundaries, with average dimension about 150 nanometer were observed. With heavy deformation and temperature decreasing, many of fine and dispersive particles with dimension about 20~80nm in grains, which is the function of strain induction.

(3) With the increasing cumulative strain during hot rolling process, the density of dislocations increases , which lead to high strength.

(4) From analysis, we concluded that the strength of hot strip produced by CSP was high than that of hot strip produced by conventional hot rolling due to fine microstructure, precipitation and high density dislocations.

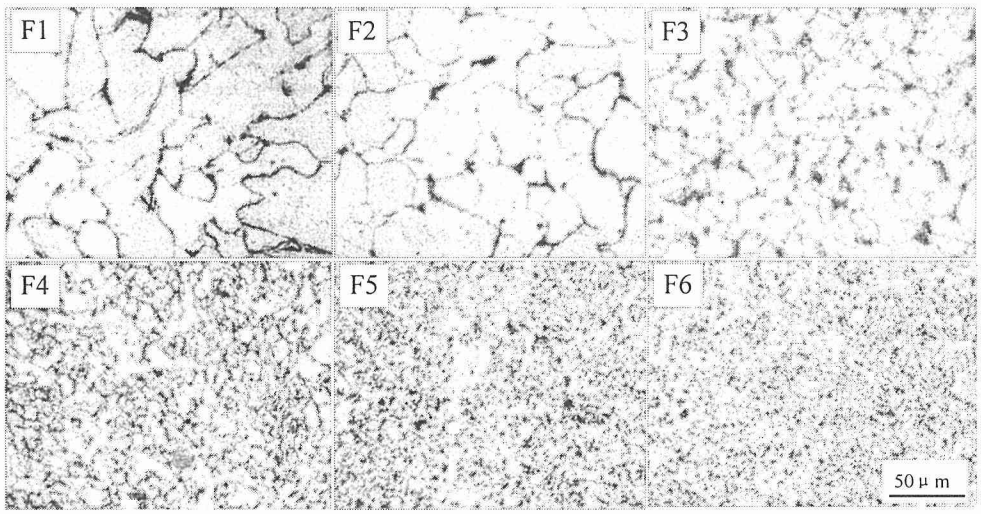

Fig.2 Optical microstructures of each stand after deformation

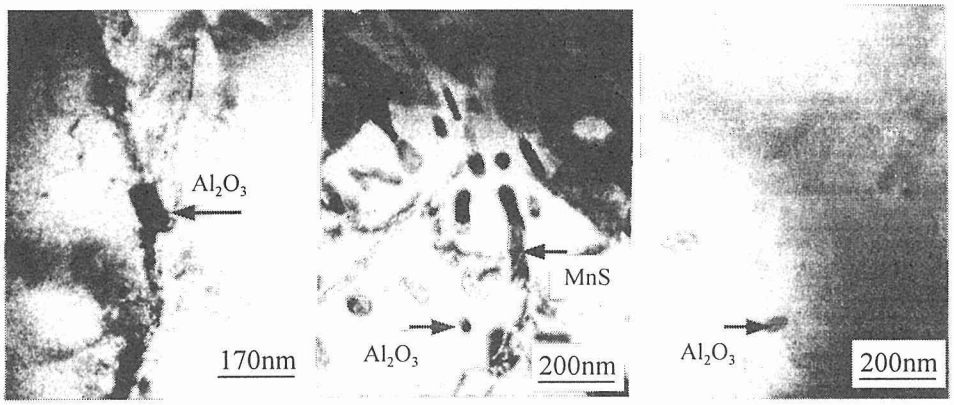

(a) F1 Deformation area (Total defomation 30%)

(b) F2 (Total deformation 79%)

(c) F5 (Total deformation 95%)

Fig.3 TEM micrographs of precipitates from thin foils

Refining Intermediate Transformation Microstructure by Relaxation Processing

X. M. Wang, X. L. He, S. W. Yang and C. J. Shang

Dept. Materials Physics, Univ Sci & Tech Beijing, Beijing, 100083, CHINA

1. Introduction:

It is well known that among the vast strengthening methods the grain refinement is the only method to improve both strength and toughness simultaneously, He[1] found that new developing RPC technique is an efficient process to refine the intermediate transformation structure. This technique includes micro-alloying design, two stages controlling rolling, relaxing and accelerated cooling/direct quenching. By this technique the strength could be increased about 25–30% comparing with the same composition steel processed by re-quenched and tempered steels[2,3]. In this paper, the influences of the RPC process parameters on the refinement of the microstructure were studied in order to obtain the best processing condition for actual rolling schedule, and to investigate the mechanism of grain refinement imparted by the RPC technique and relevant physical metallurgical issues.

2. Experimental materials and methods

The experimental steel was melted in a 25kg vacuum induction furnace, and its composition is 0.035C-1.74Mn-0.16Si-0.094Nb-0.080Ti-0.29Cu-0.33Ni-0.0020B. Besides, a Fe-40%Ni-Nb alloy was employed to retain the austenitic structure to room temperature upon quenching, while showing deformation and precipitation behavior similar to those seen in the steel.

The thermo-simulation process includes: the samples were reheated to 1250℃, thermally held for 20 minutes, cooled at 2℃/s to800℃, 850℃ or 900℃, and held for 1 minute, then deformed by a strain:ε =0.3 or 0.6. After that the samples were relaxed isothermally for different time and quenched in water.

3. Experimental results and discussions

1). The steel after different RPC processing is composed of similar microstructure constituents that mainly are lath bainite. From figure 2 it can be seen that with a certain relaxing the bainite can be refined markedly and at a best relaxing time the packet size reaches a minimum value. After various RPC processing the bainite packet size varies with the relaxing time by the same rule, but the optimum relaxing time to obtain shortest packets and the refinement effect is different.

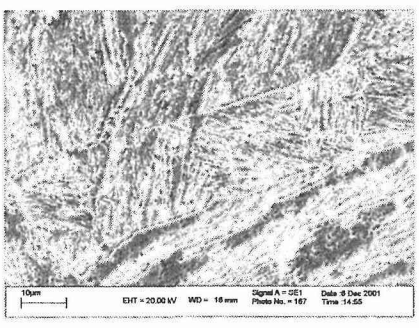

(a) relaxing 200s at 850℃

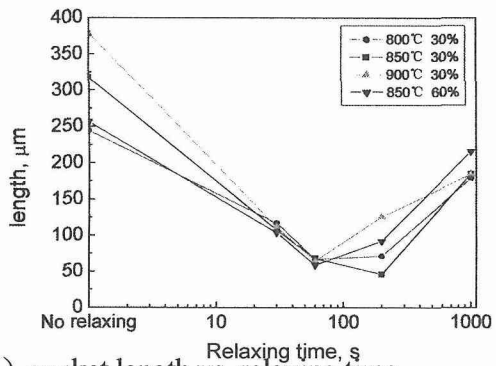

(b) packet length vs. relaxing time

Fig. 1 (a) typical microstructure and (b) packet size vs. relaxing time under various processings

2) It can be found from Figs. 2 (a, b) that during relaxation the high density of dislocation induced by deformation will be recovered and formed polygonal dislocation cells. The perfect dislocation cells boundaries would provide the preferential nucleation sites for new phase during cooling, and hinder the growth of new phases, and refine the new phase. At the same time, during the relaxation the precipitation occurs, and the surrounding matrix would become less stable so granular bainite will be formed in advance and hinder the succeeding lath bainite growth to refine the microstructure. Fig.2(c) shows a prior austenite is divided into numbers of subgrains uniformly and each subgrain is near a perfect polygon. From Fig. 2(d) it can be found after relaxing 200s at 850℃ a great number of precipitates precipitates pin the dislocation network effectively and a polygonal dislocation network structure is rather perfect. Therefore under this processing condition the optimum refinement effect could be obtained.

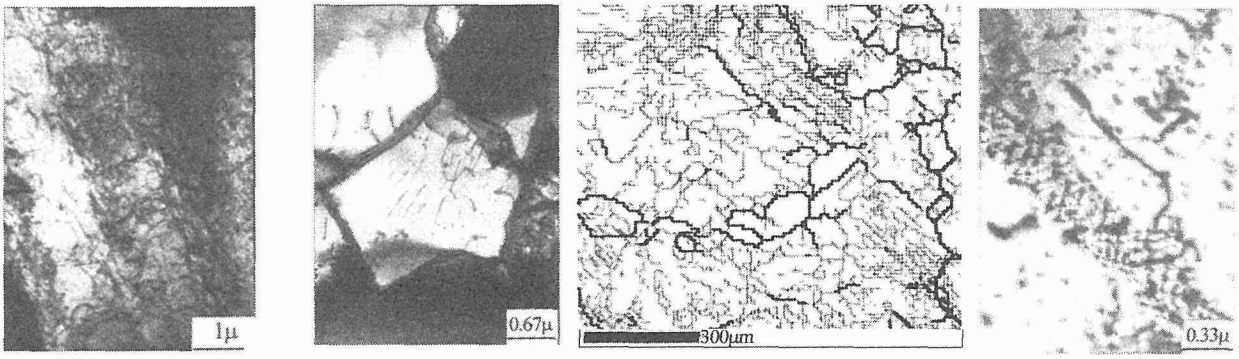

（a）900℃ 0s （b）900℃ 60s (c) 850℃ 200s (d) 850℃ 200s

Fig. 2 TEM micrographs (a, b, d) showing dislocation configuration and precipitation during relaxing and EBSD misorientation map (c) showing sub-structure for a Fe-Ni alloy.

4. Conclusions

1) By RPC process, the intermediate transformation structure could be refined, the refinement effect depends on relaxing time, deformation temperature and reduction ratio. Relaxing for a certain time the refinement would be most effective.
2) The RPC process parameter influences the refinement effect, in this thermo-simulated experiment, deformation at 850℃ by 30% and relaxing isothermally for 60-200s could have a best refinement effect. Increasing or decreasing deformation temperature and increasing the reduction ratio would also influence the refinement after relaxing for various time.
3) During relaxing the dislocation recovery and polygonizing occur, and a polygonal dislocation cells appears, meanwhile the Nb, Ti carbonitride precipitation takes place. These two mechanisms are both helpful to refine microstructure and when they cooperate and promote each other the optimum refinement could be obtained.

Reference:

[1] Yang, S. Shang, C. He, X. et al., Stability of Ultra-fine microstructure during tempering. Journal of university of science and technology Beijing 8(2001), No.2, pp.119-122.
[2] Yang, S. Wang, X. Shang, C. et al., Relaxation of deformed austenite and refinement of bainite in a Nb-containing microalloyed steel. Journal of university of science and technology Beijing 8(2001), No.3, pp.214-217.
[3] Shang, C. Wang, X. He, X. et al., A special TMCP used to develop an 800 MPa grade HSLA steel. Journal of university of science and technology Beijing 8(2001), No.3, pp.224-228.

Anisotropy of Interfacial Energy of B1-Precipitates with Iron

Z.-G. Yang* and M. Enomoto**

*Department of Materials Science and Engineering, Tsinghua University, Beijing 100084, P. R. China

** Department of Materials Science, Ibaraki University, Hitachi 316-8511, Japan

1. Introduction

The interfacial energy of non-metallic inclusions with iron may play an important role for microstructure control in steel and steel welds, e.g. the fabrication of fine, interweaving ferrite microstructure. A discrete lattice plane, nearest neighbor broken bond (DLP/NNBB) model was employed to study the chemical interfacial energy of B1(NaCl)-type inclusions in austenite and ferrite [1-2]. In this work, the anisotropy of interfacial energy and the corresponding equilibrium shape of B1-precipitates with liquid iron are studied by the NNBB model.

2. Calculation method

The chemical interfacial energy, σ, is calculated as the difference in free energy between the interfacial region and the bulk. Under the assumption that the entropy term is insignificantly small, the interfacial energy is given by,

$$\sigma = E_{\xi/L} - \frac{E_{\xi/\xi} + E_{L/L}}{2} \tag{1}$$

where $E_{\xi/L}$ and $E_{\xi/\xi}$ are the sum of the bond energy across the liq.Fe/compound interface and across the plane of the same orientation in the compound phase, respectively. $E_{\xi/L}$ is calculated from,

$$E_{\xi/L} = n_s Z e_{FeM} + n_s' Z' e_{FeI} \tag{2}$$

where $Z=\Sigma\, j z_j$, $Z'=\Sigma\, j' z_j'$, n_s and n_s' are the number of metal (M) and non-metallic (I) atoms per unit area of the interface, respectively, and z_j and z_j' are the coordination number of the nearest neighbor M and I atoms to an M atom (the liquid phase is regarded as pure Fe). $E_{L/L}$ is the sum of the bond energy across the plane in the liquid (approximately two times of the liquid surface energy). In an earlier model [3] it was considered that the structure of the liquid is unaltered up to the interfacial plane. Later, it was considered that the liquid phase is adjusted to some extent to the crystal interface in the immediately adjacent layers. On the basis of the hard sphere model it was proposed that the number of atoms in the 1st layer is approximately 0.75 of that in the crystal plane [4]. However, it is only for a close-packed crystal plane and the knowledge on the structure of high index interfacial planes is lacking. Under these circumstances it is assumed that $E_{\xi/L}$ is independent of the interface orientation, which implies that the anisotropy of the interfacial energy comes only from the orientation dependence of $E_{\xi/\xi}$. An alternative is to assume that the atom arrangement in the layers of the liquid adjacent to the interface has an almost coherent structure with the crystal phase within the 1st neighbor distance. In this case both $E_{\xi/L}$ and $E_{\xi/\xi}$ are the same as the fcc Fe/compound interfaces and only $E_{L/L}$ is independent of the orientation. The calculation is conducted with the e_{FeM} and e_{FeI} values for TiN [1].

3. Results and Discussion

Figure 1a is the (110) section through the polar plot of the chemical part of fcc Fe/TiN interfacial energy and Fig.1b is the three-dimensional polar plot and the equilibrium shape derived from Wulff construction. In contrast to a binary fcc/fcc interface {100}-type interfaces have the minimum energy and {111}-type interfaces have the maximum energy. This is because the contribution from strong M-I interaction is greater than the contribution

from M-M interaction. The corresponding equilibrium shape is a cube [1].

Figure 2a is the (110) section through the polar plot of TiN/liq.Fe interfacial energy calculated assuming a constant $E_{\xi/L}$ value, the value of which was chosen such that {100}-type interfaces has a similar energy to that in Fig.1. Although the anisotropy is considerably different from the TiN/fcc Fe interfaces, the equilibrium shape is likely to be a cube, due to the deep cusp at {100} orientation (Fig.2b). Experimentally, the cubic morphology in austenite was observed [5].

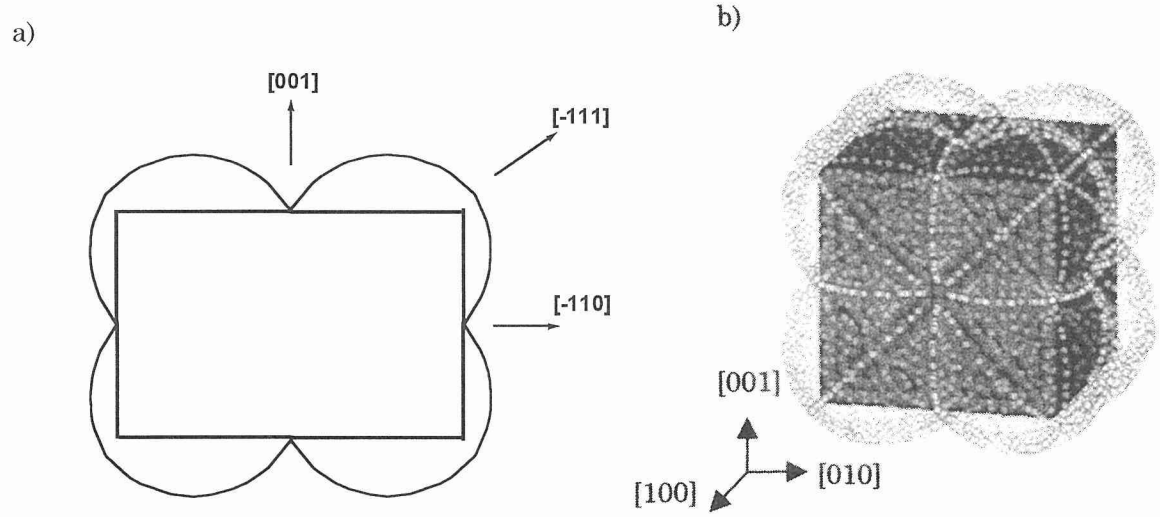

Fig.1 (a) {110}-section of the polar plot of the chemical interfacial energy and (b) the corresponding Wulff construction for the equilibrium shape of TiN in fcc Fe.

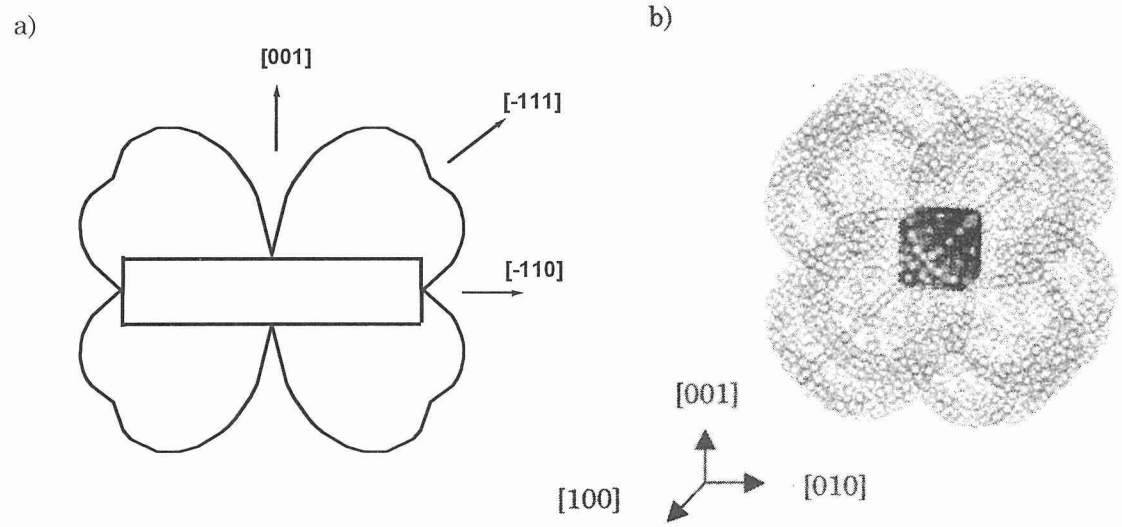

Fig.2 (a) {110}-section of the polar plot of the chemical interfacial energy and (b) the corresponding Wulff construction for the equilibrium shape of TiN in liq.Fe calculated assuming constant $E_{\xi/L}$.

References

[1] Yang Z.-G. and Enomoto M., Metall. Mater. Trans. A, 32A(2001), p.267
[2] Yang Z.-G. and Enomoto M., Mater. Sci. Eng. A, in press.
[3] Skapski, A.S., Acta Met., 4(1956), p.576
[4] Spaepen, F., Acta Metall., 23(1975), p.729
[5] Fairchild, D.P., Howden, D.G., Clark, W.A.T., Metall.Mater.Trans.A, 31A(2000), p.643

Non-classical analysis of the nucleation of Cu precipitates in Fe-Cu alloys

C. Zhang and M. Enomoto
Department of Materials Science, Ibaraki University, Hitachi 316-8511, Japan

1. Introduction

The formation of copper precipitates plays an important role in the evolution of microstructure and the mechanical properties of Fe-Cu alloys. In ageing of the supersaturated α-Fe (bcc) solid solution, the metastable phase of coherent bcc copper-rich cluster precipitates at first, and transforms to incoherent fcc α-Cu particles upon reaching a critical size, that is nearly 5 nm. It is reported that the mechanical properties change remarkably when copper-rich precipitates are still extremely small, probably at the stage of the nanoscale clustering. The FIM atom-probe analysis made earlier showed that nuclei of Cu precipitates in ferrite contain less copper than the equilibrium α-Cu phase[1,2], as shown in Table 1.

Table 1 Results of FIM atom probe analysis in the literature

Alloy composition (at %)	Aging temperature and time	Average composition in precipitates (at%)	Mean diameter of particle (nm)	Particle number (1/cm^3)	Reference
Fe-1.4Cu	500℃, 3 h	50	2.4	~1×10^{18}	[1,4]
Fe-1.14Cu	500℃, 3 h	55	N.D.	N.D.	[2]

2. Calculation method

In the classical nucleation theory, it is usually assumed that the precipitate has a sharp interface with a composition-independent interfacial energy. On the other hand, a continuum non-classical theory of nucleation developed by Cahn and Hilliard [3] takes into account the diffuse nature of the interface. This model is used to study the nucleation of copper-rich clusters in the supersaturated bcc matrix. According to the Cahn-Hilliard theory, the change in free energy accompanying the formation of a nucleus (denoted as W) is written as,

$$W = \int_v \left[\Delta f(c) + K(\nabla c)^2 \right] dv \tag{1}$$

where

$$\Delta f = f(c) - f(c_0) - (c - c_0)\left(\frac{\partial f}{\partial c}\right)_{c_0}$$

$f(c)$ is the free energy of one atom in the uniform solid solution of composition c, and K is the gradient energy coefficient. c_0 is the average composition in the matrix. Applying the variational principle, the composition profile corresponding to the critical nucleus can be obtained by solving the following Euler equation in spherical coordinates,

$$2K\frac{\partial^2 c}{\partial r^2} + \frac{4K}{r}\frac{\partial c}{\partial r} = \frac{\partial \Delta f}{\partial c} \tag{2}$$

with the boundary conditions,

$$\frac{\partial c}{\partial r} = 0 \text{ at } r = 0, \text{ and } \frac{\partial c}{\partial r} = 0 \text{ and } c = c_0 \text{ as } r \to \infty.$$

3. Results and discussion

In a regular solution, the gradient energy K is related to the critical temperature of the miscibility gap as $K = kT_c a^2/6$, where a is the lattice parameter, k is Boltzmann's constant, T_c is the critical temperature of the miscibility gap. In a sub-regular solution, K is expected to vary with the solute concentration. In Fig 1. the composition profile of a nucleus of bcc Cu precipitate was calculated at T_c = 2200℃ (determined from the solubility of Cu in α-Fe), 5830℃ (the critical temperature of the miscibility gap), and 2730℃ (roughly fitted to the observed nucleus composition). It is seen that the calculated critical radius of a Cu particle is much smaller than the observed particle radius (Table 1). From the concentration profile at 3930℃, the activation energy for nucleation W was calculated from eq.(1) at various alloy compositions, and the result is shown in Fig.2. It is seen that the non-classical theory gives a considerably smaller activation energy for nucleation compared to the classical theory. At c_0=0.014 the activation energy is equal to $W=2.8\times10^4$ J/mol and the steady state nucleation rate of Cu precipitates is calculated to be $J=1.5\times10^{18}$ nuclei/cm^{3}s. This is comparable with the observed particle number, though not only the particle radius, but also the particle density are likely to have changed during the prolonged holding. The Langer-Schwartz type analysis of the particle number and size during aging is in progress.

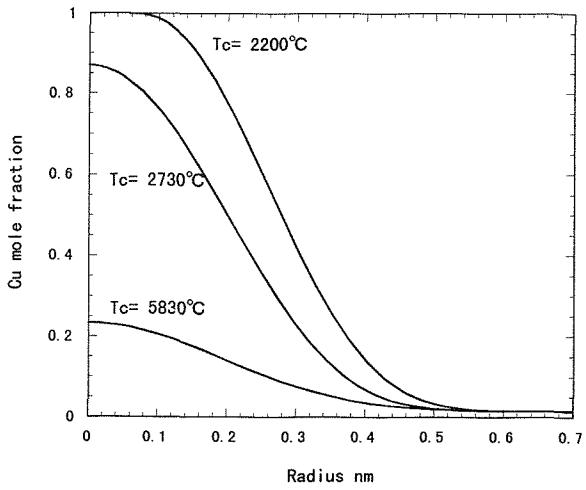

Fig.1. Calculated composition profiles of critical nucleus of Cu particle in an Fe-1.4at% Cu alloy obtained using non-classical nucleation theory. T = 773K.

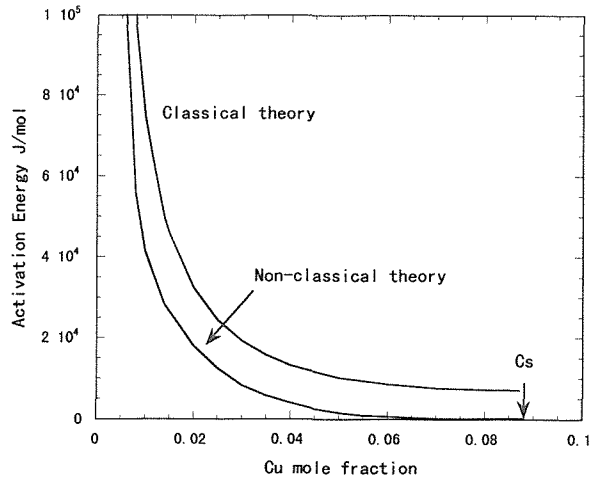

Fig. 2. Variation of the activation energy of nucleation with the bulk alloy composition, C_s is the spinodal composition.

Reference

[1] , Goodman S R, Brenner S S, Low J R, An FIM-Atom probe study of the precipitation of Copper from iron-1.4 at.pct Copper. part II Atom Probe Analyses. Metallurgical Transactions 1973;4;2371-2378.

[2], Worrall GM, Buswell JT, English CA, Hetherington MG, Smith GDW, A study of the precipitation of copper particles in a Ferrite matrix. J. Nucl. Mater. 1987;148;107-114.

[3],Cahn JW and Hilliard JE, Free energy of a nonuniform system III, Journal of Chemical physics, 1959,31,688-699.

[4] , Goodman S R, Brenner S S, Low J R, An FIM-Atom probe study of the precipitation of Copper from iron-1.4 at.pct Copper. part I Field-Ion Microscopy. Metallurgical Transactions 1973;4;2363-2369.

Structural Control of Steels through Phase Transformations in High Magnetic Field

H. Ohtsuka and H. Wada
Strong Magnetic Field Research Group, NIMS, Japan

1. Introduction

Magnetic field is expected to affect the alignment of product phase and transformed structure per se during solid/solid phase transformations and then affect the mechanical properties or some functions of materials. Therefore magnetic field is considered to be promising for structural or functional control of materials. Steels are very hopeful for such control of materials by magnetic field because steels have various kinds of solid/solid phase transformations and therefore various structures. It is expected that the nucleation and growth rates, transformation kinetics, transformed structure and variants are affected by magnetic field in these transformations since the magnetic moment of parent and product phases are different, and also due to the magnetocrystalline anisotropy, shape magnetic anisotropy, induced magnetic anisotropy and magnetostriction. So far, we have been investigating the effects of magnetic field on recrystallization, austenite to ferrite transformation, pearlite transformation, martensitic transformation, dynamic aging or processing of ceramics [1,2]. In this study, the effects of magnetic field on diffusional transformations are reported.

2. Experimental

The alloys used in the present study were an Fe-1.5Mn-0.1C-0.05 Nb (mass%) (Nb alloy hereafter) and an Fe-0.4C alloy prepared by vacuum induction melting. After homogenization specimens were machined 5x5x1 mm, and heat treated in vacuum by the furnace installed in the He-free type superconducting magnet whose bore size is 100 mm ϕ. Specimens were heat treated in the center of magnetic field and magnetic force applied to the specimen can be neglected. The surface parallel to the direction of applied magnetic field was observed by optical microscope.

3. Results and Discussion

Austenite to ferrite transformation is remarkably accelerated by high magnetic field. The reason for this enhancement of austenite to ferrite transformation by magnetic field can be classified into the following three factors, (1) increase of nucleation rate of ferrite, (2) increase of growth rate of ferrite and (3) decrease of austenite grain size. As a result, nucleation rate of ferrite is increased from several times to more than ten times larger by magnetic field of 10T, but the effects of magnetic field on growth rate of ferrite is not so remarkable. The austenite grain size is smaller in magnetic field. Among these three factors, the increase of nucleation rate of ferrite is the dominant factor for the acceleration of austenite to ferrite transformation. It is also observed that magnetic field of 10 T stimulates isothermal pearlite transformation significantly. This acceleration is due to the increase of driving force since the transformation temperature for ferrite is increased by

magnetic field.

No structural alignment of ferrite grains are observed for austenite to ferrite isothermal transformation in Nb alloy in magnetic field. However, alignment of transformed grains in high magnetic field are observed both for austenite to ferrite transformation and lath martensite to austenite reverse transformation[3] in an Fe-0.4C alloy. Figure 1 is the optical micrograph showing the effects of magnetic field on the alignment of ferrite grains in Fe-0.4C alloy. The specimens were solution treated at 1223 K for 0.9 ks, and rapidly cooled to 1123 K, and slowly cooled to 973 K at the cooling rate of 2 K/min and rapidly cooled again to room temperature with magnetic field of 10T. It is clearly observed that each ferrite grain is elongated and these grains are distributed head to tail along the direction of applied magnetic field. The conditions for the alignment of ferrite grains are (1) austenite grain size is relatively small and (2) cooling rate is relatively small, for austenite to ferrite transformation.

The conditions for the alignment of product phase in lath martensite to austenite reverse transformation were also studied. An Fe-0.4C alloy was solution treated at 1173 K for 15 min and water-quenched without magnetic field, which produces the lath martensite single phase structure. Then this specimen was reheated to 1023 K (ferrite and austenite two phase region) with or without magnetic field and held for 20 min and then rapidly cooled to room temperature by He gas. In this heat treatment, austenite is formed by the reverse transformation and then transformed to lath martensite again during the cooling to room temperature, making the final structure of ferrite and lath martensite. Without magnetic field, equiaxed ferrite grains are formed and both ferrite and lath martensite are distributed homogeneously. With magnetic field, lath martensite, that is, austenite grains in the two phase region, and ferrite grains are aligned along the direction of magnetic field. On the contrary, neither martensite nor ferrite phases are aligned along the direction of magnetic field when the solution treatment temperature is rather high such as 1423 K, that is, the prior austenite grain size is rather large. Austenite is not necessarily aligned along the direction of magnetic field, and formed along the packet or block boundaries. No alignment was observed either when the reheating temperature is relatively high. The conditions for the alignment of product phase in the reverse transformation are (1) prior austenite grain size is relatively small and (2) reheating temperature is relatively low.

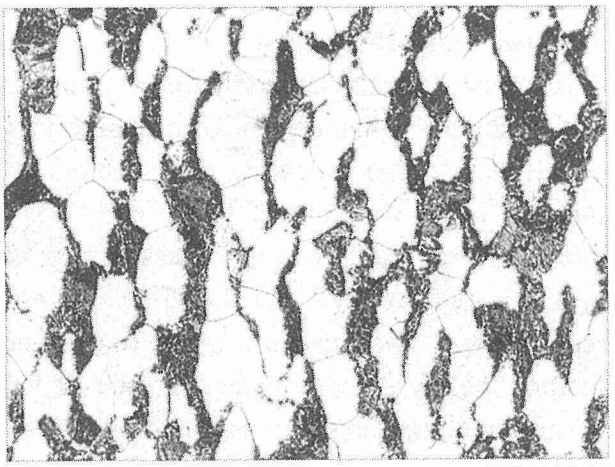

Fig.1 Optical micrographs showing the effects of magnetic field on the alignment o ferrite grains.

References

[1] Ohtsuka, H and Xu, Y, Ferrum (The Bulletin of the Iron and Steel Institute of Japan), **5** (2000), pp.9-16.

[2] Ohtsuka, H, Materia Japan、**40** (2001), pp.552-555.

[3] Shimotomai, M and Maruta, K, Scripta Materialia, **42** (2000), pp.499-503.

Influence of Refinement Processing on the Microstructure and Mechanical Properties of HSLA Plate Steel

C. J. Shang, S. W. Yang, X. L. He, X. M. Wang
Department of Materials physics, University of Science and Technology Beijing
Beijing , 100083, China

1.Inroduction

TMCP generally is recognized as a good choice to develop HSLA steel to meet less micro-alloy addition, low cost, save energy and obtain high strength and toughness. Besides, refinement the microstructure is one of the basic methods to improve the mechanical performance. New developing relaxation-precipitation-control phase transformation(RPC) technique[1] is an efficient process to refine the intermediate transformation structure. The technique includes micro-alloying design, two stages control rolling, relaxing and accelerated cooling/direct quenching. The strength of fine bainitice lath like plate steel could be improved by 25-30% comparing with the same composition steel processed by re-quenched and tempered process[2]. The influences of relaxing time and other process parameters on the microstructure and the mechanical properties have been revealed. The microstructure characteristics and the evolution of the microstructure with the tempering process were also investigated.

2.Experimental

The target composition (mass%) of the steels is: 0.04C, 1.6Mn, 0.35Si, 0.05Nb, 0.04Ti, 0.4Cu, 0.25Ni, 0.0010B. The steels were melted by vacuum induction furnace and rolled following a special TMCP+RPC process as shown in Fig.1. After the finish rolling, the steel was relaxed for certain time and then direct quenched in water. The microstructure was revealed by optical microscope (OM), SEM and TEM. The mechanical properties were also measured.

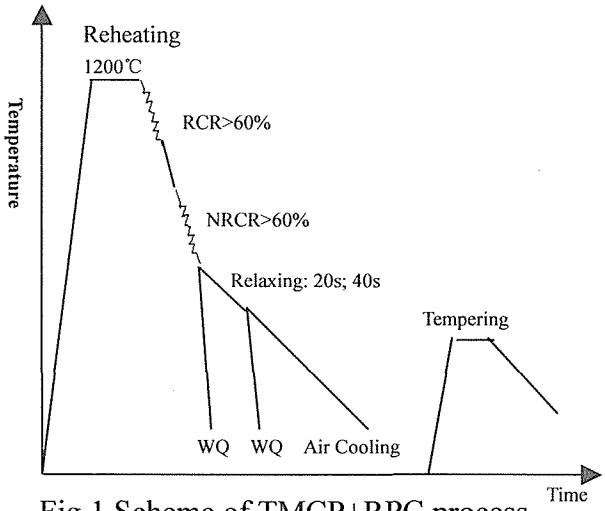

Fig.1 Scheme of TMCP+RPC process

3.Results

Fig. 2 shows the microstructures that following different TMCP. The microstructure of steel that relaxed for a certain time after finish rolling and than direct quenched in water is shown in Fig2(a), it is shown that in a pancake like prior-austenite grain, there are lots of lath like structures, the width of the lath is less than 1μm and the length is about 5-8μm, some laths(about 3-7laths) which align in the same direction form a packet and the width of packet size is about several microns. Fig. 2(b) shows the microstructure that cooled in air after finish rolling, the prior-austanite is flattening, the main structures are granular bainite and there is no lath like structure as shown in Fig.2 (a).

The yield strength of the steels that following relaxation process could be improved to more than 800MPa(as shown in Fig.3) and the strength was influenced by relaxation time. Fig. 4 shows that the hardness influenced by relaxing process too and the tempering phenomenon shows that the precipitation and microstructure recovery are complicated in this kind of steel. The microstructures after tempering are shown in Fig.5. It can be seen that after tempering even as high as at 700℃, the lath like microstructure was not completely recovery. The packet size was not bigger markedly after tempering.

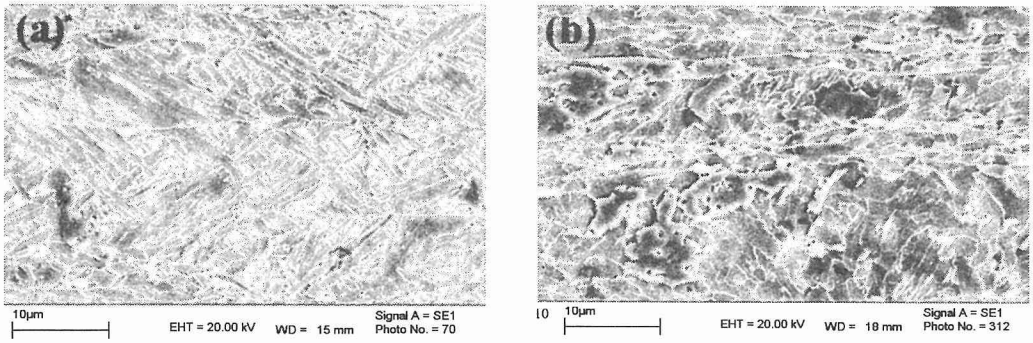

Fig. 2 The micrographs (SEM) of relaxing for 20s and direct quenched steel (a) and air cooled steel (b) after finish rolling

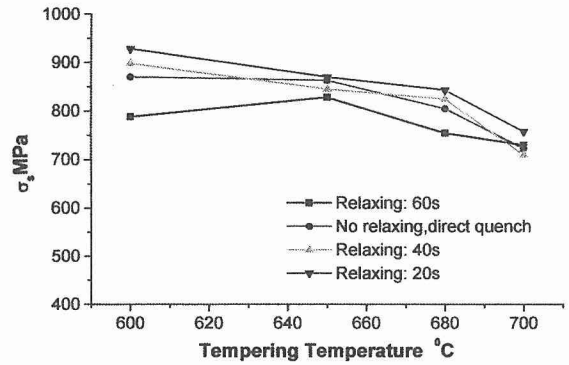

Fig.3 σ_s influenced by relaxation time

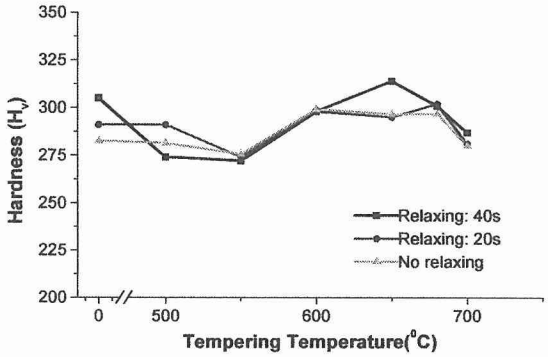

Fig.4 Hardness vs. tempering temperature

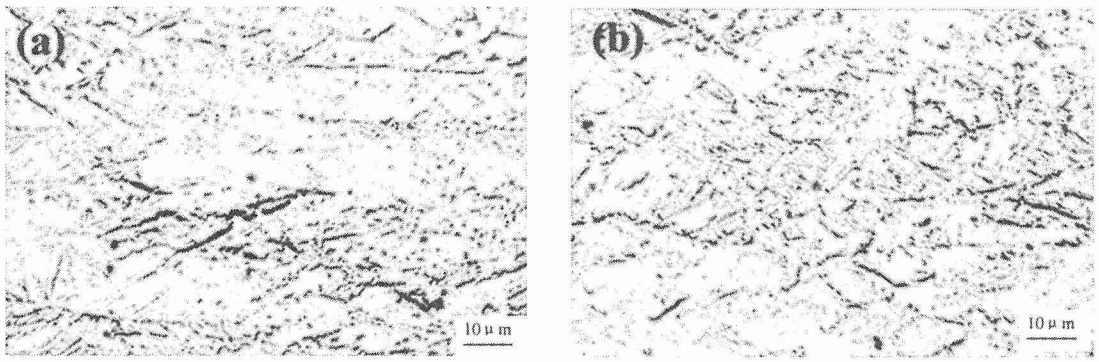

Fig. 5 Microstructures (OM) after tempering at 600℃ for1h (a) and at 700℃ for 1h (b).

4.Conclusions

The relaxation process after finish rolling could refine the inter-mediate transformation structure, the packets could be refined to several microns. The yield strength could be improved markedly by RPC process.

5.References

[1] C. Shang, S. Yang, X. Wang, Y. Yuan, and X. He: A new 800MPa grade ultra-fine composite microstructure HSLA plate steel, G.Liu and F. Wang et al. edited, HSLA steels'2000, Beijing:Metallurgical industry press,2000,304-309.

[2]C. Shang, S. Yang, Y. Yuan and X. He: The Structure and Properties of 800MPa grade HSLA Steel after treatment by RPC technique, T. Chandra, K. Higashi, C. Suryanarayana and C. Tome edited, THERMEC'2000, LasVegas, Dec 4-8, CD-ROM issue, J. of Materials Processing Technology, 2001

THE FORMATION OF ULTRA-FINE GRAIN STRUCTUREIN PLAIN CARBON STEEL

YANG Zhongmi WANG Ruizheng CHE Yanmin CHEN Qian
Central Iron & Steel Research Institute, Beijing 100081;

In last decade or so, in order to effectively improve the strength and toughness of steels, the researches on achieving ultra-fine grain structure in steel were carried out. An emphasis was put on the obtain of ultra-fine ferrite grains finer than 3μm for C-Mn steel[1~4].

The purpose of this paper is to study the processing technology and the mechanism of obtaining ultra-fine grain structure fining down to 4~5μm and microstructure constitution is ferrite(F)+pearlite(P) in the conventional low carbon steel (type Q235). By means of refining ferrite grains to 4~5 μm, the YS of Q235 steel is increased up to 400MPa level.

EXPERIMENTS

The chemical composition of plain carbon steel Q235 is shown in Table1. The size of specimens is Φ10 ×12 mm for simulating compression test at Gleeble2000. The grain size of the specimens after normalization is around 25 μm.

The temperature region of 900~600 ℃, the reduction region of 20~90% and strain rate region of 30~350 s^{-1} were selected to study the influence of processing parameters on the ferrite grains size. The experimental conditions are as follows: reheated at 900 ℃ for 2 min and followed by cooling at 10℃/s to test temperature. After deformation specimen was water quenched on the Gleeble2000.

The austenite to ferrite transformation start temperature (A_{r3}), the stop transformation temperature (A_{r1}), the eutectoid temperature of pearlite (T_s) and equilibrium temperature (A_{e3}) of steel Q235 are 780 ℃, 600 ℃, 700 ℃ and 840 ℃ respectively. The equilibrium temperature was calculated by using program Thermo-Calc, and others were measured on Gleeble 2000.

The testing results were applied on the modern continuous rod mill and produced rebars of diameter size Φ12mm and Φ20mm. The YS of rebar is achieved 400MPa level.

Table 1. Chemical composition of experimental steel.

C	Si	Mn	P	S	Al	Ti	O	N
0.18	0.21	0.60	0.016	0.020	0.0082	<0.005	0.017	0.0059

RESULTS AND DISCUSSION

Through DIFT obtained ferrite grains grow very rapidly, and during deformation the DRX of ferrite is occurred see Fig.1B. Fig.1 shows microstructure change with increase of reduction.

Fig.1A shows start of DIFT, Fig.1B shows that DRX of deformation induced ferrite no take place, Fig.1B shows DRX of deformationg induced ferrite occurs. Therefore with increase of reduction the fraction volume of ferrite increases and its grain size decreases. At the same time, the morphology of DIF also changes. Dynamic recrystallization of ferrite does not occur when amount of deformation is less than 40%.

In this case, uniformity of ferrite can be obtained by DRX of ferrite during deformation.

Fig.2 shows that 90%~95% ultra-fine ferrite of size 2-3 μm is obtained, when single pass deformation between 870~760 ℃ with reduction 80%.

The experiment of low temperature rolling of ribbed steel bars was carried out on the modern continuos bar rolling mill by means of decreasing starting rolling temperature and control cooling between stands. Water cooling after rolling was applied to control grain size. The ultra-fine grain structure can be obtained when rolling in 950-800℃ region. It is proved that the YS of the ribbed steel bar can reach 400MPa or more when the ferrite grain size is reduced to 4.5~6 μ m, see Fig.3.

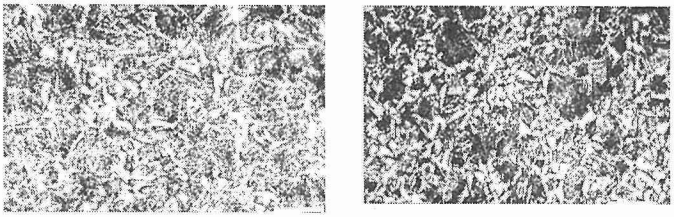

A. Reduction 40% B. Reduction 50%

Fig.1 The microstructures with different deformation at strain rate 30 S^{-1} and followed water quenching。

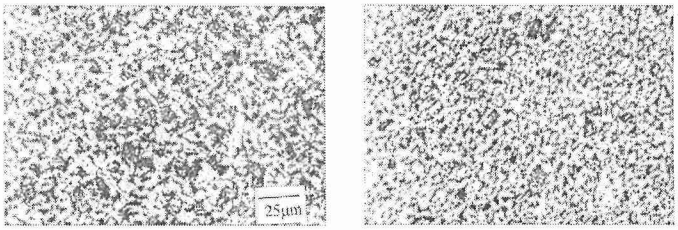

A Temperature 870℃ B Temperature 760℃

Fig.2. The microstructures at different temperature, deformation with 80% at strain rate 30 S^{-1} and followed water quenching。

CONCLUSIONS

Ultra-fine grain for the plain carbon steel (typeQ235) can be obtained by controlling deformation parameters. The result is regarded as the joint effects of both mechanisms of DIFT and DRX of ferrite.

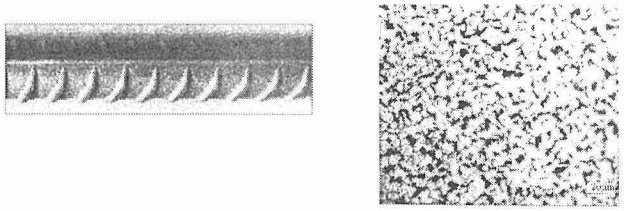

Fig.3 400MPa level (type Q235)

Under condition of hole-type rolling, Q235's ferrite grain size can be refined to 4.5~6μm and yield strength reaches to 400MPa by means of large amounts of accumulative deformation in the temperature range of A_{e3}~ A_{r3} and accelerated cooling after rolling.

REFERENCE

[1] Yada H, Matsumura Y, Proc, Int, Conf, Physical Metallurgy of Thermomechanical Processing of Steel and Other Materials; Tokyo, ed, Tamura I, Iron and Steel Institute of Japan, 1988: 200

[2]牧 正志 铁と钢, 81, 1995; 11: 547

Maki T, Tetsu to Hagane, 81, 1995; 11: 547

[3] Mintz B, Abu-Shosha R, Shaker M, Mate Sci and Technol, 1993; 9: 907

[4] Z.M.Yang, Y.Zhao, R. Z.Wang, Y. M.Chen, et al.: Acta Metallurgica Sinica, 8(2000), 818

Mechanism of Nano-Crystal Formation by Large Plastic Deformation

N. Tsuji

Department of Adaptive Machine Systems, Graduate School of Engineering,
Osaka University, Japan

1. Introduction

It has been already well-known that severe plastic deformation (SPD) of metallic materials can produce submicrometer- or nanometer-sized ultrafine grains (UFGs) [1,2]. However, the formation mechanism of the UFGs during SPD is still unclear. The present paper aims to discuss the formation mechanism of the UFGs.

2. Major Issues on Formation Mechanism of UFG

Fine grained structures have been conventionally obtained by recrystallization during annealing of deformed materials. In case of SPD, however, clear UFGs are sometimes observed in the specimens as-deformed without annealing [3]. Further, the UFGs obtained by SPD often have the morphologies similar to the deformed microstructures; that is, elongated grain shapes and dislocation substructures inside [4,5]. Is the formation mechanism of the UFGs in SPD different from conventional recrystallization ?

3. Experimental Procedures and Results

The author developed a novel SPD process applicable to continuous production of large bulky materials with his colleagues in 1998; Accumulative Roll-Bonding (ARB) [6]. An IF steel and plain low-C steel sheets were strained up to various strains ranging from 0.8 to 5.6 at 500°C and RT by ARB. The microstructural and misorientation evolution during straining was studied in details by means of TEM observations with Kikuchi-line analysis [4,7]. The observations clarified that the initial grains are finely subdivided by deformation induced boundaries with high-angle misorientations. The number of the deformation induced high-angle boundaries, in other words, the finely subdivided regions surrounded by high-angle boundaries, increases with increasing strain, and finally the microstructure in the specimen was subdivided in sub-micrometer sizes uniformly. As a result, the pancake-shaped UFGs appeared in the IF steel highly strained at 500°C. On the other hand, clear UFGs were not observed in the specimens ARB processed at RT. The UFGs with clear grain boundaries appeared only after annealing at warm temperatures, which indicates that recovery is necessary to form clear UFGs (or clear grain boundaries). The details of the experimental results will be shown in the presentation. After these results, it could be concluded that ultrafine grain-subdivision by SPD and recovery to form clear grain boundaries are the essential process of the UFG formation. This process could be called either *in-situ recrystallization* [7] or *continuous recrystallization* [8]. The whole mechanism and microstructural changes are schematically illustrated in **Fig.1**. Since the UFGs form only by recovery, clear UFGs could be observed in the as-SPD state without annealing in case of the materials with lower melting point, such as aluminum [3]

Acknowledgments

The present idea about formation mechanism is a fruit of the discussion with Professors T.Maki (Kyoto Univ.), T.Sakai (Univ. Electrocommunication), M.Umemoto (Toyohashi Inst. Tech.), K.Ameyama (Ritsumeikan Univ.) and T.Furuhara (Kyoto Univ.) in ISUGS conference at Fukuoka in 2001. The author expresses best thanks to them as well as his colleagues in Osaka Univ.

References

[1] Shaw, L.L. : J. of Metals, **52** (2001), pp.43-53.

[2] Tsuji, N. : to be published in *Tetsu-to-Hagane*, **88** (2002), No.7.
[3] Iwahashi, Y., Horita, Z., Nemoto, M. and Langdon, T.G. : Acta Mater., **45** (1997), pp.4733-4741.
[4] Tsuji, N., Ueji, R. and Saito, Y. : Materia Japan, **39** (2000), p.961.
[5] Tsuji, N., Ueji, R. and Minamino, Y. : to be published in Scripta Mater., (2002).
[6] Saito, Y., Utsunomiya, H., Tsuji, N. and Sakai, T. : Acta Mater., **47** (1999), pp.579-583.
[7] Tsuji, N., Ueji, R., Ito, Y. and Saito, Y. : Proc. of the 21st RISØ Int. Symp. on Mater. Sci., RISØ National Lab., Denmark, (2000), pp.607-616.
[8] Belyakov, A., Sakai, T., Miura, H. and Tsuzaki, K. : Phil. Mag. A, **81** (2001), pp.2629-2643.

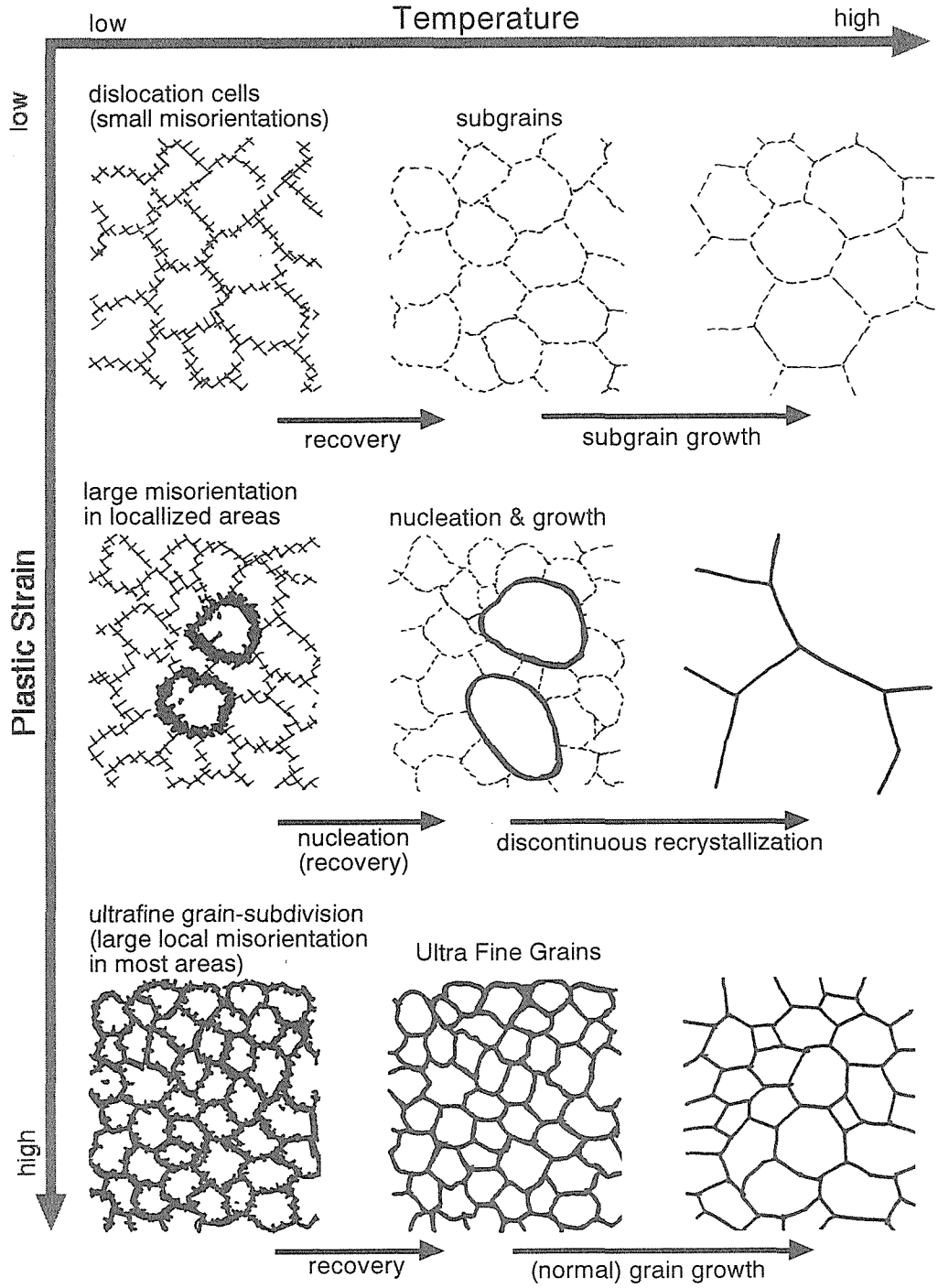

Fig.1 Schematic illustration showing the microstructural evolution in plastic deformation and annealing.

Fine-grained Structures Developed along Grain Boundaries in a Cold-rolled Austenitic Stainless Steel

T. Morikawa[1], K. Higashida[1] and T. Sato[2]
[1]Department of Materials Science and Engineering, Kyushu University,
[2]Present address : HINODE Co., Inc. Japan

1. Introduction

Plastic deformation in crystalline materials is intrinsically inhomogeneous. Particularly, in the vicinity of grain boundaries(GBs) of polycrystalline materials, the inhomogeneity is enhanced by the constraint that the displacement across GBs must be matched. Such inhomogeneous deformation near GBs causes a local crystal rotation being different from that of the inner part of grains, which is known to be essential not only for the development of macroscopic deformation texture but also for the occurrence of the nucleation sites of recrystallization and phase transformation.

In our previous works[1][2], it has been shown that shear bands(SBs) have an important role in the microstructual evolution in 310S steel: when they are cold-rolled, dense twin-matrix(T-M) lamellae develop, and then the lamellae are destroyed by the multiplication of SBs to evolve a fine-grained structure. These features are very similar to those observed in fcc alloys with low stacking fault energy.

In the present study, in addition to those features previously reported, we have found a characteristic fine-grained structure newly formed around initial GBs in cold-rolled 310 steels. This indicates that not only SBs but also GBs must contribute to the evolution of fine-grained structures. However, the effects of GBs on the microstructural evolution in cold-rolling have not been fully clarified. In this paper, therefore, we will report the characteristics of this fine-grained structure found near the initial GBs in cold-rolled 310S steels.

2. Experimental procedure

Polycrystalline plates (initial thickness:12mm, average grain size:100μm) of 310S steel were rolled by the reduction of 70% in thickness at room temperature. TEM samples were prepared by ordinary twin-jet technique. The foil surface of specimen was parallel to the longitudinal plane. The TEM observations were carried out with JEM-200CX operated at 200kV in the HVEM laboratory at Kyushu University.

3. Results and Discussion

Figure 1(a) shows a microstructure observed in the longitudinal section, which includes a GB nearly parallel to the rolling direction(RD). We can see SBs inclined by 30-40 degrees to RD. Their directions are indicated by the white arrows. Fine lamellar structures are also visible in the region between SBs. The lamellar boundaries in the upper region in Fig.1(a) are almost parallel to the RD. On the other hand, those in the lower region are inclined about 15 degrees to RD. In the middle of Fig.1(a), a band-like structure (width: around 5 μm) is lying almost horizontally. SAD patterns obtained from the areas indicated by the circles in Fig.1(a) are shown in Figs. 1(b)-1(d). As shown in Fig.1(b), the SAD pattern from the upper lamellar region exhibits the superposition of a couple of <011> diffraction patterns of twin and matrix(T-M), indicating that the lamellar structure observed here consists of alternate stacks of twin and matrix thin layers. On the other hand, the SAD from the lower area of the horizontal band (Fig.1(d)) exhibits a pattern whose incident beam direction is not <011> but near <112>. This suggests that the horizontal band observed here corresponds to the region of the initial GB, although no contrast such as a obvious boundary is observed there. Fig. 1(c) shows the SAD pattern obtained from the horizontal band. Here, Debye arcs are clearly seen, indicating that the horizontal band-like structure consists of highly misoriented regions.

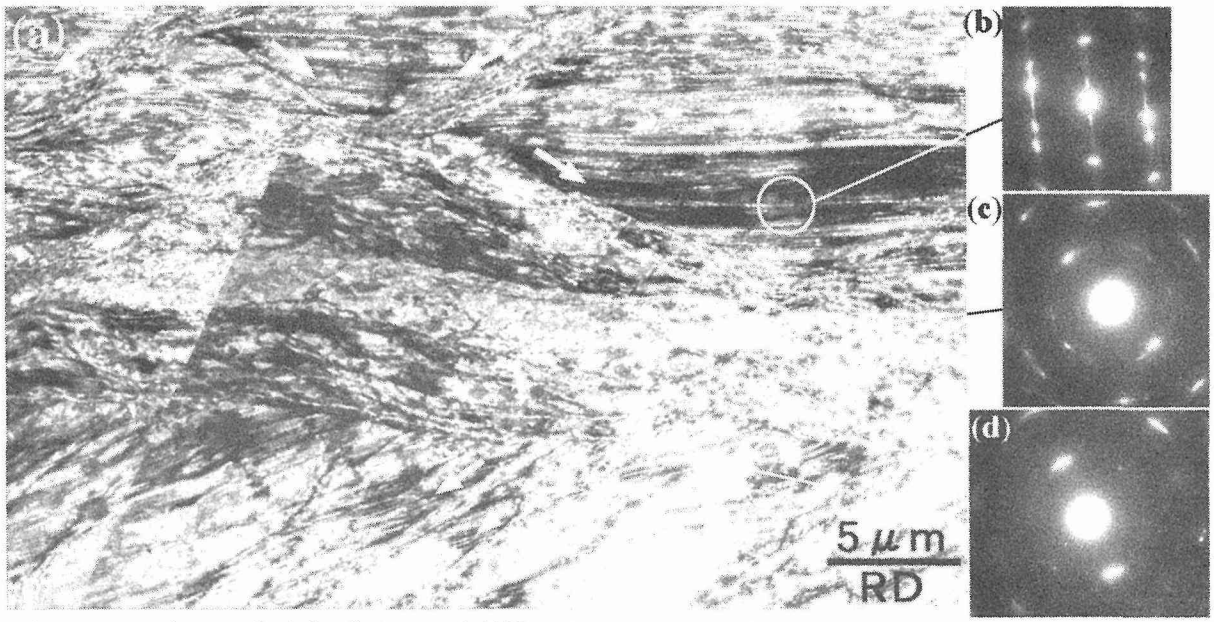

Fig.1 TEM image(bright field) and diffraction patterns of microstructures observed in longitudinal section at 70% reduction.

Considering that SBs are constructed by the aggregation of submicron-sized grains as shown in our previous study[2], these suggest that a fine-grained structure develops also in the band-like structure. In order to confirm this, we observed the band-like structure with higher magnification.

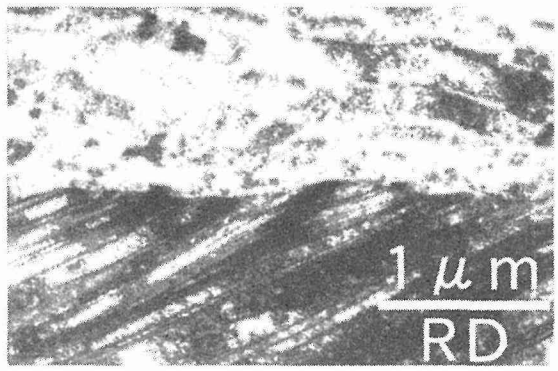

Fig.2 Enlarged TEM image of T-M lamellae(lower part) and a fine-grained structure developed along a grain boundary(upper part).

Figure 2 shows the enlarged image of the band structure. In the upper part of this figure we can see a fine-grained structure which is not equiaxed but somewhat elongated along RD. The width and length of each grain are 0.1-0.5μm and 1-2μm, respectively. Comparing those grain sizes with the spacing of T-M lamellar observed in the lower part of Fig.2, the size of the fine grains in the band structure was larger than the lamella spacing. Similar feature was observed around the border of SBs and T-M lamellae, suggesting that the collapse of T-M lamellae and one kind of grain growth occurs during the formation of fine-grained structure along GBs.

It is to be noted that such fine-grained structures were preferentially formed at the intersection of GBs with SBs(see Fig.1(a)), and they developed along the GB lying nearly parallel to rolling plane. These results suggest that the intensive shear deformation in SBs causes a stress concentration at the intersection of SBs and GBs, which highly promotes the destruction of T-M lamellae and evolution of the fine-grained structure.

References

[1]Morikawa, T., Senba, D., Higashida, K. and Onodera, R., Materials Transactions, JIM, 40(1999), No.9, pp.795-798.

[2]Morikawa, T. and Higashida, K., Proc. of the 21st Riso International Symposium on Material Science, (2000), pp467-472.

Microstructures and Tensile Properties of Ultrafine Grained Low Carbon Steels Processed by Equal Channel Angular Pressing

K.-T. Park[1], S.Y. Chang[2] and D.H. Shin[3]

[1]Division of Advanced Materials Science and Engineering, Hanbat National University, Taejon 305-719, Korea
[2]Department of Materials Engineering, Hankuk Aviation University, Koyang, Kyunggi-Do 412-791, Korea
[3]Department of Metallurgy and Materials Science, Hanyang University, Ansan, Kyunggi-Do 425-791, Korea

1. Introduction

Recently, equal channel angular pressing (ECAP) has been used as the most preferred method for producing porosity-free, ultrafine grained (UFG) metallic materials showing the superior mechanical and physical properties [1]. For a practical point of view, commercial low carbon steels processed by ECAP have shown the strong potential for the industrial application. This study was aimed at providing the guiding information for the practical use of the UFG low carbon steels manufactured by ECAP. For this purpose, particular focus was made on the effects of pressing strain and vanadium addition on the microstructural stability and tensile properties of the ECAPed steels.

2. Experimental Procedure

Two grades of low carbon steels, Fe-0.15C-0.25Si-1.1Mn (CS steel) and Fe-0.15C-0.25Si-1.1Mn-0.06V-0.0076N (CSV steel) (in wt.%), which were austenitized at 1473 K for 1 h, were used as starting materials. The CSV steel was normalized by soaking at 1223 K for 1 h before ECAP. ECAP was performed on the cylindrical samples of ϕ 18 mm × 130 mm at 623 K by utilizing a die designed to yield an effective strain of ~1 per a single pass with the rotation of the sample by 180° around its longitudinal axis between passages, i.e. route C. Annealing was conducted for 1 h in the temperature range of 693 K ~ 873 K. Tensile tests were performed using an Instron machine with the initial strain rate of 1.33×10^{-3} s^{-1} on the specimens of the gage length of 25.4 mm at R.T. The microstructure was observed by TEM.

3. Results and Discussion

The ferrite grain size after 4 passes ECAP, 0.2~0.3 μm, was nearly the same in both steels despite the different initial ferrite grain sizes of ~30 μm and ~10 μm for the CS and CSV steels, respectively. In addition, their microstructure showed the ill-defined grain boundaries, extensive extinction contour near grain boundary, and dense dislocation debris inside grain [2]. It was also evident that the misorientation angles of grain boundaries increased with increasing the ECAP strain. For the CS steel, by 753 K annealing, the dislocation density in the 4 passes ECAPed sample was low due to recovery but high dislocation density remained in the 8 passes ECAPed sample. At 813 K, abnormal grain growth occurred in the former but it did not occur in the latter. This result is contrary to the general observation that more severely worked materials exhibit faster kinetics of the microstructural evolution related to annealing. Fig. 1 shows the nano-sized cementite particles precipitated at the unrecrystallized UFG ferrite grain boundaries in the 8 passes ECAPed CS steel, resulting from the carbon dissolution from pearlitic cementite by severe plastic deformation and the precipitation of dissolved carbon atom during subsequent annealing. Consequently, this carbon dissolution would cause to the unusual annealing behavior of the UFG CS steel. It was of interest to note that high dislocation density and uniform UFG structure were preserved in the CSV steel annealed at 813 K, while the CS steel exhibited a typical recovered structure with a low

dislocation density and coarse recrystallized ferrite grains even at lower annealing temperature of 753 K. Accordingly, it is apparent that the addition of a small amount of V is effective for the enhancement of microstructural stability of ECAPed UFG low carbon steel against thermal exposure.

The strength of the CS steel annealed at 693 K was slightly lower than that of the as-ECAPed sample, and decreased rapidly with increasing annealing temperature. The loss of strength with increasing annealing temperature is attributed to two factors: the appearance of coarse recrystallized ferrite grains, and softening of the pearlite due to the spheroidization of pearlitic cementite. On the contrary, the strength of the CSV steel annealed at 693 K was higher than that of the as-ECAPed sample, probably due to the precipitation of very fine Fe_3C particles (Fig. 2). The strength of the CSV steel decreased gradually with increasing the annealing temperature. It was noted that the strength of the CSV steel annealed at 813 K was comparable to that of the CS steel annealed at 693 K (Fig. 3). This extension of the mechanical stability in the CSV steel to higher temperatures resulted mainly from the preservation of a homogeneous UFG structure at these temperatures. The CSV steel revealed smaller elongation than the CS steel above 813 K, which would result from its higher strength.

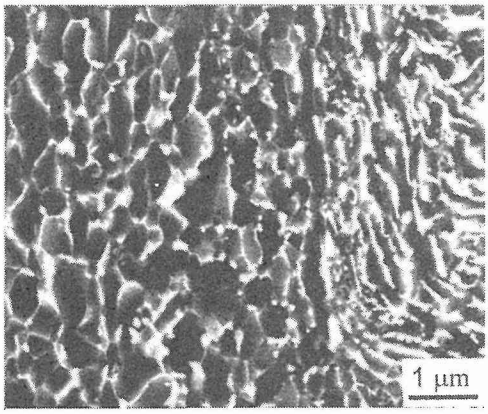

Fig.1 Nano-sized Fe_3C particles precipitated at grain boundaries of UFG ferrite grains in the vicinity of pearlite colony

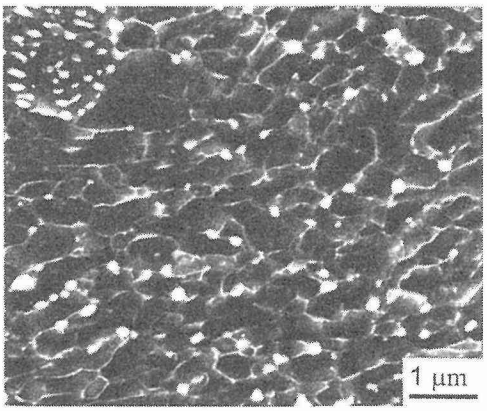

Fig.2 Nano-sized Fe_3C particles precipitated at UFG ferrite grain boundaries in the CSV steel annealed at 813K

4. Conclusions

ECAP was successfully applied to produce bulk UFG low carbon steels having ultrahigh strength. It was shown the high ECAP strain and the addition of vanadium were effective to enhance the microstructural stability without degrading the strength.

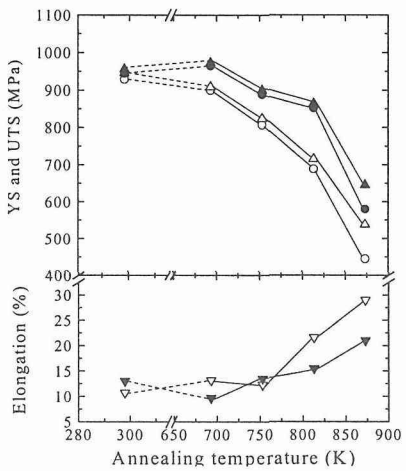

Fig. 3 Tensile properties of ECAPed CS and CSV steel as a function of annealing temperature.

References

[1] Valiev, R.Z., Islamgaliev, R.K. and Alexandrov, I.V., Prog. Mater. Sci., 45(2000), pp.103-189 .

[2] Shin, D.H., Kim, B.C., Kim, Y.–S. and Park, K.–T, Acta Metall. 48 (2000), pp. 2247-2255 .

PARTIALLY RECRYSTALLIZED STRUCTURES IN INTERSTITIAL FREE STEELS AFTER SEVERE ROLLING AND ULTRA-SHORT ANNEALING

A.C.C Reis[1], R. Petrov[1], W.J. Kaluba[2] and L. Kestens[1]

1-Ghent University, Department of Metallurgy and Materials Science,
Technologiepark 9, B-9052 Ghent, Belgium
Email: ana@metallur.rug.ac.be
2- Université du Littoral, Laboratoire Thermo Physique Matière Condensée,
Côte d'Opale, 62968 Longuenesse, France

In the past decade, several methods have been proposed in literature to obtain sub-micron or even nanocrystalline structures in Fe-based alloys. Ultra fine structures in ultra-low carbon steels (i.e. single phase ferritic structures) might offer an interesting ecological option to substitute higher alloyed high strength steels. Although there is some reports that grain refinement impairs the strain-hardening potential of these non-alloyed steels, their mechanical properties are not yet fully characterized and hence they remain an interesting object of study. Moreover, industrial steel-manufacturers generally prefer a thermo-mechanical degree of freedom over a chemical one. Bearing in mind this setting a Ti alloyed IF steel (0.0024%C and 0.044% Ti) was selected to carry out the present study on the effect of ultra short annealing treatments. By applying extreme high reheating rates on the cold rolled material it was intended to induce the α–γ transformation before the end of static recrystallization. This would operate as an instrumental grain refinement technique because it would produce a nucleation of the high temperature phase in the deformed ferrite and would automatically lead to a finer austenite structure, which would be additionally refined during the reverse transformation.

The samples were initially hot rolled and then cold rolled with a reduction of 95% ($\varepsilon = 3$). Cold rolled strips (20x80x1 mm) were submitted to an annealing treatment in which the samples were reheated to various temperatures between 600 and 1200°C, followed by a water quench. Three different reheating rates were applied of 300, 1000 and 3500°C/s, respectively. All of the samples were observed by standard metallographic methods, including optical microscopy, SEM and orientation imaging microscopy (OIM).

The results show a number of remarkable features which can be listed as follows:

i. The extreme high reheating rates have only increased the recrystallization temperature with approximately 100°C to 150°C, which was not enough to retard the recrystallization until the onset of the α–γ transformation, as also the Ac1 temperature is increased with increasing heating rate. Figs 1a and b show, as a representative example, the structures and textures for an annealing rate of 1000°C/s. In this example recrystallization started at ±690°C and was entirely completed at ±830°C, whereas Ac1 ≈ 980°C. In an additional ultra-fast annealing experiment on a steel with a typical TRIP composition (0.11%C, 1.26% Si and 1.53% Mn) it was proven that the recrystallization could be enough retarded until the start of the phase transformation. This is illustrated in Fig. 2 which shows concurrently the martensite phase (resulting from the water quench from the intercritical range) and remaining parts from the deformed ferrite structure.

ii. Even in an annealing treatment as short as 300 ms (corresponding to the reheating rate of 3000°C/s) the conventional deep drawing textures (with a strong {111} fibre texture) and microstructures (with an average grain size of ±15 μm) were observed. This shows that the recrystallization kinetics can be one order of magnitude faster than the conventional kinetics if the recrystallization temperature is increased with 100°C to 150°C. Probably this is due to the exponential dependence of the grain boundary mobility with the temperature.

iii. The structures observed after the forward and reverse α–γ–α transformation display an even larger grain size than the recrystallized structures and also show a strong memory effect from the recrystallization texture (cf. Fig. 1b). The grain coarsening was not expected, as a phase transformation is generally associated with grain refinement. In order to further investigate this strange phenomenon a similar experiment was carried out on an ELC steel (with 0.028% C) and the results of this experiment have shown that the C condition during phase transformation is of critical importance for the austenite nucleation and thus for the grain size characteristics of the final product.

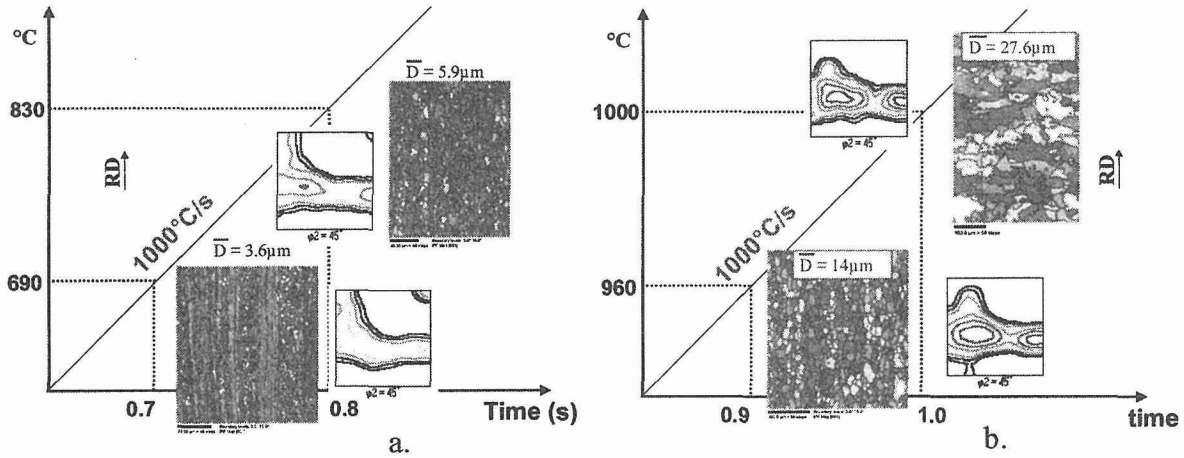

Fig. 1: Observed microstructures and textures in Ti IF steel submitted to an ultra short annealing treatment with a heating rate of 1000°C/s; (a) sample at the start and near the end of recrystallization; (b) fully recrystallized structure and after α–γ–α transformation.

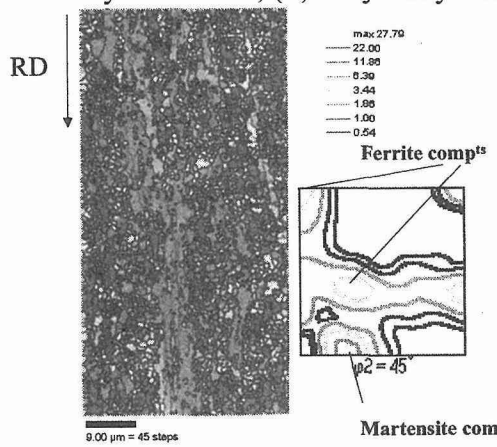

Fig. 2 : OIM scan observed on 83% cold rolled Si-Mn alloyed steel, after ultra fast annealing (with reheating rate of 3000°C/s) to 840°C and water quenching. The microstructure displays a mixture of deformed ferrite orientations and martensite grains which emerged after the quench from the intercritical regions.

In conclusion it can be stated that ultra-short annealing is not a useful grain refinement technique for interstitial free steel grades. In order to retard the recrystallization until the intercritical annealing range additional alloying elements are required. It was also proved that the double α–γ–α transformation only acts as a grain refining mechanism on condition that the austenite nucleation is homogeneously distributed throughout the structure.

Kinetics of Grain Refinement in a Stainless Steel by Large Strain Deformation

A. Belyakov[1]*, T. Sakai[2], H. Miura[2], and K. Tsuzaki[1]
[1)] Materials Creation Research Group, Materials Engineering Laboratory, National Institute for Materials Science, Tsukuba, Ibaraki 305-0047, Japan
[2)] Department of Mechanical Engineering and Intelligent Systems, University of Electro-Communications, Chofu, Tokyo 182-8585, Japan
*On leave from the Institute for Metals Superplasticity Problems, Ufa, Russia

1. Introduction

Recently, large strain plastic working at relatively low temperatures has been utilised as a novel processing method to develop ultra fine-grained structural metals and alloys with a grain size in a submicron scale. It has been shown that the new fine grain evolution results from a kind of continuous dynamic recrystallization [1]: namely, evolution of strain-induced subboundaries and a gradual rise of the misorientations, finally leading to the development of ultra fine grains with medium- to high-angle boundaries. The aim of the present work is to study the kinetics of grain refinement during severe deformation, and especially, the effect of initial microstructure on the evolution of strain-induced subboundaries.

2. Experimental Procedure

A 304 type austenitic stainless steel (0.058% C, 0.7% Si, 0.95% Mn, 0.029% P, 0.008% S, 8.35% Ni, 18.09% Cr, 0.15% Cu, 0.13% Mo and the balance Fe) was used as the samples for multiple compressions. Four sets of the specimens with different initial microstructures were used, i.e. annealed samples with a grain size of D_0 = 25 μm and 3.2 μm, and dynamically recrystallized ones with D_0 = 3.5 μm and 1.5 μm. The samples were machined into rectangles with a dimension of 1.5:1.22:1.0. The samples were deformed to a strain of 0.4 in each compression pass at 873 K under a strain rate of about 10^{-3} s^{-1}, while the loading direction was changed through 90° from pass to pass (that is x to y to z to x ...).

3. Results

The integrating flow curves (Fig. 1) are similar in appearance to those controlled by recovery. The flow stresses rapidly increase at an early deformation and approach a saturation value after third compression, leading to a steady-state-like flow at high cumulative strains. The yield stress for the D_0 = 1.5 μm samples is two times higher than that for the specimens with D_0 = 25 μm. Therefore, the strain hardening was smaller and the steady-state flow appeared at lower strains for the samples with smaller initial grain sizes, as can be seen in Fig.1.

The structural changes can be commonly characterised by the evolution of strain-induced subboundaries followed by the fine grain formation of 0.3 μm in grain size. However, the kinetics of grain refinement is strongly affected by the initial microstructure. At a strain of 1.6, the substructure composed by dense dislocation walls with medium-angle misorientations evolve in the D_0 = 25 μm samples (Fig. 2a), while a new fine-grained microstructure almost develop in the samples with $D_0 \leq 3.5$ μm (Fig. 2b). Increase in subboundary misorientations is greatly accelerated by decreasing the initial grain size (Fig. 3). The fraction of strain-induced high-angle grain boundaries rapidly increases to a typical value of dynamically recrystallized state in the samples with small initial grains, while that needs much more straining for the relatively coarse-grained initial microstructure (Fig. 4).

References

[1] Belyakov, A., Sakai, T., Miura, H. and Tsuzaki, K. Phil. Mag. A 81 (2001), pp. 2629-2643.

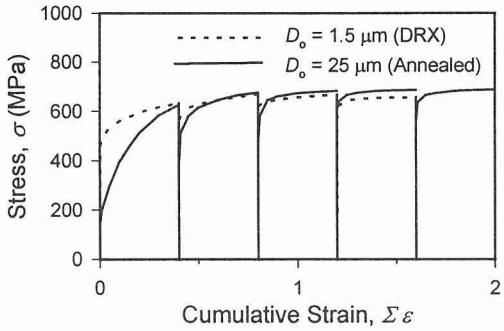

Fig. 1. Stress – strain curves for a 304 stainless steel with different initial grain sizes.

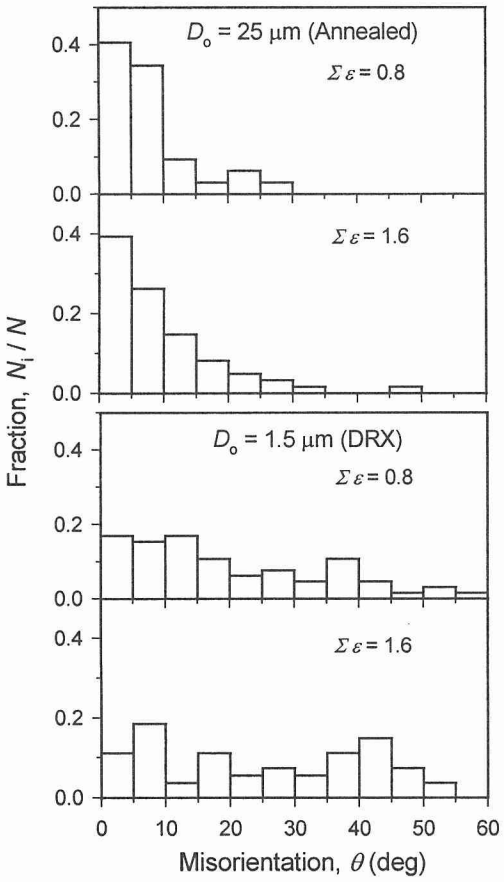

Fig. 3. (Sub)grain boundary misorientation distributions developed in a 304 stainless steel under warm multiple compressions. (a) D_o = 25 μm (annealed); (b) D_o = 1.5 μm (DRX).

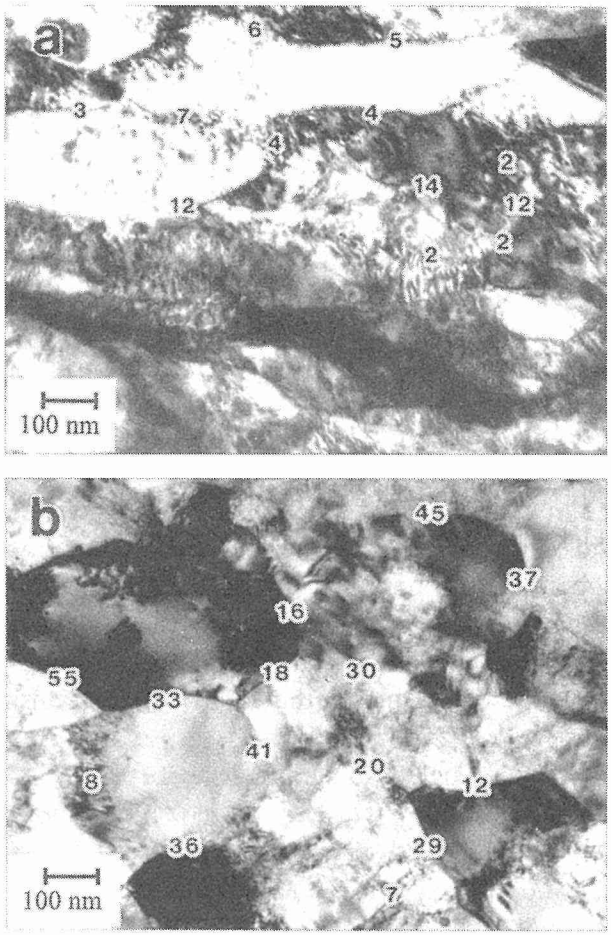

Fig. 2. Typical microstructures evolved in a 304 stainless steel after multiple compressions to a strain of 1.6. (a) D_o = 25 μm; (b) D_o = 1.5 μm.

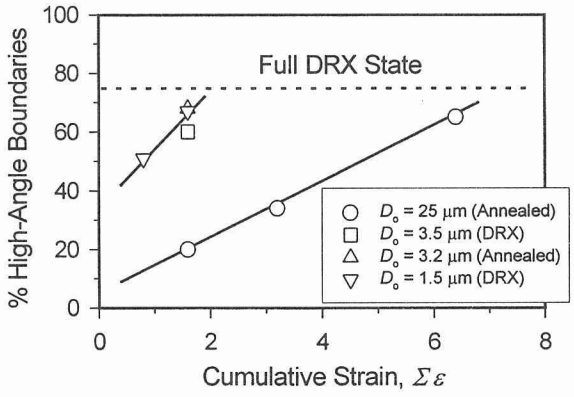

Fig. 4. Effect of initial grain size on the evolution of strain-induced grain boundaries in a 304 stainless steel.

Deformation Behavior of Ultrafine Grained Steels

S.Takaki
Department of Materials Science and Engineering, Kyushu University, Japan

1. Introduction

Ultra grain refining is a worldwide topic in the field of advanced structural steels nowadays. In Japan, we have been investigating the process to fabricate ultrafine grained steels with the grain size of 1μm or below and the mechanical properties of such ultrafine grained steels through the activity of national projects; Super Metal Project and Super Steel 21. So far, we have succeeded in the production of ultrafine grained steels with the grain size of around 1μm in a practical pilot line and the grain size of 0.2~0.3μm in a special powder metallurgy process which has been developed by author et al [1]. In this paper, deformation behavior in the temperature range from room temperature to 1200K is introduced for the ultrafine grained iron with the grain size of 0.2~1μm comparing with a usual large grain sized iron.

2. Deformation behavior at room temperature

Ultra grain refinement is very effective for increasing yield stress of iron and steel materials. So far, the grain refinement to 0.18 μm is achieved in a bulk iron material and yield stress is confirmed to follow the Hall-Petch law at least to around 0.2 μm [2]. However, it is sure that uniform elongation disappears in the ultrafine grained iron below 1μm due to the plastic deformation instability.

3. Possibility of grain boundary accommodation at room temperature

Mechanical milling (MM) to iron powder enable the ultimate grain refining to the nano-size level. Fig. 1. shows the relation between grain size and hardness in MM iron and powders. In the case of iron powder, grain refining was limited to about 25nm but it was possible to about 10nm for 0.8%C steel powder. This figure displays that the Hall-Petch relation is realized to around 0.1 μm and the data tends to deviate toward lower hardness side from the extended value. This is probably due to the contribution of grain boundary accommodation. Fig. 2. shows the relation between grain size and volume fraction (f) of grain boundary layer. Under

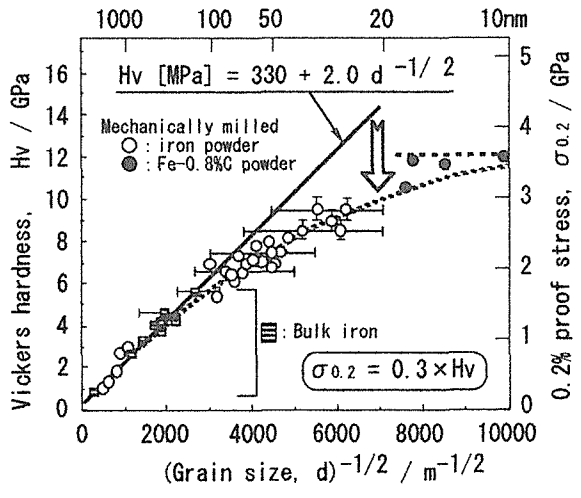

Fig. 1. Relation between grain size and hardness in iron and steel materials.

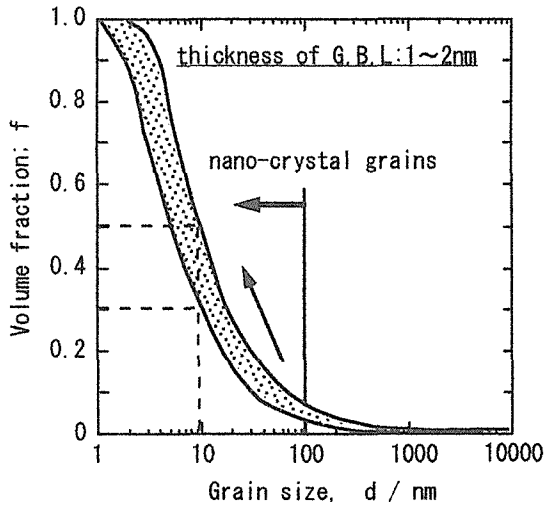

Fig. 2. Relation between grain size and the volume fraction of grain boundary layer (G.B.L).

the estimation of grain boundary thickness as 1~2nm, the value f is negligible small in the grain size above 1μm but greatly increases below 1μm, especially below 100nm. For instance, the material of grain size 10nm should be regarded as a dual-phase material of grain boundary layer and nano-crystal.

4. Grain boundary sliding at elevated temperatures in ultrafine grained iron

Fig. 3. shows temperature dependence of mechanical properties of ultrafine grained iron (0.3μm) in comparison with a usual polycrystalline iron (20μm). The fine grained iron has a high tensile strength (1.2GPa) at room temperature, but it abruptly drops above 500K and reaches to the small value above 800K, which is the almost same strength as the referential material. Fig. 4. displays the hardness at room temperature for the fine grained specimens tested for Fig. 3. as a function of testing temperature. It should be noted that hardness is kept at high value even in the specimens deformed at temperatures above 800K. The grain size was also confirmed to be around 0.3μm in the tested specimens. This means that grain boundary sliding works above 800K and grain boundary accommodation begins to contribute above 500K in the case of 0.3μm grain size. Tensile testing at 973K indicated that an inverse Hall-Petch relation appears in the grain size region above 0.6μm.

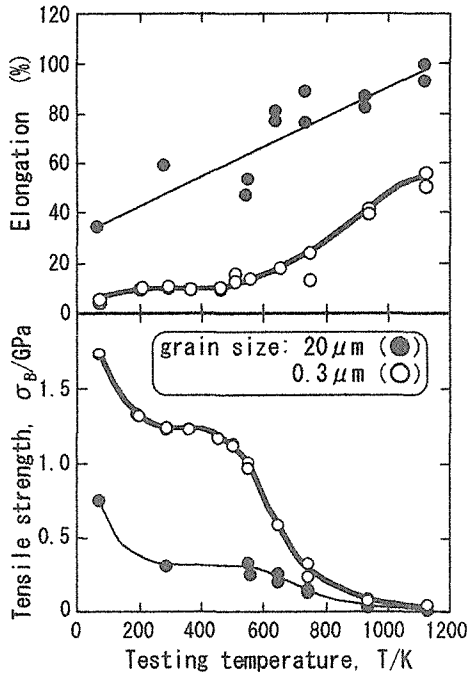

Fig. 3. Temperature dependence of mechanical properties of ultrafine grained iron.

5. Conclusion

Ultra grain refining below 1μm is probably not favorable for the mechanical properties at room temperature but an attractive subject in terms of low temperature superplastic deformation. So far, the appearance of grain boundary sliding was confirmed above 800K for the iron of 0.3μm grain size, although elongation was not so large probably due to the existence of dispersed oxide particles.

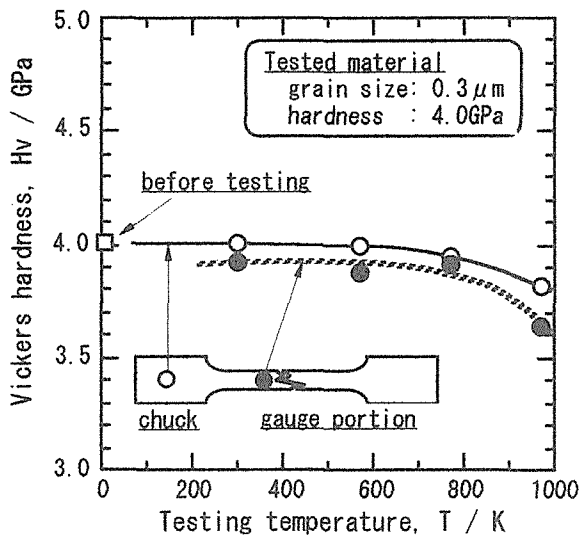

Fig. 4. Relation between tensile testing temperature and hardness at room temperature in tested specimens.

References

[1] S.Takaki: CAMP-ISIJ, 10 (1997), No.6, 1176-1178.

[2] S.Takaki, K.Kawasaki and Y.Kimura: Journal of Materials Processing Technology, 117(2001), 359-363.

High-Resolution TEM Analysis of Defect Structures in Mechanically Milled, Nanocrystalline Fe

J. M. Howe[1], M. Murayama[1]*, H. Hidaka[2] and S. Takaki[2]
[1]Department of Materials Science and Engineering, University of Virginia, USA
[2]Department of Materials Science and Engineering, University of Kyushu, Japan
*On leave from: National Institute for Materials Science, Japan

1. Introduction

Ultrafine-grained metallic materials have attracted considerable research interest because they tend to have high strength without sacrificing toughness and ductility. Factors that have been considered to account for this behavior include the grain size, grain boundary structure and internal defect structure. Gleiter [1] proposed that the structure of grain boundaries in ultrafine-grained material is different from that of conventional materials, although other investigators [2-4] showed that the structures are similar. Previous HRTEM observations revealed the presence of large local elastic strains in such materials [5,6], but characteristic defect structures were not reported. Recently, severe plastic deformation (SPD) has become a popular processing method to produce ultrafine-grained Fe and other materials [7,8]. The detailed mechanisms of grain refinement and grain-refinement strengthening during this process are not fully understood. The purpose of this study is to characterize the defect structures in ultrafine-grained Fe powder produced by SPD, i.e., by mechanical milling. HRTEM is particularly effective for characterizing these fine structures, since it can provide direct observation of the atomic arrangement in both the interior and grain-boundary regions of nanocrystalline materials.

2. Experimental

The procedure of making a mechanically milled pure Fe (MM-Fe) powder has been described in detail elsewhere [8]. In summary, a commercially pure Fe powder (Fe-0.007C-0.03Cr-0.04Si-0.24Mn (wt. %)) was mechanically milled together with stainless steel balls in a planetary ball mill up to 360ks under an Ar atmosphere. After this fabrication process, the Vickers hardness of the MM-Fe powder reached 850. TEM specimens were thinned from the as-milled Fe powder using a Gatan Model 600 Duo Ion-Mill with a liquid-nitrogen cold stage. HRTEM was performed in a JEOL JEM-4000EX microscope equipped with a UHP40H pole-piece and operating at 400kV.

3. Results and Discussion

Figure 1 shows a $<111>_{Fe}$ HRTEM image of a small grain in the MM-Fe powder, taken near Scherzer (-48.5nm) defocus. The presence of two wedge-shaped regions facing each other, as outlined by the three white lines in the figure, indicates the presence of a partial disclination dipole in the grain [9]. The partial disclinations appear to be wedge disclinations with a Frank vector $\boldsymbol{w}$ parallel to the defect line, which corresponds to the <111> viewing direction. Each partial disclination in the dipole consists of a number of terminating {110} planes, which are individual dislocations with a Burgers vector $\boldsymbol{b}=\boldsymbol{a}/2<111>$. The arrays of terminating {110} planes can also be considered terminating tilt grain boundaries [10,11]. Compared with complete tilt grain boundaries, terminating tilt grain boundaries contain missing dislocations, and these are replaced by rotational elastic deformation in the crystal [12]. The crystal rotation produced by the partial disclination dipole in Figure 1 is evident from the bending of the middle white line by about 9° relative to the other two white lines in the figure. Many such partial dislocation dipoles were observed in the MM-Fe powder.

It is not possible to determine how the partial disclination dipole in Figure 1 formed, but it is possible to envision how such dipoles facilitate the fragmentation of metals in the presence of severe plastic shear strain. The formation and migration of partial disclination dipoles allows crystalline solids to rotate [10,11]. The partial disclination dipoles in Figure 1 are only about 3.5nm apart, thereby allowing crystal volumes this small to rotate. Many such partial disclination dipoles were observed in the MM-Fe powder, as was the progressive rotation of small crystalline regions about a common <110> crystallographic axis. These features indicate that partial disclination dipoles facilitate nanocrystal rotation and thus, fragmentation of the Fe powder, under the severe shear strains produced during mechanical milling.

References

[1] Gleiter, H., Prog. Mater. Sci., 33 (1989) 233.
[2] Thomas, G., Siegel, R. W., and Eastman, J. A., Scripta Metall. Mater., 24(1990) 201.
[3] Siegel, R. W., and Thomas, G. J., Ultramicroscopy, 40 (1992) 376.
[4] Stern, E. A., Siegel, R. W., Newville, M., Sanders, P. G., and Haskel, D., Phys. Rev. Lett., 75 (1995) 3874.
[5] Wunderlich, W., Ishida, Y., and Maurer, R., Scripta Metall. Mater., 24 (1990) 403.
[6] Zhu, X., Birringer, R., Herr, U., and Gleiter, H., Phys. Rev. B, 35 (1987) 9085.
[7] Jang, J. S. C., and Koch, C. C., Scripta Metall. Mater., 24 (1990) 1599.
[8] Kimura, Y., Hidaka, H., and Takaki, S., Mater. Trans., JIM, 40 (1999) 1149.
[9] Murayama, M., Howe, J.M., Hidaka, H., and Takaki, S., Science (2002), in press.
[10] Romanov, A.E., and Vladimirov, V.I., in Dislocations in Solids, Vol. 9, F.R.N. Nabarro, Ed. (North-Holland, Amsterdam, 1992) p. 191.
[11] Seefeldt, M., Rev. Adv. Mater. Sci., 2 (2001) 44.
[12] Michler, J., von Kaenel, Y., Stiegler, J., and Blank, E. J. Appl. Phys., 83 (1998) 187.

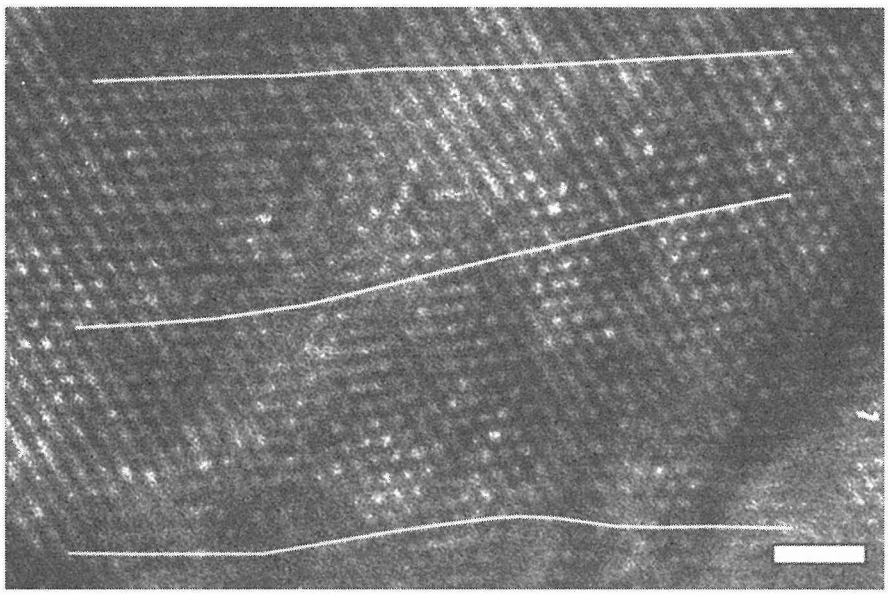

Figure 1. HRTEM image of mechanically milled, nanocrystalline Fe powder. The hexagonal arrangement of white spots in the image corresponds to columns of Fe atoms in a <111> crystal orientation. The white lines shown superimposed on three {110} planes highlight the distortion in these planes. The scale bar in the figure is 1.0nm.

Nanocrystallization in Fe-C Alloys by Ball Milling and Ball Drop Test

Y. Todaka, M. Umemoto and K. Tsuchiya

Department of Production Systems Engineering,
Toyohashi University of Technology,
Tempaku-cho, Toyohashi, Aichi 441-8580, Japan

1. Introduction

Nanocrystalline materials have attracted considerable scientific interests in the past decade. Steel companies have made large efforts to refine grain size to increase both strength and toughness of steels. Various heavy or severe plastic deformation methods have been proposed to produce nanocrystalline materials, such as torsion straining under high pressure, equal channel angular pressing and so on. In this study, microstructure evolution in steels by ball milling to nanocrystalline state is presented. To clarify the conditions to induce nanocrystallization, ball drop tests were carried out.

2. Experimental Procedures

The carbon steel (0.004 - 0.89 wt%C) powders (about 1 mm) with various microstructures (ferrite, martensite, pearlite and spheroidite) were milled in a horizontal ball mill. Ball drop tests in which a ball with weight was dropped onto a flat surface of bulk carbon steel (0.89 wt%C) with pearlite and spheroidite structures were carried out. The structure observation and property characterization of those samples were performed by SEM, TEM and micro-Vickers hardness tester.

3. Results and Discussion

Figure 1 shows SEM micrographs of the Fe-0.10C martensite steel after ball milling for 360 ks. It can be seen two types of structures, a layered structure near the surface of the powder (dark smooth contrast) and a deformed structure in the interior of the powder (bright contrast), as shown in Fig.1(a). The boundaries between these structures are clear and sharp. The layered structure near the powder surface was revealed to be nanocrystalline by TEM. These two types of structures were observed in all kind of steels studied after ball milling irrespective of the carbon content (0.004 - 0.89 wt%C) or starting microstructure (ferrite, martensite, pearlite or spheroidite) [1,2]. A drastic hardness change between these regions can be seen in Fig.1(b). The microhardness of nanocrystalline region (about 8.8 GPa) is almost double of that of the work-hardened region (3.9 GPa). The structural change of the nanocrystalline ferrite region by annealing is quite different from that of the work-hardened region. Figure 2 shows the microstructure change of the Fe-0.004C powder milled for 360 ks after annealing for 3.6 ks. The work-hardened region (lower right area) annealed at

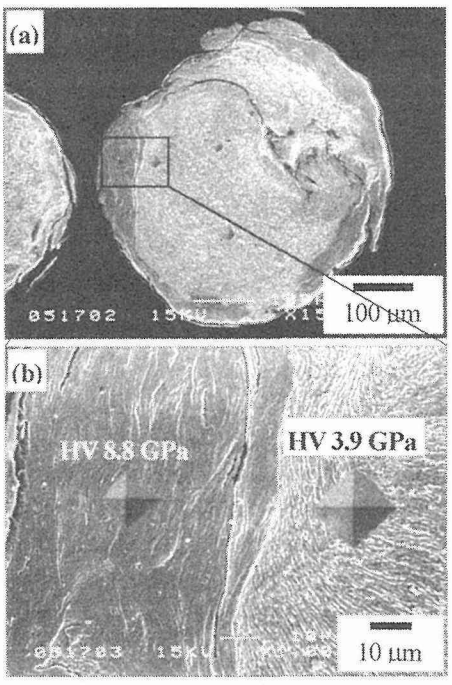

Fig.1 SEM micrographs of Fe-0.10C martensite steel after ball milling for 360 ks. (a) cross section of a powder, (b) enlargement of the boundary between the work-hardened and layered nanostructure regions.

673 K showed grains with an average size of about 1 μm as the results of recovery, as shown in Fig.2(a). On the contrary nanocrystalline ferrite region (upper left area) showed almost no detectable change. After annealing at 873 K (Fig.2(b)), the recrystallized grains in the work-hardened region become 10 μm. While, the nanocrystalline region remains almost unchanged. In a ball milling process, deformation mode is substantially complicated and contamination of powders from vial or atmosphere is hard to avoid. Thus the deformation conditions to induce nanocrystallization are unknown. The similar nanostructure with that formed by ball milling can be obtained by ball drop test. A heavy deformation with high strain rate in the drop test is similar to that in ball milling process (the estimated true strain of around 2 and strain rate of 10^4 s^{-1}), was supposed to be applied. Figure 3 [3] shows typical microstructure observed in Fe-0.89C pearlite steel specimen. A uniform dark layer with thickness of about 10 μm can be seen at the surface of the specimen. In the darkly appeared surface layer, the hardness is substantially high and cementite particles are mostly dissolved. The formation of nanocrystalline ferrite with about 100 nm was confirmed by TEM. A typical test conditions to obtain such nanocrystalline layer are 6 mm in a ball diameter, 3 kg of weight and 3 times of ball drops from 1 m height. Even a single drop showed the formation of nanocrystalline layer when the specimen is pre-deformed by rolling. From such experiments, it was found that a high strain rate deformation around 10^4 s^{-1} is important to produce nanostructure. The drop test confirmed that for nanocrystallization by ball milling deformation plays the major role but contamination has minor effect.

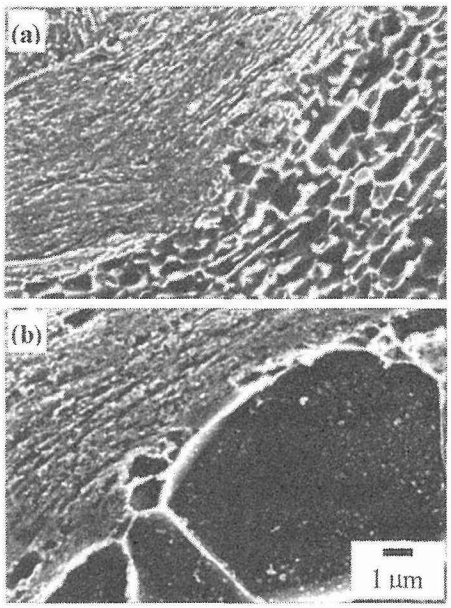

Fig.2 SEM micrographs of Fe-0.004C milled for 360 ks and annealed for 3.6 ks at (a) 673 K and (b) 873 K.

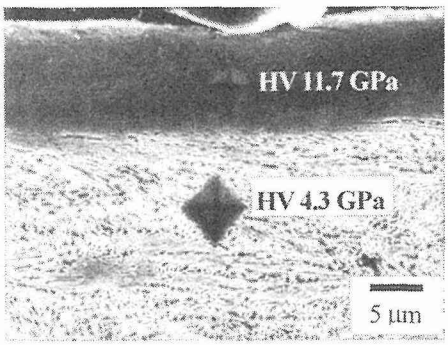

Fig.3 SEM micrograph of Fe-0.89C pearlite steel near the surface after ball drop of 8 times with a weight of 4 kg from 1 m height.

4. Conclusions

Nanocrystallization in steels by ball milling or ball drop test was studied. From the studies of both processes, it has been suggested that the nanocrystalline ferrite formed through a transition from dislocation cell wall created by work hardening during ball milling to grain boundary. The present results ensure the importance of high strain rate deformation of about 10^4 s^{-1} to produce nanocrystalline ferrite. It is realized that not only a large number of repeated deformations like ball milling but also a small number of deformations with large strain and high strain rate can produce nanostructure.

References

[1] M.Umemoto, Z.G.Liu, K.Masuyama, X.J.Hao and K.Tsuchiya, Scripta Mater., 44 (2001) pp.1741-1745.
[2] J.Yin, M.Umemoto, Z.G.Liu and K.Tsuchiya, ISIJ Int., 41 (2001) pp.1389-1396.
[3] M.Umemoto, B.Haung, K.Tsuchiya and N.Suzuki, Script Mater., 46 (2002) pp.383-388.

Fabrication of Fine-grained High Nitrogen Austenitic Steels through Mechanical Alloying Treatment

T.Tsuchiyama, H. Uchida, K. Kataoka and S. Takaki
Dept. of Materials Science and Engineering, Kyushu University, Japan

1. Introduction

Grain refining and solid solutioning of nitrogen are very effective for strengthening austenitic stainless steels without losing corrosion resistance [1,2] and ductility so much [2,3]. Each of the strengthening mechanisms, therefore, has been applied for various austenitic stainless steels to improve mechanical properties [4,5]. However, it seems to be difficult to increase proof stress over 1 GPa by a single strengthening mechanism. If the grain refining strengthening and solid solution strengthening by nitrogen can be used simultaneously, the strength of the steels could be further increased. In order to develop austenitic stainless steels having higher strength with moderate ductility, we used mechanical alloying (MA) technique which enables not only refining of grains but also alloying with variable chemical composition. In this study, microstructure and tensile properties were investigated for the high nitrogen stainless steels with fine-grained structure fabricated with the MA technique.

2. Experimental procedure

Fe-Cr alloy powders (Fe-16 or 20mass%Cr powder) and Cr_2N powder were mixed to control its mean chemical composition to be Fe-23mass%Cr-1mass%N which is enough to stabilize austenitic single structure at room temperature [6]. The powder mixture was put into a stainless steel pot with steel balls (SUJ2, 15mm in diameter), and then sealed under argon gas atmosphere. MA treatment was carried out with a planetary ball mill up to 360ks. The powder with the particle size under 45 μm (-350mesh) was separated from the as-MA powder, and it was packed in a stainless steel tube (SUS304, 16mm in diameter) in a vacuum. The sealed tube was warm-rolled to the thickness of 1.5mm at 1073K for consolidation of MA powder with full density. The bulk materials were finally heated to various temperatures (1173~1473K) followed by water quenching without holding at the temperature to avoid coarsening of grains. The bulk specimen was subjected to microstructural observation and tensile testing.

3. Results

Fig. 1 shows X-ray diffraction patterns of the as-consolidated material and the heat-treated materials (1173~1473K). In the specimens heat-treated below 1273K, the microstructure is composed of bcc phase and nitride (Cr_2N), while in the specimens heat-treated above 1373K, the matrix phase is changed to fcc phase. This result suggests that solutioning at high temperature is required for dissolving a sufficient amount of nitrogen into matrix to stabilize austenitic structure even at room temperature. Fig. 2 represents scanning electron micrographs of the heat-treated materials of 1373K (a), 1423K (b) and 1473K (c). Although the austenite grain size slightly increases with elevating heating temperature, it is kept fine under 2.2 μm in each steel. This is mainly due to the grain boundary pinning effect by finely dispersed precipitates in the matrix[7]. Chemical analysis revealed that the amount of solute nitrogen in the matrix increases with rising heating

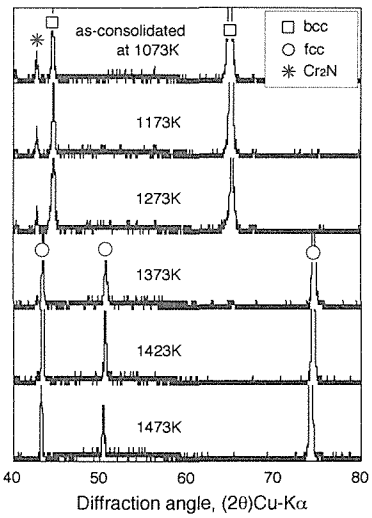

Fig. 1 X-ray diffraction parttern of bulk matrials heated to various temperatures(1173～1473K), followed by water-quenching.

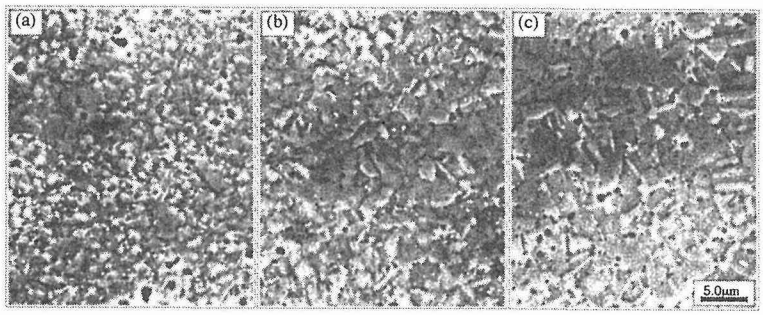

Fig. 2 Microstructures of MA bulk materials heated to 1373K(a), 1423K(b) and 1473K(c), followed by water-quenching.

temperature. The nitrogen concentrations of the heat-treated materials are 0.53%N, 0.68%N and 0.86%N for the specimen (a), (b) and (c), respectively. Fig. 3 shows an example of nominal stress-strain curves of the developed fine-grained high nitrogen austenitic steels (1473K heat-treated). The curve of a conventional austenitic steel (SUS304) is also shown for a reference. Yield strength of the developed material reaches 1.1GPa which is about four times higher than that of SUS304. According to our previous study [7,8], the increment of strength by solid solution strengthening (0.86%N) and grain refining strengthening (2.2 μm in diameter) can be estimated at 470MPa and 400MPa, respectively. Since the base yield strength of austenite is thought to be about 200MPa, yield strength of the developed austenitic steel is roughly estimated at 1070MPa by the addition of these strengths. This value well corresponds to the experimental value (1100MPa). Besides, it should be noted that the steel keeps a sufficient ductility (about 30% in total elongation) in spite of such a high yield strength. This is probably due to large work hardening rate which is introduced by a great deal of solute nitrogen.

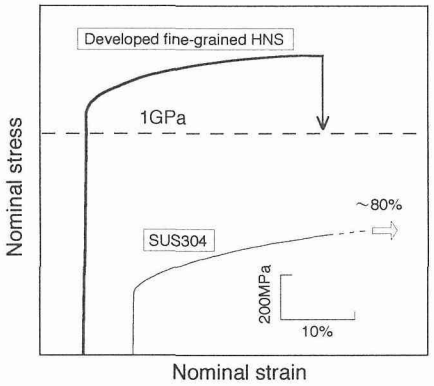

Fig. 3 Stress-strain curves of bulk materials heated to 1473K shown in Fig. 2, and of SUS304 material as a reference.

4. Conclusions

The bulk materials, which were fabricated from the mechanically milled powder, have a stable austenitic structure at room temperature in the case that the bulk materials were heated to the temperature above 1373K. In the specimen heated to 1473K, it was confirmed that the grain size of the bulk matrials is about 2.2 μm, and the amount of solute nitrogen increases to 0.86mass%. This material has a large elongation (about 30%) in spite of its high yield strength (1.1Gpa). Such a high yield stress of this steel was reasonably explained by combining strengthening mechanisms of grain refining strengthening and solid solution strengthening by solute nitrogen.

References

[1] M. Hasegawa and M. Osawa: Corrosion-NACE, 40 (1984), 371
[2] M. O. Spiedel: Proc. Int. Conf. On Stainless Steels, Chiba, ISIJ, (1991), 25
[3] H. Krauth and A. Nyilas: Austenitic Steels at Low Temperatures, ed. by R. P. Reed and T. Horiuchi, PLENUM, (1983), 159
[4] R. J. Ilola, H. E. Hanninen and K. M. Ullakko: ISIJ International, 36 (1996), 873
[5] C. A. P. Rennhard: Materials Science Forum Vols. 318-320 (1999), 175
[6] N. Nakamura and S. Takaki: ISIJ International, 36 (1996), 922
[7] Y. Kimura, S. Nakamyo, H. Hidaka, H. Goto and S. Takaki: Ultrafine Grained Materials, The Minerarl, Metals & Materials Society, (2000), 277
[8] S. Takaki, T. Tsuchiyama, H. Ito and K. Kataoka: CAMP-ISIJ, 13 (2000), 364

Effect of Oxide Addition on Thermal Stability of Ultra Fine-Grained Structure in Iron

H.Hidaka, T.Tsuchiyama and S.Takaki

Dept. of Materials Science and Engineering, Kyushu University, JAPAN

1. Introduction

Grain refining is useful technique for not only strengthening but also improving toughness at low temperature. In particular, ultra grain refining below 1μm makes the proof stress increase to 0.7GPa or more [1] without raising ductile-brittle transition temperature. However, thermal stability of the fine-grained structure is lowered with decreasing grain size. We have investigated grain growth behavior in the ultra fine-grained bulk iron fabricated from mechanical milling iron powder, and found that phase transformation from ferrite to austenite causes the abrupt grain growth to the grain size of 10μm (Transformation Assisted Grain Growth: TAGG[1,2]). In this study, oxide was added to the ultra fine-grained steel for suppressing grain growth at high temperature, and the effect of oxide addition on grain growth behavior during phase transformation was discussed in Fe-1vol.%oxide (Y_2O_3 or Cr_2O_3) material with ultra fine-grained structure.

2. Experimental procedure

The powders used in this study are commercial pure iron powder and oxide powders of Y_2O_3 and Cr_2O_3. Oxide powder (Y_2O_3 or Cr_2O_3) was mixed with iron powder by 1vol.%. Mechanical milling (MM) treatment was performed with a high energy ball milling apparatus in an argon gas atmosphere. The weight ratio of the ball to powder was 20. The mechanically milled powder was consolidated to the full density by hot-rolling technique as follows: First, the powder was put into a stainless steel tube of 16mm diameter and then the tube was sealed in a vacuum after degassing treatment of 873K-1.8ks. The sealed steel tube was rolled to 1.5mm thickness at 973K for the consolidation and densification of the MM powder. Microstructure of the consolidated materials was observed with transmission electron microscope (TEM). Hardness was represented by the average of eight measurements by micro-Vickers hardness testing.

3. Results and discussion

Fig.1 shows TEM images of the Y_2O_3 material consolidated at 973K. The bulk material has ultra fine - grained structure with the grain size of 0.25μm. The Cr_2O_3 material had similar structure as the Y_2O_3 material although the gain size is slightly large (0.3μm). Fig.2 shows relation between annealing temperature and hardness in these bulk materials. The result of MM pure iron without the intentional addition of oxides is also shown in the figure. Hardness of the Cr_2O_3 material gradually decreases with rising annealing

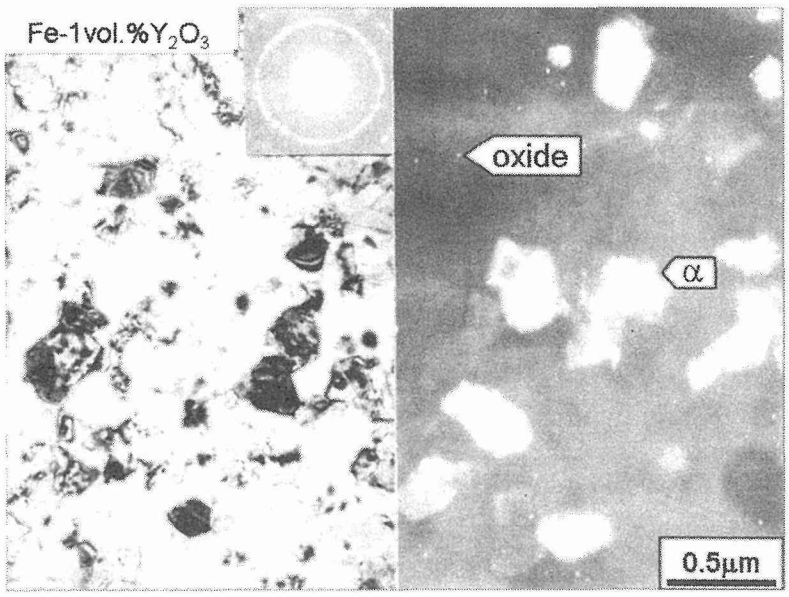

Fig.1 TEM images of Fe-1vol.%Y_2O_3 bulk materials fabricated from MM powders; bright field image, dark field image and diffraction pattern taken from observed area.

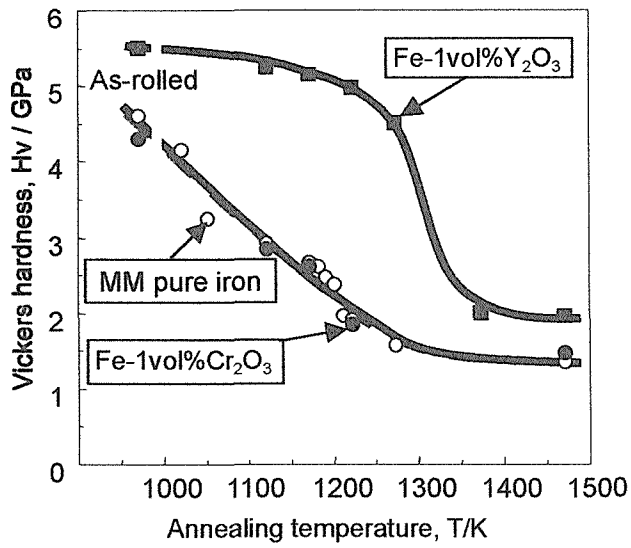

Fig.2 Relation between annealing temperature and hardness in MM bulk materials

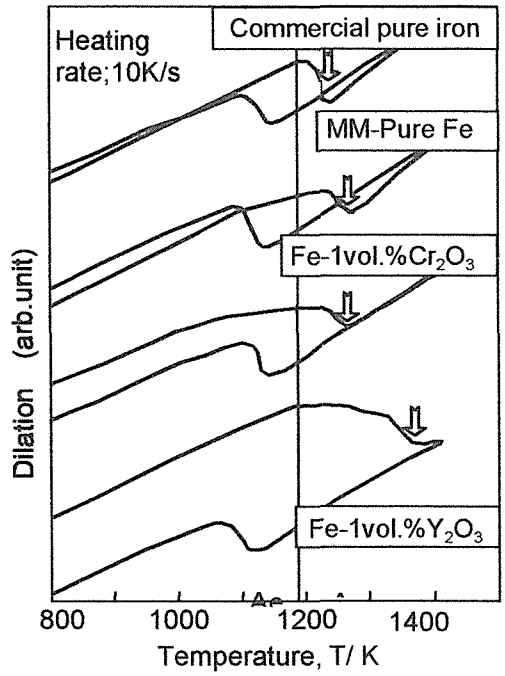

Fig.3 Dilatation curves in MM bulk materials. The result for commercial pure iron is also shown in this figure for reference.

temperature, and its softening behavior is just same as that of the MM pure iron. Since hardness of ultra fine-grained materials is dependent on the grain size yielding to the Hall-Petch relationship[1], it is found that Cr_2O_3 addition gives no effect on the thermal stability of ultra fine-grained structure. On the other hand, the hardness of the Y_2O_3 material is kept at a higher level in the temperature range below 1200K, although the hardness drops abruptly at around 1300K from 5GPa to 2GPa. This abrupt softening is thought to be due to TAGG which has caused by the phase transformation from ferrite to austenite. Fig.3 shows dilatation curves of MM bulk materials and commercial pure iron on heating and cooling. The reversion temperature of the MM pure iron and the Cr_2O_3 material is almost same as that of commercial pure iron (1223K), while the reversion temperature of Y_2O_3 material is sifted to the higher temperature of 1350K. This result demonstrates that the excellent thermal stability leads to the rise in reversion temperature in the Y_2O_3 material. The retardation of reversion by the addition of Y_2O_3 can be explained by the suppression of nucleation of austenite: Ultra fine-grained structure kept by the pinning effect of fine Y_2O_3 particles should prevent the nuclei of austenite grain (the size of nuclei>grain size.)

4. Conclusion

Addition of Y_2O_3 is useful to keep ultra-fine-grained structure in the elevated temperature below ferrite_austenite reversion temperature, and the reversion temperature is raised through the retardation of nucleation of austenite due to the characteristic ultra fine-grained structure.

References

[1]Y.Kimura and S.Takaki: Proc. of the 1998 PM World Congress and Exhibition Granada, Spain, 1998, Oct, pp573-578

[2] K.Kawasaki and S.Takaki: CAMP ISIJ Vol.13, No.6(2000),pp.18

Fabrication of Ultrafine Grained Austenitic Stainless Steels by Powder Metallurgy

R.Ishibashi, H.Arakawa*, H.Doi and Y.Aono
Hitachi Research Laboratory, Hitachi Ltd., Japan
*Hitachi Kyowa Engineering Co., Ltd., Japan

1. Introduction

Austenitic stainless steels with ultra-fine grains are expected to have high strength, high corrosion resistance and high irradiation resistance without losing their toughness. The present authors have developed ultra-fine grained austenitic stainless steels through the high strain powder metallurgy process combining mechanical milling (MM) and consolidation processes. As described in a review by Kimura *et al.*[1], mechanically milled powder (MM powder) of iron has large strain and nano-meter sized grains. A major issue during development is the suppression of the growth of nano-meter-sized grains in the mechanically milled powders during their consolidation processes at elevated temperatures. In order to suppress grain growth, consolidation at lower temperatures and dispersion of finer particles for pinning grain boundaries are desirable. Consolidation processes, such as hot isostatic pressing(HIP), hot forging and hot extrusion, are expected to compact the powders at lower temperatures than conventional sintering process. Addition of stable carbide former elements, such as Zr and Ti, is expected to precipitate fine stable carbides. This does not suppress only grain growth effectively during the consolidation processes, but also suppress significant $M_{23}C_6$ precipitation. Optimized composition and processing for fabrication of ultra-fine grained austenitic stainless steels with high strength and high toughness are proposed.

2. Experimental procedure

Prealloyed 304 base powders including about 0.8% Zr as a carbide former element were manufactured by gas atomization. Powders and steel balls were loaded into a planetary ball mill or an attrition mill under an inert gas. The MM treatment was processed at a rotation speed of 200 rpm for 360 ks in case of a planetary ball mill or for 180 ks in case of an attrition mill. The attrition mill was used to produce MM powders for hot extruded materials. The MM powders were first canned in mild steel capsules after degassing at 673 K under 10^{-4} Pa, and then consolidated by HIP or hot extrusion at 1023～1123 K. Consolidating materials were held for 3.6 ks at an intermediate temperature during temperature increase of the consolidation processes. Some materials consolidated by HIP were forged at the same temperatures as HIP.

3. Results and discussion

Consolidation by HIP or hot extrusion was able to achieve almost full density at 1023～1123 K, which are much lower in comparison to conventional sintering temperatures. However, additional forging was required to obtain a ductile tensile property for a consolidated material by HIP[2]. Mechanical properties of the developed materials by HIP + forging or extrusion are shown in Fig.1. Zr-added materials held for 3.6 ks at 823～873 K during consolidation processes. Zr-addition increased strength and Charpy absorbed energy of materials consolidated by HIP + forging. These materials had tensile strengths higher than 1000 MPa and Charpy absorbed

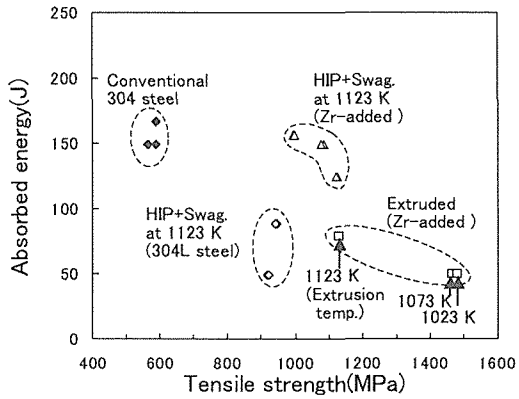

Fig.1. Strength and toughness of developed materials

energies of 150 J comparable to conventional 304 stainless steel. Although the absorbed energy decreased, an extruded material with a tensile strength of 1460 MPa was obtained by decreasing an extrusion temperature. These materials showed ultrafine grains with mean sizes of 150～300 nm. Addition of Zr caused fine ZrC precipitation. As a result, consolidated materials showed finer grains and higher strength in comparison to a material without any addition. Holding at 823～923 K during temperature increase of a HIP process improved strength of Zr-added as-HIP materials, consolidated at 1123 K, as shown in Fig.2. TEM observation revealed that the microstructure of materials processed by temperature holding was slightly finer than that processed without holding, and that, this treatment enhanced nano-meter-sized ZrC precipitation and suppressed significant $M_{23}C_6$ precipitation[3]. Suppression of $M_{23}C_6$ precipitation probably improved toughness as shown in Fig.1. As described above, addition of Zr, a stable carbide former element, and temperature control during consolidation process resulted in nano-meter-sized dispersion and ultrafine grain structure. Such a microstructure was considered to be produced due to initial microstructure of MM powders as follows. After MM, condition of powders can be considered to be similar to that of conventional solution treated materials because they are both precipitate free. High-density defects in the microstructure of the MM powders enhanced diffusion of solutes and nucleation of new phases. Therefore, stable phase transformations and precipitation processes are believed to be promoted by this microstructure without the kinetic restrictions at temperatures lower than those required for conventional materials.

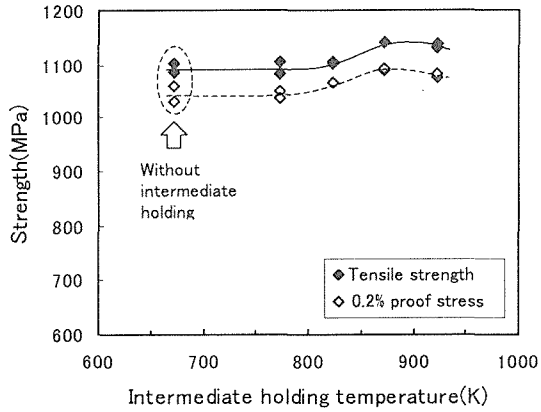

Fig. 2. Effect of holding at various temperatures during temperature increase of the HIP process on the strength of Zr-added as-HIP materials (HIP at 1123 K)

4. Conclusion

Austenitic stainless steels with tensile strengths higher than 1000 MPa and Charpy absorbed energies of 150 J comparable to conventional 304 stainless steel are obtained by a high strain powder metallurgy process applying mechanical milling with addition of Zr, a stable carbide former element, and temperature control during consolidation processes. Ductile materials are produced by the consolidation processes, such as HIP + forging or extrusion at lower temperatures in comparison to conventional sintering process. Low consolidation temperatures and fine ZrC precipitation by addition of Zr result in suppressing grain growth effectively during consolidation processes. Furthermore, the controlled consolidation process was able to enhance precipitation of nano-meter-sized carbides and suppress significant $M_{23}C_6$ precipitation. Suppressing $M_{23}C_6$ precipitation by addition of Zr is considered to be one of reasons for improving toughness.

Acknowledgements

This study is supported by the New Energy and Industrial Technology Development Organization (NEDO).

References

[1] Y. Kimura and S. Takaki: Materials Transactions, JIM, 36(1995), pp.289-296.

[2] R. Ishibashi, H. Arakawa, T. Abe and Y. Aono: ISIJ International, 40(2000), Supplement, pp.S169-S173.

[3] R. Ishibashi, H. Arakawa, H. Doi and Y. Aono: Proc. The fourth Pacific Rim Int. Conf. on Advanced Materials and Processing(PRICM4), JIM, (2001), pp.151-154.

Ultra refinement in austenite grain size through the spontaneous reverse transformation due to adiabatic deformation heating

T. Yokota[1,2], K. Sato[1,2] and M. Niikura[1,2]
[1]Ferrous Super Metal Consortium of JRCM, Japan
[2]Materials and Processing Research Center, NKK Corp. , Japan

1. Introduction

γ grain size refinement is one of the most important factors for microstructural control of steels. There are two approaches to refine γ grain size. One is recrystallization of deformed γ and the other is reverse transformation. It is known that γ grain size can be refined by static recrystallization after hot deformation as small as 6 μm [1]. On the other hand, γ grain can be refined down to 3 μm by repeated transformation under rapid heating and cooling [2]. Reverse transformation of cold rolled martensite is also known to have a beneficial effect on γ grain refinement. There have been many studies on γ grain refinement by this thermomechanical processing and ultra fine γ grain size of under 1 μm has been obtained in both high and low alloy steels [3-5].

The purpose of this investigation is to propose a new concept for ultra refinement processing in γ grain size, i.e. "Spontaneous Reverse Transformation due to Adiabatic Deformation Heating". It has been revealed that heavy deformation at a temperature in α region just below the Ae1 transformation temperature induced a spontaneous reverse transformation which resulted in ultra refinement in γ grain size to less than 1 μm[6]. In this paper, the deformation conditions to bring about the spontaneous reverse transformation were clarified, and the occurrence mechanism was discussed.

2. The deformation conditions to bring about the spontaneous reverse transformation[6,7]

Deformation conditions to bring about the spontaneous reverse transformation were investigated by means of compression type hot deformation simulator (maximum load: 10ton). 0.3%C-9%Ni steel was adopted for the investigations. This steel was designed to have high hardenability so that the extent of austenitization could be easily evaluated through hardness measurement and microstructure observation. Ae1 and Ae3 temperatures were calculated as 625℃ and 665℃ by Thermo-Calc. The initial microstructure of the specimens was martensite with a prior γ grain size of 22 μm.

Cylindrical specimens with 8mm in diameter and 12mm in height were heat treated at 550℃ for 5min and compressed with various reduction from 0% to 70% under a strain rate of 10/s followed by quenching with 30℃/s. Fig.1 shows the hardness and microstructural change of the deformed specimens as a function of reduction ratio. Hardness of the deformed specimens are less than HV400 in the reduction range from 15% to 50%. Heavy deformation such as 70% reduction brings about a drastic increase in hardness up to over HV600 which corresponds to the hardness of martensite. This result suggests that reverse transformation has completed only by deformation. The microstructure of 50% and 70% deformed specimen consisted of heavily deformed tempered martensite and extremely fine fresh martensite respectively. TEM observation revealed that grain structure surrounded by high angle boundaries were either equiaxed or elongated and the size of equiaxed grains was roughly estimated as around 0.5 μm for the 70% deformed specimen. Generally, martensite packet size is in proportion to prior γ grain size[8]. Therefore prior γ grain size in this case could be ultra refined though it couldn't be observed directly.

TEM observation was also performed for 50% deformed specimen in detail to clarify the transformation mechanism. Many globular submicron size γ precipitates located adjacent to cementite on a subgrain boundary were observed in 50% deformed specimen. These results

suggest that the spontaneous reverse transformation partially occurred even by 50% reduction and completed by 70% reduction through a diffusional mechanism. The mechanism for ultra refinement in grain size has not clearly understood yet, although both local rotation of crystals caused by dynamic transformation and grain growth suppression caused by extremely rapid heating effect are suggested as candidates.

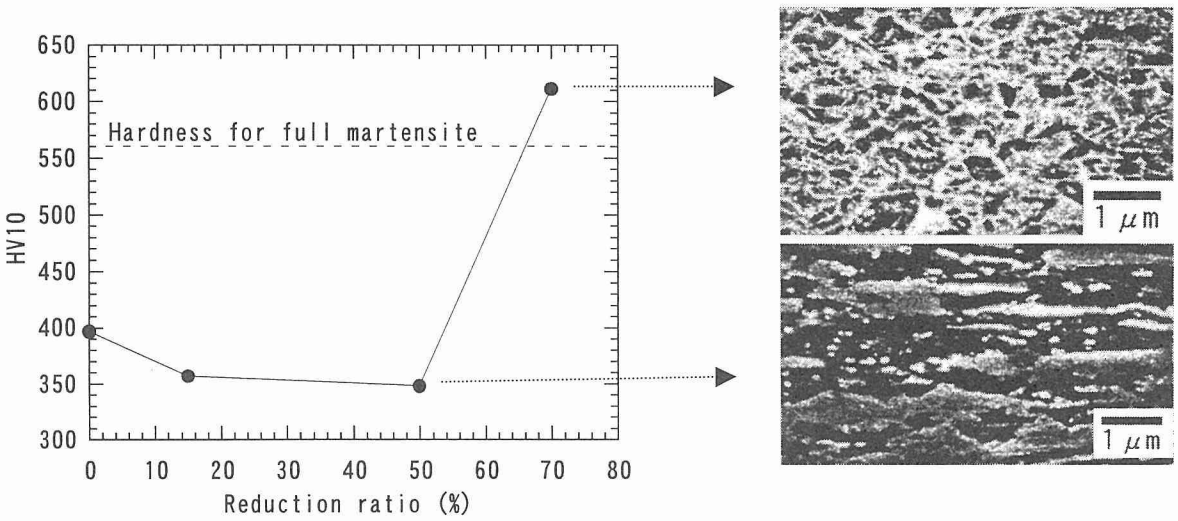

Fig.1 Hardness and microstructural change of the deformed specimens as a function of the reduction ratio

The spontaneous reverse transformation was clearly observed for the strain rate of 10/s but not observed for the strain rate of 0.1/s or 1/s in the case of 70% reduction. This suggests that the spontaneous reverse transformation results from temperature increase due to adiabatic heating induced by heavy deformation. The occurrence of the spontaneous reverse transformation was also verified by means of a 1000 ton large scale laboratory mill and ultra refined steel plate with thickness of 6mm had been obtained[9].

3. Conclusion

The spontaneous reverse transformation has been proposed as a new concept for γ ultra refinement processing. The deformation conditions to bring about the spontaneous reverse transformation were clarified and its mechanism was discussed.

Acknowledgments

This study was carried out as a part of research activities of Ferrous Super Metal Consortium of JRCM. Financial support from NEDO (New Energy and Industrial Technology Development Organization) is gratefully acknowledged.

References

[1] C.Ouchi and T.Okita, Trans. ISIJ,24(1984), pp.726-733.
[2] R.A.Grange, Trans. ASM, 59(1966), pp.26-48.
[3] R.L.Miller, Met.Trans.,3(1972), pp.905-912.
[4]K.Tomimura et.al.,Tetsu-to-Hagane,75(1989),No.7,pp.1186-1192.
[5] M.Tokizane, K.Ameyama, and K.Takao, Scr. Metall., 22(1988),No.5, pp.697-701.
[6] T.Yokota, T.Shiraga, K.Sato and M.Niikura, Tetsu-to-Hagane,86(2000),No.7, pp.479-484.
[7]T.Yokota et.al., Proc.of the 2nd Symp. on Super Metal, RIMCOF & JRCM, (1999), pp.173-181.
[8] T.Maki, K.Tsuzaki and I.Tamura, Tetsu-to-Hagane,65(1979), No.5,pp.515-524.
[9] T.Yokota, T.Shiraga , M.Niikura and K.Sato, CAMP-ISIJ,13(2000),No.3, pp.462-465.

Refinement of Austenite Grain in a Medium-Carbon Low-Alloy Steel by Thermomechanical Processing

Y.Kimura, S.Takagi* and K.Tsuzaki
Materials Creation Research Group, NIMS, Japan
*Now at Technical Research Lab.,Kawasaki Steel Corp., Japan

1. Introduction

Since coarse film-like grain boundary carbides usually cause failure, it is important for the improvement of mechanical properties of steels to minimize both the size and the amount of grain boundary carbides. Our co-workers[1] have recently reported that the modified ausforming at around 1050K makes austenite grain boundaries serrated or curved with a period of 1-2 μm and leads to the disappearance of the film-like grain boundary carbides and the refinement of grain boundary carbides in tempered martensitic steel. Thus, if the prior-austenite grains are significantly refined to a few μm or less, the film-like grain boundary carbides are expected to be refined.

In this study, the thermomechnical processing, which consists of warm working of tempered martensite and subsequent rapid austenitizing[2], was applied to a medium-carbon low-alloy steel to refine austenite grains. Here we also expect the utilization of undisoluved carbide as a way of microstructure control to attain a fine-grained structure without coarse film-like carbides. Then, the refinement of austenite grain was investigated in association with the carbide dispersed microstructures developed by the warm working of tempered martensite at different temperatures.

2. Experimental

A commercial medium-carbon low-alloy steel (JIS-SCM 440) was used and its chemical composition was 0.4%C, 0.2%Si, 0.8%Mn, 0.02%P, 0.01%S, 1.0%Cr, 0.16%Mo, and the balance Fe (mass%). A martensite billet with 40 mm diameter was tempered at 873K or 973K for 5.4 ks and subjected to multi-pass bar-rolling into 12 mm square bar (total reduction; 90%). Rod shape samples with 3mm in diameter and 10mm in length were machined from the rolled bar. Samples were heated at about 100K/s and austenitized at 1093K for 1-600s with an induction heating device and then quenched by He gas. The normalized bar was austenitized at 1153K for 1.8ks and then oil-quenched for the reference. Mean austenite grain size was determined by the Heyn's intercept method.

3. Results and Discussion

Fig.1 shows carbide microstructures after bar-rolling at 873K(a) and 973K(b). Spheroidized cementite structures are formed in both samples and the microstructures are relatively uniform. The sizes of carbide particles and matrix ferrite grains become smaller with decreasing rolling temperature. **Fig. 2** shows the hardness changes of the samples quenched after austenitizing at 1093K for various time. In this austenitizing treatment, Ac1 temperature was measured to be about 1020K for the sample rolled at 873K, and 1025K for the sample rolled at 973K. The hardness of the samples shows a sharp rise in a short period of time and then a gradual increase in response to the dissolution of carbides. Over the whole time range, the sample rolled at 873K has higher hardness than the sample rolled at 973K. That is, the dissolution of carbide particles is faster in the sample rolled at 873K than that in the sample rolled at 973K. **Fig. 3** represents the change in the austenite grain size. Fine austenite grains of 3μm or less can be obtained in a short period of austenitizing time up to 10s in both samples. But finer grained martensitic structure with higher hardness can be obtained in the sample rolled at 873K. **Fig.4 (a)** shows a carbide structure of an as-quenched sample with the austenite grain size of about 2μm (**Fig.4(b)**). Undissolved carbides exist in as-quenched state. The maximum diameter of undissolved carbides was about 100nm, and the carbide distribution is relatively uniform. In spheroidized microstructure, austenite nucleates at cementite particles associated with the ferrite grain structure[3]. Thus, the carbides are thought not only to retard the growth of matrix grains but also act as nucleation sites of austenite in a short period of the austenitizing time. These results indicate the importance of the rolling temperature to attain fine-grained martensitic structure with uniform dispersion of fine carbide particles.

References

[1] S.Yusa, T.Hara, K.Tsuzaki ; *J.Japan Inst. Metals*, **64** (2000) pp.1230-1238.
[2] M.Tokizane, K.Ameyama, K.Takao ; *Scripta Metall.*, **22** (1988) pp.697-701.
[3] G.Krauss; *STEELS : Heat Treatment and Processing Principles*, ASM International, USA, (1989), pp.182-188.

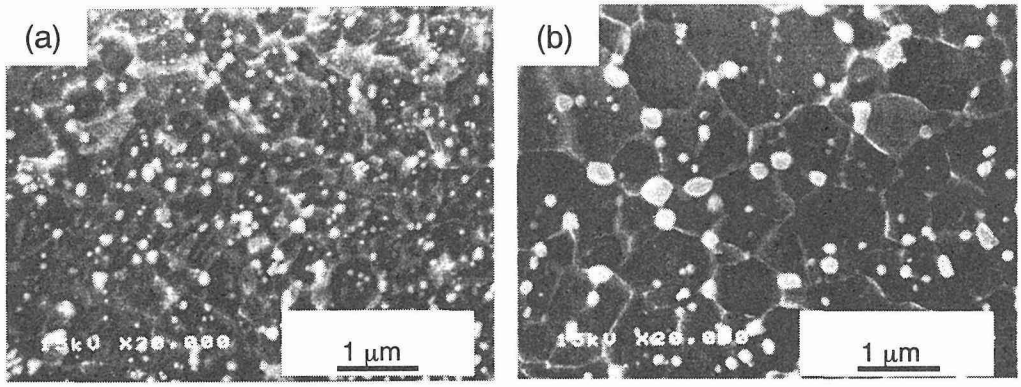

Fig.1 SEM micrographs showing carbide structures after bar-rolling of tempered martensite at 873K(a) and 973K(b). Hardness of the samples is 320HV at 873K and 245HV at 973K.

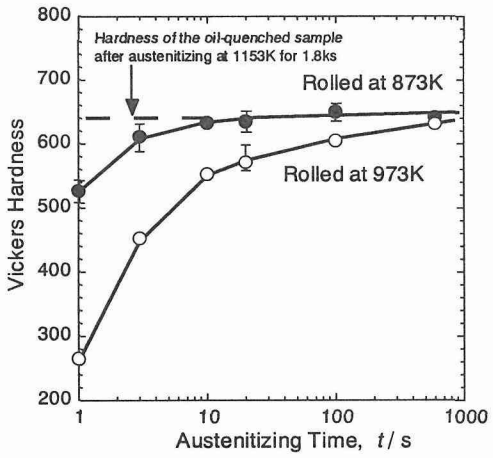

Fig.2 Changes in hardness of bar-rolled samples during austenitizing at 1093K, followed by quenching.

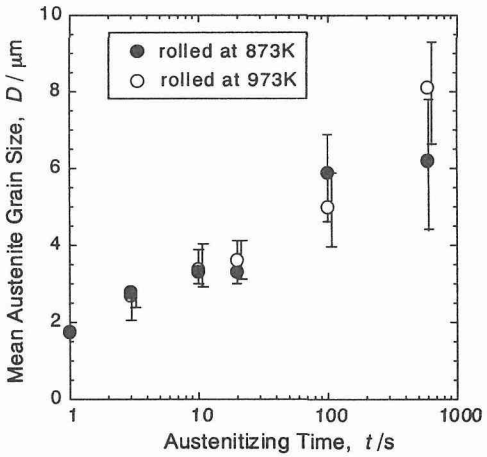

Fig.3 Changes in austenite grain size of bar-rolled samples during austenitizing at 1093K, followed by quenching.

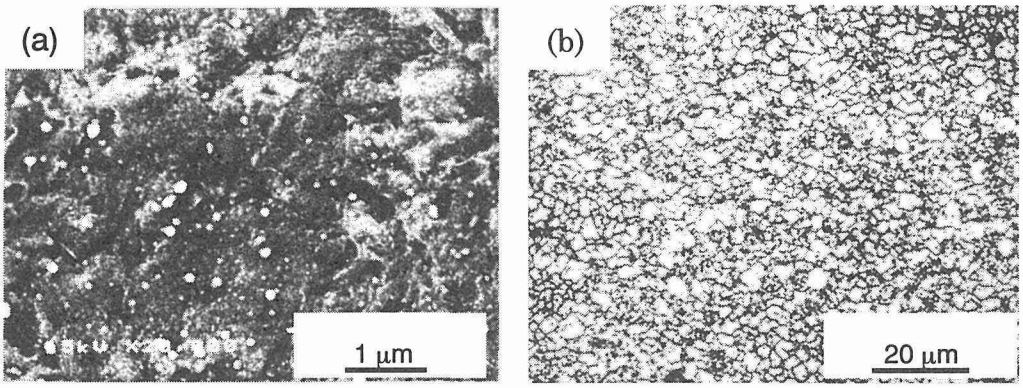

Fig.4 Carbide microstructure(a) and austenite grain structure(b) after austenitizing at 1093K for 1s in a sample bar-rolled at 873K. Mean austenite grain size is about 2μm.

Evaluation of grain size effect on the strength of Fe-C tempered martensite using nanoindentation techniques

T. OHMURA, T. HARA and K. TSUZAKI
Materials Engineering Laboratory, National Institute for Materials Science
1-2-1 Sengen, Tsukuba, Ibaraki, 305-0047 Japan

1. Introduction

A lot of previous studies have revealed that the macroscopic strength of Fe-C based martensitic steels is dominated by many factors such as matrix strengthening and grain size effect. The matrix strength is considered to be a major factor because the macroscopic strength of the Fe-C lath martensite increases drastically with carbon content in the range that is lower than about 1 mass% [1], and the dislocation density is extremely high in the Fe-C lath martensite [2]. However, the matrix strengthening factors have never been evaluated by themselves, because an effective grain size of the Fe-C lath martensite, which is block structure, is too small in sub-micron. Therefore, a direct evaluation of the matrix can make clear the each contribution of matrix strength and grain boundary efficiency.

For the subject, nanoindentation is a useful method. Some studies [3-5] with nanoindentation tests showed successful evaluation of the matrix strength of martensite. In the present study, mechanical characterization was done for the matrix of the Fe-C martensite and then the strengthening factors of the macroscopic strength of the martensite such as matrix strength and grain size effect were separately considered.

2. Experimental

The specimens investigated were Fe-C binary steels with nominal carbon contents of 0.1, 0.2, 0.4, 0.6 and 0.8 mass%. The specimens were austenitized at 1050°C for 900s in an argon gas atmosphere and then ice-brine quenched (as-Q specimens), after that only the Fe-0.4C specimens were followed by tempering at 100, 200 and 300 °C in an oil bath and 450, 550, 600 and 650°C in an argon gas atmosphere (QT specimens). Four bcc single crystals were also employed as reference. Hysitron Triboscope was conducted in nanoindentation measurements. Conventional micro Vickers hardness test with a load of 4.9 N were also performed as macroscopic strength evaluation.

3. Results and Discussion

The tempering temperature dependence of the nanohardness H_n, micro Vickers hardness H_v and the elastic modulus E_r for the Fe-0.4C specimens are represented in Fig. 1. The elastic modulus is almost constant, while the nanohardness decreases with increasing tempering temperature, which is the same behavior as the temper softening of the micro Vickers hardness. The ratio H_n/H_v is employed for further consideration of the contributions of the matrix strength to the macroscopic strength. Since the macroscopic strength is composed of the matrix strength and the grain boundary efficiency, the ratio H_n/H_v is associated with the contribution of the matrix strength to the macroscopic strength. In other words, the lower the ratio is, the larger the grain

size effect is. Figure 2 shows the ratio H_n/H_v for all the specimens plotted as a function of H_v. The ratio is much higher for the single crystals than those for the Fe-C martensite, especially for the as-Q and QT specimens tempered at or below 300 °C. These results indicate the significant grain size effect for the Fe-C martensite. For the as-quenched specimens, the grain size effect increases with increasing micro Vickers hardness, namely with increasing the carbon content. This is attributed to that the size of the block structure decreases with increasing the carbon content. In the case of the quench-tempered specimens, the grain size effect drastically depressed in the tempering temperature between 300 °C and 450 °C. According to the transmission electron microscopy observation and scanning electron microscopy with electron back scattering diffraction analysis, a grain growth at 450°C is not sufficient. On the other hand, a remarkable change of the cementite structure occurs at 450 °C. A large amount of cementite precipitates on the boundaries in a film like state at 300 °C, while most of the cementite particles are spheroidized and the film like carbides on the boundaries disappear in the specimen tempered at 450 °C. Since the film like carbides have great resistance to the dislocation glide motion, the grain boundary efficiency regarded as the locking parameter of the Hall-Petch relation is larger for the specimen tempered at 300 °C than that for 450 °C. Therefore, a significant increase of the ratio H_n/H_v corresponding to the reduction of the grain size effect at 450 °C is mainly due to the spheroidization of the cementite.

References

[1] Pickering, F. B., Hardenability Concepts with Applications to Steel (AIME, Warrendale, PA, 1978) pp. 179-220.

[2] Kehoe, M. and Kelly, P. M., Scripta Metall. 4(1970), pp.473-476.

[3] Ohmura, T., Tsuzaki, K. and Matsuoka, S., Scripta Mater. 45(2001), pp.889-894.

[4] Ohmura, T., Tsuzaki, K. and Matsuoka, S., Phil. Mag. A, (accepted).

[5] Ohmura, T., Hara, T. and Tsuzaki, K., Acta Mater., (submitted).

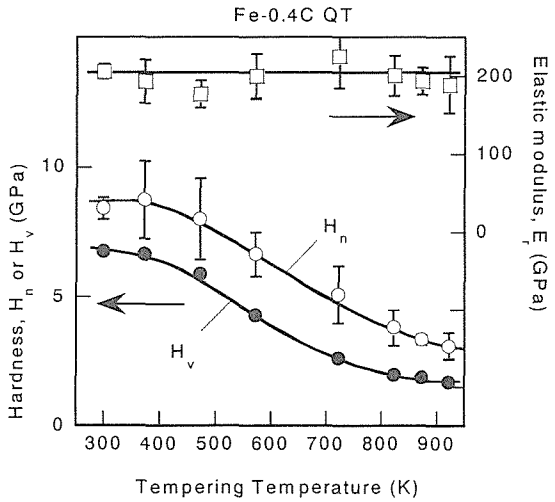

Fig. 1 Tempering temperature dependence of the nanohardness, micro Vickers hardness and the elastic modulus.

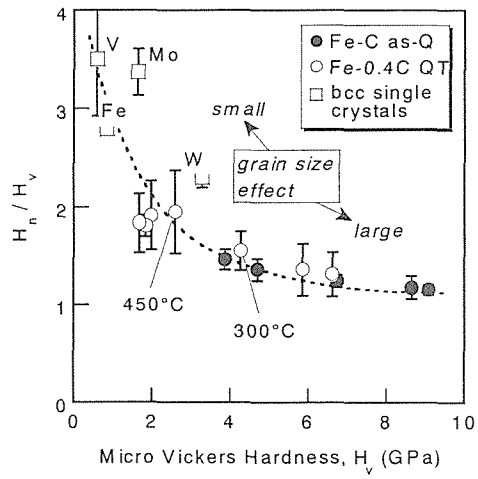

Fig. 2 The ratio H_n/H_v for all the specimens plotted as a function of H_v.

- Deformation Behavior at High Strain Rate and the Modeling
- High-Speed Deformation for TRIP Steel
- High Strength Steels for Welded Structures
- Application of High Strength Steels
- Microstructure of Welds and Mechanical Properties
- Heat Affected Zone of High Strength Steels

(Room 202)

Modeling for Common Evaluation Method in High-Speed Deformation

Y.Tomota*, N.Tsuchida and J-H.Park
*Department of Materials Science, Ibaraki University, Japan

To improve the safety for automobile collision, the quantitative description of plastic deformation of steels at high strain rates has been required. Several experimental methods to examine high-speed deformation behavior have been developed, but sufficiently accurate results with good reproducibility have not been obtained yet. In steels, plastic deformation at room temperature with strain rates below 10^3/s is controlled by thermally activated mechanisms for dislocation motion. Because the strain rate at the automobile collision is considered to be from 10^2/s to 10^3/s, the flow stress is possibly estimated by using an appropriate deformation equation based on the above thermally activated mechanisms.

Many workers have used the following equation to describe the influence of strain rate ($\dot{\varepsilon}$) on flow stress (σ) [1],

$$\sigma = \sigma_a + K\dot{\varepsilon}^{m^*} \tag{1}$$

Here, K and m^* are constants that depend on test temperature and σ_a is the athermal stress that is often expressed by Swift equation; $\sigma_a = a(b+\varepsilon_p)^N$ where a, b, N: constants and ε_p: plastic strain. This simple expression holds under the assumption that thermal activation mechanisms for dislocation motion can be represented by one hypothetic barrier. Generally, m^* is determined by utilizing stress relaxation test or strain rate change test at a concerned temperature. Equation (1) is easy to estimate the flow stress at high-speed deformation but contains several problems which include,

(1) m^* must be determined experimentally at a concerned temperature.
(2) thermal stress component σ_{th}, the second term of Eq.(1), is frequently assumed to be independent of strain, or m^* must be determined at various strains to figure the whole flow curve at a high strain rate.
(3) m^* cannot be obtained by stress relaxation test when dynamic strain aging takes place in carbon steels.

More sophisticated approach for this issue has been developed starting from the works by Kocks and Mecking [2, 3], so called Kocks-Mecking (KM) model or mechanical threshold (MT) model. The model has still been in progress but contains the following merits;

(1) the model can give the effects of temperature, strain rate, and strain on flow stress by one equation.
(2) more than two strengthening mechanisms can be superposed and hence it is convenient to investigate steel design suitable for high-speed deformation.
(3) the model is based on real phenomena so that physical meanings of parameters are more clear.

A typical example of deformation equation is given by

$$\frac{\sigma}{\mu}=\frac{\sigma_a}{\mu}+S_I(\dot{\varepsilon},T)\frac{\hat{\sigma}_I}{\mu_0}+S_D(\dot{\varepsilon},T)\frac{\hat{\sigma}_D}{\mu_0} \quad \text{where} \quad S_I(\dot{\varepsilon},T)=\left[1-\left(\frac{kT}{g_{0I}\mu b^3}\ln\frac{\dot{\varepsilon}_{0I}}{\dot{\varepsilon}}\right)^{1/q_I}\right]^{1/p_I} \tag{2}$$

where $S_D(\dot{\varepsilon},T)$ is given similarly to $S_I(\dot{\varepsilon},T)$ which indicates the aid by thermal activation for dislocation motion. Concerning the detailed explanation on Eq.(2), see refs.[2]-[7]. The equation consists of the athermal stress that is generally described as a function of strain and grain size, the thermal stress associated with the yielding (note suffix I) and the thermal stress associated with work hardening (D). The microstructure in which dislocations move is expressed by the stress at 0K ($\hat{\sigma}$) where thermal activation is no longer expected. The parameters in Eq.(2) were determined mostly from experimental results obtained by conventional tensile tests and partially from theoretical considerations.

Many applications of Eq.(2) to several materials are now found in literature. We have studied the cases of α Ti [4], SUS310S [5], and ferritic steels [6, 7]. The comparison between the flow stress estimated by KM model and measured ones obtained by Hopkinson bar method has revealed that deformation with $\dot{\varepsilon}=2\text{x}10^3/\text{s}$ is adiabatic. Hence, temperature increase during deformation is taken into account for computation of high-speed deformation. The remained problems to be solved in the future include, more advanced treatment of work hardening where microstructure evolution should be described as a function of test temperature and strain rate, superposition of strengthening by the second phase and dynamic strain aging in carbon steels. Plotting the flow stresses calculated by Eq.(2) in a form of Eq.(1), we have found reasonable m in a wide temperature regime. That is, Eq.(2) is revealed to cover Eq.(1) when concerned temperature and strain are given.

References

[1] For instance, 「High-speed deformation of steels for automotive use」 (Final report of " the research group on high-speed deformation of steels for automotive use" (chairperson: H.Takechi)), ISIJ (2001)

[2] Kocks, U. F., ASME J. Engng mater tech.: 98(1976), 76-85

[3] Mecking, H. and Kocks, U. F., Acta metall. 29(1981), 1865-1875

[4] Tsuchida, N., Moriya, H., Tomota, Y., Umezawa, O. and Nagai, K., ISIJ Int., 40(2000), 84-90

[5] Tsuchida, N., Tomota, Y., Moriya, H., Umezawa, O. and Nagai, K., Acta mater., 49(2001), 3029-3038

[6] Park, J-H., Tomota, Y., Takagi, S., Ishikawa, S. and Shimizu, T., Tetsu-to-Hagane, 87(2001), 657-664

[7] Park, J-H. and Y.Tomota: submitted to ISIJ Int.

High Strain Rate Deformation in High Strength Steels for Automotive Application

T. Shimizu, S. Takagi, K. Miura, K. Sakata
Technical Research Laboratories, Kawasaki Steel Corp., Japan

1. Introduction

The application of high tensile strength steel sheets in automotive body parts to reduce the weight while simultaneously improving the crashworthiness of the vehicle was studied. As shown as figure 1 and 2, the strength of steel increases with the rise of strain rate. But the strain rate sensitivity decreases as the strength of steel increases. [1], [2] The strain rate affecting impact-resistant parts may be as high as 10^3/s during crash of car body. For this reason, the steel sheets, which have larger strain rate dependence of deformation strength and large values of absorbed energy at high strain rates, are necessary for such parts.

High tensile strength steels are categorized into various types, depending on the method of hardening. As shown as figure 3, multiphase steels, such as dual phase steel consists of ferrite and martensite, TRIP steel consists of ferrite, bainite and residual austenite, have higher strain rate sensitivity of yield strength than other type such as solid solution hardening steel. [3]

Even within the same type multiphase steel, the microstructure may not be identical, and the volume fraction and grain size of the secondary phase may differ. However, the effect of these micro-structural factors on the strain rate sensitivity of yield strength has not been adequately clarified. Accordingly, this report will present the results of research for the effect of the volume fraction and grain size of martensite on strain rate sensitivity in dual phase steel.

2. Influence of martensite on strain rate sensitivity in dual phase steel

The hot steel sheets, consist of 0.05%C-0.96%Si-1.35%Mn-0.01%P- 0.004%S - 0.99%Cr, were cold rolled and annealed to produce the samples of 590MPa tensile strength grade dual phase steel with differing volume fractions and grain size of martensite. Tensile tests were performed on these samples at strain rates of $2x10^{-2}$/s with an Instron types tensile tester and

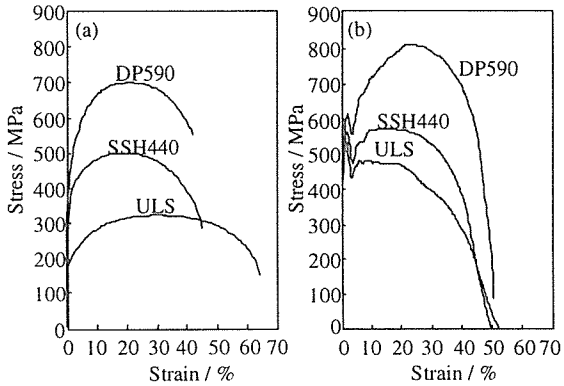

Fig.1 Stress-strain curves at strain rates of (a) 2×10^{-2}/s and (b) 2×10^{3}/s
ULS: ultra low carbon mild steel
SSH440: TS440MPa grade solid solution hardening steel
DP590: TS590MPa grade dual phase steel

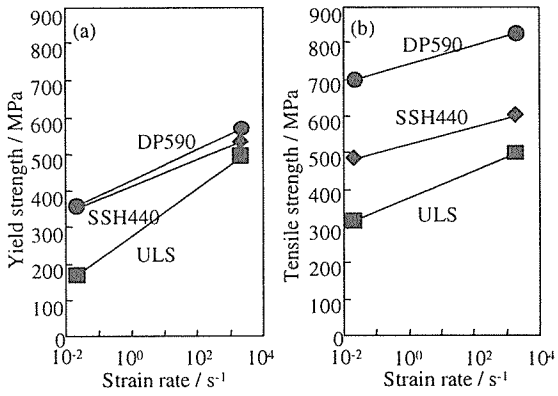

Fig.2 Effects of strain rates on (a) yield strength and (b) tensile strength

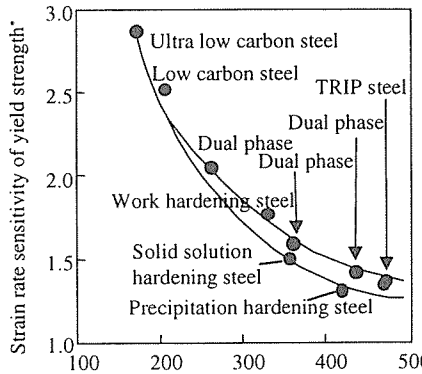

*)Strain rate sensitivity of yield strength

$$= \frac{\text{Yield strength at strain rate of } 2 \times 10^{3}\text{/s}}{\text{Yield strength at strain rate of } 2 \times 10^{-2}\text{/s}}$$

Fig.3 Relationship between strain rate sensitivity of yield strength and yield strength at strain rate of 2×10^{-2}/s

$2x10^3$/s with the Hopkinson Pressure Bar method. Figure 4 shows the effect of the volume fraction of martensite and the strain rate on yield strength. Under high strain rate deformation, yield strength increases with increasing the volume fraction of martensite. Figure 5 shows the effect of surface area of martensite grain on tensile strain hardening exponent (n-value). N-value was calculated by stress and strain at 7.5% and 12.5% strain. In this testing, the sample of martensite grain size was varied under the condition of constant martensite volume fraction in range of 4 to 6.5%. That is the increasing of surface area of martensite grain means the decreasing of martensite grain size. N-value increases with increasing the surface area of martensite grain.

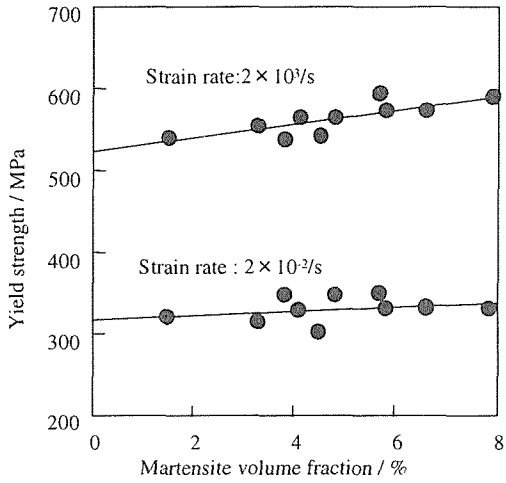

Fig.4 Effect of martensite volume fraction on yield strength of 590MPa tensile strength grade dual phase steels

3. Discussion

It is thought that dual phase steel has large n-value in early stage of deformation at low strain rate due to storage internal stress, but n-value become decrease with an increase in the deformation due to the relaxation of internal stress. [4] However, as shown as figure 6, n-value doesn't decrease with increase in the deformation at strain rate of $2x10^3$/s. The increase of strain rate reduces the influence of thermal vibration energy on dislocation activity, and it must be difficult to reduce the relaxation of internal stress. Therefore n-value increases with increasing the strain rate, and doesn't decrease with increase in the deformation. Correspondingly, the increase of martensite volume fraction must be require the large external stress to increase of the moving speed and multiplication of dislocation at strain rate of $2x10^3$/s. It is seemed that decreasing of martensite grain size reduces the relaxation of internal stress.

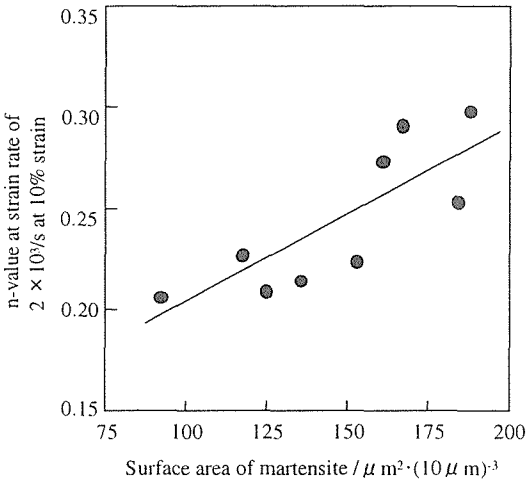

Fig.5 Effect of surface area of martensite grain on n-value at strain rate of 2 × 10³/s of TS590MPa grade dual phase steels

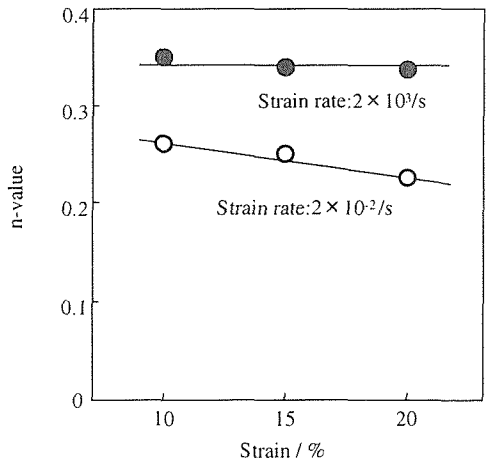

Fig.6 Effects of strain rate on relationship between n-value and strain in dual phase steel.

References

[1] K. Miura, S. Takagi, T. Hira, O. Furukimi: SAE Technical Paper Series, #980952(1998)

[2] S.Takagi, K.Miura, T.Hira, T.Shimizu, S.Tanimura: 31st ISATA Proceeding(1998) 98NM008

[3] S. Takagi, K. Miura, O. Furukimi, T. Obara, T. Kato, S. Tanimura: Tetsu-to-hagane 83 (1997), No.11, pp.748-753.

[4] Y. Tomota, I. Tamura: Tetsu-to-hagane 68 (1982), 1147.

Modelling of Microstructural Evolution and Prediction of Mechanical Properties of Strip Steel in Hot Rolling Process

L.M. WANG, D.Z. LI, Y.J. LAN, C.L. MO, Y.T. ZHANG and Y.Y. LI
Institute of Metal Research, Chinese Academy of Sciences, 110016, P. R. China

1. Introduction

Number of groups have been actively studying the evolution of austenite during roughing and finishing process, phase transformation during cooling process and grain growth during coiling process, and the quantitatively relationship between microstructure and mechanical properties [1-2]. The work in laboratory is mainly concerned the development of concept of metallurgical modeling, and the industries applied the developed models in mill plant, and several in- house software had been developed [3-4]. Each model is limited to its own production line, and must modify the coefficients when it is used in other mill plant. Our institute incorporated with Ansteel in China has been developing its own computer model for rolling analysis (ROLLAN), which incorporates thermal-mechanical, recrystallization, transformation and mechanical properties. Firstly, it is used off-line, and then on-line based on the research work of plain carbon steel, C-Mn steel and micro-alloyed steel. Large production data and testing has been used to check the models.

2. Thermal-mechanical/microstructural models

The core of thermal-mechanical models is the temperature evolution model. In the roughing and finishing part, the key factors are air cooling, water spray cooling, heat transmission by conduct, heat generation by friction and heat generation by deformation. The contribution of each item to the temperature evolution is calculated respectively. In typical points, such as roughing exit temperature (RT2), finishing exit temperature (FT7) and coiling point (CT), the calculated results will compare with the measured results. If deviation is large, the self-learning coefficient will be used to adjust the data and satisfy the accuracy requirements.

The recrystalization and phase transformation model of plain carbon steel was mainly based on the work of Sellars and Hodgson, but modified to cover the requirements of Ansteel. The decomposition of austenite is predicted based on Avrami equation. The grain size of ferrite is calculated along length direction. Considering the gradually growth of grains during coiling process, the model of coarsening is adopted to predict grain size after coiling process. For structure-property equations, Hall-Petch equation is used to predict yield strength, tensile strength. As for elongation, there is no distinct relationship with grain size, for individual mill line, the regression equation should be changed.

3. Application

Plain carbon steel Q235 in 1780 mill line of Ansteel covers a wide thickness strip from 2mm to 15mm, and it is applied to examine the model. The routes include seven passes for roughing and seven passes for finishing. As shown in Fig.1, ROLLAN has four main functions, which can optimize alloy design and prediction of mechanical properties. The database in Fig.1 includes much information about physical properties of materials, and reduction rate in each pass.

If primary austenite grain size is 300μm, after repeated recrystalization and refine of grain

size, the entrance grain size is about 70μm, and the exit is about 20μm. Other important parameters is also calculated, such as rolling force, inter-pass time and 50% recrystallization time, temperature evolution, strain and strain rate, residual strain and critical strain. Temperature is the most important parameter in the process, RT2, FT7, CT should be controlled, the vibration of RT2 should be less than 20 °C, FT7 should be 15 °C, and CT should be limited to 10°C.

Fig.2 shows the ferrite grain size after coiling, the finest grain size is in the tail section, about 8μm, while head section is in the medium, about 10.5μm, the coarsest grain size is 11.5μm, near the center section. The tail section has the better tensile strength, yield strength and elongation, while the center part has lower properties. Compared the target properties with real properties, nearly 20MPa difference is found in tail end.

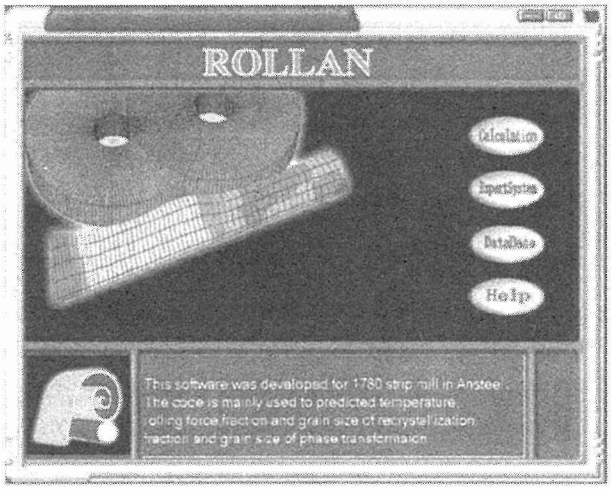

Fig.1 The main interface of ROLLAN software in hot rolling process.

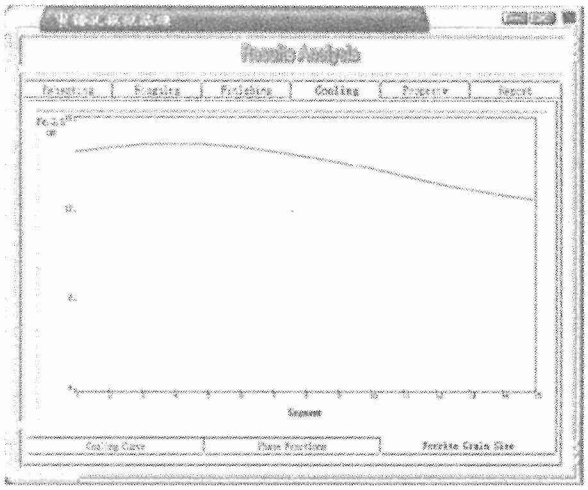

Fig.2: The ferrite grain size evolution after coiling.

4. Conclusions

ROLLAN software is developed to predict the microstructure evolution and mechanical properties in Ansteel strip steel line. The off-line models have been used to analyze the influence of key parameters and optimize the chemical composition of strip steel. The good agreement between measured and calculated values is obtained. Through sensitivity analysis, typical temperatures RT2, FT7 and CT have been accurate controlled.

References

[1] Fulvio SICILIANO, and Jonas, J, Mathematical modeling of the hot strip rolling of microalloyed Nb, multiply –alloyed Cr-Mo, and plain C-Mn steels. Metall. and Mater. Trans., A, 31(2000), pp.511-529.

[2] Cobo S.J. and Sellars C.M, Microstructural evolution of austenite under conditions simulating thin slab casting and hot direct rolling. Ironmaking and Steelmaking 28(2001), No.3, pp.230-236.

[3] Andorfer Josef, Dietmar Auzinger and Gerhard Hubmer, Operational experience with VAI-Q Strip: on-line system for controlling hot rolled strip mechanical properties. Steel Technology, July/August 2000, pp.43-46.

[4] Maccagno T.M., Jonas J. and Hodgson P.D, Spreadsheet modeling of grain size evolution during rod rolling. ISIJ Inter., 36(1996), No.6, pp.720-728.

High Speed Deformation for an Ultrafine-grained Ferrite-Pearlite Steel

N.Tsuchida[*1], Y.Tomota[*2] and K.Nagai[*3]

[*1] Domestic Research Fellow, Japan Society for the Promotion of Science, Japan

[*2] Department of Materials Science, Ibaraki University, Japan

[*3] Steel Research Center, National Institute for Materials Science, Japan

1. Introduction

Ultrafine-grain strengthening is effective to increase strength without using alloying elements. Dual phase strengthening like in ferrite-pearlite (FP) steels also plays an important role to improve a balance between strength and elongation [1]. According to the Hall-Petch equation [2] describes the effect of grain size on flow stress; $\sigma=\sigma_0+\mathbf{k}\mathbf{D}^{-1/2}$, where σ means flow stress, σ_0 and $\mathbf{k}$ constants and $\mathbf{D}$ ferrite grain size, flow stress increases abruptly in ultrafine-grain range below 5 μm. We have investigated the effects of temperature, strain rate and ferrite grain size on stress-strain curve for FP steels with ferrite grain size between 3.6 and 46.2 μm [3]. Results of static tensile test for the FP steels showed that the effects of temperature and strain rate on tensile flow stress were almost the same independent of ferrite grain size and that effect of ferrite grain size on tensile flow stress was almost independent of temperature and strain rate. In this study, a high speed tensile test with a strain rate of 10^3 s^{-1} for an ultrafine-grained FP steel below 5 μm was conducted to investigate high speed deformation. We also investigate the effects of temperature, strain rate and ferrite grain size on tensile flow stress by comparing with the results obtained by static tensile test.

2. Experimental procedures

Three ferrite-pearlite (FP) structures with ferrite grain sizes of 3.6, 9.8 and 46.2 μm were prepared by microstructural control for a JIS-SM490 (0.15C-0.4Si-1.5Mn (mass%)) steel. The ultrafine-grained FP steel with 3.6 μm was obtained by austenitization for 3.6 ks at 1173 K, and then was subjected to rolling with an accumulated area reduction of 90 % at 1053 K. The FP steels with 9.8 and 46.2 μm were prepared by furnace cooling after austenitization for 600 s at 1173 K and for 5.4 ks at 1423 K, respectively. A sheet specimen for dynamic tensile test with a gauge length of 3.8 mm was prepared. A split Hopkinson pressure bar tester [4] was used to conduct the high speed tensile test with the strain rate of 10^3 s^{-1} at 77, 210 and 296 K. Tensile tests with strain rates between 10^{-6} and 10^0 s^{-1} were performed by using test specimens with diameter of 3.5 mm and gauge length of 25 mm at the same temperatures.

3. Results and discussions

Figure 1 shows nominal stress-nominal strain curves for the ultrafine-grained FP steel with strain rates between 10^{-6} and 10^3 s^{-1} at 296 K. Flow stress became higher with

increasing strain rate and decreasing ferrite grain size. Uniform elongation became smaller with decreasing ferrite grain size. **Figure 2** shows 10% flow stress as a function of inverse square root of ferrite grain size ($\mathbb{D}^{-1/2}$) with 10^{-4}, 10^{0} and 10^{3} s^{-1} at 296 K. The 10% flow stress can be described as a function of $\mathbb{D}^{-1/2}$ by the Hall-Petch equation. The constant k of the equation is almost constant independent of temperature and strain rate. The effect of ferrite grain size on flow stress was independent of temperature and strain rate. That means the effect of ferrite grain size on flow stress contributes to only athermal stress which does not depend on temperature and strain rate.

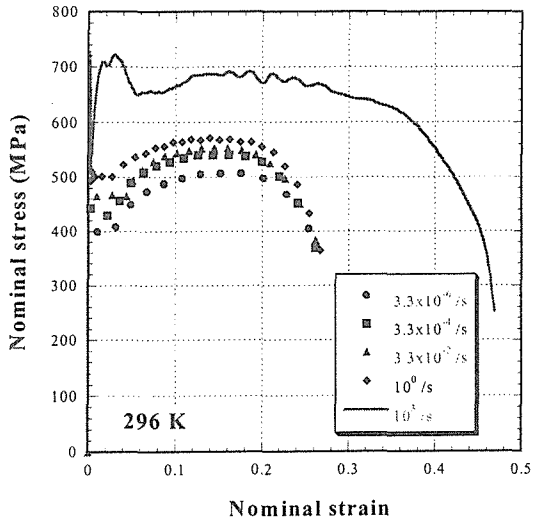

Fig. 1 Nominal stress-nominal strain curves for the ultrafine-grained FP steel with strain rates between 10^{-6} and 10^{3} s^{-1} at 296 K.

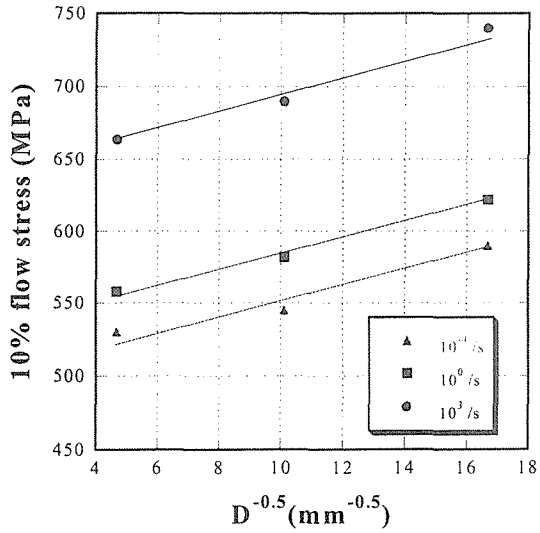

Fig. 2 10% flow stress as a function of inverse square root of ferrite grain size with strain rates of 10^{-4}, 10^{0} and 10^{3} s^{-1} at 296 K.

References

[1] For example, K.Nagai, *J. Materials Processing Technology*, **117**, (2001), pp.329-332.

[2] N.J.Petch, *J. Iron and Steel Inst.*, **174**, (1953), pp.25-28.

[3] N.Tsuchida, T.Ono, Y.Tomota and K.Nagai, *to be submitted.*

[4] K.Miura, S.Takagi, O.Furukimi, T.Obara and S.Tanimura, SAE960019 (1996).

High Strength Steels and Their Application to Improve Crash Energy Absorption Property of Auto Bodies

M. Takahashi, H. Yoshida, A. Uenishi and Y. Kuriyama
Steel Research Laboratories, Nippon Steel Corporation, Japan

1. Introduction

There is an increasing demand for improving crashworthiness of vehicle to meet the requirement of the safety regulation. To satisfy the requirement, the weight of auto body tends to increase due to the introductions of various types of reinforcements. This trend contradicts to the energy consumption requirement from CO_2 emission point of view. One of the solutions to answer these contradictory requirements is an intensive use of high strength steels. Effects of the geometry of structures and mechanical properties of steels used on the absorbed energy during crash event will be discussed here.

2. Crash energy absorption property of square tubes

In the case of frontal crash of vehicles, the energy absorbing components such as front side members receives axial forces, which cause buckling deformation of the thin wall tube structure. The absorbed energy during an axial crush test of thin wall tubes increases with the wall thickness [1], size of the cross section [2], number of corners and strength of the materials used [1]. Fig.1 is an example of the calculated absorbed energy during crush test of a square tube. The dynamic deformation behavior has been visualized and analyzed in detail using finite element method (FEM). The FEM analysis has revealed that the strain rate during the crash event of thin wall tubes can reach 10^3/s [1]. When the ratio between the size of the cross section and the wall thickness of square tubes is altered, the mode of buckling changes from compact to non-compact (Fig.2). For a given size of the cross section, the thinner the wall thickness, the less regular buckling (non-compact mode) is observed. It should also be noted that the buckling mode changes from non-compact to compact when the work hardenability of material at high strain rate is increased [3].

3. High strength steels for crash energy absorption

The absorbed energy during an axial crush event of a square tube increases with the strength of the steel used as shown in Fig.1. It is, however, reported that multi-phase type-high strength steels such as ferrite-martensite dual-phase steels and ferrite-bainite-retained austenite TRIP type steels show higher energy absorbing property than conventional high strength steels (Fig.3). There are two different factors which enhance strength of steels during high strain rate

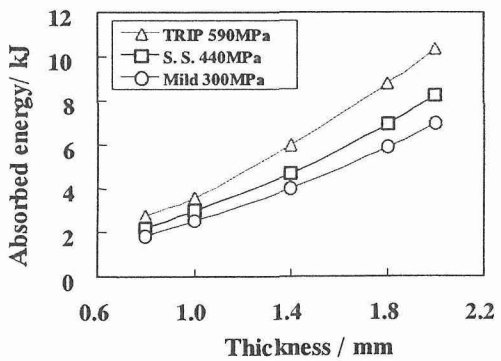

Fig.1. Calculated absorbed energy during an axial crash event of a 70×70mm square tube. Materials used are TRIP-type 590MPa, solution strengthened 440MPa and 300MPa mild steels.

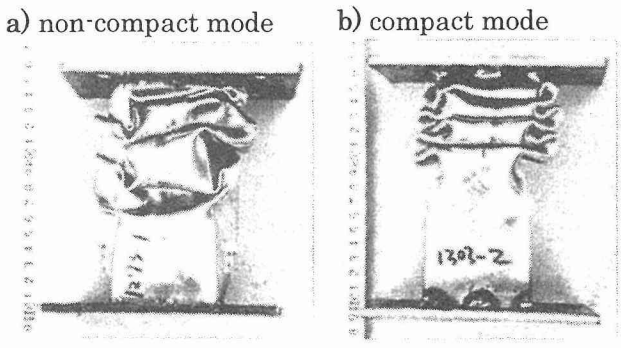

Fig.2. Square tubes after an axial crush test. The ratios between the wall thickness and the width of the 70×70mm tubes are a) 0.011 and b) 0.026 respectively.

deformation. The first factor is a high strain rate dependence of these multi-phase type-high strength steels mainly due to soft ferrite phase. The strain rate dependence of TRIP type steels is enhanced by an accelerated martensite transformation during deformation at higher strain rates. Martensite transformation is observed to be accelerated at higher strain rates during uni-axial tensile tests as shown in Fig.4.

The second factor is the effect of pre-strain and baking. When the steel contains carbon or nitrogen in solid solution, these interstitial atoms cause an increase in flow stress during baking after press forming. Multi-phase type-high strength steels are known to show relatively large amount of bake hardenability. Although the strain rate dependence of flow stress decreases with increasing the quasi-static strength of steels, the increase in quai-static strength by pre-strain due to press forming and baking does not deteriorate the strain rate dependence of the flow stress (Fig.5).

Since the formability of these multi-phase type-high strength steels are better than conventional high strength steels, dual-phase type and TRIP type high strength steels show excellent press formability-energy absorption combination as shown in Fig.6.

4. Conclusions

Multi-phase type-high strength steels such as dual-phase steels and TRIP type steels are found to show higher energy absorbing property than conventional high strength steels. Pre-deformation and baking are found to enhance the superiority. These formable high strength steels are believed to contribute to improve crashworthiness of auto bodies without deteriorating the fuel consumption.

References

[1] Uenishi,A., Suehiro, M., Kuriyama, Y. and Usuda, M.: IBEC'96, Aotomotive Body Interior & Safty Systems, (1996), p.89.

[2] Sato, K., Yoshitake, A., Hosoya, Y. and Yokoyama, T.: IBEC'97, Automotive Body Materials, 31(1997), p.1.

[3] Uenishi, A., Kuriyama, Y., Usuda, M. and Suehiro, M.: IBEC'97, Automotive Body Materials, (1997), p.59.

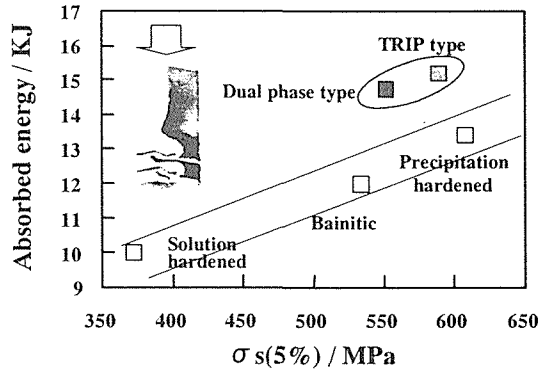

Fig.3. Calculated absorbed energy during an axial crash event of a 70×70mm square tube as a function of the flow stress at 5% of strain during quasi-static tensile test.

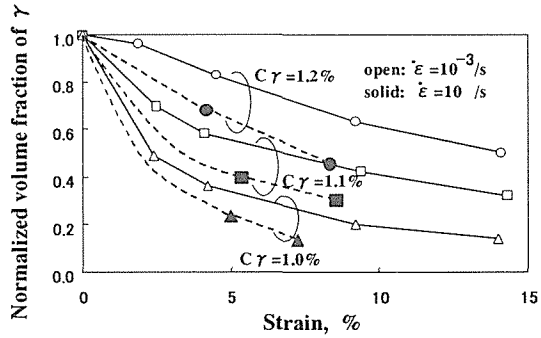

Fig.4. Effect of strain rate on martensite transformation during uni-axial tensile test on TRIP type-high strength steels. The carbon concentration in retained austenite was altered by heat treatment.

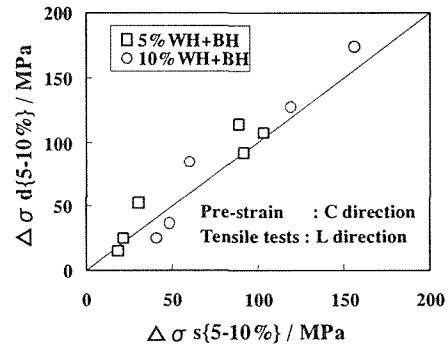

Fig.5. Relation between increases in quasi-static flow stress and increases in dynamic flow stress by baking for 20 minutes at 170 ℃ after 5% and 10% of pre-strains (WH) in the transverse direction (C).

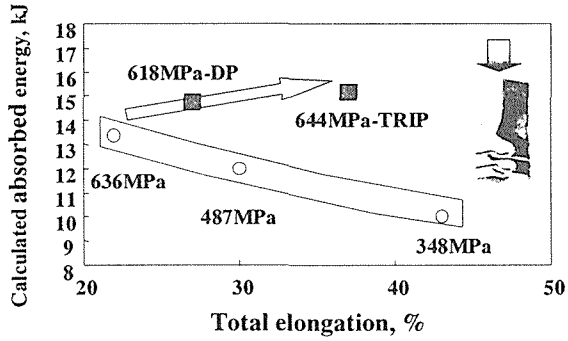

Fig.6. Combination between total elongation and calculated absorbed energy during an axial crush event of a square tube.

Behavior of Fine Lath-Like Microstructures during Tensile Test

S.W. Yang, C.J. Shang, X.M. Wang, X.L. He

Materials School, University of Science and Technology Beijing, China

Hall-Petch formula has provided a basis for predicting the strength of polycrystal materials. However, it is difficult to define their grain size while the formula is applied to lath-like microstructures. Experimental investigation on deformation behavior is essential to establish the relation between their mechanical properties and structures. Deformation of lath-like martensite in shape memory alloys has been widely studied[1-5], but the emphasis is put on different aspects. This paper aims at elucidating the change of fine lath-like microstructures during all stages of tension.

1. Materials and Experimental Procedures

The material utilized in this investigation is a microalloyed steel which contains (in mass%) 0.033C, 0.0013B, 1.74Mn, 0.094Nb, 0.057Ti, 0.25Ni and 0.31Mo. The steel was melt in a 25kg vacuum induction furnace and then rolled in two stages to obtain 6mm thick plates before cooled in air or water. One of the plates was reheated to 1200℃ and isothermally held for 1h, then cooled in water. All the plates cooled in water was tempered at 675℃ for 3h.

Plate-shaped tensile samples were cut from the steel plates with axes of samples paralleling to rolling direction. The samples were tensioned monoaxially at a rate of 3mm/min until fracture took place. Optical examination was carried out along side-faces of the samples, which were etched with a 3% nital, on undeformed parts, uniformly deformed parts and regions near fracture (necking parts) respectively.

2. Experimental Results

By optical examination, it was found that all samples exhibit microstructures mainly constituted by lath-like bainite (Fig.1), the lathes arrange as sheaves. In the undeformed parts of all samples, orientation of sheaves is random. A distinction between reheated samples and the others is that lathes in the former are longer than 50μm in general while the latter is composed by lathes shorter than 10μm. When deformation occurs, lathes show a tendency to turn their long axis towards tensile direction. But in the uniformly deformed part of all samples, the turn is not obvious. In the reheated samples, lathes in the region next to fracture turn and become curved. In the other samples with short lathes, it is surprising to find out that almost all lathes parallel to tensile axis in the necking parts, displaying that some lathes have turned near 90 degrees angle. In the necking part of sample cooled in water after rolling, cracks paralleling to tensile direction can be seen. This kind of crack is caused by large turn of lathes. If a sample possesses good plasticity, as the sample cooled in air, or the extent of turn is small, as that occurring in the reheated sample, cracks may not occur. The distinction is also demonstrated on steps of fractures due to same reason (Fig.2).

3. Discussion

All the results mentioned above point to a reason that not only the sheaves boundaries but also the boundaries between lathes can inhibit movement of dislocations and the effect causes a natural selection of practically movable glide system. The glide system with its glide plane at the least angle to wide face of lath has a advantage over other systems, so that mono-glide of the system dominates during the deformation and the orientation of lathes continue to turn. In the long lath microstructure, due to difficulty on coordinate movement of neighboring sheaves and lathes, the turn cannot be thorough.

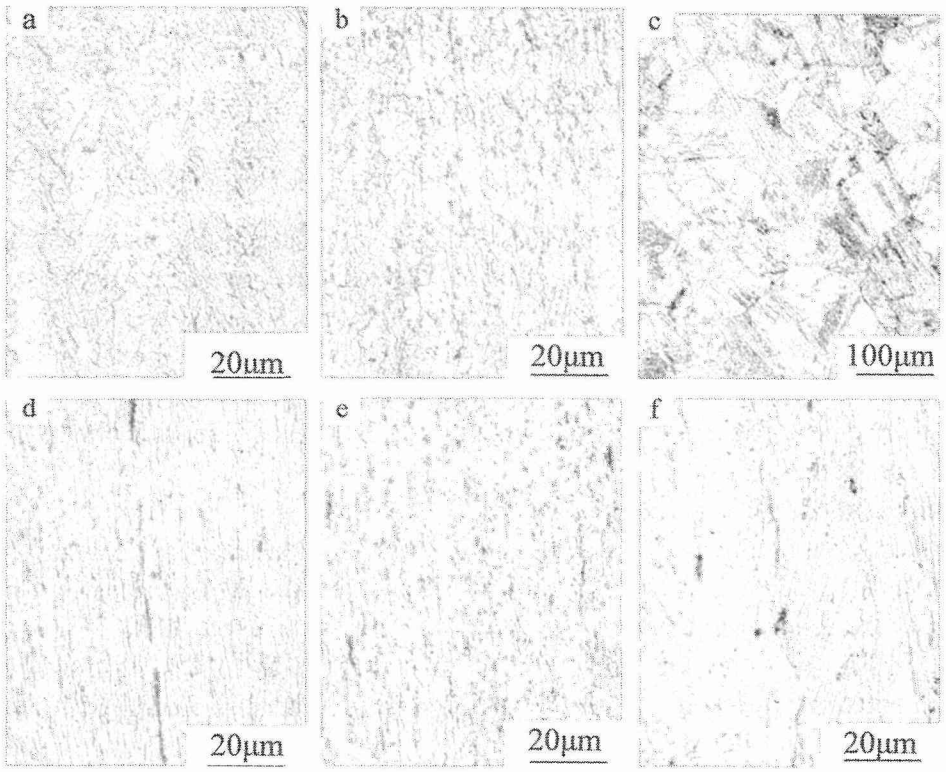

Fig.1 Micrographs of sample cooled in water (a, d), sample cooled in air (b, e) and reheated sample (c, f), including undeformed parts (a, b, c) and necking parts (d, e, f)

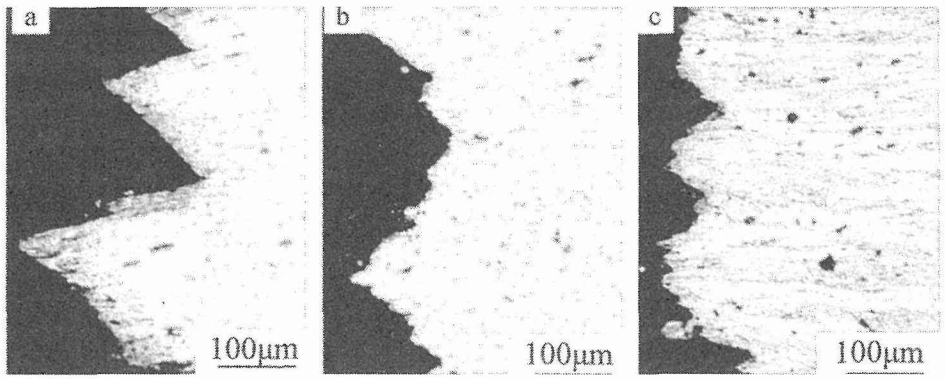

Fig.2 Fractures of sample cooled in water (a), sample cooled in air (b) and reheated sample (c)

References

[1] Schroeder, T. A. and Wayman, C. M, The formation of martensite and the mechanism of the shape memory effect in single crystals of Cu-Zn alloys. Acta Metall 25(1977), pp.1375-1391.

[2] Saburi, T. and Wayman, C. M, The shape memory mechanism and related phenomena in Ag-45at.% Cd. Acta Metall 28(1980), pp. 1-14.

[3] Kim, Y. D. and Wayman, C. M, Shape recovery and phase transformation behavior in Ni-Al alloys. Metall Trans 23A(1992), No.11, pp.2981-2986.

[4] Liu, Y. N. Liu, Y. and Van Humbeeck, J,. Two-way shape memory effect developed by martensite deformation in NiTi. Acta Mater 47(1999), No.1, pp.199-209.

[5] Liu, Y. Xie, Z. L. and Van Humbeeck, J. et al, Effect of texture orientation on the martensite deformation of NiTi shape memory alloy sheet. Acta Mater 47(1999), No.2, pp.645-660.

EFFECTS OF TITANIUM ADDITION ON PRECIPITATE AND MICROSTRUCTURAL CONTROL IN C-Mn MICROALLOYED STEELS

M. Vedani, F. D'Errico, A. Mannucci

Politecnico di Milano, Dipartimento di Meccanica
Piazza Leonardo da vinci 32, I-20133 Milano, Italy
maurizio.vedani@polimi.it

INTRODUCTION

Transverse and edge cracking can be a serious concern in several continuously cast structural steels. Cracking is found to develop along austenite grain boundaries and it is encouraged by precipitation of Al and Nb rich compounds. Titanium is known as one of the elements that can alleviate such form of hot cracking by refining the austenite grains. Although its effects are known from practice experience, some doubt still remain on the optimal Ti/N content to be used in different steel grades and on the detailed sequence of precipitate and inclusion generation, especially in HSLA steels.

The effects of Ti addition on precipitation and microstructural behaviour of a microalloyed steel grade was studied with the aim of improving the knowledge on interaction between titanium nitrides formed at high temperatures, and other phases that precipitate in the austenite matrix in a following time during cooling. A linepipe C-Mn steel grade microalloyed with Nb and V was considered both in a standard heat, produced according to established practice, and in a modified version, alloyed with 0,14% Ti. The composition of the heats investigated are given in table I

Table I. Chemical compositions of the materials investigated (mass%)

	C	Cr	Cu	Mn	Mo	N	Nb	Ni	P	S	Si	Sn	Ti	V	Al
STD	0,11	0,12	0,12	1,05	0,09	0,0066	0,024	0,09	0,010	0,001	0,30	0,010	0,005	0,044	0,026
Mod. Ti	0,11	0,08	0,12	1,02	0,08	0,0056	0,022	0,09	0,012	0,002	0,25	0,006	0,014	0,044	0,026

Investigations were carried out to microstructurally and mechanically characterise the two heats by optical, scanning and transmission electron microscopy and by impact and tensile testing. Particular emphasis was given to inclusion and microprecipitate effects found in the steels.

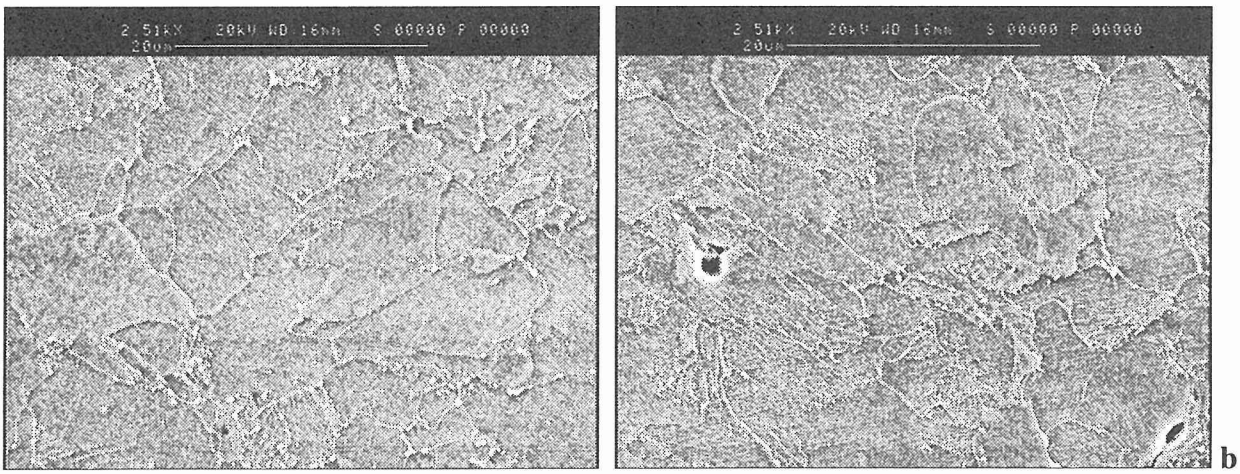

a b

Figure 1. SEM micrographs of the steel investigated; a) STD grade, b) Ti modified grade

Representative SEM micrographs of the steels investigated are given in figure1. The two heats had a duplex ferrite-bainite structure, the Ti modified heat featuring a slightly higher amount of bainite.

A theoretical study was then undertaken by using a commercial thermodynamic calculation code (Thermocalc) and a more specific numerical model developed to assess microalloying element precipitation (ref.: H. Adrian, Proc. Int. Conf. "Microalloying '95", Pubblisher: Iron and Steel Society, Warrendale, PA (1995) pp.285-305) to elucidate phase stability as a function of temperature for the specific compositions studied. In figure 2 a plot of the predicted phase obtained by Thermocalc is presented for the Ti modified steel grade.

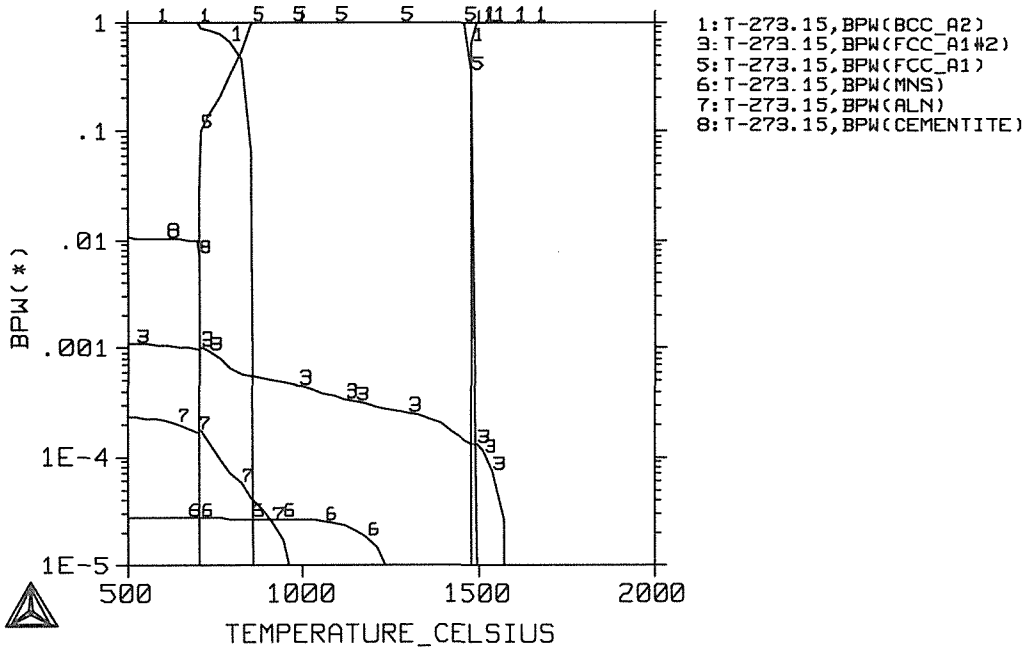

Figure 2. Theoretical predictions of equilibrium phases formed as a function of temperature (content in weight %) in the Ti modified heat. Label 1) liquid; label 3) Ti-rich (carbo)nitride; label 5) austenite; label 6) MnS; label 7) AlN; label 8) cementite

Comparative calculations performed on the standard grade allowed to state that in the Ti alloyed steel, carbonitrides significantly rich in titanium and nitrogen (curve 3 in figure 2) precipitated in the liquid phase at temperatures exceeding 1500°C whereas Nb and V rich carbonitrides formed in the standard grade only at 1400°C. In addition, the AlN phase would form at equilibrium at about 900°C in the Ti modified steel while in the standard grade it would precipitate at 1100°C.

TEM studies contributed to elucidate the actual microprecipitate morphology and distribution and allowed to draw conclusions on both fundamental and practical aspects related to microalloyed steels and to their steelmaking practice.

Supra-Ductile High-Manganese-TRIP-TWIP-Steels for High Energy Absorption Purposes

G. Frommeyer and P. Neumann

Max-Planck-Institut für Eisenforschung GmbH, Düsseldorf, Germany

1. Introduction

Newly developed austenitic iron-manganese-aluminium (silicon) alloys are showing promising mechanical and technological properties, such as high strength, reduced specific weight, excellent ductility and formability - even at high strain rates and cryogenic temperatures - which are suitable for the development of new types of high strength lightweight steels.

2. Experimental Results

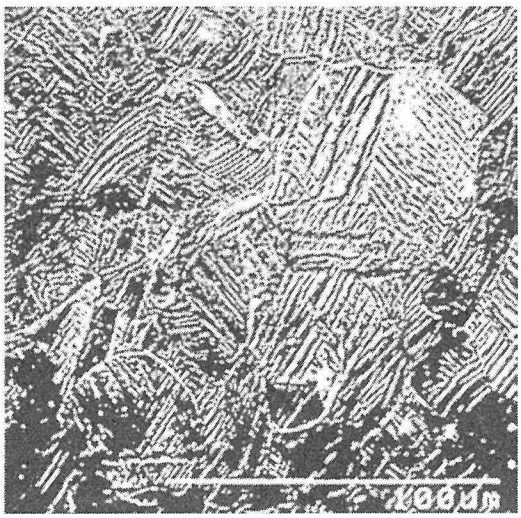

Fig.1.Heavily twinned microstructure of the TWIP steel deformed in tension

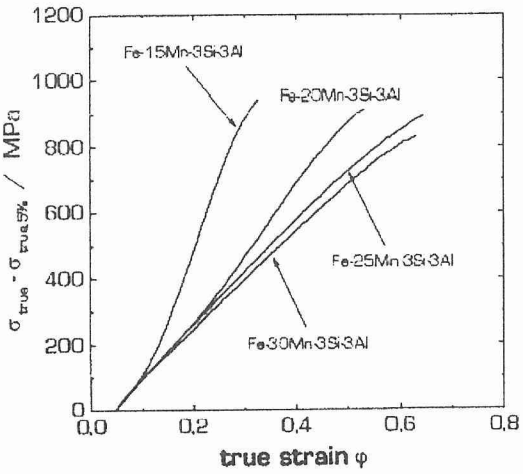

Fig.2.Strain hardening increment vs. true plastic strain.

At high manganese contents of about 20 to 30 at-% and at medium aluminium contents of about 10 to 15 at-% with certain amounts of carbon, the austenitic γ-phase is fully stabilized. Addition of silicon to the high manganese-aluminium steels destabilizes the austenite and decreases the stacking fault energy so that subsequent martensitic transformations ($\gamma_{fcc} \rightarrow \varepsilon_{hcp}$, α'_{bcc}) occur (multiple TRIP effect [1]) or enhanced mechanical twinning formation ($\gamma \rightarrow \gamma'_{TWIN}$) takes place (TWIP effect). Both mechanisms will contribute a considerable amount of plasticity to the total plastic deformation potential of these steels [2].

Which mechanism dominates, depends on the manganese to aluminium and silicon ratio resulting in different stacking-fault energies, γ. With $\gamma < 20$ mJ/m^2, the $\gamma \rightarrow \varepsilon$ phase transformation is favoured and the TRIP effect is obtained, and with $\gamma > 20$ mJ/m^2, the phase transformation is suppressed [3] and heavy twinning formation is sustained (TWIP effect).

In the present work, the mechanical properties of Fe-Mn alloys with additions of aluminium and silicon were investigated. Specifically, the tensile properties of the Fe-25Mn-3Si-3Al alloy were determined at different strain rates and temperatures in order to correlate micro-structural features with flow stress and elongations. Deformation twinning and the formation of strain-induced martensite were analysed.

The characteristic microstructure of the TWIP steel is illustrated in figure 1. The TWIP steel reveals pronounced mechanical twinning $\gamma_{fcc} \rightarrow \gamma^*_{twin}$. This deformation mechanism causes linear

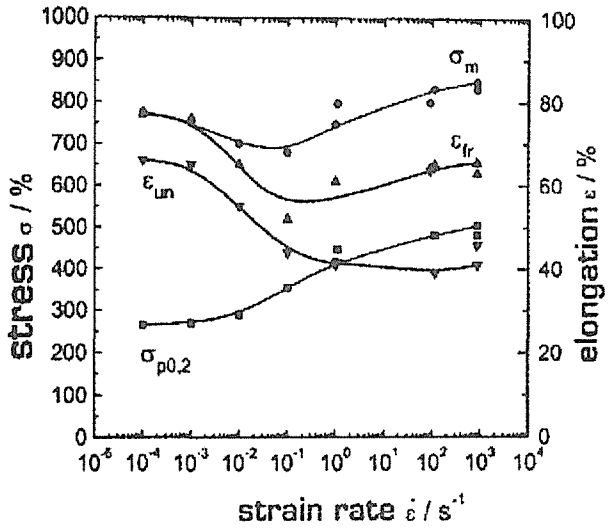

Fig.3.Mechanical properties as a function of the strain rate of the TWIP steel at 20°C.

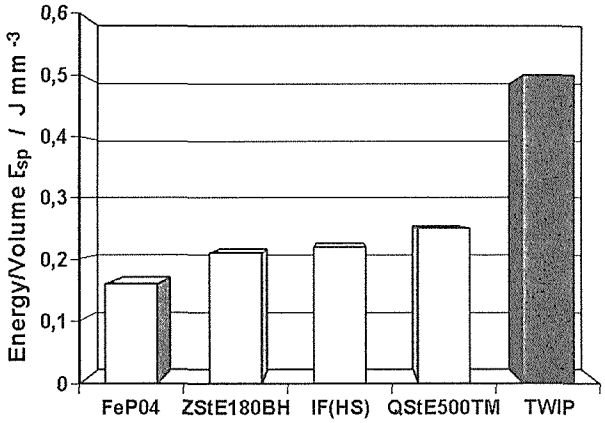

Fig.4.Energy absorption per unit volume of conventional deep drawing steels and the TWIP steel at 20 °C and $\dot{\varepsilon} = 10^2\ s^{-1}$.

work hardening over a large stress range (figure 2), which in turn - due to Considère's criterion – results in a large uniform elongation and a large strain to failure for tensile samples. The changes in yield stress $\sigma_{p0.2}$, tensile strength σ_m, uniform elongation ε_{un} and strain to failure ε_{fr} of the TWIP steel as a function of the strain rate from 10^{-4} to $10^3\ s^{-1}$ are shown in figure 3. With increasing strain rate the yield strength is increasing from 250 MPa at $10^{-4}\ s^{-1}$ to about 530 MPa at very high strain rates of $10^3\ s^{-1}$. The steady increase of the tensile strength from 600 to 800 MPa beyond the strain rate of $10^{-2}\ s^{-1}$ is remarkably high. The uniform elongation is decreasing with increasing strain rate up to about $10^{-1}\ s^{-1}$. The total elongation has a minimum value of 55 % at the strain rate of $10^{-1}\ s^{-1}$. No phase transformation was detected by X-ray diffraction and TEM investigations.

A very important parameter which characterizes the impact behaviour of deep drawing steels for automotive bodies and frame structures is the specific energy absorption E_{spec}, defined as the deformation energy per unit volume at a given temperature and strain rate of the order of 10^2 to $10^3\ s^{-1}$. The block diagram of figure 4 represents the specific energy absorption of the TWIP steel in comparison with some selected conventional deep drawing steels, such as FeP04, ZStE180BH, high strength IF(HS) and QStE500TM, respectively. It is obvious from the diagram that the specific energy absorption value of the TWIP steel is about twice of that of conventional deep drawing steel qualities. This extraordinary energy absorption of the extraordinary crash and impact resistant high strength TWIP steel is due to the extensive twinning formation under high strain rate conditions.

3. References

[1] Hong, S.H. and Han, Y.S. Scripta Met. et Mater., 32(1995), pp. 1489-1494.

[2] Grässel, O., Frommeyer, G., Derder, and C.,Hofmann, H. J. Phys. IV France 7(1997), C5, pp. 338-388.

[3] Sato, K., Ichinose, M., Hirotsu, Y., and Inane, Y. ISIJ Int., 29(1989), pp. 868-877.

Deformation Behavior of Low Carbon TRIP Steels at High Strain Rates

I.D. Choi[1], S.J. Kim[2], C.G. Lee[2], S.H. Park[3], D. Bruce[4], D.K. Matlock[4]
1. Dept. of Mech. & Mat. Eng., Korea Maritime University, Busan, Korea
2. Dept. of Materials Processing, KIMM, Changwon, Korea
3. Automotive Steels Research Center, POSCO, Kwangyang, Korea
4. Dept. of Met. & Materials Eng., CSM, Golden, CO, USA

The safety of passengers is very important during an automobile collision. Because the collision is the event of high speed deformation, the data and deformation mechanisms of materials under high strain rates are needed to choose proper materials for automobiles.

Therefore, in this study, dynamic mechanical properties of low carbon TRIP steels with various amount of retained austenite were evaluated over a wide range of strain rates (10^{-3} to $2.5x10^{2}$ s^{-1}) using a high-velocity hydraulic tensile testing machine. The effects of retained austenite and carbon content on the strain rate hardening capability were studied.

Two kinds of steel ingots, termed ECO-5 and ECO-6 were fabricated by vacuum induction melting and aluminum killing. Steel ingots were rough rolled to slabs of 25mm in thickness and then cold-rolled to sheets of 0.8mm in thickness. Table 1 lists their chemical compositions together with the A_{c1}, A_{c3} and martensite start (M_s) temperatures measured using a dilatometer. Steels were intercritically annealed for 5 minutes at 810°C for ECO-5 and 790°C for ECO-6. After intercritical annealing, specimens were isothermally treated at 450°C for 3 minutes (ECO-5A) and at 430°C for 5 minutes (ECO-6A) to attain the highest volume fraction of retained austenite. ECO-5B and ECO-6B steels, which aimed to have a low volume fraction of retained austenite, were isothermally treated at 470°C (ECO-5B) and 500°C (ECO-6B) for 20 minutes, respectively. Tensile specimens (longitudinal direction) with gage length of 50mm and width of 12.7mm were prepared from the cold-rolled steel sheets. All tensile specimens were machined according to ASTM E-8 specification, with one grip section elongated to accommodate a strain gage. The specimens were tensioned at room temperature over the strain rate range of 10^{-3} to $2.5x10^{2}$ s^{-1} using an MTS high rate testing system. The volume fraction of retained austenite was measured using X-ray diffratometry.

Table 1: Chemical compositions (weight percent) critical temperatures (°C) for the TRIP steels studied.

	C	Mn	Si	Cu	P	S	Al	A_{c1}	A_{c3}	M_s
ECO-5	0.10	1.52	1.48	0.51	0.0016	0.0036	0.046	912	750	450
ECO-6	0.14	1.51	1.49	0.51	0.0018	0.0030	0.050	900	750	432

All steels show a homogeneous microstructure with uniform distribution of secondary phases such as bainite and retained austenite. According to X-ray diffractometer analysis, the amounts of retained austenite for ECO-5A and ECO-6A are 11% and 16%, respectively, and the amount of retained austenite for both B steels is less than 3%.

Ultimate tensile strength (UTS) versus true strain rate data are plotted in Figure 1. In general, UTS increases with increasing strain rate. The UTS values for ECO-6 are higher than those for ECO-5 since ECO-6 has higher carbon content. Also, heat treatment "A" produced higher UTS values than heat treatment "B." This behavior was expected since the higher retained austenite

content creates more martensite transformation with strain, which increases both uniform strain and UTS. Figure 1 also displays increasing strain rate sensitivity with increasing strain rate. The strain rate sensitivities of the ECO-5 steels appear higher than those of the ECO-6 steels.

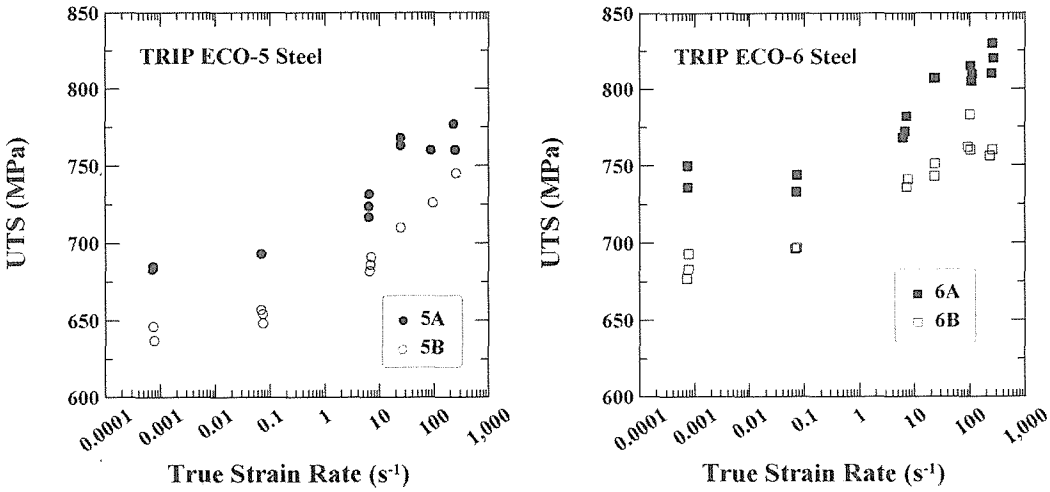

Figure 1 - Ultimate tensile strength versus true strain rate for four different TRIP steels tested at many strain rates.

Flow stress values at 5% true strain were calculated for all tensile samples. 5% flow stress values were chosen instead of yield strength values because a filter present in the data gathering device did not allow collection of accurate yield strength values at strain rates above 10 s^{-1}. Flow stress at 5% true strain versus true strain rate data are plotted in Figure 2. In general, heat treatment "A" produced lower 5% flow stress values than heat treatment "B." This suggests that the yield strengths of the "A" samples are also lower than those of the "B" samples. It is concluded that strain rate hardenability is increased with increasing the amount of retained austenite.

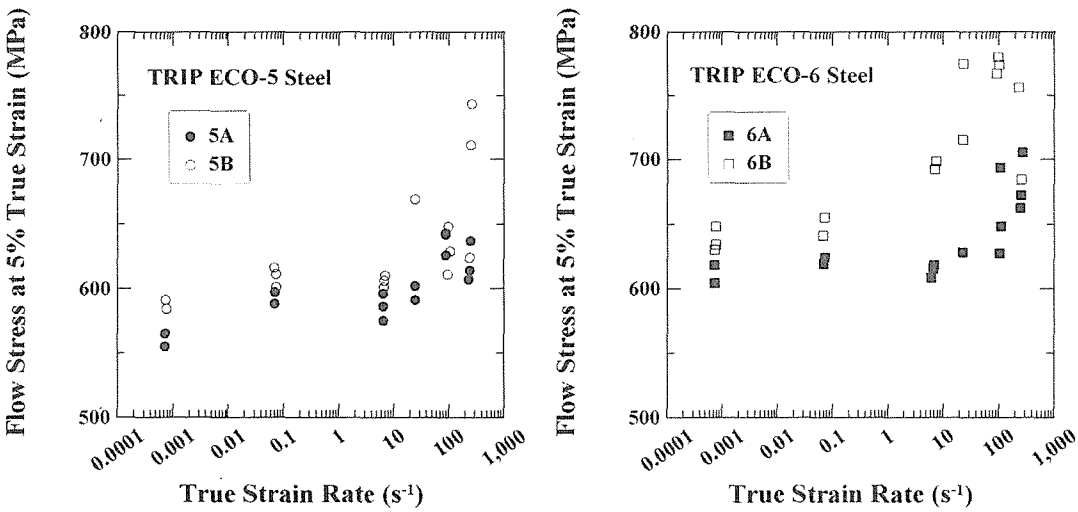

Figure 2 - Flow stress at 5% true strain versus true strain rate for four different TRIP steels tested at many strain rates

Thermal and Mechanical Stability of Retained Austenite in Al-bearing TRIP Steels

S. van der Zwaag[1,2], L. Zhao[1,2], S.O. Kruijver[1,2] and J. Sietsma[2]

[1.] Netherlands Institute for Metals Research, P.O.Box 5008, 2600 GA Delft, The Netherlands

[2.] Laboratory of Materials Science and Engineering, Delft University of Technology, Rotterdamseweg 137, 2628 AL Delft, The Netherlands

The stability of retained austenite is the key issue in low-alloyed multiphase transformation induced plasticity (TRIP) steels. It has been found that many factors, for instance the chemical composition of retained austenite, grain size and morphology, influence the stability of the retained austenite. To understand this subject, both thermal stability and mechanical stability were investigated in this work, by means of magnetic and diffraction techniques.

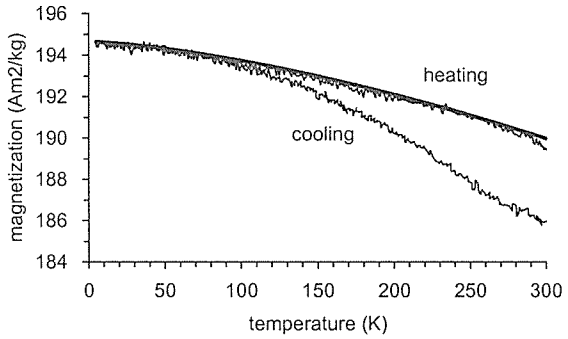

Fig. 1. Temperature dependence of mass magnetization during a thermal cycle.

The thermal stability of austenite in a 0.20C-1.52Mn-0.25Si-0.96Al (wt.%) TRIP steel was studied via thermo-magnetic measurements [1] in the temperature range between 5 K and 300 K at a constant magnetic field of 5 T (Fig. 1). It is found that almost all austenite transforms to martensite upon cooling to 5 K. The M_S and M_f temperatures were derived from the present experimental data to be 355 K and 115 K, respectively. The austenite fraction was calculated from the difference of the magnetization during cooling and heating. The transformation kinetics is found to be well described by the following thermodynamic model [2]

$$f^{\gamma} = f_0^{\gamma}[1-(M_S-T)/(M_S-\beta M_f-(1-\beta)T)]$$

where β is the ratio of the slopes of Gibbs free energy for martensite and austenite versus temperature. Based on this transformation kinetics, the M_S temperature of individual retained austenite grains is analyzed and is mainly attributed to the distribution of carbon concentration in retained austenite.

The mechanical stability of retained austenite in a 0.17C-1.46Mn-0.26Si-0.01P-1.81Al (wt.%) TRIP steel was measured *in situ* using both conventional x-ray diffraction and 3D microdiffraction with synchrotron radiation. From the conventional XRD measurements it is found that the volume fraction of retained austenite f^{γ} decreases as the strain increases according to the Ludwigson and Berger relation [3] ($1/f^{\gamma}-1/f_o^{\gamma}=k\varepsilon$) with $k=72$, in which k describes the mechanical stability of the

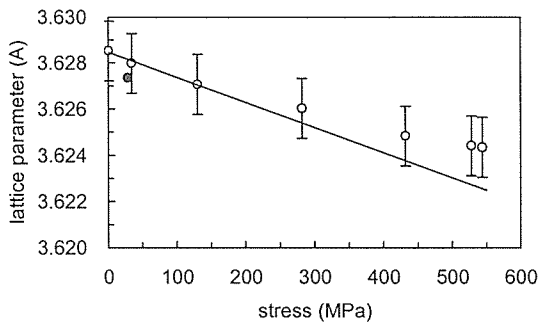

Fig. 2. Stress dependence of austenitic lattice parameters, determined from the in situ x-ray measurements.

retained austenite. From the increase in austenitic lattice parameter with respect to the linear decrease due to elastic strain (Fig. 2), one can see that the average carbon concentration in retained austenite increases with increasing stress, since austenite grains with a low carbon concentration transform at the lower stress values. The integral breadth of the diffraction peaks was also calculated and the dislocation density was thus estimated. The increase in the dislocation density in ferrite increases with increasing plastic strain is thought to assist the martensitic transformation of retained austenite but it is not a predominant factor in comparison with carbon concentration in retained austenite.

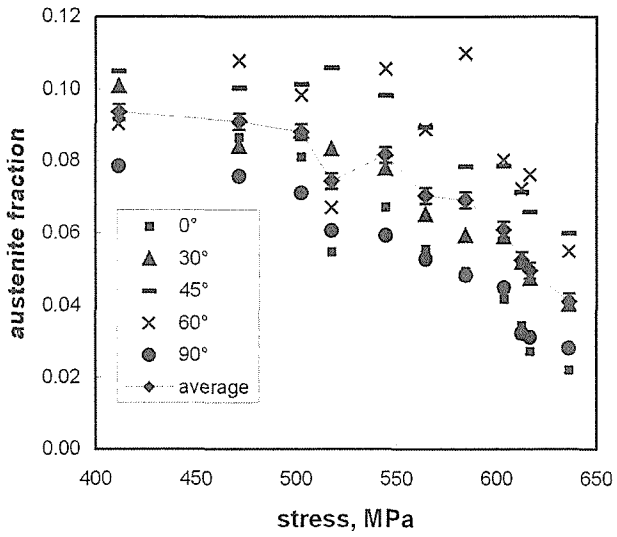

Fig. 3. Orientation dependent austenite volume fraction during in situ tensile testing.

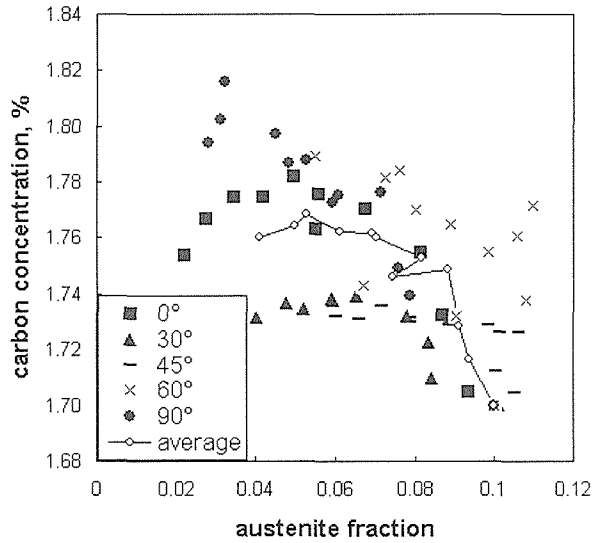

Fig. 4. Carbon concentration versus the retained austenite fraction for different orientations.

From the microdiffraction measurements using synchrotron radiation, the effect of the orientation of the grain with respect to the direction of the applied stress on the mechanical stability was observed (Fig. 3). It is found that the austenite grains at an angle of 45° or 60° to the tensile direction are more stable than those at lower or higher angles. Taking the contribution of the strain tensor to the lattice parameter into account, the increase of carbon concentration as a result of martensitic transformation was observed (Fig. 4).

The above results show that the range of temperature and stress in which the martensitic transformation occurs is related to the distribution of carbon concentration over different austenite grains, which results from the different formation mechanism of retained austenite during the heat treatment. Conclusions can be thus drawn that the inhomogeneity of carbon distribution in retained austenite is the main cause for both thermal and mechanical stability of retained austenite. The austenite grains with a low carbon concentration transform more readily than grains with a higher carbon concentration.

References:

1. Zhao, L., Van Dijk, N.H., Brück, E., Sietsma, J. and Van der Zwaag, S., Mat. Sci. Eng. 313A (2001)145–152.
2. Yu, H.Y., Metall. Mater. Trans. 28A (1997) 2499–2506.
3. Matsumura, Y., Sakuma, Y. and Takechi, H., Scripta Metall. 21 (1987) 1301–1306.

Achievements in Creation of Ultrafine –Grained Steel

S. Torizuka, T. Inoue, A. Ohmori, T. Yamashita, T. Hanamura and K. Nagai
Materials Creation Research Group, NIMS, Japan

1. Introduction

In this paper, we discuss three guidelines to create ultrafine-grained steels, i.e. metallurgy to form ultrafine-ferrite grains, methodology to fabricate bulky ultrafine grain samples, and the microstructural design to achieve a good combination of strength, ductility, and toughness.

2. Ultra grain refinement

Heavy deformation produces ultrafine ferrite grains. The so-called continuous recrystallization generates ultrafine ferrite grains on deforming the ferrite heavily at elevated temperatures [1]. The austenite-to-ferrite transformation also introduces ultrafine ferrite grains from the heavily deformed austenite in the non-recrystallized temperature region on cooling or deformation [2].

Recrystallization Route The grain size is a function of the Z-H parameter as shown in Table.1. The larger the parameter, the finer the grain size becomes. Namely, a sub-micron grain size can be obtained at a lower deformation temperature or at a higher strain rate. However, a critical strain exists for either initiating or completing the recrystallization. A higher critical strain seems to be necessary for a higher Z-H parameter. Hence, an ultrafine grain structure is created through a rather heavy plastic strain.

Transformation Route The ultrafine grain ferrite structure can be formed by introducing a plastic strain larger than 2 in the temperature range in a non-crystallized austenite state where the austenite grain size is between 17 and 300μm [2]. The ultrafine ferrite grain structure having an average grain size of 2μm can be obtained even from a large austenite grain of 300μm. However, the

Table 1 Guidelines for ultra grain refinement.

	Rex (deformed $\alpha \rightarrow \alpha$)	Transformation (deformed $\gamma \rightarrow \alpha$)
Key point for Ultrafine grained ferrite	Large strain – High Z ・Critical strain $\varepsilon > 2\text{-}3$ ・Controlling parameter for d_α $d_\alpha = aZ^b$ $Z = \varepsilon \exp(Q/RT)$	Small thickness of pancake γ THγ –under cooling ・ Controlling parameter for d_α THγ (or recovered γ size) Deformation temp. Cooling rate $d_\alpha = cTH\gamma^d$ $10 > TH\gamma > 2$ μm d_α=const. $2 > TH\gamma$ μm
Minimum grain size achieved	0.5μm	2μm
Texture	Strong (Deformation texture) Control by multi-dir. deformation	Weak (Transformation texture)

ferrite grain size is dominated by the thickness of the pancake-like deformed austenite grain THγ. A smaller austenite grain size is favorable for obtaining the ultrafine grain structure in terms of reducing the THγ.

3. Multidirectional deformation for fabricating a bulky ultrafine grain sample

We have employed multidirectional deformation to fabricate a bulky ultrafine grain sample. The effect of multidirectional deformation is verified from the both viewpoint of numerical simulation and experimental analysis [3]. First, the multidirectional deformation was applied to make bar samples by using caliber rollers [4]. The samples were rotated 90 degrees at every pass and severely deformed with a cumulative strain larger than 3. A 18 mm thick and 20 m long bar was fabricated with ultrafine grains of 0.6 μm. Second, a thick plate with a thickness of 12mm, a width of 70mm and a length of 2m was fabricated by bidirectional rolling as illustrated in Fig. 2 [5]. The tensile properties are shown in Fig.3.

4. Microstructural design for good strength-ductility-toughness combination

The yield strength of the ultrafine-grained steels is determined from the ferrite grain size and the Hall-Petch relationship. However, grain refinement into a sub-micron size deteriorates ductility, particularly, uniform elongation. We propose a strain hardening design using a fine dispersion of the second phase to improve the ductility [6].

[1]A.Ohmori, S.Torizuka, T.Hanamura, and K.Nagai, CAMP-ISIJ, 14(2001), pp.665.
[2]S.Torizuka, J.Takahashi, O.Umezawa, K.Tsuzaki, K.Nagai, S.Genda and Y.Kogo, CAMP-ISIJ, 12(1999), pp.365-368.
[3]T.Inoue, S.Torizuka, and K.Nagai, Materials Science and Technology,17,(2001), pp.1329.
[4] S.Torizuka, K.Nagai and A.Sato, Journal of the JSPS, 42 (2001), pp.287-292.
[5] A.Ohmori, S.Torizuka and K.Nagai, CAMP-ISIJ, 14(2001), pp.1050.
[6] T. Hayashi, K.Nagai, T.Hanamura, H.Nakajima and T.Mitsui, CAMP-ISIJ, 13(2000), pp.473-476.

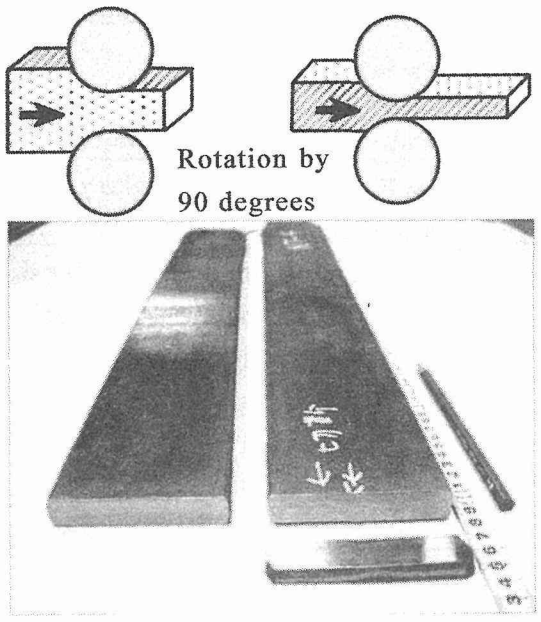

Fig.2 Thick plate with a thickness of 16 mm fabricated by warm bidirectional rolling. Initial thickness was 120 mm.

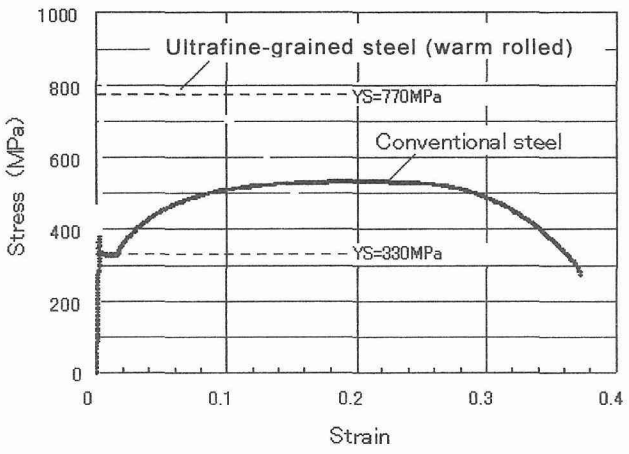

Fig.3 Nominal stress-strain curves of an ultrafine-grained steel (0.6μm) and a conventional steel (10μm).

Steel Plate having Surface-layers with Ultra-Fine Grained Microstructure (SUF Steel) and its Welding Joint Properties

T. Ishikawa、 T. Inoue
Steel Research Laboratories, Nippon Steel Corporation, Japan

1. Introduction

Steel plates with ultra-fine-grained surface layers (SUF steel) has been developed applying an advanced thermo-mechanical control process. Since ultra fine-grained microstructure in surface layers of the steel promotes the formation of shear lips when brittle crack propagates in the steel plate, the SUF steel possess high crack arrest fracture toughness against brittle fracture (crack arrestability). The safety of welded steel structure such as ships will be increased by the use of steel having high crack arrestability for important components of welded structures. Therefore, the SUF steel has been already applied to important members of large welded structures such as large ships in order to improve structural integrity.

In the present paper, the basic properties of SUF steel are summarized and the results of large-scale fracture model tests were discussed in order to evaluate the efficacy of SUF steel for the welded structures as a crack arrestor.

2. SUF steel plate

Figure 1 shows the macrostructure of the SUF steel plate together with the microstructures of the surface layers and midsection regions. The ultra-fine-grained region is the black layer observed at the surface of the steel plate, as shown in Fig. 1. The average value of grain sizes in the surface layers is less than two micrometers. The distribution of the average grain size in the thickness-direction is also shown in Fig. 1. In the surface layer, the grain sizes are relatively homogeneous. The grain size changes significantly at the border of the surface layers and the mid-thickness of the plate.

Charpy impact test results for SUF region suggested that remarkably lower brittle-ductile transition temperature is obtained in 'SUF' than in mid-thickness', although the chemical composition of the SUF steel plate is the same as that of ordinary steel plates without any special alloy elements. The tensile strength of the SUF steel plate is comparable to that of the 490 N/mm^2 class steel. Mechanical properties and welding performance of SUF steel satisfy the requirements of KE36 (EH36) class steel according to the NK (IACS).

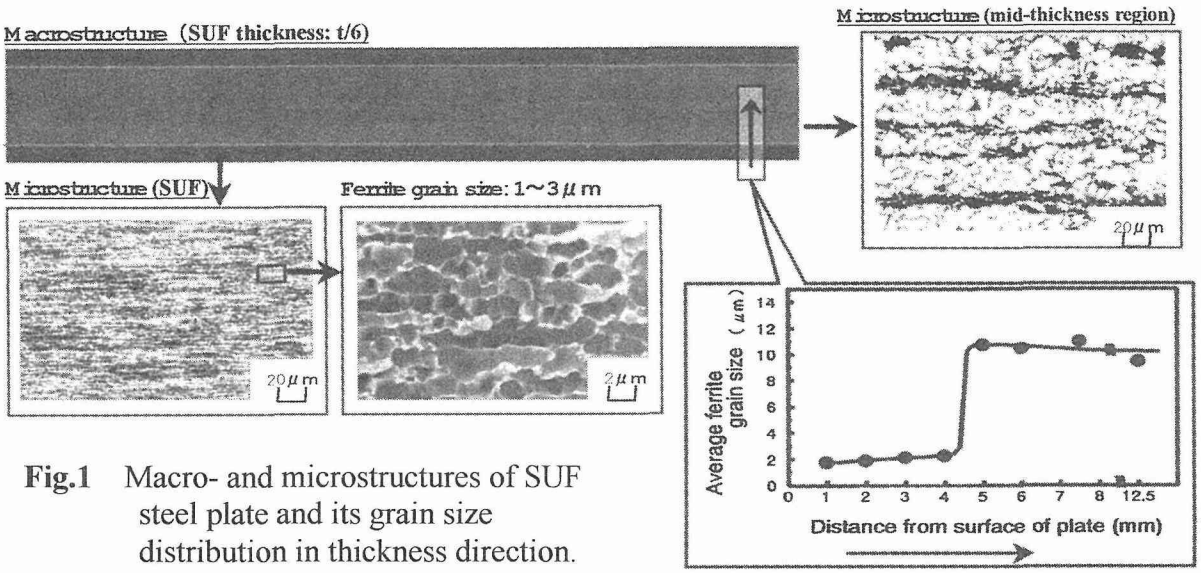

Fig.1 Macro- and microstructures of SUF steel plate and its grain size distribution in thickness direction.

Figure 2 shows the fracture surface of the SUF steel plate used for the temperature gradient type ESSO test. The inside of the plate was fractured brittlely, while the surface regions of the plate were not fractured in a brittle way but in a ductile way. The surface regions fractured ductilely with plastic deformation are called shear-lips, and these have a braking effect on unstable brittle crack propagation and further enhance the crack arrestability of the steel plate. Therefore, the SUF steel possess high crack arrest fracture toughness against brittle fracture.

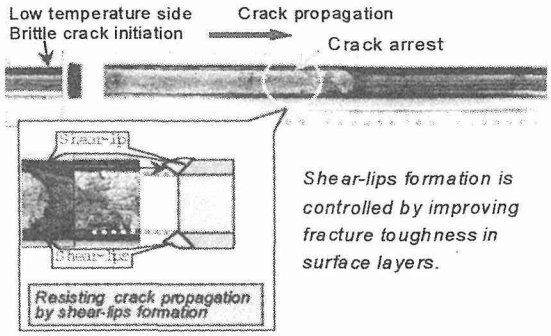

Fig.2: Fracture surface of standard ESSO test specimen for SUF steel plate

3. Large scale fracture tests for welded structures using SUF steel

Figure 3 shows a schematic illustration of the ship hull as an example of welded steel structure. It was assumed that the SUF steel plates were used for the shear strakes and bilges. When collisions or other accidents occur, brittle cracking may occur in various members, such as in the shear strakes. This paper discusses Cases A to E in which tests using large-scale fracture models were conducted. Case A assumes that a brittle crack (which occurred in some part of the deck) propagated across the deck into the shear strake. Case B assumed that the brittle crack propagates from the side plating to the shear strakes or bilges. Case C assumes that a brittle crack propagates along a vertical butt-welded joint corresponding to one in the block segment and penetrates into a weld of the shear strake or that a brittle crack occurs and propagates in a welded joint in the shear strake. In Cases D and E, the structure of the SUF layer on one side of the SUF steel plate was changed by applying heat in welding or line-heating for fabrication.

These large-scale fracture tests revealed that the SUF steel plates used in the shear strakes can serve as an effective crack arrester even in serious accidents, such as collisions, etc.

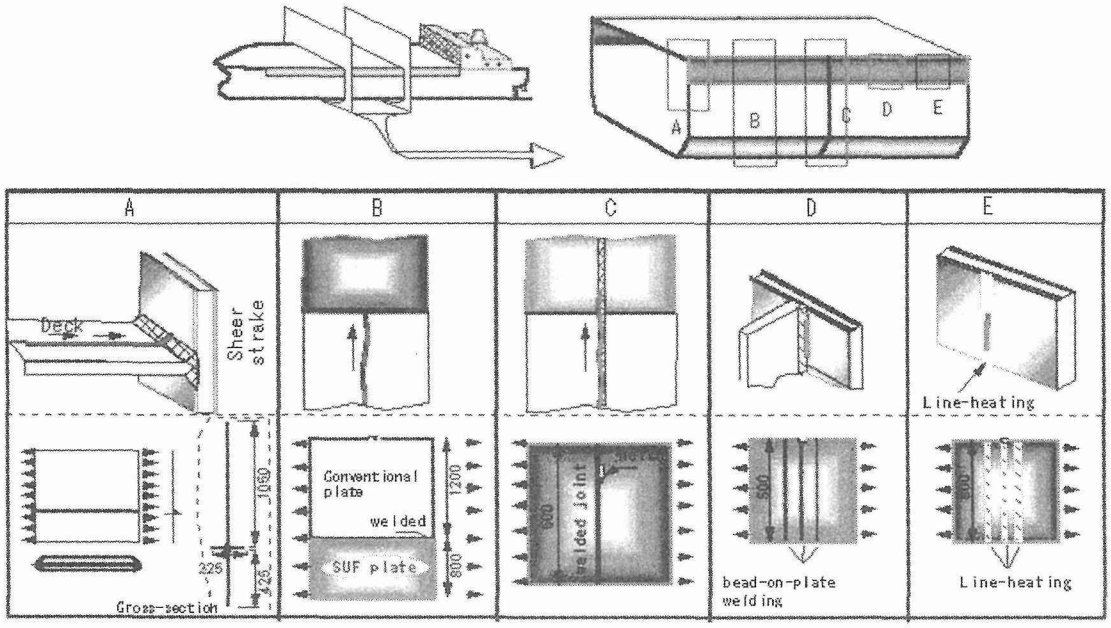

Fig.3 Large scale fracture model tests to evaluate the usage of SUF steel for welded structures.

Development of Ausformed Bainite Steel and its Welding Joint Properties

K.Fujiwara, S.Okaguchi, Y.Komizo, K.Arimochi, T.Kawabata and A.Nagayoshi
Sumitomo Metal Industries Ltd., Japan

1. Introduction

TMCP has been already expanded in manufacturing high tensile strength steel plates lowering susceptibility to low temperature cracking in welding. This is because TMCP enables to decrease carbon content to obtain same strength in comparing with conventional process such as normalizing, quenching and tempering. On the other hand, decreasing carbon content brings remarkable deterioration of toughness in base metal of 600MPa class tensile strength (HT570) steel because of coarse upper bainite formation. In this situation, we have developed HT570 steel with superior toughness and weldability by utilizing fine ausformed bainite. This type of steel, named "Ausformed Bainite HT570", is characterized by the reduction control in unrecrystallized austenite region and by the cooling control in bainite transformation region. This advanced HT570 steel has been applied to various fields such as penstock, tank, bridge and so on.

2. Effect of Deformation on the Characteristics of Bainite Structure

0.1C-1.4Mn-Nb-Ti-B steels is used for laboratory test. Small specimens were austenitized at 1000℃ for 300s by induction heating and deformed 0 to 75% at 900℃. After that, specimens were accelerately cooled and isothermally kept at 500℃. Deformation less than 30% is not effective on the reduction of the length significantly. Heavy deformation is required for the remarkable refinement of bainitic ferrite lath. Fig.1(a) shows typical B1 type[1] upper bainte structure having large packet size. On the contrary, Fig.1(b) shows fine ausformed bainite strcture in which coarse bainite packet is not observed.

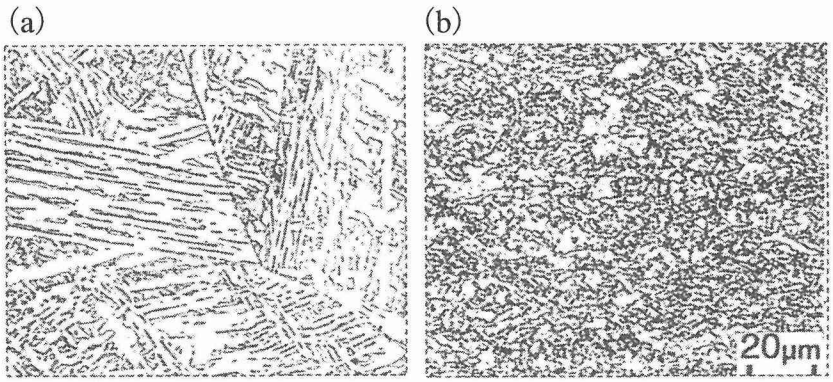

Fig.1 Microstructure of conventional upper bainite (a) and ausformed bainite (b)

3. Development of Ausformed Bainite type HT570 Steel

Typical chemical compositions of developed steels for manufacturing scale are shown in Table 1. The chemistry design has enabled site welding without preheating even in

Table 1 Chemical composition (mass%)

Application	Thick.	C	Si	Mn	others	Pcm
Penstock	40mm	.06	.19	1.37	Cu,Ni,Mo,Nb,V,Ti	.17
Tank	45mm	.09	.32	1.50	Mo,Nb,V,Ti	.19
Bridge	45mm	.08	.16	1.36	Cr,Nb,Ti,B	.18
Bridge	100mm	.08	.20	1.46	Cr,Mo,Nb,Ti	.19
conventional	40mm	.13	.30	1.37	Mo,V	.23

80% humidity condition as shown in Fig.2. Conventional HT570 steel for penstok required preheating up to 100℃. Moreover manufacturing concept has made this steel developed superior toughness of base metal and welded joint as shown in Table 2.

In consideration of applying the steel developed to tank, steel properties on stress relief (SR) or PWHT and stress corrosion cracking (SCC) should be investigated. Change of mechanical properties of base metal and welded joint is very small even after 600℃ SR due to containing Vanadium. Moreover susceptibility to ammonia SCC of steel developed is confirmed to be less than that of conventional QT steel by four point bent test, as shown in Fig.3.

Mechanical properties of HT570 steel developed for bridge are shown in Table 3. High tensile strength and superior toughness have been obtained both in base metal and welded joint up to 100mm in thickness. High heat input electro-gas arc welding up to 20kJ/mm can be also applicable to this steel.

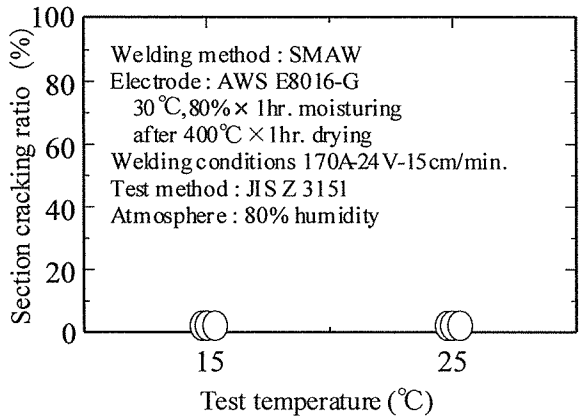

Fig.2 y-groove weld cracking test result

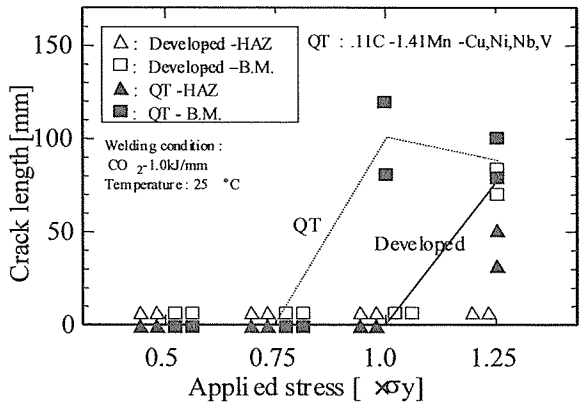

Fig.3 Ammonia SCC test result

Table 2 Mechanical properties of developed HT570 steel for penstock

	Base Metal				SAW Welded Joint			
Thickness [mm]	YS [N/mm^2]	TS [N/mm^2]	vE-40 [J]	vTrs [°C]	Heat Input [kJ/mm]	Edge Preparation	TS [N/mm^2]	vE0(FL) [J]
40	520	635	333	-107	4.5	double V	659	225

Tensile test specimen:D14×GL50 (1/4t,C-dir.) Tensile test specimen:Full thick. 25width
Impact test specimen:2mmV (1/4t,full size,L-dir.)Impact specimen: 2mmV(1/4t,full size)

Table 3 Mechanical properties of developed HT570 steel for bridge

	Base Metal			Welded Joint (t=45mm)			
Thickness [mm]	YS [N/mm^2]	TS [N/mm^2]	vE-5 [J]	Heat Input [kJ/mm]	Welding Process	TS [N/mm^2]	vE-5(FL) [J]
45	523	632	306	20.0*	EGW	643	115
100	508	628	317	5.0	SAW	664	217
				10.0		650	195

Tensile test specimen:D14GL50 (1/4t,C-dir.) Tensile test specimen:Full thick. 25width
Impact test specimen:2mmV (1/4t,full size,L-dir.) Impact specimen: 2mmV(1/4t,full size)
*Thickness decreased to 35mm

[1] Y.Ohmori, H.Ohtani and T.Kunitake:Trans. Iron Steel Inst. Jpn.,11 (1971),250.

Mechanical Properties of Welded Joints of Ultra-Fine Grained Steels

Y.Kawaguchi
Joining and Interface Research Group, NIMS, Japan

1. Introduction

Strength and toughness of the welded joints are the fundamental properties for structural steels. In STX-21 project, the material production began with tiny samples and now it has reached to the plates of 16mm in thickness and 100mm in width. The properties of the welded joints have been investigated along with the development of the materials production and the basic properties are reported here.

2. Strength and deformability of welded joints

Softening in the heat affected zone (HAZ) is a serious problem for the performance of the welded joints. In the ultra-fine grained steels, the softening in HAZ is deep and wide compared with the conventional high strength steels which contain the various additional elements for base metal strengthening. In the tensile test of the welded joints, sometimes the rupture occurs from HAZ and the strength is far lower than that of the base metal.

The basic concept to attain the rupture from the base metal is the use of strength miss-matching between the base metal and the weld metal. Over-matching weld metal neighboring HAZ constrains the plastic deformation of the softening in HAZ and the deformation can occur in the base metal. But the conditions to attain the rupture from the base metal are much complicated. Extent and configuration of the softening, over-matching degree and configuration of the weld metal, and the plate thickness and width of the tensile test specimen are the main factors for the rupture from the base metal.

Rupture from the base metal is the most preferable for the fitness for purpose of the welded joints. It assures the strength of the welded joints so far as the base metal has enough strength. But another required property for structural steels is the deformability of the welded joints in the tensile test. The distribution of the elongation in the ruptured specimen should be wide in the base metal because the deformation should be wide spread apart from welded joints for the safety of the actual steel structures. This property is

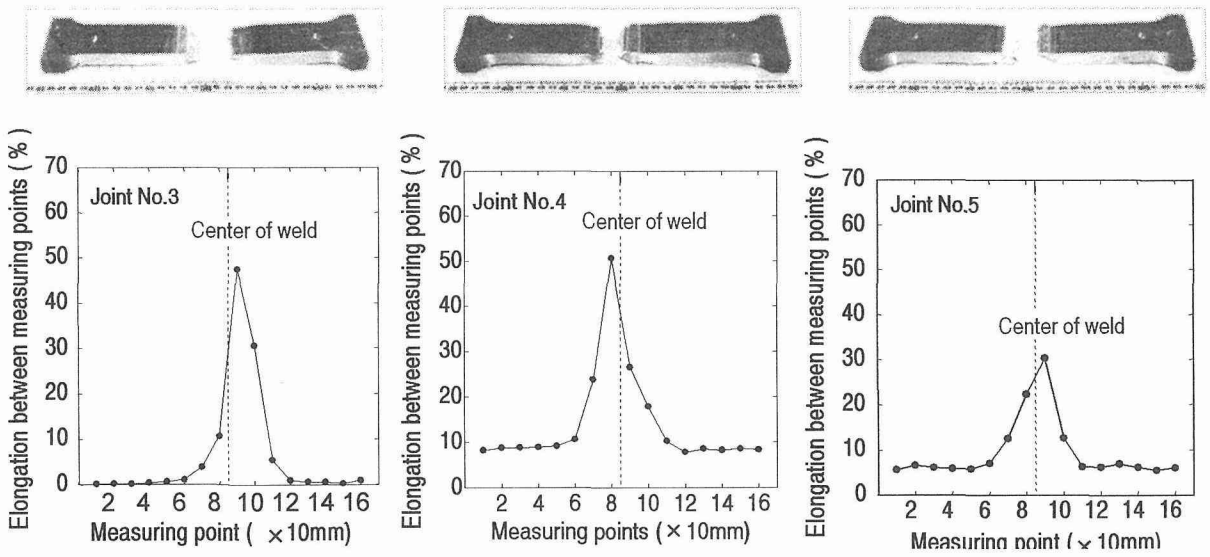

Fig.1 Rupture from HAZ and variety of elongation distribution (t=16mm, W=40mm)

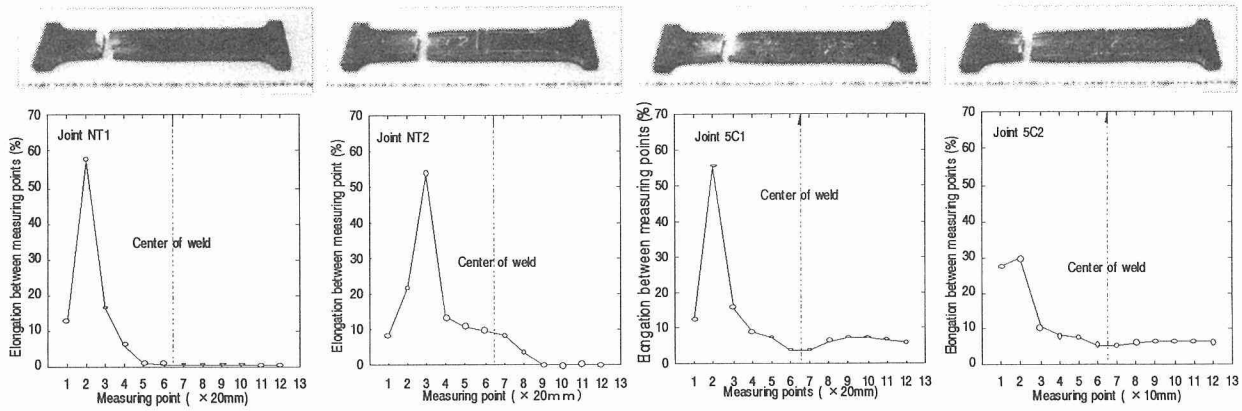

Fig.2 Rupture from base metal and variety of elongation distribution (t=16mm, W=60mm)

dependent on a base metal property, the yield to tensile strength ratio (YR), because the base metal should yield and be deformed before the rupture of the specimen occurs.

3. Toughness of heat affected zone

HAZ is the most deteriorated portion for toughness in the welded joints, but the toughness evaluated by Charpy test is fairly good compared with conventional high strength steels.

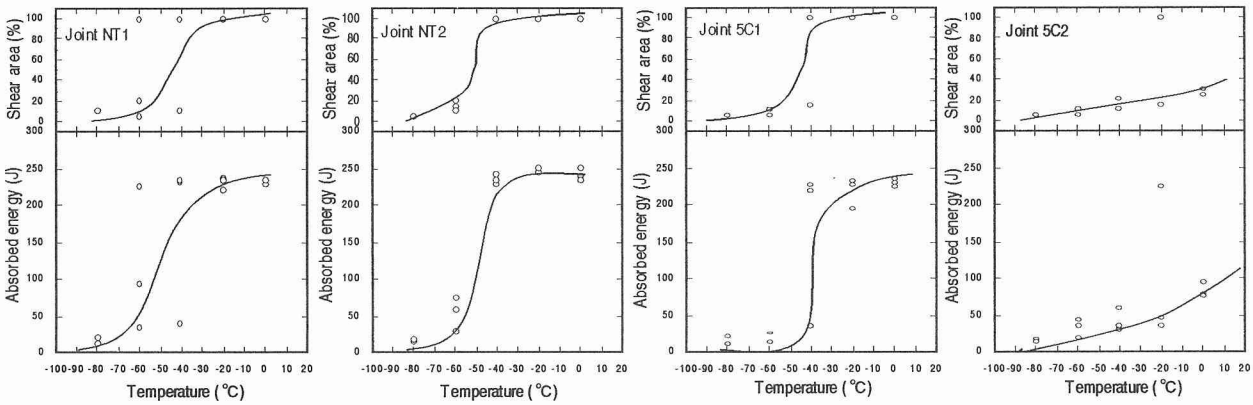

Fig.3 Toughness at HAZ with varied base metals and welding heat inputs

4. Conclusion

Ultra-fine grained steels has a weak point of softening in the heat affected zone (HAZ), but the practical countermeasures such as low heat input to narrow HAZ, over-matching of weld metal to constrain the plastic deformation of the softening zone, adding slight elements to base metal to resist softening and the appropriate design of welding groove and reinforcement give compound effect to the strength of the welded joints, and the most preferable rupture from the base metal can be attained. The deformability of the weld joints can be approved by the appropriate yield to tensile ratio of the base metal. The superiority of the toughness of HAZ is an advantage of ultra-fin grained steels but corresponding to the welding methods and heat input, improvement to the chemical compositions of the base metal may be required.

Ultra-fine grained steels have great advantages compared with the conventional steels, but the disadvantages should be overcome for practical application to welded structures.

High Strength Extremely Low Carbon Bainitic Steels for Bridges and Buildings

T.Hoshino, M.Okatsu, T.Kimura, and K.Amano
Technical Research Laboratories, Kawasaki Steel Corporation, Japan

1. Introduction

The thermo-mechanical control process (TMCP) is a representative technology for manufacturing a non-heat treated high-strength steel product [1]. Because of the increase in the scale of welded structure due to the improved efficiency of welding process, it has been required to be produced a large section steel product with higher strength, better weldability, in on-line process. By using the conventional TMCP, however, we can not easily satisfy these demands. With the intention of solving these issues, authors have paid attention to the bainitic structure of extremely low carbon steel, particularly that with a carbon content of about 0.02mass% or less, as well as to its transformation behavior and have established the concept called TPCP (Thermo-mechanical Precipitation Control Process) for solving the problems. This paper introduces the concept of TPCP and its application to non-heat treated high-strength steels for bridges and buildings.

Table 1 Chemical compositions of the ELCB and SM490 steels, mass%

Steel	C	Si	Mn	Cu	Nb	Ti	Al	B
ELCB	0.007	-	1.75	0.95	0.015	0.021	0.030	0.0014
SM490	0.14	0.40	1.30	-	0.015	0.013	0.024	-

2. Concept of TPCP

The TPCP is the method for control of mechanical properties of steels through invariable microstructure control integrated with precipitation hardening and basically different from the conventional TMCP. Lowering carbon content below 0.02mass%, which is the maximum solid-soluble limit to ferrite, and optimizing the other alloying elements such as Mn, Nb, and B for lowering the transformation temperature can make the steel have a uniform extremely low carbon bainitic microstructure independent of a cooling rate. Figure 1 shows the continuous cooling transformation (CCT) diagrams with deformation for the extremely low carbon bainitic and a conventional low alloy steel corresponding to JIS grade SM490, whose chemical compositions are listed in Table 1. The microstructure of extremely low carbon bainitic steel (hereafter ELCB) was identified to an extremely low carbon bainite [2] and not changed in the wide range of cooling rate. The cooling rate dependence of hardness is shown in Fig.2. As for the ELCB steel, the increment with the rise of cooling rate from 0.1 to 55°C/s was 4 points while 89 points for the SM490 steel. This weak cooling rate dependence of

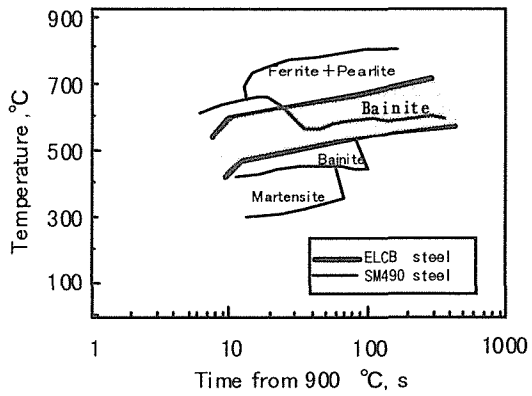

Fig.1 Comparison of the CCT diagrams between the ELCB and SM490 steels.

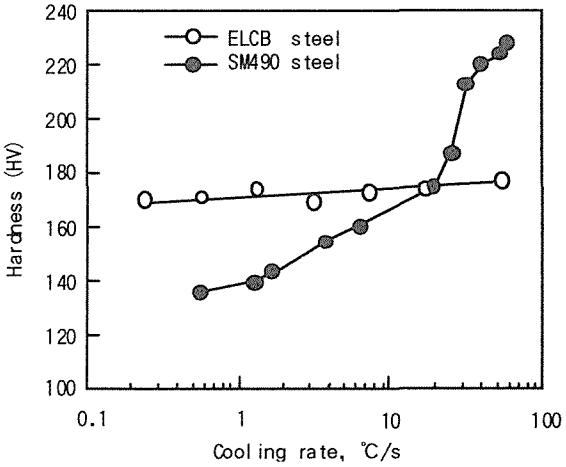

Fig.2 Relationship between cooling rate and hardness of the ELCB and SM490 steels.

the microstructure and the hardness for the ELCB steel indicate that a large section steel products with higher strength, lower hardenability of HAZ in welding process, can be easily produced by using the TPCP. Furthermore, the TPCP can vastly improve the strength of a steel by invariable microstructure control associated with precipitation hardening.

3. New Products and Features in Performance

3.1 600MPa grade plates for bridges

A typical chemical composition of the ELCB steel plates of 600 MPa class with thickness up to 75 mm is of 0.012mass%C-0.3mass%Si with micro-alloying elements. For this application, the basic TPCP is adopted so that precipitation hardening is not necessarily used. Both values of Ceq and Pcm, 0.294 and 0.137 respectively, are remarkably smaller than those the conventional 600 MPa plate products.

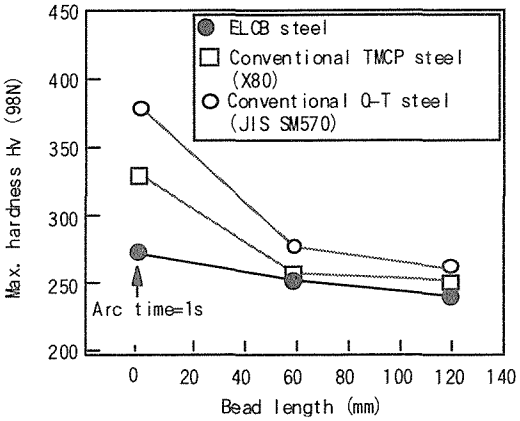

Fig.3 Results of maximum hardness tests

The ELCB steel plates exhibit the excellent uniformity in microstructure and therefore in strength. The extremely-low carbon also makes the high strength steel be free from a preheating owing to its low hardenability as demonstrated in Fig. 3. The ELCB steel plate keeps quite gentle rise in hardness even though attacked by short time arc melt while those of the other conventional steels shoot up. The ELCB steel was also verified to exhibit good heat-affected zone toughness for a wide range of welding heat input owing to its little dependency on cooling rate.

3.2 600 MPa TS grade heavy gauge H-shapes for buildings

For this application, the amount nearly 1 mass% of Cu is typically micro-alloyed to the basic extremely-low C steel of 0.02%C-0.3%Si-Mn-Cu-Ni-Nb-B type in order to obtain 600 MPa in the tensile strength. The moderate Cu self-ageing is supportively used. The ELCB steel covers the heavy gauge H-shape products with the flange thickness range from 30 to 125 mm. The tensile strength (TS), yield ratio (YR), and V-notch Charpy absorbed energy at 21 °C were shown satisfactory with the ASTM A913 grade 65 standard for all the heavy gauge H-shapes with several flange sizes as shown in Fig. 4.

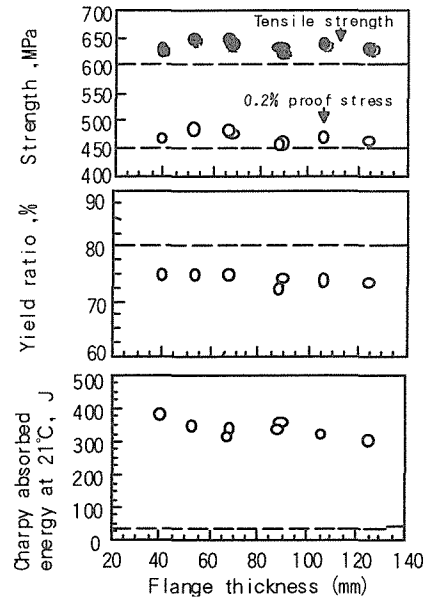

Fig.4 Mechanical properties of developed heavy gauge H-shapes of the ELCB type.

4. Conclusions

A new as-rolled process for high strength steel products of heavy section, which is called TPCP, has been developed and the features of the ELCB steels and products were described from the metallurgical and the application's points of view. The new TPCP products showed the distinguished performances in the applications from the conventional steels.

References

[1] T.Maki, 161st Nishiyama Memorial Lecture, ISIJ, Tokyo, 1996, p11, in Japanese
[2] T.Araki, Atlas for Bainite Microstructure, ISIJ, 1992, p4

Development of High Strength and Excellent formability Steel Tube by Warm-reducing

Y. Kawabata, T. Toyooka, M. Nishimori, M. Aratani
Tubular Products & Casting Laboratory, Technical Research Laboratories,
Kawasaki Steel, Japan

1. Introduction

Aiming at the weight reduction, improvement of collision safety and manufacturing cost saving, the amount of the steel tubes used for automobile parts has been increasing in recent years. Especially, high strength steel tubes with excellent formability are significantly demanded these days. Based on this background, Kawasaki Steel has developed a new steel tube manufacturing process termed The HISTORY (High speed tube welding and optimum reducing technology) process. This process consists of a newly developed thermo-mechanical control process based on the new metallurgy by the warm-stretch-reducing. This production line was built in October 2000 at Chita Works and has been operating

2. Features of the developed process and steel tube

The newly developed manufacturing process of steel tubes is shown in Fig. 1. The steel strip is formed to the circular shape semi-formed tube by roll forming process and its both edges are welded by the electric resistance welding. The steel tube is heated and reduced by the stretch reducer in the warm temperature (923~ 1173K).

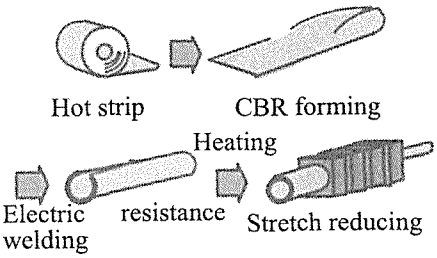

Fig.1 Newly developed steel tube manufacturing process

The warm-reducing has not been applied to the actual production mill. Because the flow stress in the warm temperature becomes several times compared with that in the hot temperature(>1173K). However, the warm-reducing process is the innovative steel tube making process which can produce both higher strength steel tubes and more excellent formability steel tubes compared with a conventional ERW (electric resistance welding) steel tubes, made of the same chemical composition steel by the controlling of reducing conditions.

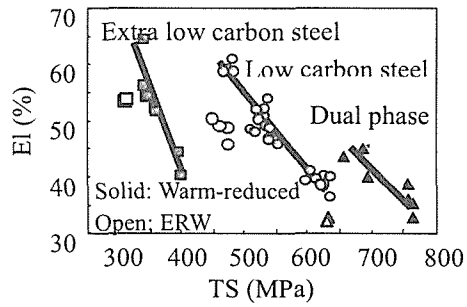

Fig. 2 Mechanical properties of the warm-reduced steel tubes and ERW steel tubes

Fig. 2 shows the comparison of tensile properties between in the ERW steel tubes and in the warm-reduced steel tubes. Comparing at the same strength in the low carbon steel; about 450 MPa, the elongation of the warm-reduced steel tube is 10 % higher than that of the ERW steel tube. Comparing at the same elongation in the low carbon steel; about 50 %, the strength of the warm-reduced steel tube is 80 MPa higher than that of the ERW steel tube. The same result is obtained in the warm-reduced steel tube of the extra low carbon steel and dual phase steel.

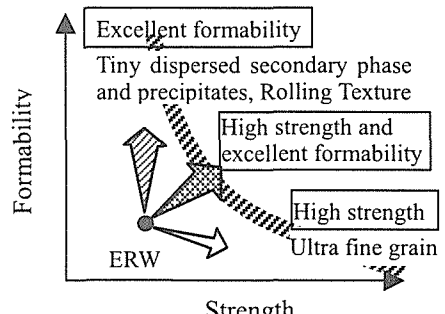

Fig. 3 Concept of the warm reducing for high strength and excellent formability

3. New metallurgy of the warm-reducing

The effects of the warm-reducing on the strength and

the formability of a steel tube is schematically shown in Fig. 3. The warm-reducing process can obtain the high strength due to refining of ferrite and the excellent formability due to tiny dispersed secondary phase and precipitates and due to the rolling texture.

(1) Refining of microstructure

Photo. 1 shows the microstructure of the warm-reduced steel tube in comparison with that of a conventional ERW steel tube. In the warm-reduced steel tube, ferrite grain size is refined to approximately 1 ~ 2 micrometers, resulting in high strength.

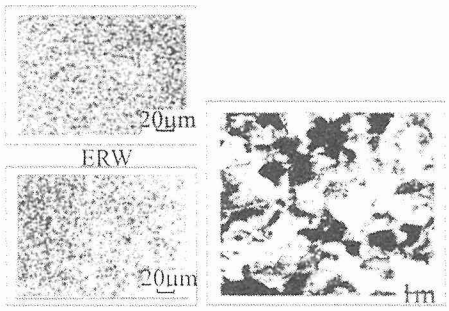

Warm-reduced Optical | Warm-reduced TEM

Photo. 1 Microstructure of the warm-reduced steel tube and ERW steel tube

(2) Tiny dispersion of secondary phase (On-line spheroidizing of cementite)

Photo. 2 shows the comparison of microstructure between the ERW steel tube and the warm-reduced steel tube. In the warm-reduced steel tube, tiny spheroidized cementite is dispersed homogeneously. Generally spheroidizing of cementite needs a long time annealing at about 973K. However, the warm-reducing process can complete spheroidizing of cementite in several seconds.

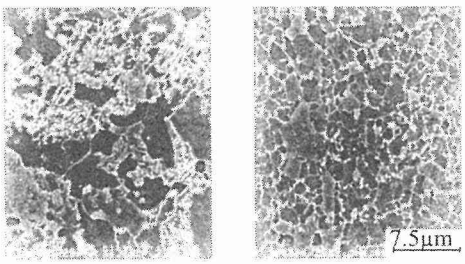

Normalized ERW | Warm-reduced

Photo. 2 SEM images of the warm-reduced steel tube and normalized ERW steel tube, 0.42%C-1.4%Mn steel

(3) Rolling texture

The warm-reducing process can form the rolling texture of high r value especially in the longitudinal direction. This rolling texture of high r value can not be obtained by rolling of steel sheet because of the difference of the deformation between in reducing and in rolling. The direction of reduction in reducing of steel tube is the transverse direction, on the other hand, the direction of reduction in rolling of steel sheet is the normal direction.

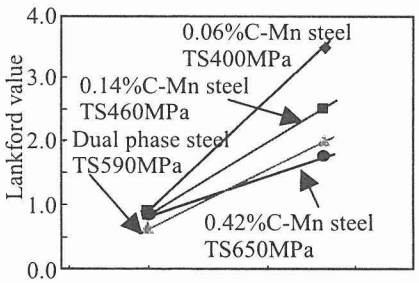

Fig. 4 r value of the warm-reduced steel tube, Reduction: 60%

The formation of rolling texture is independent on the solute carbon or secondary phase[1]. Therefore higher r value than 1.5 can be achieved in the low carbon steel tube, high carbon steel tube, dual phase steel tube as shown in Fig. 4. In steel sheets of those steels, high r value has not be obtained. Because the solute carbon or secondary phase of those steels prevent the formation of recrystallization texture which is used to obtain high r value in the steel sheet[2].

4. Conclusion

Kawasaki Steel has developed the new steel tube by the newly developed warm-reducing process. The warm-reduced steel tube has high strength and excellent formability those can not be obtained in the conventional ERW steel tubes and steel sheets.

References

[1] S. Nagashima, Shuugousosiki. (1984), pp.117, Maruzen

[2] Saikesshou shuugousosiki to sono soshikiseigyo eno ouyou (1999), pp228, ISIJ

Development of Low C HSLA Steel Plates and the Properties of Welded Joints for Pressure Vessel Use

K.Hayashi, K.Takahashi, M.Yuga, S.Suzuki, T.Kojima, T.Maeda
Materials & Processing Research Center, NKK Corporation

1. Introduction

NKK's new 610N/mm^2 class high-performance low-C high-strength low-alloy (HSLA) steel plates, "NK-HITEN 610 "series have been developed for penstock, tank, and pressure vessel use, and they have been already applied to many plants. These are designed in order to meet the needs of improvement of weldability and reliability of weldments. This paper deals with the outlined of NK-HITEN 610 series and their weldability and mechanical properties of welded joints.

2. NKK's new 610N/mm^2 class high-performance steel plates for pressure vessel use

The alloy design concept of new NK-HITEN 610 series is shown in Fig.1. C content and Pcm values of any steel plates are suppressed to extremely low levels, which decrease the susceptibility to weld cracking through the decrease of maximum hardness in HAZ, that enable a great reduction in preheat temperature for welding (Fig.1), and that enhance the reliability of welded structure through the decrease of hardness and improvement of HAZ toughness. NK-HITEN 610U2 is the standard grade with excellent weldability.

The chemical compositions of NK-HITEN 610U2L, which is developed for low temperature use, are also optimized in addition to the suppression of C and Pcm to obtain superior toughness at lower temperature.

Regarding NK-HITEN 610E2 for high-heat input welding (~100kJ/cm), Ceq. values of the steel are suppressed and microalloy elements are utilized in addition to the suppression of C and Pcm to obtain both strength and HAZ toughness of welded joints for high-heat input welding. The coarse grain HAZ (CG-HAZ) with upper bainite microstructure which is transformed at a temperature around 550-600℃, has lower toughness. HAZ toughness of 610E2 has been improved through controlling microstructure to avoid upper bainite structure by suppressing the Ceq and utilization of microalloy elements.

The chemical compositions (Table 1) and the mechanical properties of any steel plates satisfy those of SPV490 (JIS G 3115) and the steel plates have obtained the quality certification of WES 3001, 3009 (U2,U2L,E2), and 3003(U2L).

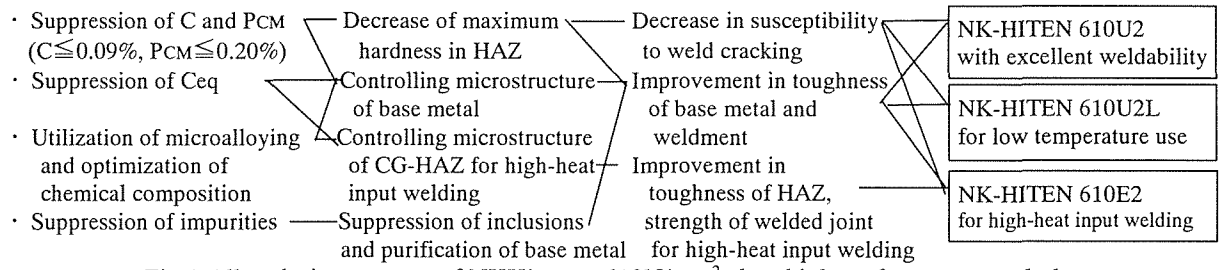

Fig.1 Alloy design concept of NKK's new 610N/mm^2 class high-performance steel plates

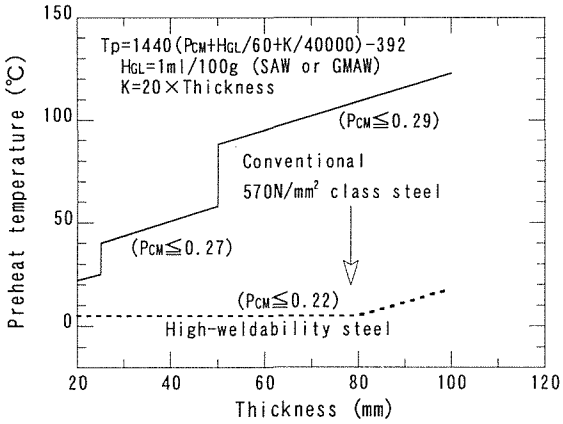

Fig.2 The decrease of required pre-heat temperature by using low Pcm HSLA steel plates[1]

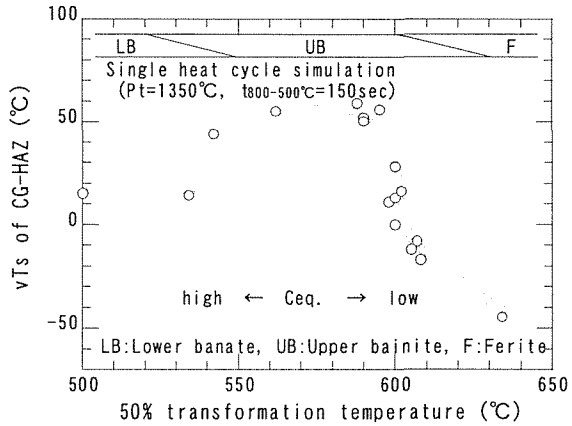

Fig.3 Influence of microstructure and its transformation temperature on toughness (vTs) of simulated CG-HAZ for high-heat input welding[1]

Table 1 Chemical compositions of new NK-HITEN 610 Series (wt.%)

	t (mm)	C	Si	Mn	P	S	Others	Ceq.	Pcm
NK-HITEN 610U2	38	0.08	0.21	1.34	0.006	0.001	Mo,V etc.	0.33	0.17
	75	0.08	0.26	1.44	0.005	0.002	Mo,V etc.	0.39	0.18
NK-HITEN 610U2L	50	0.07	0.20	1.32	0.007	0.001	Cu,Ni,Cr,Mo,V etc.	0.41	0.19
NK-HITEN 610E2	22	0.09	0.20	1.37	0.010	0.002	Mo,V etc.	0.35	0.18
	45	0.09	0.20	1.37	0.010	0.002	Mo,V etc.	0.35	0.18
NKK Specification 610U2,U2L,E2	6-75	0.09 max.	0.15 -0.55	1.00 -1.60	0.020 max.	0.010 max.	Cu,Ni,Cr,Mo:0.30 max., V:0.06max., Nb:0.03max.	0.44 max.	0.20 max.
JIS G 3115 SPV490	6-75	0.18 max.	0.15 -0.75	1.60 max.	0.030 max.	0.030 max.	Alloying elements other than those listed may be added.	0.45[1] max.	0.28[1] max.

Ceq= C+Si/24+Mn/6+Ni/40+Cr/5+Mo/4+V/14

Pcm = C+Si/30+Mn/20+Cu/20+Ni/60+Cr/20+Mo/15+V/10+5B

1) 50<t≦75mm : Ceq:0.47 max., Pcm.:0.30 max.

3. Weldability and mechanical properties of new NK-HITEN 610 series' welded joints

Typical properties with respect to weldability and welded joints of new NK-HITEN 610 series are shown as follows. Maximum hardness below 300HV10 in HAZ can be achieved under any conditions in Fig.4, even when heat input is low and initial plate temperature is RT. These values are lower than those of conventional 610N/mm^2 class steel plates. As far as the y-groove weld cracking test results are concerned, no cracks occur even at the temperature of 0℃, any welding conditions and any plate thickness up to 75 mm tested.

The tensile strength of NK-HITEN 610U2L's SMAW welded joint is high enough and satisfies the specification, and the Charpy impact properties of them are also good enough, which satisfy the specification LT490-75 -50G Q (vTE≦-50℃) of WES 3003.

As far as mechanical properties of NK-HITEN 610E2'sEGW welded joints with high-heat input are concerned, the tensile strength of welded joints is high enough and satisfies the specification, and enough Charpyimpact energy values are obtained at -15℃

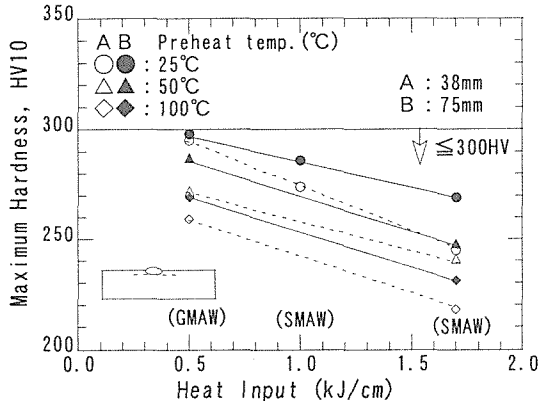

Fig.4 Maximum hardness of NK-HITEN 610U2

Table 2 Mechanical properties of NK-HITEN 610U2L's SMAW welded joint

t (mm)	Welding condition	Tensile Properties TS (N/mm^2)	Tensile Properties Fracture position	Charpy impact properties Position	Charpy impact properties vE-50℃ (J)	Charpy impact properties vTs (℃)	Charpy impact properties vTE (℃)
50	H.I.=23kJ/cm LB-62L (φ5)* Preheat : none Inter pass temp : ≦150℃ PWHT:580℃×2h×2 times	676 681	WM WM	WM FL HAZ	133 183 208	-63 -63 -62	-58 -64 -74

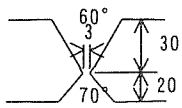

*Supplied by KOBELCO

Table 3 Mechanical properties of NK-HITEN 610E2's EGW welded joints

t (mm)	Welding condition	Tensile Properties TS (N/mm^2)	Tensile Properties Fracture position	Charpy impact properties Position	Charpy impact properties vE-15℃ (J)
22	H.I.=80kJ/cm DWS-60G (φ1.6)* Built-up : 1 side 1 pass Preheat : none	620 623	HAZ HAZ	WM FL HAZ	69 159 254
45	H.I.=93, 85kJ/cm DWS-60G (φ1.6)* Built-up : both side 1 pass Preheat : none	639 642	HAZ HAZ	WM FL HAZ	56 129 248

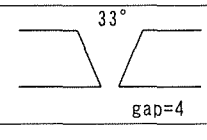

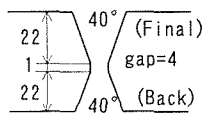

*Supplied by KOBELCO

Reference

[1] K.Matsui et.al., NKK Technical Report (JA). No.165, p11-16 (1999).

The application and the problems of high strength steel on penstock in Chinese hydroelectric station

Li Ming, Jiang Wenlin
Quality Inspection & Test Center of Hydro Steel Structure
Ministry of Water Resource, P. R. China

1. introduction

China has the richest waterpower resource in the world, which, however is only limited developed. With the increasing construction of waterpower station in China, which have larger capacities and higher water heads, especially in the case of pumped storage power station, high strength steel being employed in penstocks is becoming a trend.

The application of high strength steel has increasingly improved the technology on penstock manufacture and assembling, as well as management, with economy benefit being equally obtained.However, some misunderstandings on using high strength steel plate are still existed, which weaken their advantage. In this paper, the following problems are discussed.

2.Overly request on welding and nondestructive test (NDT)

High strength steel is generally regarded as bad weldability, which causes high request on welding technology and NDT test. As a matter of fact, the new type of high strength steel has excellent weldability, with low C_{eq} and P_{cm}, as well as low components of S and P.

Table1 shows that the 600MPa class steels SM570Q, NK-HITEN610U2, 07MnNiCrMoVDR respectively have lower C_{eq} and P_{cm} than 500MPa steel 16MnR. However, 800MPa steel SHY685NS has relatively higher C_{eq} than 16MnR, with equal P_{cm}. Besides, the welding materials applied to high strength steel are more reliable than they were before. Table2 shows that some projects in China are overly requested on technologic parameters, such as pre-heating temperature and heat input, especially stress on controlling heat input to improve the impact toughness of welded joint. However, largely increasing tolerance of impact toughness is neither economically, nor quality promised.[1]

NDT was also overly requested before, and RT dominated the testing. However, in recent years, RT has been decreasingly applied in testing thanks to UT, which has more advantages to inspect crack or likeness.

Table 1.Main technical statistical results for penstocks materials of several projects

name of project	material	thickness (mm)	Ceq	Pcm	P	S	A_{kv}(J)
Ming Tomb	SM570Q	30-48	0.30-0.41	0.21-0.24	0.006-0.015	0.008-0.05	(-5℃)142-358
	SHY685NS	32-70	0.49-0.55	0.24-0.26	0.004-0.007	0.008-0.003	(-40℃)125-313
	16MnR	40-44	0.39-0.46	0.23-0.27	0.014-0.024	0.013-0.02	(-20℃) ≥20
Three Gorges	NK－HITEN 610U2	60	0.38-0.41	0.16-0.19	0.004-0.013	0.002≤	(-40℃)175-385
Xiangshui	07MnNiCrMo VDR	36-40	0.40-0.43	0.18-0. 20	0.0014-0. 0022	0.004-0. 01	(-40℃)50-152

C_{eq}=c+Mn/6+Si/24+Ni/40+Cr/5+Mo/4+V/14, P_{cm}=C+Mn/20+Si/30+Cu/20+Ni/60+Cr/20+Mo/15+V/10+5B

Table 2. Requirements of heat input and preheating in several projects

name of project	Okuyoshino	Shimogo	Imaichi	Sabigawa	Okouchi	Okukiyotsu-II	Lubuge	Ming Tomb	Xiangshui	Three Gorges
metrial	SM570Q	SM570Q	SM570Q	SM570Q	SM570Q	SM570Q	A537CL.1 A537CL.2	SM570Q	07MnNiCr MoVDR	NK－HITEN 610U2
	HT-80		HT-80	SHY685NS-F	SHY685NS-F	SHY685NS-F	A517GrF	SHY685NS		
upper limit of heat input (kJ/cm)	<80	<60	<75	<75	<75	<75	<60	<45	<36	<40
	<50		<50	<60	<50	<50	<50	<40		
pre-heating temperature (℃)*	100	80	50	50	80	50	80	100	100	75
	150		100	80	80	80	120	100		

*Take SMAW for example

Take Ming Tomb Project for example, which requested 100% UT + 25% longitudinal weld (10% girth weld) RT, Nevertheless, RT was finally cancelled in the testing on slanted pipe (underground pipe), following the comparison between the two testing results.

Besides, penetrant inspection and magnetic particle inspection are being emphasized on surface defect testing. Further more, acoustic emission testing has also begun being used on welding supervision. All these show the recent development of testing technology and realization on welded defect of high strength steels.

However, confusing technology with management would cause attending to one thing and losing another. With qualified welded joints being promised, working conditions of welding and NDT testing could be improved and going efficiently, cost being reduced by lowering pre-heating temperatures, less controlled heat input, as well as applying reasonable testing.

3. The penstock standards are behind the development of high strength steel

The standards do not clarify what requirements could support the new materials, as prevents the application of new materials.

The present high strength steel , has low components of S and P (see table1), as well as high purity thanks to measures that reduces gases in steel, such as vacuum degassing, which improves toughness, as well as largely reduces strain aged sensitivity. However, the standards specifies that the higher strength steel allows lower cold rolling deformation, which limits the application of high strength steel under the conditions of high water head and small pipe diameter. It should not be regarded the higher strength is the steel, the smaller is the allowable cold rolling deformation, which, the writer thinks, should be based on test results.[2]

The hydraulic testing is emphasized in the standards, but in terms of developing trend of penstock technology, it is sort of backward testing and passive after testing, and will be likely cancelled. Therefore, carefully choosing materials, strict technology management and NDT are effective ways of improving structure safety. In the special case when hydraulic testing be considered necessary, using acoustic emission testing could effectively inspect crack growth, it's effective to insure the safety of structure.

The standards emphasize on relieving welding residual stress. However, they were set for the conditions under conventional materials, low level of welding and NDT technology in the past time. Furthermore, almost all the measures on stress relieving have their limitation, therefore, SR is generally not performed on high strength steel. In China, this problem has been being argued for almost every project on the requirement of standards.

Experts have different opinions about SR for thicker parts of penstock in Three Gorges Project. With the reference of WES 2805-1997 Method of Assessment for Flaws in Fusion Welded Joints with respect Brittle Fracture and Fatigue Crack Growth, the writer's calculation figures based on Charp-V impact testing, proved that this structure is safe enough and doesn't need to be applied SR. [3]

Xianshui Project is a good example of this kind. The bifurcation was cancelled hydraulic testing and SR treatment, following discussions and research, and its surface defects were grinded carefully, as well as extending NDT to insure its safety. This practice provides precious information for the application of high strength steel in Chinese hydraulic stations.[4]

4. Establishing of Economic comment system for application of high strength steel

Hydraulic Projects applies high strength steel for both structural and economic reasons, therefore, a recognizable comment system need to be established in the near future.

Reference

[1] Gao Lisheng etc. China Three Gorges Construction 2001. No.1 P14-17
[2] Li Ming etc. Journal of Hohai University Vol.25 Special Issue 1997.10 P85-89
[3] Li Ming etc. Journal of Hydroelectric Engineering 2001 No.3 P96-107
[4] Li Wei etc. Guizhou Water Power 2000 Vol.14 No.2 P42-44

Weldability of high strength stainless steel developed for hydrofoils

S Koga*, A Murakami** and Y Kojima**
*Corporate Technology Division and **Shipbuilding Company,
Kawasaki Heavy Industries, Ltd., Japan

1. Introduction

For submersible struts and foils of ultra high-speed vehicle "Kawasaki Jetfoil", precipitation hardened stainless steel (15Cr-5Ni PH steel) was conventionally used. To eliminate the need to perform costly post-weld heat treatments (PWHT) that are essential to 15-5PH steel, 13Cr-5Ni-1Mo, a new martensitic stainless steel has been developed by Kawasaki Heavy Industries in partnership with Kawasaki Steel Corporation. This paper outlines the material properties of 13Cr-5Ni-1Mo and presents a study on its required welding processes. [1]-[2]

2. Characteristics of base metal

Table 1 shows an example of chemical analysis result of 13Cr-5Ni-1Mo base metal. Rolled plates in thickness ranging from 12.7 to 205mm were prepared. After 833K annealing, at any sampling location and testing direction, the base metal showed 1050 MPa in tensile strength, 1000 MPa in 0.2% proof stress and 70 Joule and higher in Charpy absorbed energy at 273K.

Table 1 Chemical analysis result of base metal

C	Si	Mn	P	S	Ni	Cr	Mo	Nb
0.021	0.32	0.55	0.021	0.004	5.30	13.10	1.06	0.060

3. Weldability

To apply to actual fabrication of Jetfoil, authors examined the weldability of 13Cr-5Ni-1Mo for various welding methods including shielded metal arc welding (SMAW), gas metal arc welding (GMAW), gas tungsten arc welding (GTAW) and electron beam welding (EBW). For arc welding methods, preheating temperature to prevent cold cracking was established by performing Y-slit cracking test. Test results are shown in Fig.5. With SMAW, it was found that the preheating temperature that prevents cracking is 350K, which is lower than the temperature required for high-strength steels of this class. With GTAW, 13Cr-5Ni-1Mo showed very low susceptibility of cold cracking.

Fig.2 shows cross sections of welds (30mm in thickness) prepared by several welding methods.

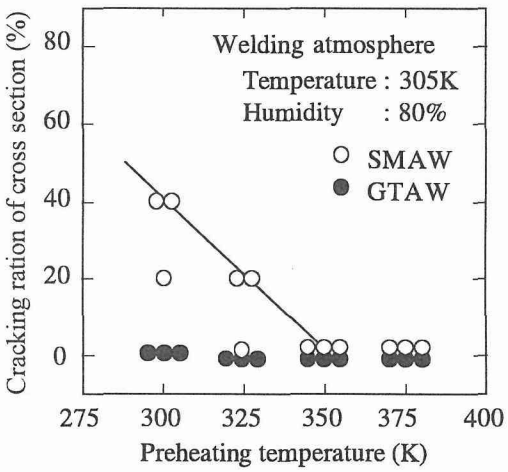

Fig.1 Effect of preheating temperature on Cracking ratio in Y-slit craking test

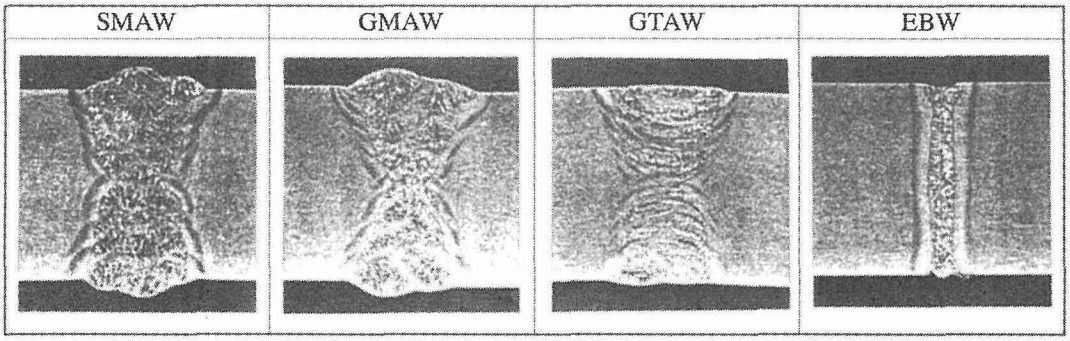

Fig.2 Cross sectional macrostructures of welds with various welding processes

4. Properties of weld joints

Fig.3 shows the distribution of residual stress of 30mm thick GMAW joint in the as-welded condition and after PWHT in the welding direction. As shown in the figure, the residual stress is sufficiently reduced by PWHT of 798K that is very low temperature for stress relieving. This is because a larger percentage of residual stress is relieved through volume expansion at austenite/martensite transformation. As shown in Fig.4, 13Cr-5Ni-1Mo shows high Mf point that allows nearly complete martensitic transformation to finish at room temperature.

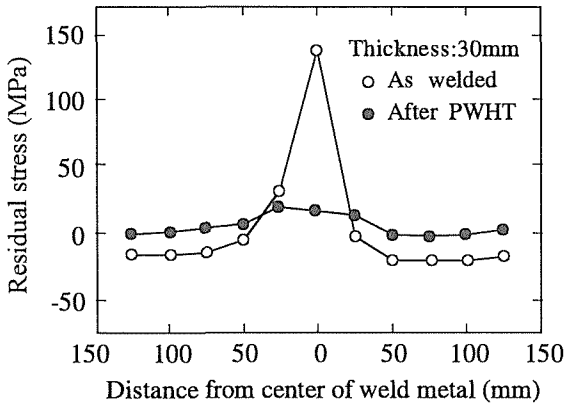

Fig.3 Distribution of longitudinal residual stress in 30mm thick GMAW joint

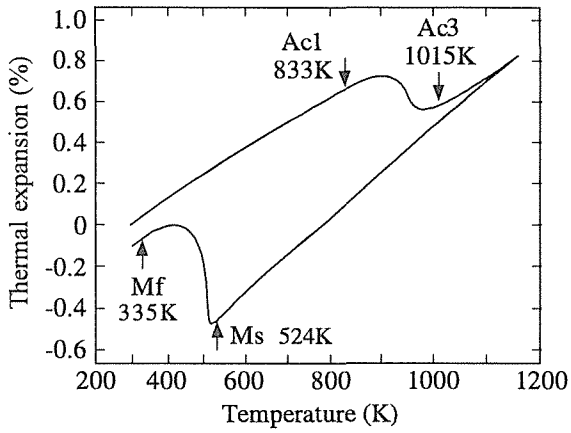

Fig.4 Formaster test result of GMAW weld metal

Tensile and impact properties of welds are shown in Fig.5 and Fig.6, respectively. Each welding method satisfied the values required for the base metal (tensile strength: 960MPa, 0.2% proof stress: 890MPa, vEo: 27J). GTAW, in particular, showed superior tensile and impact properties among welding methods tested.

Other properties of welds such as hardness, corrosion resistance, and cavitation erosion resistance were also examined and satisfactory results were obtained.

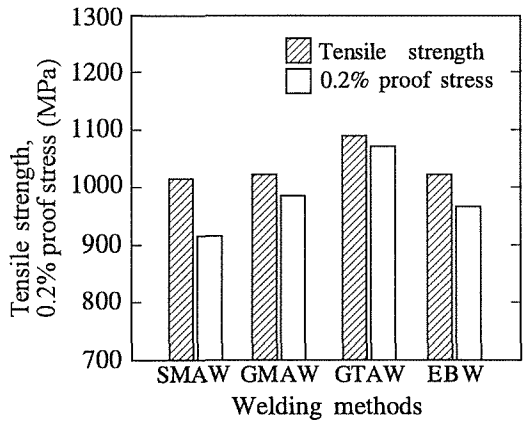

Fig.5 Tensile properties of weld metals

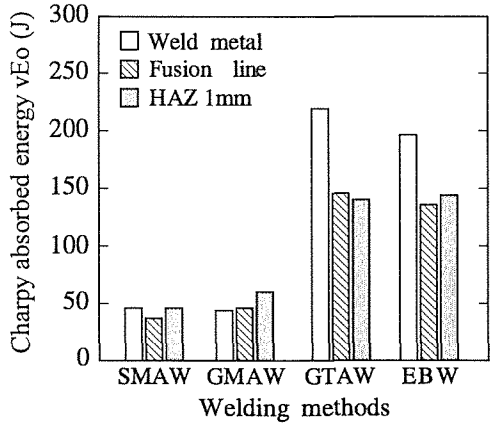

Fig.6 Charpy impact test results of welds

References

[1] Matsui, S., Kamoi, N., Matsumura, H., Imamura, M., Nakayama, S., Takeda, T., Murakami, A., Koga, S., and Ohkubo, K., IIW Doc. IV-509-89, Annual Mtg., International Institute of Welding, Sept. 1989.

[2] Kamoi, N., Murakami, A., Kojima, Y., Matsumura, H., Koga, S., Nakazawa, Y., Nihei, K., Uekado, M., and Mizuta, A., Journal of Ship Production, Vol. 9(1993), No. 1, pp.33-42.

Application of the High Strength Steel to the Building Structure

Sung-Woo Im, In-Hwa Chang

Steel Structure Research Laboratory, RIST, Korea

1. Introduction

Adaptability of the current building design codes, which are based on the results from theoretical and experimental researches on the conventional structural steels, to the design with high strength steels is not sufficiently verified. High strength steels may have mechanical properties that are significantly different from those of the conventional steels. The application of high strength steels to building structures should be reviewed in point that whether inelastic behavior equivalent to that of conventional steels can be attained or not. The main purpose of the use of high strength steels is to reduce the column size which is under high axial load. As for the experimental check, performance tests of high strength steel beam-column subjected to the simple compressive and the combined bending and axial compressive load were carried out. It was found that as far as the limit of width-to-thickness ratio was satisfied with current design code, the local buckling strength reached the maximum strength of the stub column. As the width-to-thickness ratio increased over the design limit, the stub columns did not provide the sufficient strength and the local buckling strength decreased rapidly. The compression buckling strength of the high strength steel was higher than that of code value. Beam-column test results showed that the ultimate strength was satisfied with both of ASD and LRFD codes.

2. Experimental Procedures

Stub column tests, centrally loaded column tests and beam-colum tests were performed to estimate the adaptability of high strength steel to the building structure. The box-type and H shaped welded specimens were fabricated using 570MPa grade high strength steel(Table 1). The test variable were the width-to-thickness ratio for stub column tests and the slenderness ratio for centrally loaded column tests and beam-colum tests, respectively. Experimental results were analyzed and compared the current design codes.

Table 1. Mechanical Properties of 570MPa grade high strength steel

Thickness (mm)		Upper Yield Strength (MPa)	Lower Yield Strength (MPa)	Tensile Strength (MPa)	Upper Yield Ratio (%)	Lower Yield Ratio (%)	Total Elongation (%)
570 MPa Grade	7	590.9	547.8	623.3	94.8	87.9	27.6
	9	580.1	557.5	638.7	90.8	87.3	29.6
	12	551.7	546.8	638.0	86.5	85.3	31.4
	16	590.9	587.6	668.5	88.4	87.9	34.2

3. Results

Fig. 1 showed the normalized buckling strength- $D/t\cdot\sqrt{\sigma_y/E}$, $B/t\cdot\sqrt{\sigma_y/E}$ or $H/t\cdot\sqrt{\sigma_y/E}$

ratio relations of 570 MPa grade box-type and H shaped welded stub columns, respectively. It was implied that the experimental buckling strengths reached the maximum strengths of the columns if the normalized buckling strength was higher than 1.0. The vertical dick lines indicated the limits of width-thickness ratios. It was found that as far as the limit of width-to-thickness ratio was satisfied with current design code, the local buckling strength reached the maximum strength of the stub column. As the width-to-thickness ratio increased much over the design limit, the stub columns did not provide the sufficient strength and the local buckling strength decreased rapidly [1]. Fig. 2, 3 and 4 showed ASD, LRFD and ECCS column strength curves of 570MPa grade high strength steel, repectively. As far as the limit of width-to-thickness ratio was satisfied with current design codes, all of the experimental results had excceded the theoretical strengths[1]. In case that the beam-columns were bent in reverse curvature, the ultimate strength was satisfied with both of ASD and LRFD codes.

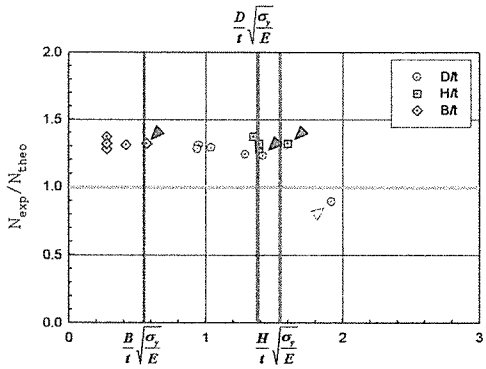

Fig. 1 Effect of Width-Thickness Ratios on Buckling Strengths

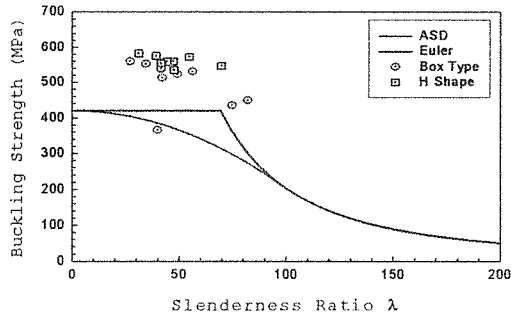

Fig. 2 ASD Column Strength Curve

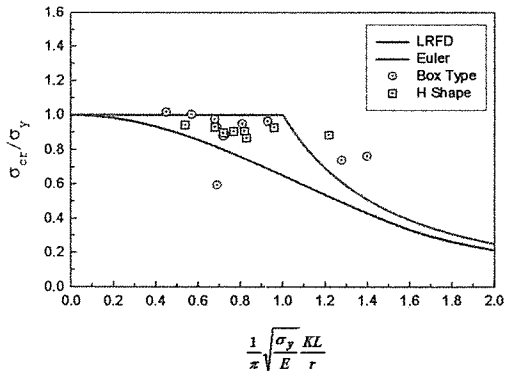

Fig. 3 LRFD Column Strength Curve

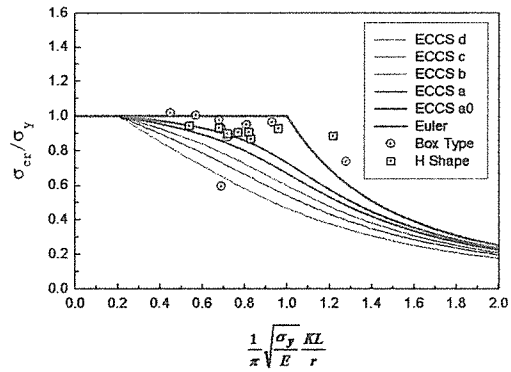

Fig. 4 ECCS Column Strength Curves

4. References

[1] S.W. Im, S.K. Ko and I.H. Chang, A Study on the Characteristics of High Tensile Strength Steel (SM570) Plates in Compression Members, Magazine and Journal of Korean Society of Steel Construction, 2001, Vol.13, No.3, pp.223-232

Study on Design for High Strength Steels Structure

K. INOSE, Dr. Y.NAKANISHI, Dr. I.IMOTO
Ishikawajima-Harima Heavy Industries Co., Ltd. Japan

1. Introduction

By using high strength steel, dead weight of structure is decreased. As a result, performances of structure, space for service, earthquake resistance, scale of structure etc, are improved. However, high strength steels have been used for large-scale structure mainly. In light of these facts, the study for rational usage of these materials has been conducted on the viewpoint of design.

2.Advantage of high strength steels and points to be considered on design

A studied bridge design characteristic was shown in Table 1. Usually, Cable-stayed Type Bridge is applied for a span of 500m long. By employing Nielsen Lohse-system Bridge with HT780 steel, quantities of materials were decreased and the work period of erection was shortened. Points to be considered on design were shown in Fig.1. Safety and serviceability are required for structures. This means these functions, ultimate strength, stiffness, and fatigue, shall be consistent for the purpose of a structure entirely. High strength steels contribute ultimate strength, especially tensile load. However it is not so effective for increasing of elastic buckling strength, stiffness for stability, and fatigue at welding joints.

3.Problem of design for high strength steels structure

Further study for high strength steel is necessary to review the present design criteria. In a design code, allowable stress of high strength steel is limited to low value as shown in table 2(Allowable stress design method). Shown in Fig.2 is the buckling strength, which was provided according to experiments and analysis based on conditions of low strength steels [1]. (E.g. residual stress due to welding was considered as $\sigma_R=0.30\,\sigma_Y$). These conditions are applied for high strength steels. Developing the new type of steel structure is also required. One of a prototype structure has been proposed shown in Fig.3. Closed section ribs filled with elastic solid prevent from local buckling in order to improve the compressive strength.

4. Subject of Economical Efficiency resulting from Material

A studied design for medium scale bridge shown in Fig.4 has been examined. And resultant of the study was shown in table 3. Total cost of materials was increased linearly with strength of steels and unit price of material. Generally, fabrication cost of high strength steel structure tends to be expensive because of troublesome quality control. Consequently, medium scale bridges using high strength steels not have ability to compete without rationalization for material cost and workability. Considering present status, which most share of bridge market occupied by medium and small-scale bridges, resolving these issues is necessary to increase high strength steels adoption.

5.Conclusion

-High strength steels should be used at appropriate part of structures.
-Reviewing present design criteria and developing new type of structure are required.
-It is expected that demand of high strength steels will increase due to rationalization of material cost and workability.

References

[1] Yuhshi FUKUMOTO, Guidelines for Stability Design of Steel Structure, October 1987.

Table. 1. Estimation of 500m span Bridge

	Tyep of super structure	Quantity of the fabrication		Erection procedure
A	Cable stayed bridge 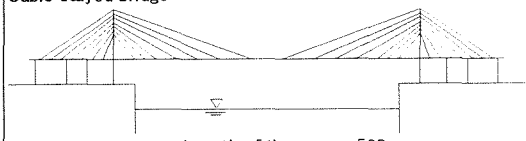 Length of the span=500m	Material	SM570, etc	Cantilever erection (25months)
		Tower	4,000ton	
		Girder	6,000ton	
		Cable	4,400ton Φ7mm×214×14,700m	
		Others	100ton	
		Total	13,500ton	
B	Lohse bridge 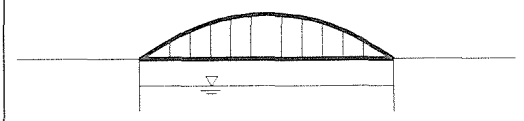 Length of the span=500m	Material	HT780, etc	Large block erection (15months)
		Arch	5,000ton	
		Girder	5,500ton	
		Cable	400ton Φ7mm×163×4,200m	
		hanger	720ton	
		Total	11,620ton	

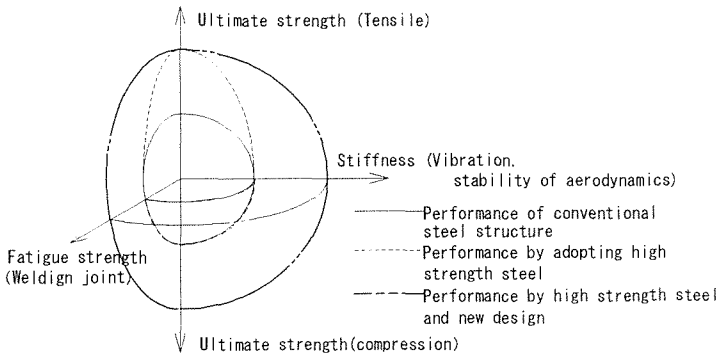

Fig.1. Key points to be considered for the Design

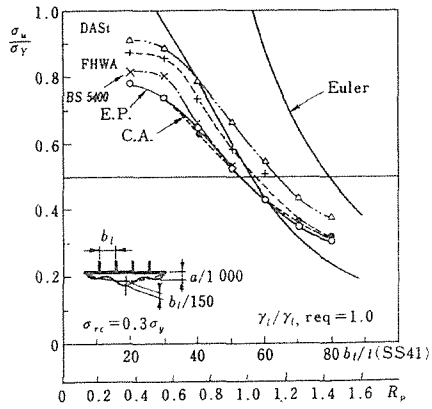

Fig.2. Buckling strength of the Design code [1]

Table.2. Allowable stress of the steels in the Design code

	Tensile strength σB	Yield point σY σY0.2%	Yield ratio σY／σB	σY／1.7	σB／2.2	Allowable stress σca0
SM400	410	240	58.5	140	190	140
SM490	500	320	64.0	190	230	190
SM490Y	530	360	67.9	210	240	210
SM570	58	460	79.3	270	260	260
HT690	700	600	85.7	350	320	320
HT780	800	700	87.5	410	360	360

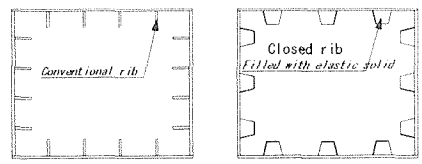

Materials per unit [m]

Paint (inside) 19.96m²→15.62m² (78%)
Welding length of ribs 72.0m(eauivalence s=6mm)
→24.0m (33%)
Number of Ribs 16→12
Heat input by welding 85536kJ→28512kJ(33%)
Elastic solid 0m² → 0.768m²

Fig.3. Comparison between Conventional pier and prototype pier

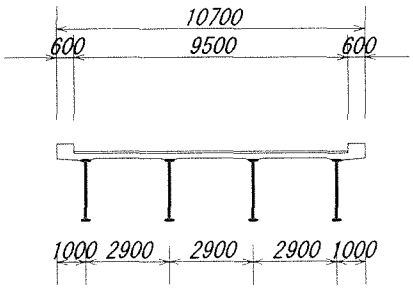

Fig.4. Cross section of the bridge which is used for estimation

Table.3. Relation between the strength and material cost

	Strength	Unit price	Quantity	Total cost
SM400	1.00	1.00	1.00	1.00
SM490	1.36	1.12	0.78	0.87
SM490Y	1.50	1.13	0.73	0.82
SM570	1.86	1.62	0.66	1.07
HT780	2.57	3.16	0.60	1.90

(comparison with SM400 steel)

Role of inclusions on acicular ferrite and bainitic transformations in steels†

S. S. Babu and S. A. David
M&C Division, Oak Ridge National Laboratory, Oak Ridge, TN 37831

Introduction

Creation of advanced structural steels is achieved by reducing ferrite grain size through mechanical alloying, excessive plastic deformation and or low-temperature phase transformations. However, fusion welding with remelting and resolidification of these steels is expected to destroy the optimum microstructure that is obtained before welding. Therefore, new methods must be developed and conventional technology must be optimized to induce fine ferrite grain size even in the weld metal. However, this requires precise control of various physical processes that occur during welding of steels as shown schematically in Fig. 1. The inclusion formation must be controlled through gas-slag-liquid reactions. The solidification, austenite grain size, and the decomposition of austenite to ferrite must be controlled through weld metal composition and cooling rate. The present paper reviews research activities at Oak Ridge National Laboratory (ORNL) to describe each of the above phenomena through characterization and modeling.

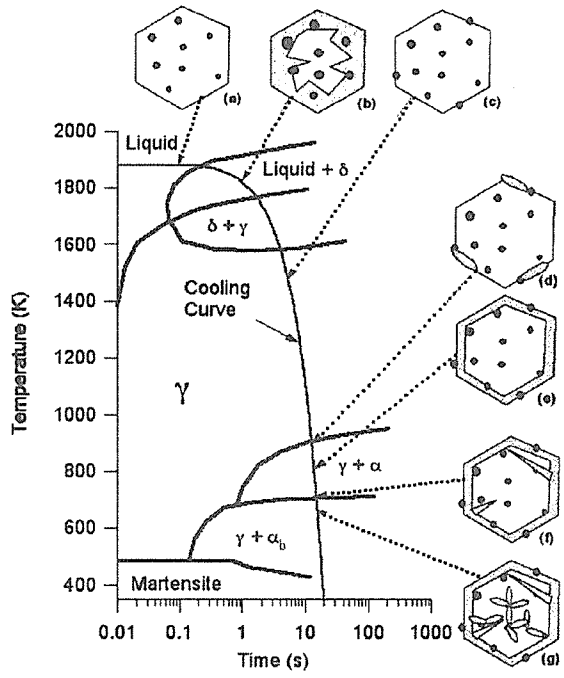

Fig. 1 Schematic illustration of overall microstructure evolution during fusion welding of high-strength low-alloy steels illustrating different stages of microstructure evolution

Inclusion Formation

In previous research, detailed thermodynamic and kinetic models for describing oxide inclusion formation have been developed by the authors and other researchers. Recent collaborative work with Lincoln Electric Company showed that there is a competition between oxide and nitride formation depending upon the dissolved aluminum, titanium, oxygen and nitrogen concentration in self-shielded flux cored arc welds. In welds containing large concentrations of aluminum and nitrogen, aluminum nitride formation was observed. In contrast, the welds with low-aluminum and low-nitrogen with small additions of titanium promoted the simultaneous formation of aluminum oxide and titanium carbonitride. Computational thermodynamic models successfully predicted these reactions. Implications of such inclusion formation on subsequent solidification and solid-state transformation will be highlighted.

Phase Selection during weld solidification

It is well known that increase in weld cooling rates may induce nonequilibrium changes in solidification structure morphology as well as nonequilibrium phase selection. The change in primary phase solidification from equilibrium δ-ferrite to austenite in stainless steels and are well known. However, investigations of such transitions in high-strength low-alloy steels are difficult due low-temperature decomposition of austenite to ferrite. Recent collaborative research of ORNL and Lawrence Livermore National Laboratory (LLNL) using *in-situ* time-resolved X-ray diffraction technique with Synchrotron radiation showed similar change in primary solidification mode in a Fe-C-Al-Mn steel weld. Theoretical evaluation of such transformations using computational thermodynamics and interface-response functions will be presented.

Competition between Bainite and Acicular Ferrite Formation

Role of oxide inclusions in promoting acicular ferrite formation in welds is well known. Research has shown that the transformation of austenite to acicular ferrite or to bainitic ferrite occurs by displacive mechanism except for the nucleation sites. In this research the transformation kinetics of austenite were measured in welds with similar hardenability, with different microalloying additions, under continuous cooling conditions. A transition from bainite to acicular ferrite was observed in these welds with a change in the inclusion characteristics. In addition, the transformation kinetics of austenite to bainitic ferrite was slower than that of austenite to acicular ferrite. The above phenomenon was attributed to subtle changes in the inclusion composition and allotriomorphic ferrite formation along the austenite grain boundaries. Attempts to model the above transition using simultaneous transformation kinetic theories will be discussed.

Relevance to Fusion Welding of Fine-Grained Structural Steels

The goals of fusion welding fine grained advanced structural steel are as follows (1) Minimize the heat-affected-zone width to reduce the deterioration of base-metal microstructure and (2) Obtain a fine-grained high-toughness weld microstructure that is comparable to that of base - metal. The first goal can be achieved by employing high-energy density welding process such as laser welding processes. However, for satisfying the second goal, we need to control the inclusion formation through consumable composition, shielding gas, and cooling rate. In this regard, role of hybrid arc-laser welding processes will be highlighted.

Summary

The formation of oxide and nitride inclusions in low-alloy steels will be discussed. The roles of weld metal composition and cooling rate on primary solidification and the decomposition of austenite to acicular ferrite or bainite will be presented. The methodology to predict the above microstructure evolution using computational thermodynamic and kinetic model will be presented. The relevance of these phenomena towards the creation of fine-grained ferrite microstructure in welds will be discussed.

Acknowledgement

This research was sponsored by the Division of Materials Science and Engineering, U.S. Department of Energy, under contract DE-ACO5-00OR22725 with UT-Battelle. The authors thank Ms. M. A. Quintana of Lincoln Electric Company, Cleveland Ohio for supplying Fe-All-C-Mn steel welds, G. M. Evans for providing titanium containing steel welds and Dr. J. W. Elmer of Lawrence Livermore National Laboratory for in *in-situ* TRXRD investigations using Synchrotron radiation.

Microstructure and Mechanical Properties of GMA Weld Metal for 950 MPa Class Steel

M.A. Gouda, M. Takahashi, T. Kuroda and K. Ikeuchi
JWRI, Osaka University

Abstract

The present study provides a detailed assessment of the effect of the shielding gas composition on the microstructures and mechanical properties of welds produced on 950MPa high strength steel. For these purpose several mixtures of argon plus carbon dioxide were used as shielding gas. An increase in CO_2 content in the shielding gas was accompanied by an increase in the O content, decreases in Si, Mn, Ti and Al in the deposited weld metal, deterioration in mechanical properties, and the microstructural changes from martensite + acicular bainite to granular bainite with the formation of M-A constituents.

Introduction

Welding of 950MPa class high strength steel is strongly demanded in the construction of large steel structures. Significant literatures on the welding of high-strength steel have been reported, but most of them focused on the heat-affected zone microstructures and properties[1-5]. There are only limited published researches on the microstructures and properties of the weld metals of high strength steel [6-9]. Recently weld metal of 950MPa class high strength steel is under development to obtain the required strength and toughness, which strongly depend on the formed microstructures. Generally, the microstructure and properties of weld metal are controlled by two factors, its composition and cooling rate[10]. The major problems in welding 950MPa class high strength steel are the microstructural instability during the thermal cycle of welding[11]. Many researches has been tried to clarify the weld metal microstructures, but till now they are not well-understood[12-14]. The aims of this research are to give a clear definition to the weld metal microstructure of 950MPa class high strength steel and to investigate the effect of gas composition on weld metal properties.

2. Experimental Procedure

950MPa class steel welding coupons, 12 X 120 X 200mm, were used. A groove was cut at the center of coupon. The groove angle was 65^0, groove depth 9mm and gap distance 3mm. Welding was done by gas metal arc welding (GMAW). Single pass welding was performed with different shielding gas compositions: Pure Ar, 10% CO_2-Ar, 15% CO_2-Ar, 20% CO_2-Ar, and 25%CO_2-Ar. The traveling speed and welding current were fixed, to give heat inputs 3kJ/mm. The cooling rate of the weld metal was measured with a thermocouple immersed into the weld pool just behind the arc as described in reference[15]. The chemical compositions of the base metal and commercial filler metal are shown in Table1.

Table 1 Chemical composition of high strength steel base metal and filler metals (mass %).

	C	Si	Mn	P	S	Cu	Ni	Cr	Mo	V	Al	Nb
Base metal	0.12	0.17	0.74	0.001	0.004	0.24	3.13	0.56	0.65	0.003	0.053	0.012
Filler	0.07	0.49	1.49	0.003	0.001	0.15	3.12	0.58	0.91	-	-	-

The distribution of elements in the weld metal was analyzed with an EPMA. To estimate mechanical properties of all weld metals obtained, Vickers hardness, and Charpy impact tests were utilized. Observations of microstructure were carried out with optical, scanning electron and transmission electron microcopies.

3- Result and discussion

Compositions of the weld metals were varied with CO_2 content in the shielding gas as listed in Table 2. The increase in the CO_2 content of the shielding gas increases the oxygen content in the deposited weld metal. The consequent decrease in Mn, Si, Al, and Ti contents suggested that, the content of these elements were reduced by the oxidation in the weld pool.

The effect of the CO_2 content on hardness and absorbed energy are shown in Fig. 1.The average of hardness and absorbed energy increased as the CO_2 content in shielding gas decreased. Optical microstructures of weld metals by the shielding gases of pure Ar and 25% CO_2-Ar that were revealed by Nital etching are presented in Fig. 2a and 3b, respectively. Weld metal by pure Ar showed well-developed lath structure. With the increase in CO_2 content of the shielding gas, the lath became obscure.

Table 2 Compositions of the weld metals (mass%).

Shielding Gas	C	Si	Mn	Cu	Ni	Cr	Mo	Ti	V	Al	O	N
Pure argon	0.089	0.36	1.26	0.22	3.13	0.59	0.83	.025	.015	0.031	.0024	.011
Ar +10% CO_2	0.092	0.25	1.00	021	3.11	0.58	0.82	.01	.015	0.023	.025	.0034
Ar +15% CO_2	0.089	0.21	0.94	0.22	3.12	0.57	0.83	.01	.013	0.016	.027	.0033
Ar +20% CO_2	0.094	0.20	0.89	0.22	3.12	0.57	0.82	.01	.013	0.016	.029	.0032
Ar +25% CO_2	0.092	0.16	0.80	0.21	3.12	0.57	0.81	.008	.013	0.014	.031	.0034

Where sulfur and phosphorus were 0.001, and 0.0043% consequently.

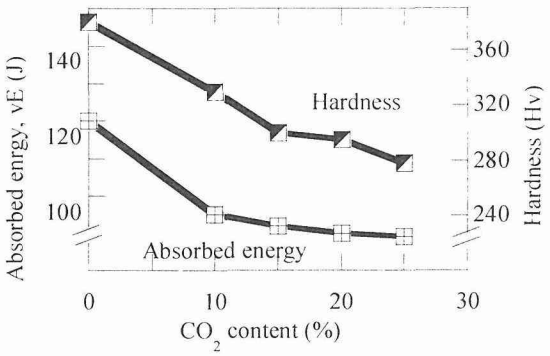

Fig. 1 Hardness and absorbed energy of the deposited metals as a function of CO_2 content in the shielding gas.

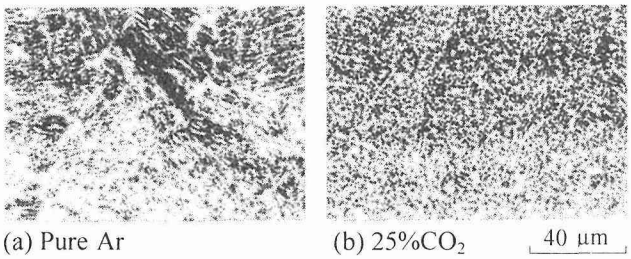

Fig. 2 Weld metal microstructures of weld metals by pure argon and 25%CO_2 shielding gas

References

1. H.Ikama,, H.Oshige, and T. Tanque,: Transaction of Japan Welding society, 11(1980), February, p. 50.
2. H Suzuki: IIW (1983), DOC.IX – 1280-83.
3. R.E. Dolby and J. F. Knott: Journal of Iron and Steel Institute, (1972), November, p.857.
4. M.J., Godden and J. D. Boyed: Microstructural Science, 9 (1981), p.343
5. K.Hrivnak: Welding in the World, 16(1978), July, p.130.
6. J. Cabelka and C. Million: Welding Journal, (1966), October, p.587.
7. P. J. Konkol and A.M. Rathbone: Welding Journal, 45(1966), December, p.525.
8. G.G Saunders: Welding Institute, 7(1977), February, p.91.
9. E.F. Nippes, W.F. Savage and J.M.Paez: Welding Journal, 38(1595), December, p.475.
10. P.T. Oldland, C.W. Ramsay, D.K. Matlock and D.L. Olson: Welding Journal (1989), April, p. 158.
11. Z. Yang and T. Debroy: Metallurgical and Material Transactions, 30B(1999), June, p. 483
12. J.E. Ramirez, S. Liu, and D.L. Olson: Material Science and Engineering, A212 (1996), p.91.
13. J. Liao, H. Kametani, H. Okada and K. Ikeuchi: Journal of Japan welding Society 18(2000), August, p. 496.
14. D.A. Fleming, A.Q. Bracarense, S. Liu and D.L. Olson: Welding Journal, (1996), June, p.171.
15. J.B. Brozda and M. Kubica: Welding International, 9(1995), April, p. 257.

Fatigue Strength Improvement of Welded Joints by Low Transformation Temperature Welding Material

Akihiko OHTA, Naoyuki SUZUKI and Yoshio MAEDA
Strength and Life Evaluation Research Group, NIMS, Japan

1. Introduction

The fatigue strength of welded joints is far below that of base metal due to the existence of high tensile residual stress and stress concentration. In this situation, the fatigue strength of welded joint is independent from the yield strength of base metal, though the fatigue strength of base metal increases with the strength of steel.

In order to overcome this situation, the authors developed the welding material to inducing the compressive residual stress around weld in the as-welded condition. The developed welding material expands in the final process of welding due to the transformation from austenite to martensite. This expansion is constricted by the surrounding base metal, and induces the compressive residual stress. The compressive residual stress acts as the mean stress, and improves the fatigue strength.

In this review, some experimental results showing the improved fatigue strength of welded joints and another properties of developed welding wire are introduced.

2. Concept of Residual Stress Inducement

The mechanism of the inducement of residual stress is shown in Fig.1. The relationships between temperature and strain or stress are measured during cooling process of welding. The former was measured in the free deformation condition; the later, in the strain constrained condition.

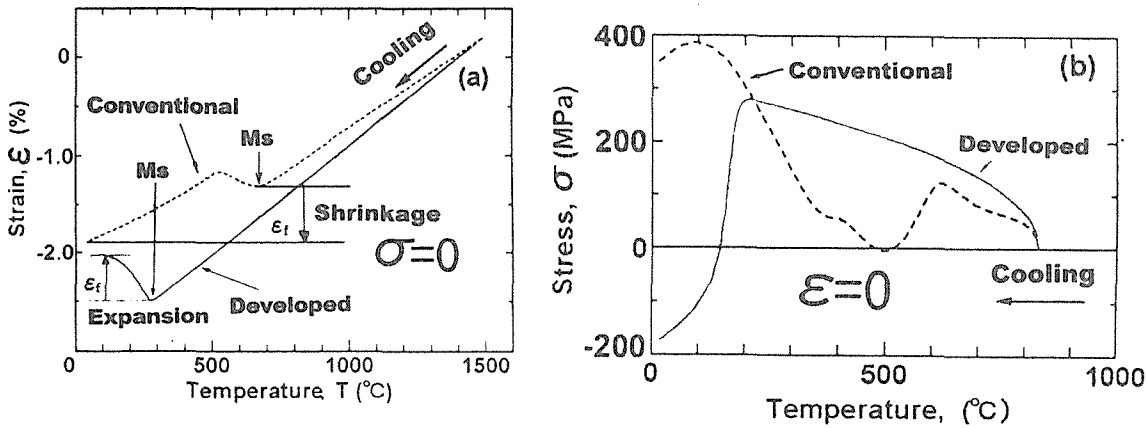

Fig.1 Relationships between temperature and strain or stress during cooling process.

In case of conventional welding material, the expansion due to the transformation from austenite to martensite is observed around 500℃ as shown in Fig.1(a) with a broken curve. However, the shrinkage occurs after the finish of transformation. So, the shrinkage becomes dominant. The tensile stress is induces when the strain kept to be zero as shown in Fig.1(b).

In case of developed welding material, the transformation temperature is low as shown in Fig.1(a) with a solid curve. The expansion finished around room temperature. That is, the expansion becomes dominant. The compressive stress can be induced at room temperature in the as-welded condition.

This compressive residual stress acts as a compressive mean stress, and improves the fatigue strength of welded joints.

3. Examples of Fatigue Strength Improvement of Welded Joints

3.1 Additional Welds around Box Weld of Attachment

The fatigue limit could be improved about twice of the original welded joint by additional welds around box weld of attachment.

3.2 Box Section Welded Member

The fatigue strength at $2x10^6$ cycles for box section of 250mm high and 200mm wide with 15mm thick plates was improved about 1.3 times.

3.3 Lap Welded Joints

The fatigue limit of lap welded joints of 2mm thick plate of 540MPa and 780MPa class steel was improved about 1.3 times and 1.6 times, respectively as shown in Fig.2. That is, the fatigue strength of stronger steel became high in case of developed welding wire, though it is same in case of conventional welding wire.

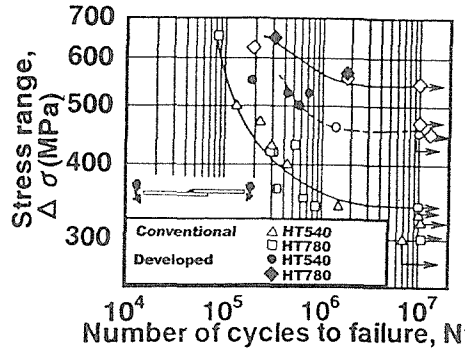

Fig.2 S-N curves of lap welded joints.

4. Prevention of HAZ Fracture of Ultra-Fine Grained Steel Butt Welded Joint in Tensile Test

The butt welded joint of 19mm square ultra-fine grained steel bar was prevented from fracture at softened HAZ in case of developed welding wire and the fracture strength became that of base metal, though it fractured at softened HAZ in case of conventional welding wire.

5. Corrosion Test Results

The heavy corrosion near the weld line exposed in shower of synthetic seawater for 4 years was not observed both in joints made with conventional and developed welding wires.

References

[1] Fisher, J., Fatigue Strength of Welded A514 Steel Beams, Proc. Conf. Fatigue of Welded Structures, The Welding Institute1(1871), pp135-148.

[2] Sander,W.W., Derecho,A.T. and Munse,W.H., Effect of External Geometry on Fatigue Behavior of Welded Joints, Welding Journal(1965), pp49s-55s.

[3] Ohta,A., Watanabe,O., Matsuoka,K., Shiga,T., Nishijima,S., Maeda,Y., Suzuki,N. and Kubo,T., Fatigue Strength Improvement by Using Low Transformation Temperature Welding Material, Welding in the World 43(1999), pp38-42.

[4] Ohta, A., Suzuki,N. and Maeda, Y., Doubled Fatigue Strength of Box Welds by Using Low Transformation Temperature Welding Wire, Properties of Complex Inorganic Solids 2(2000), pp401-408.

[5] Ohta,A., Maeda,Y., Nguyen, N.T. and Suzuki,N., Fatigue Strength Improvement of Box Section Beam by Low Transformation Temperature Welding Wire, Welding in the World 44(2000), pp26-30.

[6] Ohta,A., Watanabe,O., Matsuoka,K., Maeda,Y. and Suzuki,N., Fatigue Strength Improvement of Box Welds by low Transformation Temperature Welding Wire and PWHT, Welding in the World 44(2000), pp52-56.

[7] Ohta, A., Maeda,Y. and Suzuki,N., Fatigue Life Extension by Repairing Fatigue Cracks Initiated around Box Welds with Low Transformation Temperature Welding Wire, Welding in the World 45(2001), pp3-8.

[8] Ohta,A., Suzuki,N. and Maeda, Y., Extension of Fatigue Life by Additional Welds around Box Welds Using Low Transformation Temperature Welding Material, submitted to ASCE.

[9] Ohta, A., Suzuki,N. aand Maeda,Y., Fatigue Strength Improvement of Lap Welded Joints by Low transformation Temperature welding Wire –Superior Improvement with Strength of Steel-, to be presented at Annual Assembly of IIW Committee XIII(2002).

Improvement of Fatigue Strength of Welded Joints by Using Low-Temperature Transformation Welding Consumables

by Y. Morikage*, T. Kubo*, K. Yasuda* , K. Amano* and C. Shiga**

*Technical Research Laboratories, Kawasaki Steel Corporation
1 Kawasaki-cho, Chuo-ku, Chiba 260-0835, Japan
**Materials Engineering Laboratory, National Institute for Materials Science
1-2-1 Sengen, Tsukuba, Ibaraki 305-0047, Japan
(Present address : Japan Science and Technology Corporation)

1. Introduction

The fatigue strength of welded joints is independent of the yield strength of steel plate while that of steel plate increases as the yield strength of steel plate because of tensile residual stress around weld toes[1]. Therefore, higher strength steels are hardly applied to steel constructions which subjected to cyclic load. It has been shown that the low-temperature transformation welding consumable that contains large amount of Cr and Ni can bring compressive stress into around weld toes[2, 3] and is expected to improve the fatigue strength of welded joints of higher strength steel plate. In this study, the effect of yield strength of steel strength on fatigue property has been investigated by using non-load-carrying cruciform joints welded with the low-temperature transformation welding consumable.

2. Experimental Procedures

Fatigue strength was examined for non-load-carrying cruciform welded joints. The geometry of specimen is shown in Fig.1. The steel plates were the 400, 590 and 780MPa grade steels.

The steel plates were welded using two shield metal arc welding rods. One was the low-temperature transformation welding consumable with 11%Cr and 9.5%Ni, and the other was the conventional welding consumables.

Non-load-carrying cruciform welded joints were made by horizontal fillet welding under the welding condition of 200A-30V-15cpm. Neither preheat nor PWHT were applied. Not only horizontal fillet welding but also flat position welding was applied when 11Cr-9.5Ni shielded metal arc welding rods were used for the purpose of revealing the effect of stress concentration factor (K_t). The sequence of welding was carried out by one pass welding. Fatigue tests were carried out under cyclic axial condition($R \fallingdotseq 0$), constant sinusoidal wave and 8Hz repetition rate.

3. Results and Discussions

Figure 2 shows the fatigue test results of welded joints in case of a 780MPa grade steel. The fatigue strength of welded joints which applied 11Cr-9.5Ni shielded metal arc welding rod was about 170MPa at 2×10^6 cycles and was 60MPa higher than that of conventional welded joints.

The relation between the fatigue strength at 2×10^6 cycles of welded joints and yield strength of steel plates is shown in Fig. 3. The fatigue strength of welded joints of the 11Cr-9.5Ni shielded metal arc welding rods increased as the strength of steel plate while that of conventional welded joints is hardly improved as the strength of steel plate. Furthermore, in case of 11Cr-9.5Ni shielded metal arc welding rods, the fatigue strength of the welded joints under flat position welded joint was much higher than that of horizontal fillet welded joint.

Figure 4 shows the relation between the fatigue strength at 2×10^6 cycles and K_t of steel plates and welded joints[1]. In case of steel plate, the difference between fatigue strength of higher yield strength steel and that of lower yield strength steel is remarkable and

the difference becomes less as the stress concentration factor is higher. The fatigue strength of 400MPa and 780MPa grade steel welded joints, however, are almost same because of the existence of tensile residual stress near weld toes.

The result in this study is also plotted in Fig. 4. The fatigue strength of welded joint using 11Cr-9.5Ni shielded metal arc welding rod improves to almost same fatigue strength of steel plate with same K_t. This tendency is suitable to not only 780MPa grade steel but also 400MPa grade steel. This result means that the fatigue strength of the welded joint using 11Cr-9.5Ni comsumable rod is almost same as that of the same grade steel plate.

4. Conclusions

The fatigue strength of the weld joints using the 11Cr-9.5Ni shielded metal arc welding rod increases as the yield strength of steel plate while that of conventional welded joints is independent of the steel plate.

Acknowledgments

The authors would like to acknowledge the support by Research Laboratories, Nippon Welding Rod Corporation on manufacturing the 11Cr-9.5Ni shielded metal arc welding rod.

Reference

1) O.Watanabe, S.Matsumoto, Y.Nakano and Y.Saito: Quarterly J. Japan Welding Soc., **13**(1995), p.438-443

2) A.Ohta, O. Watanabe, K.Matsuoka, C.Shiga, S.Nishijima, Y.Maeda, N.suzuki and T.Kubo: Quarterly J. Japan Welding Soc., **18**(2000), p.141-145

3) F.Machida, T.Fujita, K.Yoshie, T.Kubo: *Proc. 52nd IIW Annual Assembly* (1999), *International Institute of Welding*, IIW Doc. XIII-1771-99

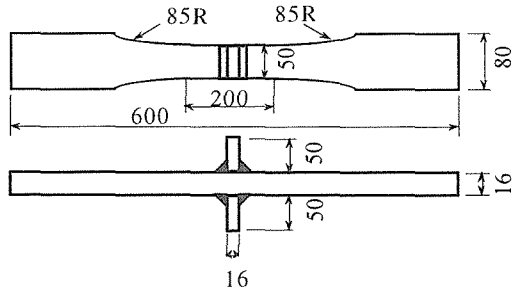

Fig. 1 Fatigue test piece of non-load-carrying cruciform welded joints

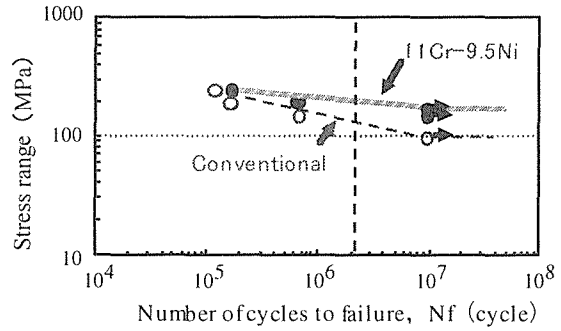

Fig. 2 S-N diagrams of welded joint (780MPa grade steel)

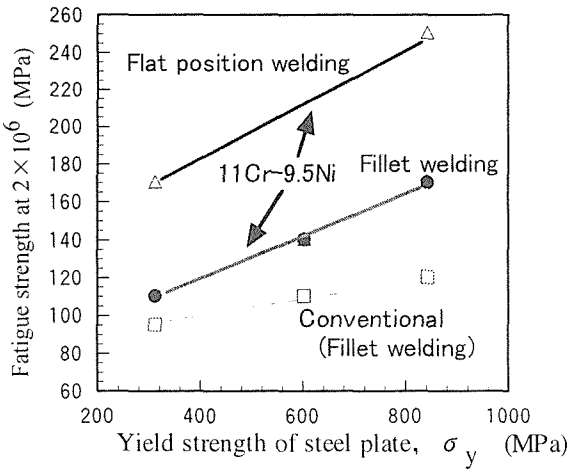

Fig. 3 Relation between yield strength of steel plate and fatigue strength of welded joint at 2×10^6 cycles

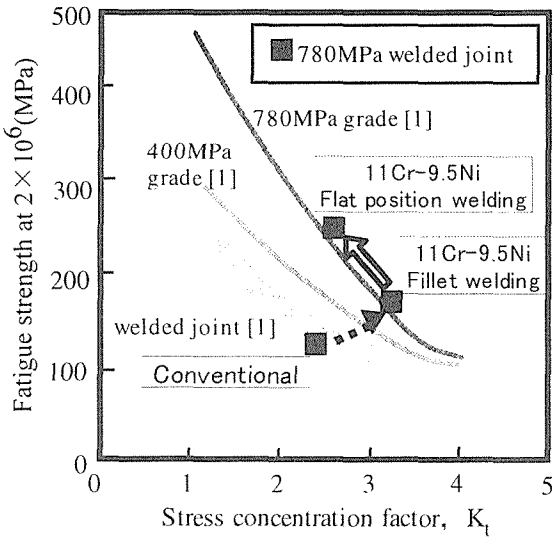

Fig. 4 Relation between fatigue strength, stress concentration factor and strength of steel

Chemical Overmatching of Weld Metal in Welding of Advanced High-Strength Steel

N. Yurioka

Technical Development Bureau, Nippon Steel Corporation, Japan

1. Introduction

The hot rolling process of steel plates have been developed continuously since half century ago. This results in a decrease in alloying elements in steels and thereby a significant improvement of weldablity of steels. On the other hands, the chemical composition of a weld metal has remained unchanged because it is formed as solidified without hot rolling and heat treatment. It follows that a gap between HAZ and weld metals has been increasingly widening concerning their compositions and thus weldability.

2. History of hot rolling process

Before and during World War II, high strength steels are produced as hot rolled (AR) without any heat treatment. The Ducole steel and St52 steel were used for bridges and war ships. In welding of them, cold cracking caused by hydrogen generated during welding was the most important concern. Armor plates of very high strength grades could not be welded by ferritic electrodes because of cold cracking and austenitic electrodes had to be used in order to shut hydrogen in the austenitic weld metal.

In 1952, the US Steel successfully produced T-1 steel of a TS 780MPa grade with chemistry similar to armor plates but with the reduced carbon content to 0.15% by the quenched-tempered (QT) process. This steel was famed for a highly weldable and tough steel. However, hydrogen cracking still occurred in many steel bridges made of T-1 steels and preheating of quite high temperatures were needed. In the late 1960s, the roller quenching process replaced the conventional press quenching process, enabling to reduce the carbon content.

In the late 60's, the controlled rolled (CR) process was developed to mostly produce C-reduced line-pipe steels. They need to be provided with desirable weldability becasuse they are girth-welded with high hydrogen electrodes. In the early 80's, Japanese steel manufactures succeeded to employ TMCP (CR and accelerated cooling) and produce structural steels with further reduced alloying elements. TMCP enabled to refine steel microstructures, and thereby improve strength and toughness resulting in the significant reduction of CE.

3. Chemical compositions of steel and weld metal

Weldability of steels is considered to preferably evaluated by the following carbon equivalent (CE):

$$CE = C + \frac{Mn}{6} + \frac{Cu + Ni}{15} + \frac{Cr + Mo + V}{5}$$

Table 1 shows chemical compositions of steels and weld metals of various grades and differently produced by AR, N(normalized), QT and TMCP. It is seen that with an increasing development of hot rolling processed, CE has been further decreased. For instance, CE of HT490 steels decreases from 0.442 to 0.380 and 0.302 as the process advances from the as-rolled process to the normalized process and TMCP. Since the composition of weld metals remains unchanged, the chemical balance of welded joints changed from undermatching (weld metal with lower CE) to overmatching (weld metal with higher CE). It is obvious that the

degree of overmatching becomes more intensive as the steel strength increases.

4. Cold cracking and toughness in high-strength steel welded joints

As seen in Fig.1 of a macro-photograph of a Y-groove weld of HT780 grade steel, hydrogen- assisted cold cracking occurs in the weld metal not in HAZ. This is because CE is higher in the weld metal than in HAZ. Not only for cold cracking but also for toughness, the weld metal remains not improved. Fig.2 is a typical example of toughness discrepancy between the weld metal and HAZ of a 9Cr steel.

5. Remarks

The weld metal is an important part of a welded joint as HAZ is. The performance of welded joints in advanced high strength steels is governed by the property of the weld metal because of higher CE of the weld metal than HAZ. High strength steels has already been enough improved. It is now time to make a great effort to improve properties of weld metals by decreasing their CE.

Table 1 Chemical Compositions of Steel and Weld Metal

	Process	C	Si	Mn	Cu	Ni	Cr	Mo	Nb	V	B	CE
HT490	As Rolled	0.19	0.39	1.51								0.442
	Normarized	0.14	0.41	1.44								0.380
	TMCP	0.10	0.24	1.19					0.020	0.020		0.302
	Weld Metal(SAW)	0.09	0.25	1.49	0.07				0.010	0.010		0.345
HT590	Ducole(AR)	0.21	0.16	1.58	0.35							0.497
	QT	0.11	0.23	1.39					0.050	0.050	0.0010	0.352
	Weld Metal(SAW)	0.09	0.23	1.42			0.05	0.28		0.030	0.0050	0.399
HT780	Armor	0.25	0.29	0.63		3.15	0.85	0.60				0.855
	T-1(QT)	0.15	0.22	0.85	0.35	0.85	0.62	0.50		0.040	0.0040	0.604
	QT	0.11	0.21	0.85	0.22	0.97	0.53	0.43		0.050	0.0050	0.534
	Weld Metal(SAW)	0.07	0.22	1.47	0.08	2.21	0.49	0.56		0.011	0.0000	0.680
HT980	DQT	0.11	0.22	0.90	0.23	2.32	0.58	0.53	0.012	0.040	0.0013	0.660
	Weld Metal(SAW)	0.08	0.16	1.44	0.10	2.85	1.00	1.03	0.030	0.007	0.0005	0.924

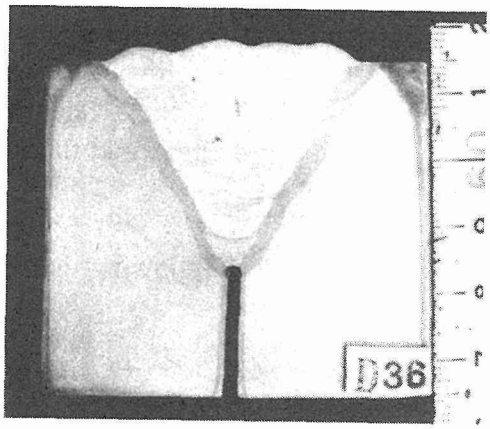

Fig. 1 Weld metal cold cracking in TS780MPa welded joint

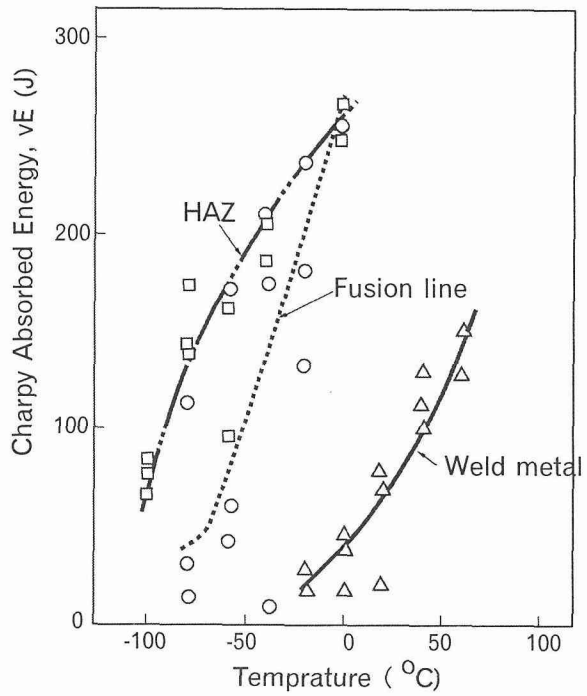

Fig.2 Charpy energy of SAW weld of mod. 9Cr-1Mo large diameter pipe

Factors Controlling Cold Crack Susceptibility of Weld Metal

H. J. Kim
Materials Reliability Center, KITECH, Korea

1. Introduction

In the past, heat affected zone (HAZ) hydrogen induced cold cracking (HICC) was the most common type of cracking observed in steel weldments. However, recently steel producers have produced a new generation of high strength steels with improved weldability such as TMCP steel and HSLA steel, and are developing ultra-fine grained steel. A consequence of this is the matching weld metal can be more susceptible to cracking compared to the HAZ of base steel it joins. There is therefore a need to improve the cracking resistance of current high strength steel weld metal so that it is at least equivalent not only to the recently developed steels but also to the new generation of steels, thereby allowing overall reductions in preheat costs to be achieved.

It has generally been accepted that regardless of the location, hydrogen induced cracking will only occur given the co-existence of a sufficient quantity of diffusible hydrogen, a residual tensile stress and a susceptible microstructure. Several equations proposed for the preheat temperature to prevent weld metal cracking in the multipass welds were expressed by the relationship of the form[1];

$$T(℃) = A\,Rm + B \log [H] + C$$

Unlike the equation for HAZ cracking, preheat temperature is related with weld metal tensile strength(Rm), which is the term counting the microstructural contribution to weld metal cracking in the above equation. The present study therefore mainly focused to study the direct evidence of microstructural contribution to weld metal cracking, since it was envisaged this could provide a basic solution to the problem of weld metal hydrogen cracking expected in the next generation of high strength steels.

2. Residual Stress Control

This could be accomplished with the expansion obtained by $\gamma \rightarrow \alpha$ transformation. The martensitic transformation taking place at sufficiently low temperature can induce a compressive residual stress in the weld. This concept has been applied by Hiraoka *et. al.* [2] in developing welding consumables and found that a weld metal of Ms temperature around 150℃ had a strong resistance to cracking compared with the commercial product.

3. Hydrogen Control

Probably the most popular method of avoiding hydrogen cracking lies in the control of weld hydrogen levels by limiting hydrogen input to the weld. On the other hand, addition of compounds such as fluorides, carbonate or rare earth metals(REM) has been reported[3] to be beneficial in suppressing the hydrogen input to the weld.

4. Microstructural Control

With a low C-Ni-Mn-Mo system experimentally designed in the laboratory, it was found that the increase of Mn eventually changed the microstructure to one that had no grain boundary ferrite. It appears that this microstructure consists of acicular ferrite in the martensite matrix. The tensile strength also increased with Mn content and reached around 840Mpa with Mn content of 1.4%. Preliminary study on cold cracking susceptibility on the experimental wires showed no pre-heating is required in the restraint submerged-arc multipass cracking tests, while for the commercial wire numerous transverse cracks were observed in the bead surface even at the preheating temperature of 125℃. As a result of this study, it has been demonstrated that the preheating temperature required for the same strength level were quite different with the modification of microstructure through the change in chemical composition. Increase in tensile strength is not necessarily related to a decrease in the resistance to cold cracking.

5. Conclusions

It has been shown that changes in alloy design, and hence composition and microstructure, can be employed to produce high strength weld metal with improved resistance to cold cracking. It has been further demonstrated that weld metal of tensile strength over 800Mpa could be deposited with multipass welding even at room temperature.

Reference

[1] N. Okuda, *et. al*: Hydrogen induced cracking susceptibility in high strength steel weld metal, Welding Journal, 66(1987), No.5, p. 141s

[2] K. Hiraoka, *et. al.:* Performance of welded joint using low-temperature transformation welding consumable, The 4th Ultra-steel Workshop, Jan. (2000), Tsukuba, Japan

[3] I. K. Pokhodnya *et. al.*: Technology and metallurgy methods for decreasing diffusible hydrogen content, Welding in the World, 43, (1999), No.4, p. 2

Development and Improvement of Welding Consumables for High Tensile Strength Steels

Y. Matsushita, N. Hara, T. Sugino, M. Otsu and K. Suenaga
Welding Company, KOBE STEEL, LTD., Japan

1. Introduction

The applications of high tensile strength steels are expanding in conjunction with the need of larger structures, due to advantages of this type of steel such as decreasing plate thickness, reducing components weight and increasing allowable stress. Most of the structures need welding to assemble; therefore, it can be said that the advancement in welding technology as well as in steel production technology has contributed to the development in high tensile strength steels and extensive applications.

It was 1951 when a low hydrogen covered electrode was developed and used in Japan; that is, it has passed half a century since the year of development of the first high tensile strength steel welding consumable. This report reviews this history of development and improvement in welding consumables for high tensile strength steels, centering on steels of 780N/mm^2 or higher classes from three points of view: higher tensile strength, higher impact toughness and higher resistance to cracking.

In addition, for a recent topic, characteristics of the HT950 class welding consumables for penstock that were developed by reducing oxygen content of weld metal to improve impact toughness are also discussed in this paper.

2. Development and Improvement for Higher Tensile Strength

Steel plates have been improved in tensile strength with controlled Pcm values by properly designing chemical composition and by using innovated steel production technology. Tensile strength of weld metal has been improved by properly adjusting chemical composition in most cases because the heat treatment of quenching and tempering as for steel is not applied.

Figure 1 shows tensile strength as a function of carbon equivalent of weld metal by a low hydrogen covered electrode. It reveals that an increase of tensile strength of weld metal significantly depends on alloying elements. The carbon content of weld metal is controlled generally at approximately 0.09% or lower levels in order to minimize the susceptibility to hot cracking and assure impact toughness; thus the tensile strength is ensured by alloying with other elements such as Mn, Cr and Mo. The compositional formula of welding consumables for HT780-HT950 steels is C-Si-Mn-Ni-Mo type or C-Si-Mn-Ni-Cr-Mo type in general. The amount of Ni is determined taking into account impact toughness requirement and permissible material cost.

3. Development and Improvement for Higher Impact Toughness

Welding consumables for HT610 or lower-strength steels can be improved in impact toughness by adding both Ti and B, thereby refining the ferritic microstructure; however, this technique is ineffective for welding consumables for the higher-strength steels that exhibit a bainitic or martensitic microstructure. Therefore, impact toughness of the weld metals matching higher-strength steels has been improved by adding Ni that strengthens the matrix. For further improvement of impact toughness, the low C-high Ni type weld metal with minimized oxygen content has been a solution that strengthens the matrix of the weld metal.

It had been believed that approximately 300ppm of oxygen content was the lowest limit for weld metals by shielded metal arc welding and submerged arc welding; however, recently, it is reported that the new technique has reduced the oxygen content of weld metal to 200ppm or

lower levels to develop the welding consumables for HT950 steel penstock. **Figure 2** shows absorbed impact energy as a function of oxygen content of weld metal by shielded metal arc welding [1], which exhibits a marked increase in absorbed energy with the oxygen level of 200ppm or lower.

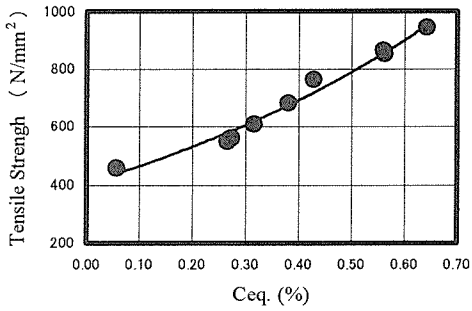

Fig. 1 Tensile strength as a function of carbon equivalent (Ceq) of weld metal by shielded metal arc welding
Ceq. (%) = C + Si/24 + Mn/6 + Ni/40 + Cr/5 + Mo/4 + V/14

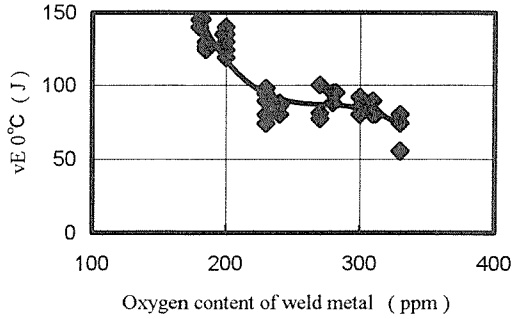

Fig. 2 Absorbed impact energy as a function of oxygen content of weld metal by shielded metal arc welding

4. Development and Improvement in Resistance to Cracking

Figure 3 shows test results of Restraint Multi-pass Welds Cracking Test by using a thick plate and submerged arc welding consumables for high tensile strength steel [2], with the testing variables of tensile strength and diffusible hydrogen content of weld metal. It reveals that preheat and interpass temperature to prevent cracking can be decreased with lower diffusible hydrogen or lower tensile strength weld metals.

Based on the test results shown in Fig. 3, reducing hydrogen content and designing proper tensile strength for welding consumables have been researched to improve resistance to cracking. For submerged arc welding fluxes, the bonded type flux containing carbonates reduces hydrogen content to 1.0ml/100g by the gas chromatographic method; therefore, this type of flux is mainly used in welding high tensile strength steels of HT780 or higher classes.

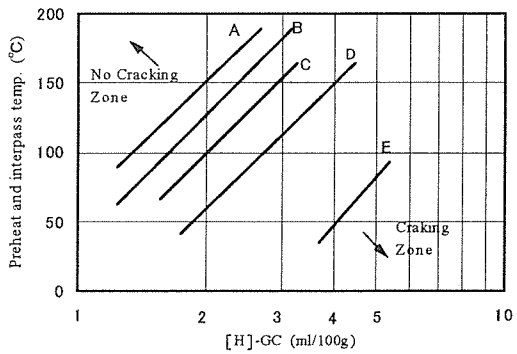

Fig. 3 Critical preheat and interpass temperature as a function of diffusible hydrogen content ($[H]_{GC}$) of HT690-980N/mm^2 class high tensile strength weld metal

Tensile strength of weld metal (N/mm^2)
A: 1043-1074
B: 965-1016
C: 875-920
D: 805-844
E: 755-778

References

[1] Hara, et al., Improvement of Toughness of Welding Consumables for HT950, Symposium on Welding Structure, '97 Lecture Paper Collection, pp44-47.

[2] Okuda, et al., Hydrogen Induced Cracking Susceptibility of Weld Metal, IIW-No.11-1072-86 (1986)

Effect of Argon Ion Bombardment on Diffusion Bonding of SUS304L Stainless Steel and Pure Iron

A. Wang, O. Ohashi, M. Aoki and N. Yamaguchi
Graduate School of Science and Technology, Niigata University, Japan

1. Introduction

Diffusion bonding has a problem for the large deformation of the bonded joints in bonding process because the bonding is carried out at a high temperature and with a high pressure. It has been desired that the bonding temperature is lowered and the applied pressure is reduced for the diffusion bonding process. Ion bombardment treatment for the bonding surface is considered to be an effective method. It has been reported that it is possible to make micro-bonding of similar and dissimilar materials at a room temperature after the ion bombardment treatment [1-2]. However, it is not clear about the effect of ion bombardment treatment for the diffusion bonding of various materials yet. In the present study, the effect of argon ion bombardment on diffusion bonding of SUS304L stainless steel and pure iron were investigated.

2. Experimental methods

SUS304L stainless steel and pure iron rods with 12 mm in diameter were used in this study. Faying surface was prepared by lapping method, and the roughness (Ry) was about 0.1μm. The specimen surface to be bonded was bombarded for 20 min by argon ion beam with 2.1 kV accelerating voltage and 20 mA ion current. The incident angle of argon ion beam was 10°. After an ion bombardment treatment, the specimens were joined in a vacuum of about 1×10^{-4} Pa. Bonding pressure applied to the specimens were 2.0 kN for SUS304L stainless steel and 600 N for pure iron, respectively. Holding time at bonding temperature was 20 min. The mechanical properties of the bonded joints were evaluated by the tensile tests using AG-250KNG autograph tester. The tensile velocity of 1 mm/min was used. The observation of the fractured surfaces and the analysis of the inclusion were carried out using JSM-6400 scanning electron microscopy (SEM) equipped with JED-2110 energy dispersive X-ray microanalyzer (EDX).

3. Results and discussion

Figure 1 shows the results of tensile strength for the SUS304L stainless steel with two different surface treatments by argon ion bombardment and no bombardment. The tensile strength of joints increased with an increasing in bonding temperature for both treatments. The joints using the ion bombardment treatment could be bonded at 600℃, but the bonds could not be formed until 700℃ for joints with no bombardment treatment.

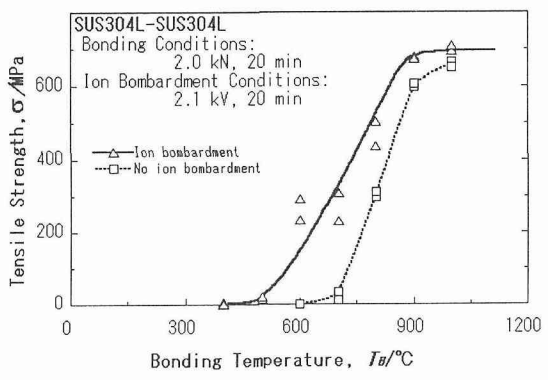

Fig. 1 Relationship between tensile strength and bonding temperature of joints with two different surface treatments by argon ion bombardment and no bombardment for SUS304L stainless steel.

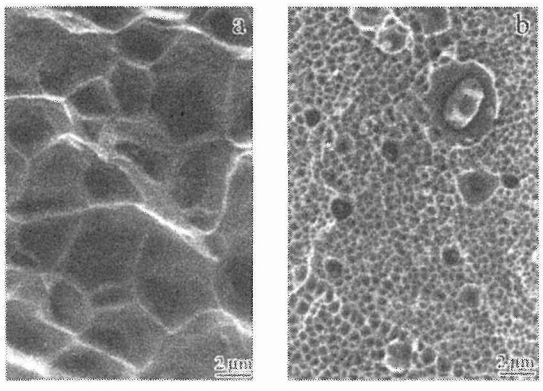

Fig. 2 SEM images of the fractured surface of the SUS304L stainless steel joints at 1000 ℃ with (a) argon ion bombardment; (b) no bombardment treatment.

In order to investigate the effect of argon ion bombardment, the fractured surfaces of the joints were observed by SEM. Figure 2 shows the fractured surfaces of the joints bonded at 1000℃. For the joints by argon ion bombardment treatment, the ductile fractured surface and very small amount of the inclusions at the fractured surface were observed. For the joints of no bombardment treatment, the small dimples at the fractured surface and the numbers of the inclusions in the dimples were seen. The EDX analysis indicated that the main of inclusions was oxide from the condensed surface film. Figure 3 shows the relationship between inclusion ratio at the fractured surface and bonding temperature. It indicates that ion bombardment treatment is effective to clean the bonding surface and reduce the inclusions.

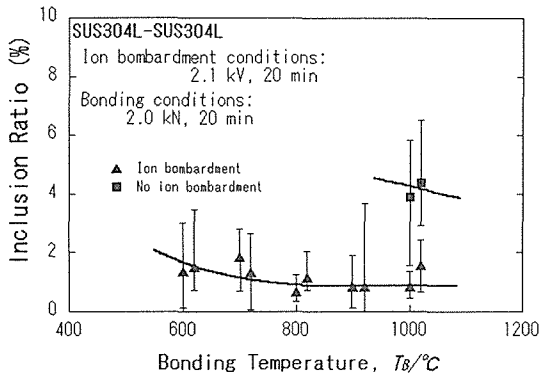

Fig. 3 Relationship between inclusion ratio and bonding temperature for the 304 stainless steel joints with the surface treatment by argon ion bombardment and no bombardment.

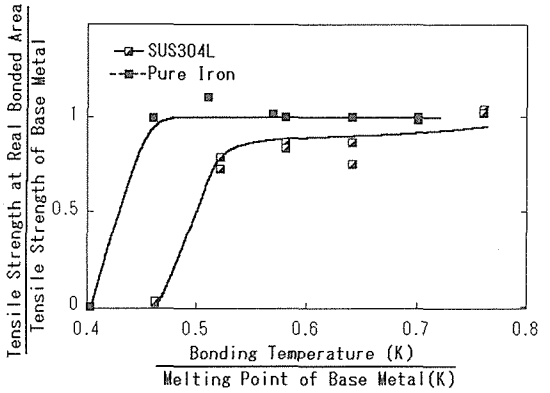

Fig.4 Relationship between joint efficiency (tensile strength at real bonded area to base metal) and equivalent temperature (bonding temperature to melting point of base metal) for the 304 stainless steel and pure iron joints by argon ion bombardment treatment.

On the other hand, to investigate the effect of ion bombardment on the various materials, the tensile tests and the fractured surface observations for pure iron were carried out. The results showed that there was the similar tendency with the SUS304L stainless steel joints, i.e. the ion bombardment treatment was also effective to lower the bonding temperature and reduce the inclusions at the bonding interface for the pure iron joints. However, the bonding properties between the SUS304L stainless steel and pure iron were different. Figure 4 shows the comparison of joint efficiency between the SUS304L stainless steel joints and pure iron joints by argon ion bombardment treatment. As SUS304L stainless steel has more active element such as Cr, the bonding surfaces are polluted again after sputter-cleaning, and a little inclusions are formed at the bonded interface. Therefore diffusion bonding properties of SUS304 stainless steel is inferior to those of pure iron.

4. Conclusions

Effect of ion bombardment on diffusion bonding of the SUS304L stainless steel and pure iron was investigated. The results obtained are shown as follows.

1. Ion bombardment treatment is effective to clean the bonding surface, reduce the precipitates, and results in lowering of bonding temperature.
2. Diffusion bonding properties of pure iron is excellent to those of SUS304 stainless steel.

References

[1] Suga, T., Takahashi, Y., Takagi, H., Gibbesch, B. and Elssner, G., Acta Metall. Mater., 40(1992), Suppl., pp.133-137.

[2] Takagi, H., Maeda, R., Hosoda, N. and Suga, T., Jpn. J. Appl. Phys., 38(1999), pp. 1589-1594.

[3] Ohashi, O., Tanuma, K. and Kimura, T., J. Jpn. Weld. Soc., 4-1(1986), pp.53-59.

[4] Ohashi, O. and Meguro, S., Mater. Trans., JIM, 38(1997), No.9, pp.801-805.

The Significance of Softened HAZs in High Strength Structural Steels

H G Pisarski and R E Dolby, TWI, UK

1. Introduction

The features and characteristics of HAZ softening have been well described by Denys [1] and Lundin [2]. Such zones can show hardness drops (ΔHV) from parent plate levels of up to ~40HV, but the actual ΔHV depends on the detailed chemistry and processing route of the steel while the softened zone width is determined by the welding process and procedure.

There have been few published investigations which have studied the fracture toughness of HAZ softened zones. A key factor which must be considered is the degree of mismatch in strength between the weld deposit and the parent steel, because this can influence both ΔHV and the constraint on the softened HAZ during test or service loading.

TWI and EWI have recently managed a study on strength mismatch in a 550 MPa QT steel which showed significant HAZ softening following submerged arc welding. Different mismatch ratios between the weld deposit and parent metal yield strength were achieved by varying the weld deposit strength level for the same parent steel. CTOD and mini-wide plate tests were used to measure the HAZ toughness for the different mismatched conditions.

In this paper the toughness data are used to calculate maximum allowable hoop stresses in a notional pipe made from 550 MPa QT steel containing a reference HAZ flaw. This is done by employing improved flaw assessment procedures which take into account strength mismatch, a recent development of BS 7910:1999. The interaction between HAZ toughness and mismatch is presented in terms of the maximum allowable hoop stress.

2. Experimental Work

The roller quenched and tempered plate (Table 1) was submerged arc welded at 2.4kJ/mm and PWHT at 580°C for one hour. Two sets of consumables were used to produce panels showing a mismatch of weld metal to parent plate yield strength of 0.65 (undermatch) and 1.51 (overmatch). Hardness traverses showed significant HAZ softening with ΔHV ~ 45 HV10.

Table 1 Chemical analysis of 25mm thick parent plate (RQT 501) (elements in wt%)

C	Si	Mn	P	S	Cr	Mo	Ni	Al	Cu	V
0.11	0.28	1.29	0.012	0.003	0.02	0.18	0.01	0.022	0.01	0.05

Surface notched 25mm square SENB specimens to BS 7488:Part 2 1997 were tested over a range of temperature, with the fatigue crack tips sited in the HAZ for both the undermatched and overmatched welds. Critical crack mouth opening displacement estimates were used to calculate J and K_J, and then CTOD values at the initiation of fracture was estimated from J, taking strength mismatch into account.

Welded specimens of 100mm width and 485mm length were produced with semi elliptical surface notches which were grown by fatigue into the HAZ. These precracked mini-wide plate specimens were tested at −70°C for the undermatched and overmatched conditions. Metallographic sections were used to confirm the fatigue crack tip locations in all CTOD and mini-wide plate specimens.

3. Results

The surfaced notched SENB test data are shown in Fig.1. This shows that the overmatched weld gave lower HAZ toughness values than the undermatched weld. Despite the scatter, an upwards shift in transition temperature of around 50°C is apparent. This was confirmed by a toughness distribution analysis of K_J data to find the 50^{th} percentile. The results from the mini-wide plate test specimens are also plotted in Fig.1 and confirm the lower HAZ toughness of the overmatched weld.

Some through-thickness notched HAZ toughness tests performed at EWI on similar welds supported the finding that weld strength overmatching gave the lowest HAZ toughness values.

4. Discussion

Three mismatch situations can arise in TMCP or QT steels:

(a) the weld deposit undermatches in strength both the HAZ and parent steel

(b) the HAZ undermatches in strength both the weld deposit and the parent steel

(c) the parent steel undermatches in strength both the HAZ and weld deposit

The experimental work described covered situations (a) and (b) and situation (b) gave the worst case HAZ fracture toughness. In related work, Harrison [3] used a 700MPa QT steel and situation (c) showed a higher HAZ toughness than situation (b). Thus situation (b) will give lowest measured HAZ toughness in welded TMCP or QT steels because strain concentrates in the softened HAZ at tips of HAZ flaws leading to a lower cleavage resistance and higher transition temperature.

Taking a notional 900mm diameter pipe with wall thickness 25mm and the yield strength and HAZ fracture toughness data from the 550 MPa QT steel, the maximum allowable hoop stresses for an axial reference flaw 4mm deep x 50mm long were calculated for a service temperature of –40°C.

The maximum allowed hoop stress for the overmatched weld is 613 MPa and higher than that for the undermatched weld at 419 MPa despite the HAZ fracture toughness being lower. Thus, whilst local HAZ softening can result in a significant reduction in fracture toughness in overmatched welds, the defect tolerance is not necessarily compromised because overmatching is beneficial to plastic collapse resistance. However, the sensitivity of this analysis to the measured HAZ fracture toughness must be emphasised. The maximum allowable hoop stress falls sharply as the fracture toughness reduces below about 120 MPa $m^{0.5}$ (Fig.2), and illustrates that fracture rather than plastic collapse would then become the dominant failure mode.

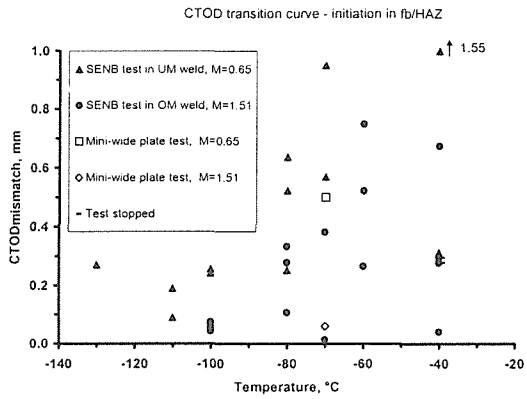

Fig.1 CTOD results for HAZ/fb.regions

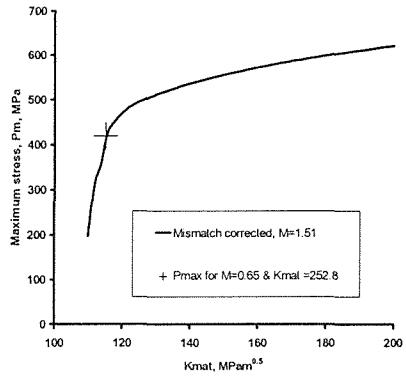

Fig.2 Maximum allowable hoop stress at -40°C vs HAZ fracture toughness

5. Conclusions

- The overmatched weld deposit gave the lowest measured HAZ fracture toughness in both CTOD and mini-wide plate tests.
- The lower HAZ toughness in overmatched welds in TMCP/QT steels does not necessarily compromise the defect tolerance in structures such as pipelines where plastic collapse is the dominant failure mechanism. However, defect tolerance depends on the measured HAZ toughness value and can fall rapidly as HAZ toughness is reduced.

6. References

[1]Denys, R. EVALMAT 89, Japan, ISIJ 1989, vol.2 pp 1013.

[2]Lundin, C D, et. al. "Recent Trends in Welding Science & Technology" May 1989, ASM International 1990.

[3]Harrison, P L, SINTAP report BS/24, March 1999. Project BE95-1426.

The Effect of Ferrite Grain Size and Impurity Elements on the Growth of Primary Austenite in the HAZ of Steels

Z. Tian, G. Zou, C. He, X. Zhang

Central Iron and Steel Research Institute, 100081 Beijing, China

Abstract

The new generation steels are characterized of ultra-fine grained structure and high cleanliness. This will dramatically enhance its' mechanical properties. However, the properties in a welded joint can hardly be maintained because of grain coarsening in the HAZ. In this paper, the effect of ferrite grain size and impurity elements on the growth of primary austenite in the HAZ was studied.

A low carbon steel was annealed at 900°C with different holding times to generate samples of different ferrite grain sizes. These samples were executed to welding thermal cycles to study the effect of ferrite grain size on the growth of primary austenite in the coarse grained zone (CGHAZ).

Three group of test steel plates of 8 mm thickness with respectively different levels of oxygen, nitrogen and sulfur content were prepared to study the effect of impurity elements on the growth of primary austenite in the CGHAZ. Table 1 lists the chemical compositions of the test steels:

Table 1: Chemical compositions of the test steels

Steel	C(%)	Si(%)	Mn(%)	P(ppm)	Al(ppm)	S(ppm)	T.O(ppm)	N(ppm)
S-10	0.15	0.30	1.41	<10	210	9	28	38
S-20	0.15	0.30	1.30	<10	220	20	20	-
S-30	0.14	0.31	1.38	<10	230	37	19	-
S-50	0.14	0.28	1.33	<10	170	50	21	-
S-100	0.13	0.26	1.33	<10	170	110	19	-
N-10	0.13	0.37	1.30	<10	<100	6	20	10
N-20	0.14	0.36	1.36	<10	<100	12	15	16
N-30	0.12	0.27	1.40	<10	120	12	16	37
N-50	0.14	0.33	1.35	<10	<100	8	17	73
N-100	0.13	0.26	1.32	<10	<100	6	15	120
O-10	0.12	0.30	1.42	<10	240	11	12	40
O-20	0.12	0.27	1.40	<10	180	12	18	-
O-30	0.12	0.22	1.37	<10	140	10	42	-
O-50	0.11	0.17	1.37	<10	150	12	52	-
O-70	0.12	0.28	1.47	<10	100	6	73	-
O-100	0.14	0.26	1.21	<10	100	8	100	-

The effect of ferrite grain size on the growth of primary austenite in the HAZ is shown in Fig. 1. It can be seen that the growth of primary austenite in the HAZ becomes severer with the decrease of ferrite grain sizes in the base metal. This means that the ultra-fine grained steel is more prone to HAZ grain coarsening. This could be explained by the declination of Ac3 and Ar3 temperature with decreasing ferrite grain size, which resulted in a longer existing time of growing at high temperature. For the same reason, the HAZ with finer ferrite grain size is also wider.

The effect of [O], S and [N] content are respectively shown in Fig. 2, Fig. 3 and Fig. 4, where T8/5 is the cooling time from 800 to 500°C. As shown in Fig. 2, the primary austenite grain size in the HAZ decreases with the decrease of oxygen content. When nitrogen content is less than 73 ppm, the

austenite grain size decreases with nitrogen content as well. With sulfur, there is a turning point. When sulfur content is higher than 42 ppm, the size of HAZ austenite decreases with sulfur content. When sulfur content is lower than 42 ppm, however, the size of HAZ austenite increases with sulfur content.

In general, higher cleanness retards phase transformation, and hence retards grain coarsening in the HAZ.

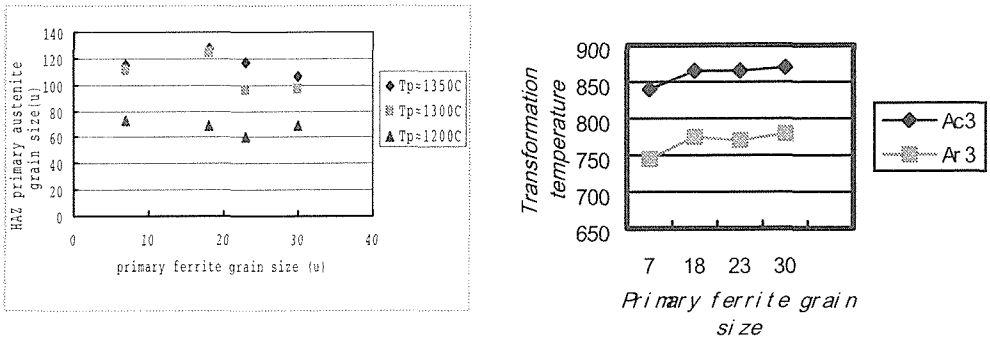

Fig. 1: The effect of ferrite grain size on HAZ grain growth and transformation temperature

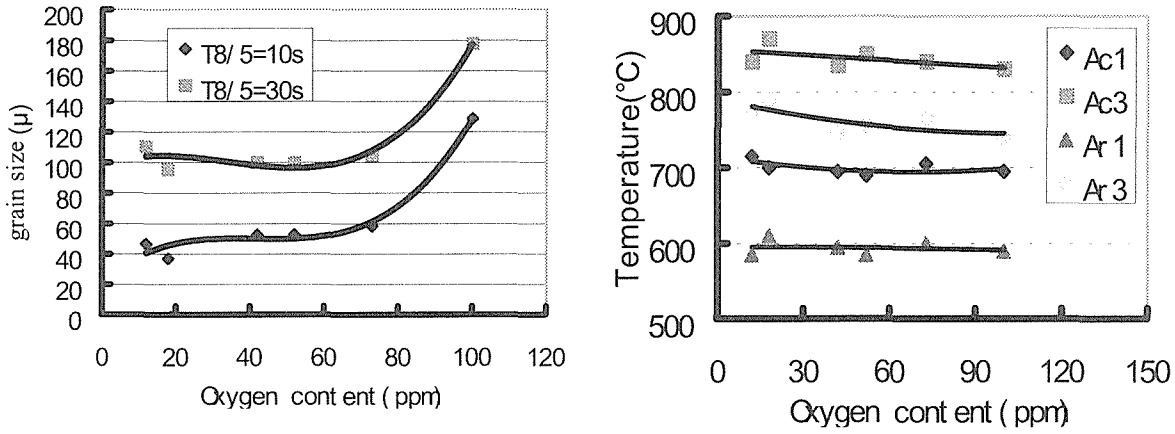

Fig. 2: the effect of oxygen content on HAZ austenite growth and transformation temperature

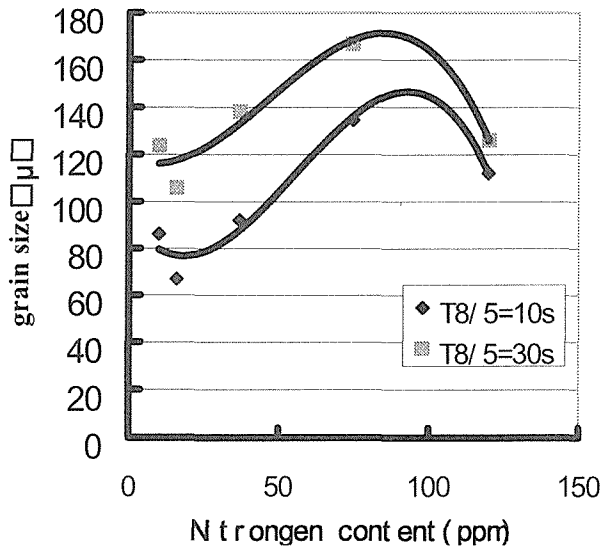

Fig. 3: the effect of nitrogen

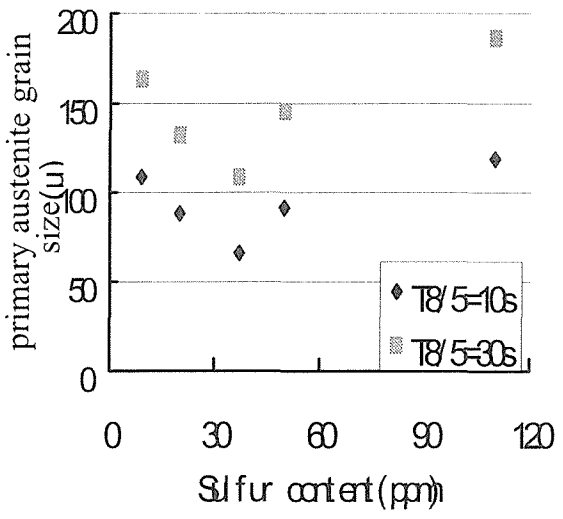

Fig. 4: the effect of sulfur

Effect of Heat Input on Properties of the Ultra-Fine Grained Steel Weldment

JoongGeun Youn and TaeDong Park

Hyundai Industrial Research Institute, Hyundai Heavy Ind. Co., Ltd.
1 Jeonha-Dong Dong-Gu Ulsan, Korea 682-792

1. Introduction

New structural steels characterized by high strength, high toughness and good weldability have been developing in order to support the infrastructure of incoming modern society [1,2]. A basic approach for developing the steel is to refine the grain size down to few μm with lean chemical composition. The developing steel is then called a fine grained steel or ultra-fine grained steel (hereafter it is noted as UFGS.). Welding causes remarkable changes in both the microstructure and the mechanical properties of the parent material, resulting in the formation of a heat affected zone (HAZ) adjacent to the weld metal. A typical feature at the UFGS weldment is the HAZ softening, which results in a noticeable reduction of tensile strength of the weldment [3]. The purpose of this study is to evaluate the effect of heat input on the properties of a 600MPa grade UFGS weldment, in particular tensile strength. Based on this result, a guideline for welding will be established for minimizing the HAZ softening of the UFGS.

2. Experiment

A 12mm thick 600MPa grade steel was used, which mainly consisted of very fine grained ferrite of average about 5 μm in size. With major chemical compositions of 0.1C-0.26Si-1.5Mn, the steel was made experimentally under the controlled rolling and accelerated cooling technology. In order to evaluate the effect of heat input on the properties of the steel weldment, FCAW, SAW and laser welding were performed without preheating in a heat input range of 6 - 30 kJ/cm. The heat input value for laser welding was the apparent value (laser power/welding speed). For laser welding, filler metal feeding technique was employed in order to improve weld metal toughness. The welding consumables used were the 600MPa grade commercial products selected by the G-BOP test. Mechanical properties of the weldment were evaluated by hardness measurement and transverse tensile test.

3. Results and Discussion

Fig.1 shows the hardness distributions along the UFGS weldments as a function of heat input. Compared with the base metal, a region having lower hardness values at the HAZ are found, the so-called HAZ softening. This resulted in the fracture at the HAZ during the transverse tensile test of the UFSG weldment. The tensile strength of the each weldment was clearly lower than that of the UFGS. The HAZ softening may be associated with a slow cooling rate after welding, which can deprive the base metal of the accelerated cooling effect. Fig.1 also indicates that the degree of the HAZ softening is a function of welding heat input applied.

In order to increase the cooling rate after welding, low heat input welding techniques such as high speed and laser welding has been applied. Hardness measurements along the high speed FCA weldment and the laser weldment showed that all the HAZ were hardened. The failure at these weldments during the transverse tensile test occurred at the base metal. The toughness values of their weld metal and HAZ were quite satisfactory.

Fig.2 shows the effect of heat input on the tensile strength of the 12mm thick UFGS weldment. The tensile strength of the UFGS weldment formed by either high speed or laser welding technique is higher than that of the other weldments and is enough to satisfy the target value of 600MPa. It is therefore very important to keep the welding heat input less than about 10kJ/cm in order to suppress the HAZ softening for the 12mm thick UFGS.

4. Conclusions

1. A typical feature at the UFGS weldment is the HAZ softening, which can reduce the tensile strength of the weldment less than that of the UFGS.
2. For suppressing the HAZ softening at the 12mm thick UFGS, it is recommended that the welding heat input should be less than about 10kJ/cm.

References

1. Japanese Ministry of Technology, J. of Iron & Steel, 12 (1996), pp.2
2. POSCO, Developing strategy of Hipers-21 steel (1997)
3. J.G.Youn, T.D. Park and K.S. Kim, Proc. of 1999 Annual Autumn Meeting of Korean Welding Society, pp.174 (in Korean)

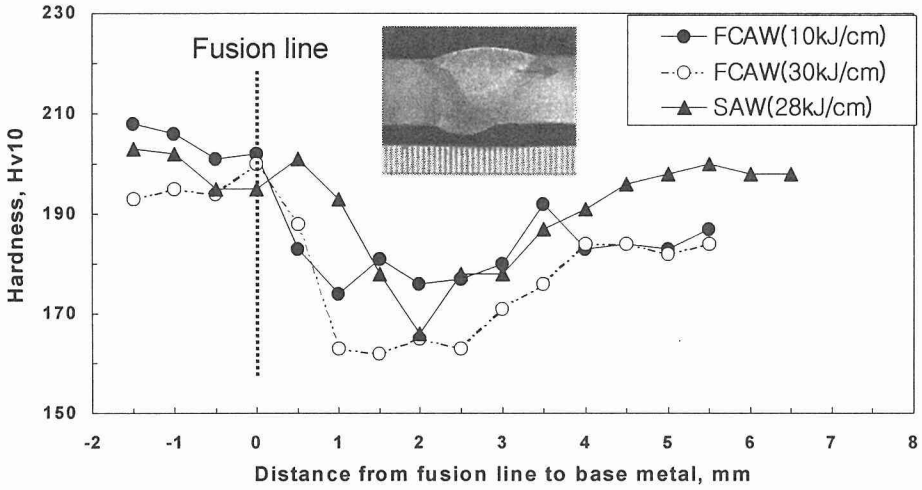

Fig. 1 Hardness distributions of the UFGS butt weldment with FCAW and SAW

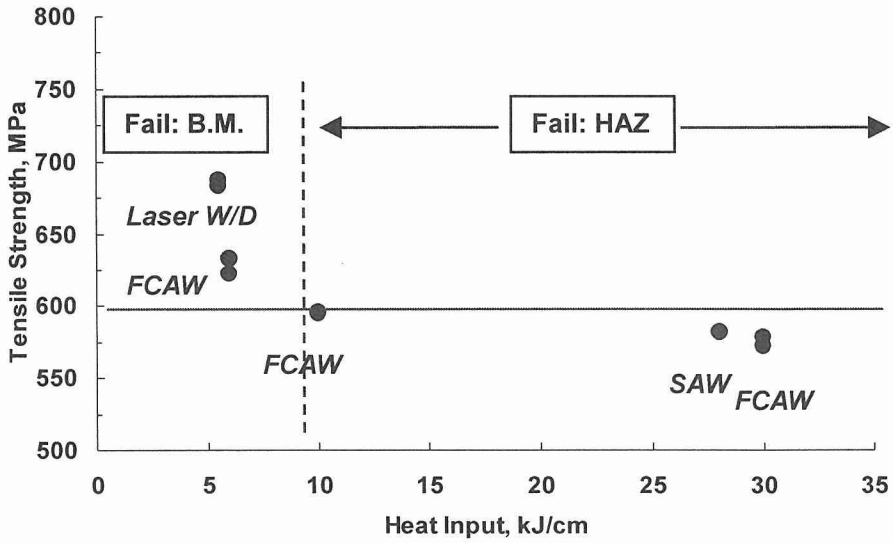

Fig. 2 Effect of heat input on the tensile strength of the 12mm thick UFGS weldment

Characteristics of HAZ of Ultra-Fine Grained Steel in Arc Welding

R. Ito, T. Nakamura, and K. Hiraoka
Joining and Interface Research Group, NIMS, Japan
K. Kasugai
Intelligent Materials Research Group, NIMS, Japan

1. Introduction

Ultra-fine grained steel (UFGS), which was increased from 400MPa to 800MPa by grain refinement, has been developed [1]. The softening region, however, was occurred in the welding HAZ of UFGS. In order to minimize the softening region, an ultra-narrow gap GMA welding (UNGW) has been developed as a higher efficiency, lower heat input welding process [2]. Then, the width of HAZ can be minimized to within 1-2mm.

In order to obtain good joints by UNGW, it is important to study the HAZ characteristics of UFGS. In this paper, the microstructures at HAZ are discussed under a rapid heating and cooling as the UNGW.

2. Welding process for ultra-fine grained steel

Table 1 shows chemical compositions of the UFGS, which consists of a ferrite phase with a grain size of less than 1 μm and fine particles of Fe_3C as shown in Fig. 1. In UNGW process, the arc distribution along groove walls with groove gap of less than 5mm can be controlled by using low frequency pulse current waveform as shown in Fig. 2. The adaptable welding conditions can be determined from the wire-melting numerical simulation, because there are many welding parameters in this welding process. Two pass welding under arc current 350A, welding speed 7.5mm/s and groove gap 5mm were carried out with 19mm thickness.

3. Results and discussions

Ac_1 and Ac_3 temperatures were measured by a program-controlled high-frequency induction heating apparatus (modified Formaster-F). The peak temperatures in the HAZ were estimated by thermal conduction theory referring to positions of fusion line and A_{C1} [3] as plotted in Fig. 3. Estimated peak temperature (solid line) showed good agreements with the measured results (△).

The hardness distribution of the welded joint was shown in Fig. 3. It was found that the softening zone existed in the range that the peak temperature raised between 980K and 1150K.

The schematic illustration of microstructures in the peek temperature range between 980K and 1,150K is summarized in Fig. 4. The microstructures heated below 1150K (A_{C3}) were mainly polygonal ferrite, and the hardness in this zone of HAZ was lower than that of the base metal.

In the state heated just above the A_{C1} temperature, the Fe_3C slightly dissolved and then austenite (γ) was formed around Fe_3C. During cooling from A_{C1} temperature, the polygonal ferrite and Fe_3C were formed, and ferrite grain was almost the same size of UFGS although the hardness became lower.

In the state heated between A_{C1} and A_{C3} temperature, the austenite was formed around Fe_3C, but the Fe_3C did not completely dissolve. During cooling from the peak temperature, the austenite transforms to the polygonal ferrite and M-A constituent, and then the Fe_3C and M-A constituent were observed at room temperature. Ferrite grain size increased in 1-2μ m.

In the region raised to A_{C3} temperature, the polygonal ferrite and large amount of M-A constituent were formed. The hardness was not high because the ferrite grain size becomes larger.

When the HAZ heated over 1200K, the amount of polygonal ferrite decreased. The hardness of the HAZ was higher than that of the base metal, because the amount of bainitic ferrite, bainite and lath-martensite increased with increasing the peak temperature.

References

[1] T. Hayashi, K. Nagai, T. Hanamura, H. Nakajima and T. Mitsui: CAMP-ISIJ, 13 (2000), 473
[2] T. Nakamura, and K. Hiraoka, :Science Technology of Welding and Joining, 6(2001),No.6,355-362.

[3] T. Kasugai, A. OkadaK and M. Inagaki :TETSSU-TO-HAGANE, 67(1981),No.6,2201-2207

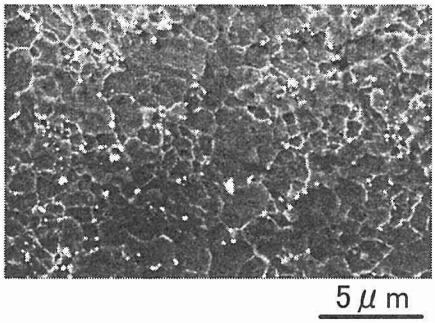

Fig. 1 Microstructure of UFGS.

Table 1 Chemical compositions of UFGS (mass%)

C	Si	Mn	P	S	C_{eq}
0.15	0.30	1.45	0.009	0.0008	0.26

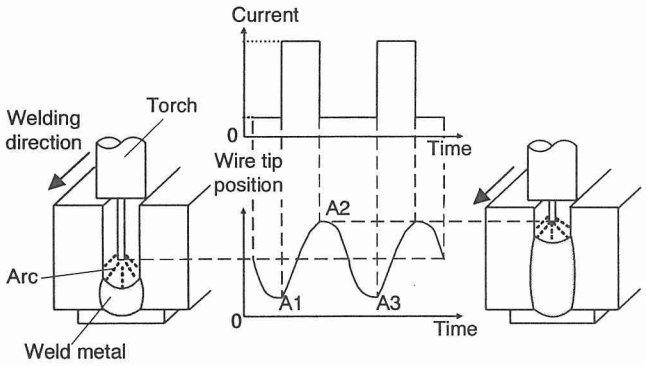

Fig. 2 Ultra-narrow gap welding process controlled by DC pulsated current waveform.

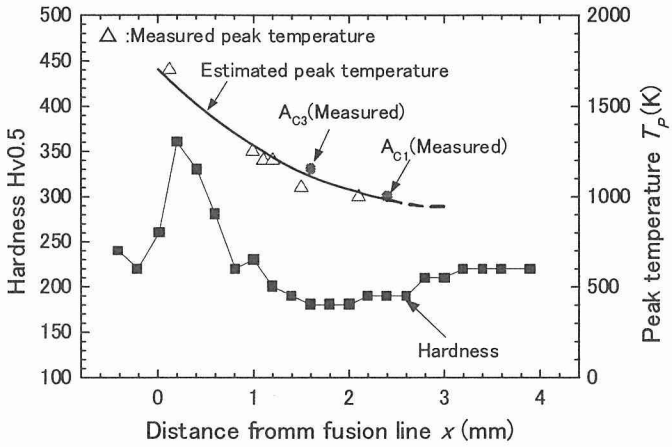

Fig. 3 Hardness distribution and peak temperatures at HAZ.

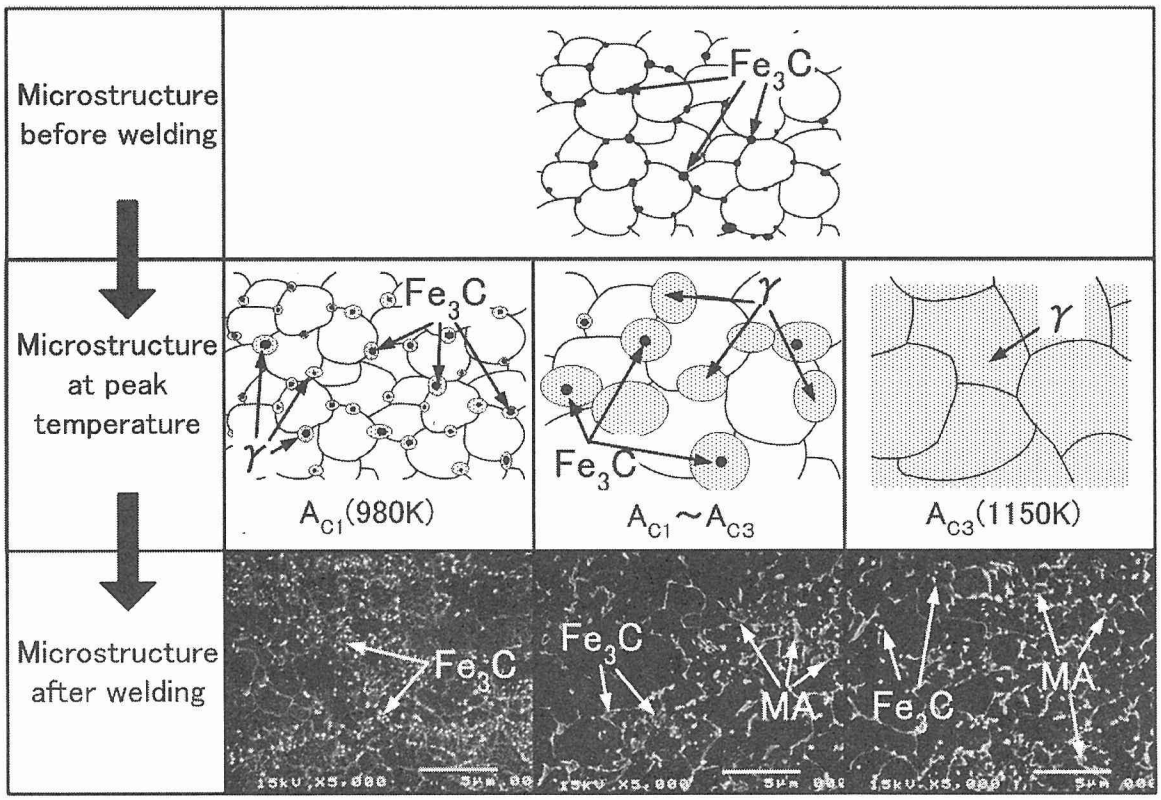

Fig. 4 Microstructures at HAZ of UFGS in UNGW.

High Power Laser Welding of Ultrafine Grained High Strength Steels

S. Tsukamoto, I. Kawaguchi, T. Otani, G. Arakane & H. Honda
Joining and Interface Research Group, NIMS, Japan

1. Introduction

Low heat input welding is desirable for ultrafine grained steels to suppress grain coarsening in the HAZ, but high efficiency welding is also required to reduce production times. To meet these objectives, a deep penetration laser welding with the depth of 20 mm has been developed using a 20 kW CO_2 laser facility. One of the major problems, in this case, is formation of large porosities. In the present study, suppression of the porosity formation has been attempted by laser power modulation. HAZ properties of the laser welded ultrafine grained steel have also been investigated.

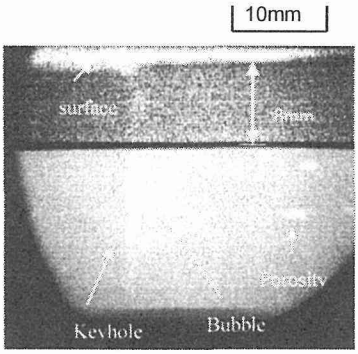

Fig.1 X-ray transmission image of keyhole and bubble formation.

2. Formation mechanism and suppression of porosity in deep penetration LB welds

Deep penetration welding in excess of 20 mm can be attained even at a high welding speed of 16.7 mm/s using 20 kW CO_2 laser. However, large porosities are always remained in the weld metal with the penetration depth of more than 10 mm. To elucidate the formation mechanism of the porosity, dynamic keyhole behaviour was observed using a microfocused X-ray transmission imaging system. Figure 1 shows a typical example of the transmission image. Large bubbles are formed at the fluctuated keyhole tip and most of them are trapped in the weld metal as the porosity. The bubble formation is closely related to spontaneous fluctuation in the keyhole depth. The bubble is formed only while the keyhole depth rapidly decreases. Figure 2 shows the formation process of the bubble. During rapid decrease in the keyhole depth, the neck is formed near the bottom by capillary instability (Fig.2 (c)). Then, the tip is broken up and forms the bubble (Fig.2 (d)).

In order to prevent the porosity formation, it should be effective to suppress the spontaneous keyhole fluctuation by

(a) CW welding.

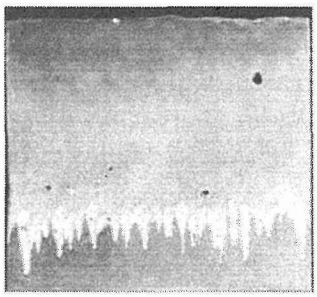

(b) Square wave power modulation.

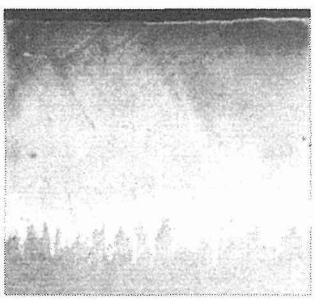

(c) Power modulation with modified waveform

Fig.3 Suppression of porosity by laser power modulation.

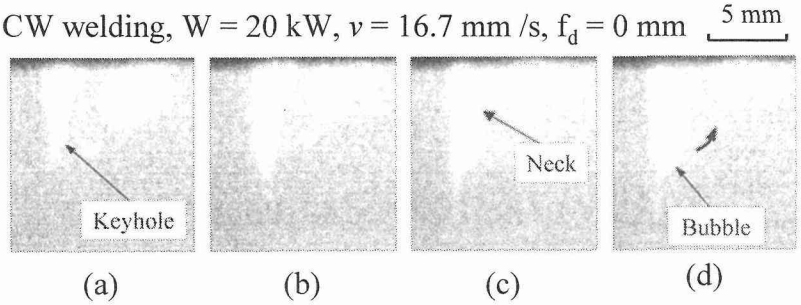

Fig.2 Formation process of bubble during abrupt decrease in the keyhole

controlling the keyhole behaviour. Laser power modulation is one of the solutions. Figure 2 shows the longitudinal sections of the laser welds. The large porosities formed in the continuous wave (CW) welding (Fig.3 (a)) are effectively reduced by square wave power modulation (Fig. 3(b)), if the modulation frequency coincides with the eigenfrequency of the molten pool oscillation on the pool surface. Furthermore, the porosity suppression effect is enhanced using the modified waveform as shown in Fig.3 (b).

3. HAZ properties of ultrafine grained high strength steel

Bead on plate laser welding was carried out on ultrafine grained steel (UFG steel) for various welding speeds to examine the suppression effect of HAZ softening. The grain refinement was achieved by multi-pass deformations of a grooved rolling. The microstructure of the base metal consists of ultrafine grained ferrites and tiny dispersed cementites. The ferrite grain size in the transverse and longitudinal sections are 1 and 1～3 μm, respectively. Figure 4 shows the hardness profiles for various welding speeds. HAZ softening can be suppressed for the welding speed of more than 33.3 mm/s, whereas clear reduction in the hardness from 220 to 170 Hv can be seen in the narrow HAZ for 16.7 mm/s. The maximum ferrite grain size in the HAZ decreases with the welding speed, but it shows an approximately constant value of 3 μm above 33.3 mm/s as shown in Fig.5. HAZ softening for 16.7 mm/s must be caused by coarsening of the ferrite grain. However, grain coarsening from 1 to 3 μm is also found even at the highest welding speed of 166.7 mm/s, where HAZ softening is prevented. To elucidate the hardening mechanism of the coarsened ferrite, microstructures of the base metal and HAZ were observed using two-step electrical etching, which can distinguish MA constituent with cementite. Tiny dispersed MA constituents are clearly seen in the HAZ near the fusion boundary as shown in Fig.6. The ferrite grain size increases with increasing the peak temperature during welding. Similarly, the volume fraction of the MA increases with the peak temperature. This means that the formation of tiny dispersed MA suppresses the HAZ softening in spite of the grain coarsening.

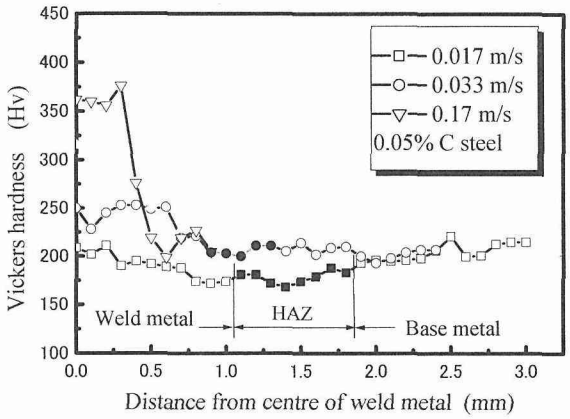

Fig.4 Hardness distributions in laser welds of UFG steel.

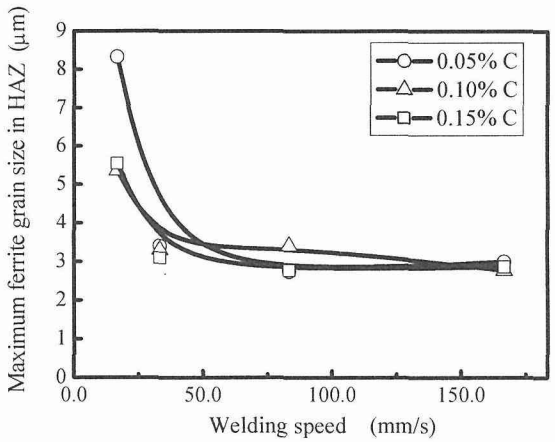

Fig.5 Effect of welding speed on maximum ferrite grain size in HAZ

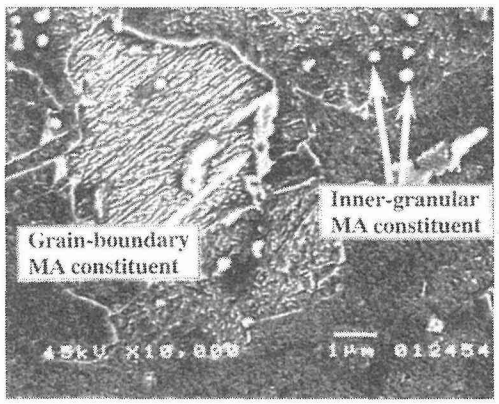

Fig.6 SEM microstructures of laser welded HAZ near fusion boundary.

- Advanced Coal-Fired Power Plants
- Advanced Coal-Fired Power Plants (Steel Development)
- Welded Joints of Creep Resistant Steels
- Microstructural Aspects of Creep Resistant Ferritic Steels
- High Temperature Properties of Creep Resistant Steels

(Room 201)

State-of-the-Art of Heat Resistant Steel Technology in Japan and Prospects for the 21st Century

K. Maruyama
Department of Materials Science, Tohoku University, Japan

Global warming is a serious problem caused by the greenhouse effect of CO_2 gas. In Japan, 30% of CO_2 is emitted from thermal power plants, and 20% from transportation such as cars and trucks. Reduction of CO_2 emission from the power plants is an essential requirement for preventing the global warming. It is well known that the reduction can be achieved by raising the operation temperatures of the power plants. High creep and creep-fatigue strength and good oxidation resistance are the major requirements on the steels to be used in the power plants.
Most of waste-to-power generation plants in Japan are operated at temperatures lower than 400°C. The temperature is substantially lower than those of coal-fired power plants (600°C), and the higher temperature operation is a strong environmental demand also on the waste-to-power generation plants. The higher temperature operation can suppress the synthesis of dioxins in the waste treatment plants. High temperature corrosion is a crucial problem of the materials to be used in such a plant.

NOx gas formed in automobile engine is removed by catalyses. The effective reaction of the catalysts requires a lower content of sulfur in fuel. To reduce the sulfur content, the hydro-desulfurization plants should be operated at temperatures higher than the present situation. High temperature strength and hydrogen attack are the major problems of the steel uses as high temperature components of these plants.

Heat resistant steels have been used extensively in these elevated temperature plants because of their good combination of low cost and reasonable performance at elevated temperatures. Developments of advanced heat resistant steels are necessary to fulfill the aforementioned requirement of the higher operation temperature. Researched and developments on advanced heat resistant steels are in progress in Japan as well as in Europe.
A number of elevated temperature plants were built in 1970s. Their structural components have been in operation beyond their design lives. The extension of service lives of those aged plants is a strong economical demand, but serious assessment of their residual lives is necessary for the safe operation of the aged plants. The life assessment is an important issue on heat resistant steel technology.

The Japan Ultra-High Temperature Materials Center has drawn a road map on the heat resistant steel technology for the early 21st century, and has published a report in 2000 [1]. This talk is based on the report, and focuses on the following aspects of the heat resistant steel technology:

1. Heat resistant steels for coal power plants
2. Heat resistant steels for waste-to-power generation plants
3. Heat resistant steels for chemical plants
4. Material database and evaluation of long-term creep properties

References

[1] New Energy and Industrial Technology Development Organization: NEDO Investigation Report (NEDO-P-9955), March 2000.

Present Status of Advanced Coal-Fired Power Plants Worldwide

Fujimitsu Masuyama

Mitsubishi Heavy Industries, Ltd.

1. Introduction

Coal-fired power plants produce major energy resources throughout the world, thus making efforts imperative for improvements in efficiency by elevating steam conditions to even higher ranges of pressure and temperature, as well as the development of new power generation systems. In general, from the standpoint of the material research and development, USC power plants require the development of high creep strength alloys, while IGCC and FBC power plants require the development of corrosion and/or erosion resistant alloys. In order to conduct the appropriate study on the material for power plant applications, it is highly important to understand trends in the advancement of power plant systems.

2. Present Status of Advanced Steam Cycle Power Plants Worldwide

Fig.1 [1] shows an overview of international research and development on advanced steam cycle power plants in three major areas of the world. In Japan, the Phase 2 program was started in 1994 for the development of single reheat steam conditions of 30MPa and 630/630℃ with ferritic steels, and was completed in 2001 after the success of the Phase 1 for the double reheat steam temperature of 593℃ and 649℃. This work was conducted by EPDC under contract with the Ministry of International Trade and Industry. Concurrently the NRIM (now NIMS) has been conducting an R&D project since 1997 aimed at ferritic heat resistant steels to be applicable for 650℃ class steam conditions

In the US, a large scale and comprehensive development project was started by EPRI in 1986 and conducted for over a period of 8 years. Recently the Department of Energy has provided backing for the first industry-led design and engineering project, known as the Vision 21 program. The overall goal of this effort is to develop the critical building blocks for fossil fuel plants that can produce power, fuels, and chemicals at high efficiency, and with virtually no emissions. This program includes the needs of development of heat resistant materials for service in components operated under high stress and high temperature conditions.

In Europe, the COST 522 project was initiated in 1998 after the success of COST 501 over the period from 1983 to 1997, aiming at steam parameters for ultra-supercritical pressure power plants of 29.4MPa and 620/650℃ with ferritic steels. Further efficiency improvements are targeted by the European R&D project known as Thermie Advanced (700℃) PF Power Plant, for which the project objectives are steam temperature of up to 700℃ and efficiency of around 55%.

Modern ultra-supercritical pressure power plants are already in service and/or under construction in Japan, Denmark and Germany. Table 1 [1] shows plants in service or under construction that were commissioned between 1997 and 2002, including the materials used for the boiler superheater, steam line pipe work and turbine rotor, as well as information concerning power plant design parameters. Fig.2 [2] shows steam parameter plots for ultra-supercritical pressure power plants at past, present and future points on a graph of pressure vs temperature. Time-wise service temperature ranges are also indicated on this graph for ferritic and austenitic steels for heavy section components such as steam line pipe and turbine rotors. The upper temperature limit for ferritic steels has thus far risen from around 560℃ to 630℃, and will increase to 650℃ in the future.

3. The Future of Coal-Fired Power Generation Systems

Fig.3 [3] shows a flow diagram of the progress of coal-fired power generation systems such as steam turbines, fluidized-bed combustion, gas turbines, integrated gasification combined cycle and fuel-cell direct power generation, together with thermal efficiency and requirements for future technology development. In the future, (with the exception of USC steam turbines) systems will be merged into the gas turbine combined type so as to obtain high efficiency of over 50%, although this will not require enhancement of creep strength exceeding that of existing heat resistant materials for steam boilers and turbines. However, USC steam turbine systems with high steam parameters of over 630℃ will require stronger and better anti-corrosion materials than those currently available.

References

1) R. Blum and J. Hald: VGB-ESKOM Int. Mat. Conf., Pretoria, South Africa, (2000)
2) F. Masuyama: ISIJ Int., 41(2001), No.6, pp. 612-625
3) Ministry of International Trade and Industry, Report on Development of Coal-Fired Power Technology for the 21st Century, (1998)

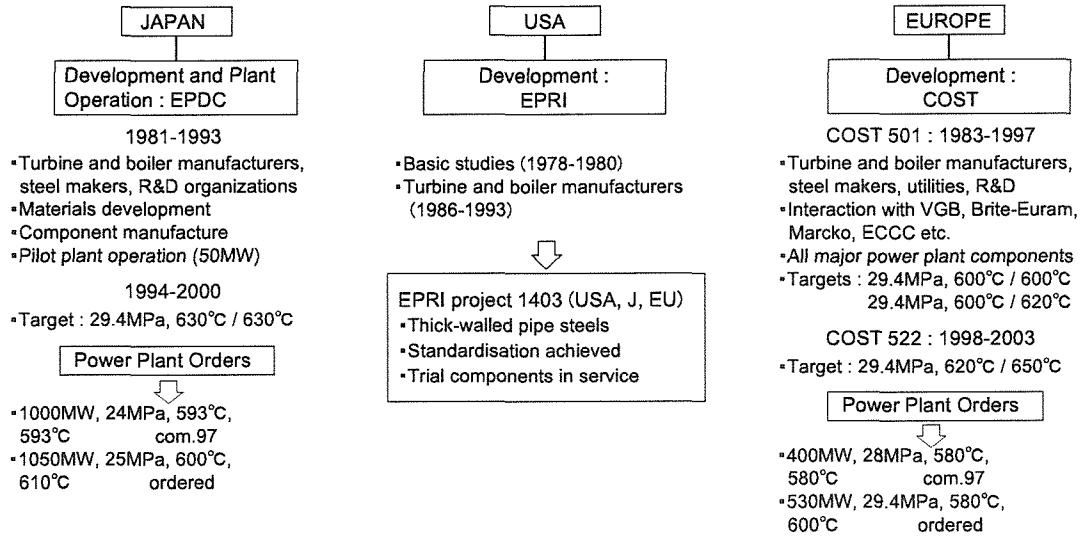

Fig. 1 International Research and Development Projects on Advanced Steam Power Plants

Table 1 Ultra Supercritical Pressure Power Plants in Service or Under Construction

Power Station	Cap. (MW)	Steam Parameters		Fuel	Year of Comm.	Eff. (%)	Boiler/Steam Line Materials	Turbine Materials
		Pressure (MPa)	SH / RH / RH Temperature (℃)					
Matsuura 2	1000	25.0	598/596	PC	1997		18Cr9NiCuNbN/P91	10.3Cr1.5MoVNbN
Skaerbaek 3	400	28.4	580/580/580	NG	1997	49	TP347HFG/P91	10Cr1MoVNbN (501F)
Haramachi 2	1000	25.4	604/602	PC	1998		18Cr9NiCuNbN/P91	10.3Cr1.2Mo0.3WVNbN
Nordjylland 3	400	28.4	580/580/580	PC	1998	47	TP347HFG/P91	10Cr1MoVNbN (501F)
Nanaoota 2	700	25.0	593/593	PC	1998		TP347H/P91	10Cr1Mo1WVNbN
Misumi 1	1000	25.4	604/602	PC	1998		18Cr9NiCuNbN/P91	10.2Cr0.5Mo1.8WVNbN
Lippendorf	934	26.4	554/583	Lignite	1999	42.3	18Cr12NiMo/P91	10Cr1Mo1WVNbN (501E)
Boxberg	915	26.4	555/578	Lignite	2000	41.7	18Cr12NiMo/P91	10Cr1Mo1WVNbN (501E)
Tsuruga 2	700	25.0	597/ 597	PC	2000		18Cr9NiCuNbN/P122	10Cr1Mo1WVNbN
Tachibanawan 2	1050	25.9	605/613	PC	2001		18Cr9NiCuNbN/P122/P92	10.2Cr0.5Mo1.8WVNbN
Avedore 2	400	29.4	580/600	NG	2001	49.7	TP347H/P92	10Cr1Mo1WVNbN (501E)
Niederaussen	975	26.0	565/600	Lignite	2002	>43	TP347HFG/P911	10Cr1Mo1WVNbN (501E)

PC : Pulverized Coal. NG : Natural Gas SH/RH/RH : Superheater/Reheater/Reheater

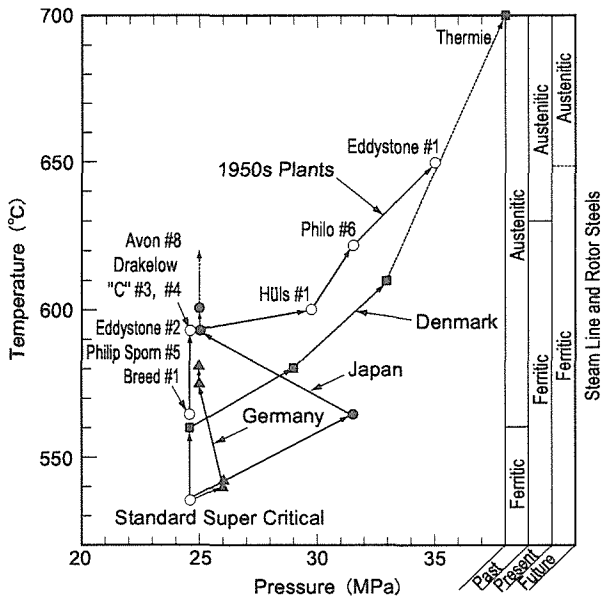

Fig. 2 Steam Parameter Plots for Ultra Supercritical Pressure Power Plants

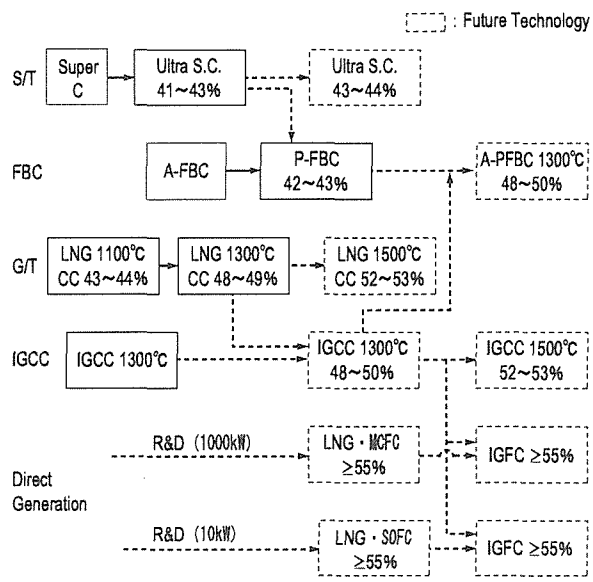

Fig. 3 Coal-Fired Power Generation Systems

Recent Advance of Elevated-Temperature Design Based on Thermal Stress Criteria

Takashi Shimakawa
Kawasaki Heavy Industries, Japan

1. Introduction

Coal-Fired power plants are required to supply middle and peak demand of electricity. Such operation requires daily start and shutdown (DSS) to cause cyclic thermal stress in structural component. The dominant failure mode considered in design and maintenance is creep-fatigue under the operation at elevated temperature. Structural design standard such as ASME Sec.III, NH[1] is adopted to exclude assumed failure modes. Elevated temperature design guidelines have been also developed in many countries to apply the designing of Fast Breeder Reactor components. Theses guidelines employ a similar concept to ASME. Design guideline BDS for prototype FBR Monju was developed in 1984 in Japan[2]. RCC-MR[3] was developed in France to apply a demonstration FBR Super-Phoenix in 1985. Evaluation scheme and criterion for creep damage employed in these standards are based on static creep concept useful for constant pressure loading. However elastic-plastic behavior and stress relaxation are key issues to estimate creep-fatigue damage under thermal stress, because design limit for computed thermal stress is allowed to exceed yielding due to displacement-controlled characteristic. Another issue is the applicability of the time fraction rule to calculate creep damage under creep-fatigue loading. R5[4] developed in UK to apply an advanced gas cooled reactor employs ductility exhaustion rule. This paper presents recent advance to estimate inelastic behavior and to calculate creep damage under thermal stress condition.

2. Estimation of inelastic behavior

It is required to estimate strain range and creep relaxation history to evaluate creep-fatigue life of the component operated at elevated temperature. Some simplified inelastic methods have been proposed to predict more accurate behavior at stress concentration portion in the vicinity of structural discontinuity. Neuber's rule is based on the concept that the product of stress and strain is constant. An elastic follow-up model is also employed in design standards. The most conservative line of elastic follow-up is employed in BDS and RCC-MR.

These concepts are defined for a linear bending stress component obtained from stress classification of computed stress through the thickness. However it is expected to calculate a peak stress/strain behavior directly from surface stress computed from elastic FEM analysis. Stress Redistribution Locus (*SRL*) for peak stress/strain is effective to perform direct prediction without equivalent linear treatment.

It is crucial issue that ***SRL*** of peak strain can be decided independently of configuration of structure, material properties and/or applied stress. The characteristic of proposed method is to use normalized stress σ/σ_e and strain $\varepsilon/\varepsilon_e$, where σ_e and ε_e are

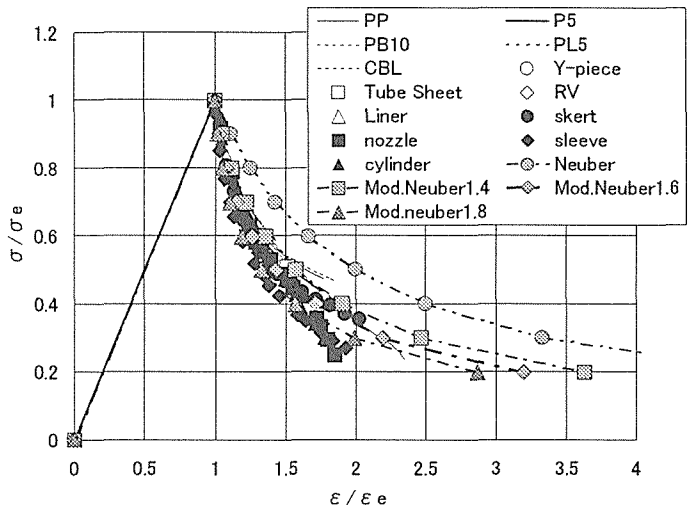

Fig.1 SRL for various geometries and constitutive models

computed by elastic FEM analysis. Another characteristic of *SRL* is to be obtained by modification of Neuber's locus with introduction of coefficient κ. FEM analyses were performed for various kinds of configuration of structure, material properties and/or applied stress. Figure 1 shows that master curve of *SRL* exist independently from geometry and applied stress level.

3. Evaluation of creep-fatigue damage

Creep-fatigue life is estimated from calculated strain range and creep relaxation behavior based on *SRL* concept. Though the material with low yield strength causes high strain range related to higher fatigue damage, it gives lower initial stress which cause lower creep damage. The material under creep-fatigue loading is required higher ductility rather than higher strength. Figure 2 shows creep-fatigue test results for Modified Type 316 stainless steel, 316FR, performed by Takahashi[5]. Creep damage calculated by a time fraction rule adopted in ASME, BDS and RCC-MR can count little damage as shown in Fig. 2(a), while those by ductility exhaustion rule count reasonable damage as shown in Fig.2 (b). It is considered that primary creep is applied in every cycle because creep hardening is recovered by plastic unloading. It is noted that primary creep is dominant under creep-fatigue loading especially in low strain range condition. Though secondary creep and rupture strength are important in the design for pressure loading, primary creep and creep ductility are essential in the design for thermal stress.

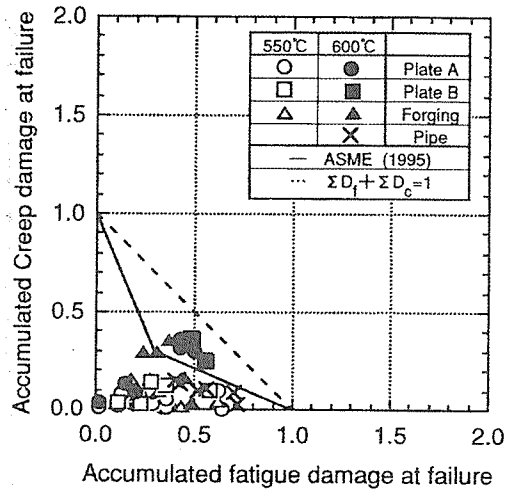

(a)Time Fraction Rule

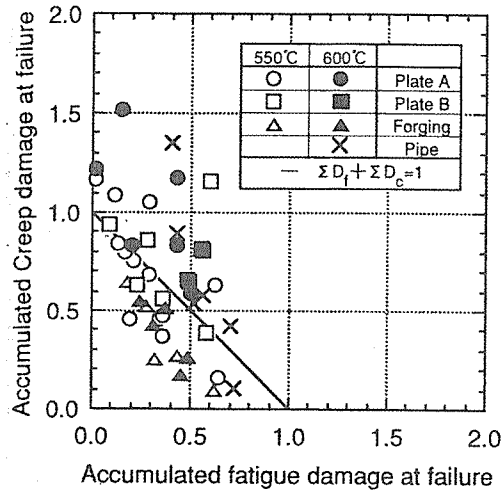

(b) **Ductility Exhaustion Rule**

Fig.2 Creep-Fatigue Damage Evaluation of 316FR

4. Conclusions

Creep-fatigue damage induced by thermal stress becomes the dominant failure mode due to the increasing of operating temperature and frequently start and shutdown of the coal fired plants. Inelastic behavior under creep-fatigue loading is simply evaluated by *SRL* method for most of configurations and loading conditions considered in pressure vessel. Designing of these components requires the material harmonized among strength, deflection and ductility.

References

[1] ASME Boiler & Pressure Vessel Code, Sec.Ⅲ、1998

[2] Iida, K., Asada, Y., Okabayashi, K. and Nagata, T., "Simplified Analysis and Design for Elevated Temperature Components of Monju", Nuclear Engng. and Design, 98(1987), pp305-317

[3] "Design and Construction Rules for Mechanical Components of FBR Nuclear Island, RCC-MR", AFCEN, 1985

[4] "An Assessment Procedure for High Temperature Response of Structures", Nuclear Electric R5, Issue 2, 1995

[5] Takahashi,Y., "Further Evaluation of Creep-Fatigue Life Prediction Methods for Low-Carbon Nitrogen-Added 316 Stainless Steel", Trans. ASME Vol.121, 1999

The European Efforts in Material Development for 650C USC Steam Power Plants – COST 522

T.-U. Kern, Siemens Power Generation, Germany
M. Staubli, Alstom Power, Switzerland

COST (Co-operation in the field of Science and Technology) is a long established European programme aimed at co-ordinating pre-competitive research activities in numerous areas of science and technology. The COST 522 programme started in April 1998 and has a planned duration up to year 2003. It involves 16 European countries and co-ordinates well over 100 research projects involving over 70 different organisations across Europe including all of the main utilities, manufacturers, materials suppliers and research establishments. COST522 is founded on the success of earlier related COST actions, specifically COST 501 (1986-1997), which have established strong trans-European networks in this field.
The overall COST 522 programme is focusing on the development of suitable materials, coatings and surface treatments for Steam Power plants (with inlet temperatures of up to 650°C) and Gas turbines (with combustion temperature of up to 1450°C and NO_x emissions <10ppm). The new COST 522 action is therefore divided into three different sub-projects which are Steam Power plant (turbine, boiler), Gas Turbines and Ancillary Components for plants with Advanced Processes. The use of ferritic-martensitic steels for the Steam Power plants is foreseen in order to allow a flexible operating mode in medium-load and peak-load operation. The COST501 project has shown that there is still a further high potential for steels up to 650°C based on the success with the 600°C-materials.

Materials for 625°C Application
Based on microstructural efforts and on the careful evaluation of already available long term test data, a new alloy concept for the further modification of cast and forged steels for 625°C application was formulated including

- Reduction of the Ni-content/ alloying with Co/ addition of Boron/ modifying N-content
- Increase of the Cr-content in order to improve the oxidation resistance at application temperatures of up to 625°C
- Variation of the proven and investigated elements such as Mo, W, B and N on the basis of a C-Cr-Co-Nb matrix

Five different alloy compositions have been selected and produced as trial melts of 100 to 500kg [1]. The ruling elements are varying from 9,5-11,5Cr/ 0-2,5W/ 0,2-1,5Mo/ B-N. A large test programme has been carried out with these melts, and the still ongoing creep tests have reached > 40´000 hours.
The best creep strength with a potential to meet the target of 100MPa at 625°C for 100'000h was measured for the melt FB2 with 9,5Cr-1,5Mo-1Co-B-N. This composition is based on the good experience with the B-containing trial rotor within the previous round of COST501 [2]. As compared to this trial rotor the C-content is reduced, and Co was added to avoid delta ferrite formation in large cross-sections.
The long term stability of strength and toughness after exposure at 600°C and 650°C for this melt FB2 is better than for conventional 12%Cr steels at 530°C [3]. Therefore two full-size pilot rotors with different production routes (both not ESR) were manufactured and tested using the chemical composition of FB2. The overall testing has been started including the determination of the mechanical properties like tensile test, toughness, LCF, crack growth, creep rupture strength and long term strength and toughness stability. First results are reported.

In addition five trial melts for cast applications were made as plates (up to 200mm thick) or 5to stepped blocks (up to 500mm thick) and were subject to a large test programme similar to the forged trial melts. The test programme has been completed apart from the creep tests which have reached >40'000 hours. With respect to creep strength, the trial melts CB2 (G-9,5Cr-1,5Mo-1Co-B-N) exhibits promising results.
A 5to pilot valve with this composition has been cast and is currently under testing including fabrication weldments.
For both product groups forgings and castings the applied Co-content in the other trial melts (W-bearing) did not affect the creep rupture strength in a positive way.

Materials for 650°C Application

A further improvement of the 625°C ferritic-martensitic grades is necessary with respect to creep strength but under consideration of the increased oxidation occurring at this temperature level. The compositional selection is based on the knowledge acquired under the COST 501 programme especially the intensive microstructural investigations, the commercially available computing tools such as ThermoCalc and Dictra and the newly developed calculation methods of the equilibrium transformation temperature as well as the diffusion parameters of potential candidate test materials. On the basis of the promising compositions FB2 and CB2 modifications were made in the C-, Cr-, Co-contents and by the addition of W=0,5% in some cases with the idea to keep it soluted [1]. The new compositions for forged and cast trial melts show a strong similarity. The main elements cover ranges of 10-11,2Cr/ 1-1,5Mo/ 3-6Co/ 0-0,5W/ 0,2V/ 0,06Nb/ 0,02N/ 0,007-0,01B.
For the forged and cast trial melts as well as for the large components an extended test programme has been started including metallographic investigations, short-term and long-term mechanical properties, oxidation tests, evaluation and qualification of filler metals for the new cast steels and the investigation of production welds on the components.
Some creep tests have currently reached durations of >15'000h. The time is still to short to define best melts. First tendencies are reported.

References

[1] Staubli, M. and Mayer, K.H., Kern, T.-U., COST 522 – Power Generation into the 21st Century, Advanced Steam Power Plants. 3rd EPRI conference on Advances in Materials Technology for Fossil Power Plants. Swansea 2001.

[2] Kern, T.-U. and Scarlin, R.B., Vanstone, R.W., Mayer, K.H., High Temperature Forged Components for Advanced Steam Power Plants. 6th COST Conference, 5-7. October 1998, Liège, Belgium.

[3] Kern, T.-U. and Cerjak, H., Mayer, K.H., Staubli, M., Vanstone, R., Development and Qualification of Rotor Steels for 600 to 650°C Application in COST 501/COST 522. 14th International Forgemasters Meeting, 3-8. September 2000, Wiesbaden, Germany.

Research Activities in Ultra-Steel Project for 650°C USC Boilers

F. Abe, H. Okada, S. Wanikawa, M. Tabuchi, T. Itagaki, K. Kimura

and K. Yamaguchi

National Institute for Materials Science, Japan

1. Introduction

Since 1997, National Institute for Materials Science (formerly, National Research Institute for Metals) has been conducting the research and development of advanced ferritic steels for application to thick section boiler components of ultra-supercritical (USC) power plant at 650 °C, as a part of Ultra-Steel project. The project on ferritic steels for 650°C USC boilers involves the improvement of creep strength, oxidation resistance and creep-fatigue properties for ferritic heat resistant steels, including welded joints. In parallel with the development of new steels, degradation behavior of creep strength at long times has been examined for 9 - 12Cr steels in order to obtain guiding principles for the improvement of long term creep strength. This paper describes our activities in the Ultra-Steel project.

2. Alloy Design Philosophy

Preferential recovery of lath martensitic microstructure in the vicinity of prior-austenite grain boundaries promotes the preferential or inhomogeneous creep deformation in the vicinity of grain boundaries in Mod.9Cr-1Mo steel at 600 to 650°C. This causes a significant decrease in creep strength at long times. Therefore, for the improvement of long-term creep rupture strength, special attention should be paid to the suppression of preferential recovery of the microstructure near prior-austenite grain boundaries.

3. Present Status of Steel Development

We have been trying to stabilize lath martensitic microstructure in the vicinity of prior austenite grain boundaries. Several steels developed in this project exhibit higher creep rupture strength than ASME-T91 (9Cr-1Mo-VNb) and ASME-P92 (9Cr-0.5Mo-1.8W-VNb) at 650°C, as shown in Figure 1. The stabilization of $M_{23}C_6$ at lath boundaries by boron addition is effective for the suppression of preferential recovery of microstructure near grain boundaries, resulting in the improvement of creep rupture strength (9Cr-3W-3Co-VNb -0.0139B[1]). No nitrogen was added to the steel, because excess addition of boron and nitrogen promotes the formation of boron-nitrides at grain boundaries, which offsets the benefit due to boron and nitrogen. New attempts have been also demonstrated for tempered martensitic 9Cr steels strengthened by Fe-Pd $L1_0$ (9Cr-3W-VNb-1Pd[2]) and by MX nitrides (9Cr-3W-3Co-VNb-0.05N-0.002C[3]), a carbon-free Fe-Ni-Co martensitic alloy (18Ni-9Co -5Mo[4]) and a full-annealed ferrite matrix 15Cr steel (15Cr-1Mo-6W-3Co-VNb-0.07N -0.003C[5]). The pre-oxidation treatment in impure argon gas and the addition of Pd cause the formation of very thin, protective Cr-rich oxide scale on the surface of 9Cr steel, which significantly improve the oxidation resistance in steam at 650°C, as shown in Figure 2. Creep-fatigue life is proportional to the reduction of area in creep rupture test, namely, creep ductility but not proportional to creep rupture strength. The boron addition improves the reduction of area as well as the long-term creep rupture strength. The fine grains in heat-affected-zone (HAZ) in welded joints are responsible for Type IV creep fracture in welded joints. Decreasing the width of HAZ by electron-beam welding extends the creep life of welded joints.

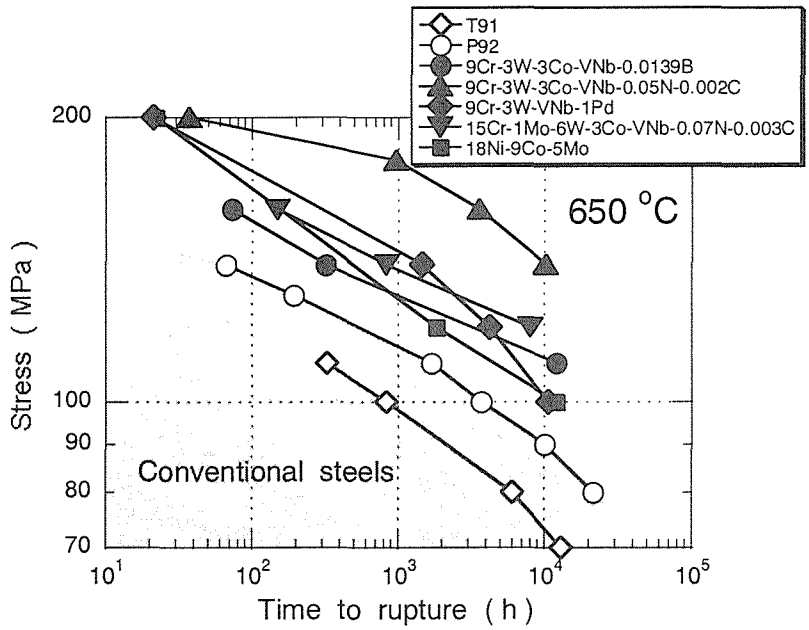

Figure 1 Creep rupture data for the new steels at 650°C, together with those for conventional steels ASME-T91 and ASME-P92.

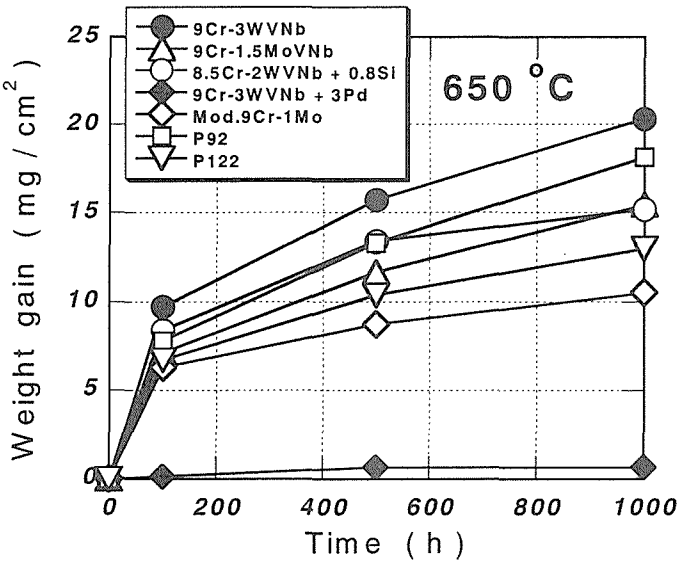

Figure 2 Weight gain of the steels in steam at 650 °C.

4. Summary

Several types of advanced ferritic heat resistant steels have been developed in a laboratory scale. Further improvement of creep strength of welded joints can make it possible to use the present steels as thick section boiler components of 650°C USC plant.

References

[1] T. Horiuchi et al., ISIJ International, 42 (2002) in press.
[2] M. Igarashi et al., ISIJ International, 41 (2001) S101 - 105.
[3] M. Taneike et al., this proceedings.
[4] S. Muneki et al., Tetsu-To-Hagane, 88 (2002) 95-100. (in Japanese)
[5] K. Kimura et al., Rep. of 123 Committee, JSPS, 43 (2002), 33-42. (in Japanese)

Martensitic/ferritic super heat-resistant 650°C steels – Design and testing of model alloys

V. Knezevic[1], G.Sauthoff[1], J.Vilk[1], G.Inden[1], R.Agamennone[2], W.Blum[2], Y.Wang[3], A.Scholz[3], C.Berger[3], J.Ehlers[4], L.Singheiser[4]

[1] Max-Planck-Institut für Eisenforschung GmbH, Düsseldorf, Germany,

[2] IfWW, Universität Erlangen-Nürnberg, Germany,

[3] IfW, TU Darmstadt, Germany,

[4] IfWE2, Forschungszentrum Jülich GmbH, Germany

1. Introduction

9-12%Cr martensitic/ferritic heat resistant steels are needed for 650°C Ultra Super Critical (USC) Power Plants. The aim of the present research is to design new super heat-resistant 12%Cr martensitic/ferritic steels for application at 650°C.

2. Design of model alloys

The alloy design concept for the new martensitic/ferritic super creep resistant 12%Cr steels is shown in Fig.1. Various carbide, nitride and Laves phase alloying elements - Cr, W, Nb, V, Ta, Ti - are used for precipitation hardening. The aim is to produce a sequence of precipitates with different kinetics: when the early precipitate ($M_{23}C_6$) over-ages and becomes less effective, the later precipitate (Laves phase) comes into operation. The Thermocalc software and database are used to study the conditions for avoiding δ-ferrite formation at the austenitization temperature (right dotted line at Fig.2.), obtaining equilibrium $M_{23}C_6$, Laves phase (and MX carbonitrides) at service temperature of 650°C (left dotted line at Fig.2.) and providing precipitation of the MX carbonitrides mostly in low- temperature ferrite (arrows).

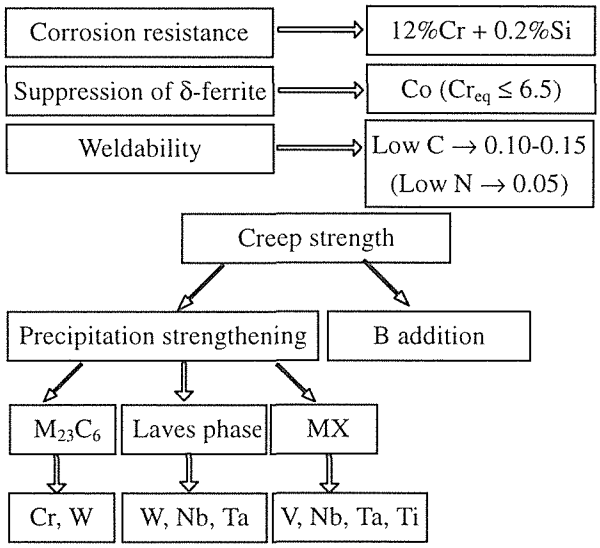

Fig.1. Alloy design concept for new martensitic/ferritic 12%Cr model alloys.

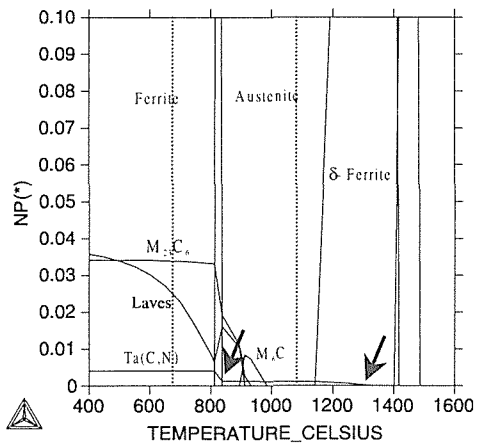

Fig.2. Calculated types and mole fractions (NP) of phases as a function of temperature for alloy DT4-30 (0.2Ta4W).

3. Results

The initial microstructure of the prepared model alloys is fully or almost fully tempered martensitic. The presence of a limited amount of δ-ferrite is a result of deviations from the nominal compositions. Relatively coarse $M_{23}C_6$ particles have been found on grain and subgrain boundaries in the initial state. A few coarse Laves phase particles have been observed in the alloy with increased W content and fine, homogeneously distributed TaX particles have precipitated inside subgrains in the alloy with Ta, Fig.3. A distinct coarsening of the subgrains, as well as of $M_{23}C_6$ carbides, and a pronounced precipitation of Laves phase has been observed after creep. TaX particles grow only very slowly, as was expected [1].

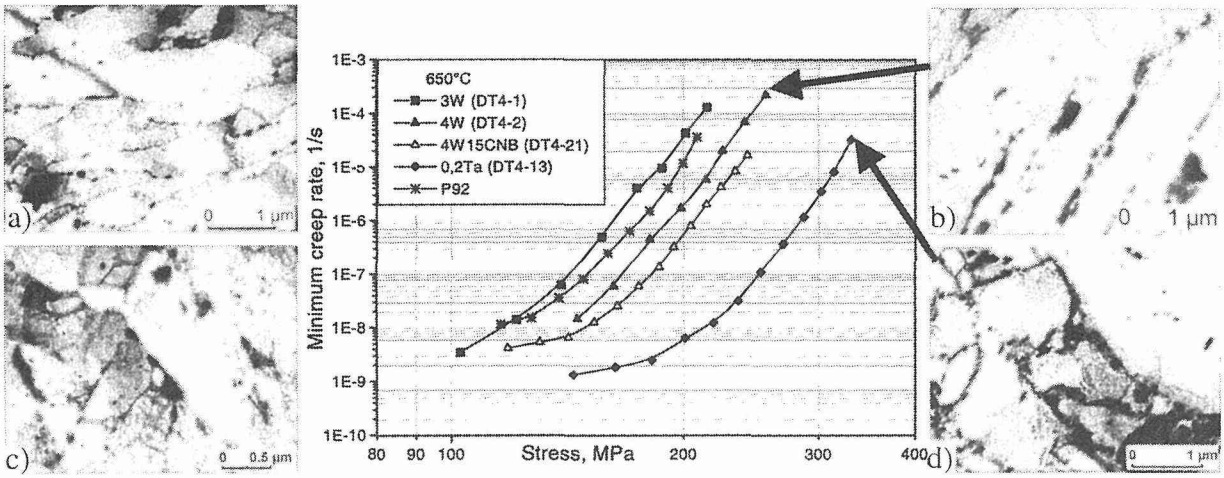

Fig.3. Stress dependence of the compressive minimum creep rate at 650°C for selected alloys and TEM micrographs of alloys DT4-2 (4W) (a, b) and DT4-13 (0.2Ta) (c, d) after heat treatment (a, c) and subsequent creep (b, d).

The results of compression creep tests for higher stress levels have indicated a high potential for reaching a sufficient creep resistance at 650°C by increasing the W content, by addition of MX forming elements, especially Ta and Ti, and by microalloying with B, Fig.3.

The iso-stress data for lower stresses demonstrate the prolongation of creep life and the reduction of creep rate, including minimum creep rate, with increase of W and addition of MX forming elements, Fig.4a. Additionally, the higher content of N and Co as well as precipitation of fine MX phase in the solid state obviously lead to better creep properties, Table 1. The simultaneous increase of W content and addition of MX forming elements together with microalloying of B have beneficial effects on creep strength, according to first results, Fig.4b. The further optimization of the composition and microstructure is in progress and is expected to result in alloys with a satisfying creep resistance at 650°C. The long-term creep testing up to 20000h will provide data for the estimation of long-term creep strength.

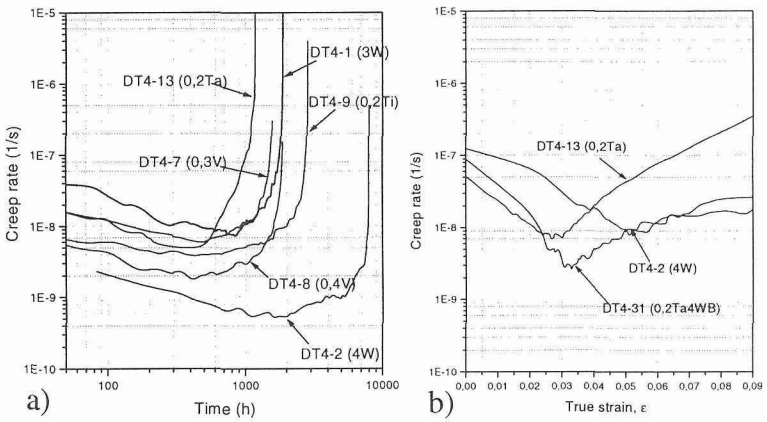

Fig.4.a) Creep rate vs. time and b) creep rate vs. creep strain for selected alloys at 650°C (stress level a) 100MPa and b) 120MPa)

Table 1. N and Co content for selected alloys and characteristics of MX particles.

Alloy	$\dot{\varepsilon}_{min}$	wt.%N	wt.%Co	MX precip.
DT4-2	5,05E-10	-	5,6	-
DT4-8	1,76E-09	0,0093	3,9	in solid
DT4-9	3,82E-09	0,0210	2,5	from liquid
DT4-13	4,58E-09	0,0098	2,05	in solid
DT4-7	5,95E-09	0,0015	3,6	in solid
DT4-1	7,16E-09	-	4,8	-

The first results of long-term corrosion tests indicate the improved corrosion behaviour compared with the 9%Cr steel P92.

Acknowledgment: The financial support by the Deutsche Forschungsgemeinschaft (DFG) is gratefully acknowledged.

Reference

[1] Knezevic, V., Vilk, J., Inden, G., Sauthoff, G., Agamennone, R., Blum, W., AG warmfeste Stähle/AG Hochtemperaturwerkstoffe, Düsseldorf, 2001, pp.78-85.

Selected Properties of High-Strength Ferritic Steels for Advanced Steam Power Plant

F. Schubert, R.J. Ehlers, P.J. Ennis, W.J. Quadakkers, L. Singheiser
Research Centre Jülich GmbH Institute for Materials and Processes in Energy Systems, Microstructure and Properties of Materials

The requirements to reduce both CO_2 emission and fuel consumption in conventional steam power plants has given rise to considerable effort to achieve higher thermal efficiency in power generation. This can be done by raising steam temperature and pressure. An enhancement from 535 to 650°C and from 185 to 300 bar would lead to an enormous reduction in fuel consumption and CO_2 emission. The development of the advanced modified 9% chromium steels P91, P92 and E 911 has provided the constructional materials for components capable of operation at temperatures up to 620°C. For application under such arduous condition, the new 9 to 12% Cr- steels are being introduced, initially because of the improved long term creep rupture behaviour.

The increases in the long term creep resistance have been achieved by alloying the basis of 9% Cr, 1% Mo steel with small amounts of V, Nb and N to provide precipitates of fine stable phases e.g. Nb and V carbides nitrides and carbo nitrides. The strengthening mechanisms are the martensitic transformation which provides a high starting dislocation density, precipitation of carbides (M23C6) at the former austenit grain boundaries and as well at the martensite lath boundaries. In addition, fine precipitation of carbides, nitrides or carbonitrides within the subgrains contribute substantially to the strengthening effect.

Very limited amounts of boron may also increase the creep resistance. Solid solution strengthening has been enhanced by W addition. The importance of the martensite transformation in achieving a suitable sub-gain structure will be discussed based on results from P92 given a high temperature tempering treatment.

Cooling after austenising produces a martensitic structure with a high dislocation density within the martensite laths. During operation recovery causes the formation of subgrains and a dislocation network, and a marked reduction in the dislocation density. The average sub grain and the dislocation density are discussed with TEM examination.

During operational exposure the precipitates of M23C6 retard the subgrain growth and therefore increase the strength of the material. The long term creep behaviour is of great importance. From the creep curves, the secondary creep rate was derived. After long testing duration, the dislocation density was examined, a decreased of about 75% compared with the as heat treated material is observed. At high stress levels, the differences in the secondary creep rates of the alloy P91, P92 and 911 is small. The low stress levels, however, the differences becomes more pronounced.
The results of the creep evaluation and the oxidation tests are discussed. It is shown that microstructural changes that occur in the first few thousand hours must be taken into account in assessing the long-term creep rupture strength.

The oxidation resistance is, however, becoming an increasingly important selection criterion. These steels exhibit during exposure in air good oxidation resistance, but in expected operational atmospheres which will contain water vapour, the oxidation rates of these new

steels increase significantly, which means that the oxidation resistance is becoming design relevant.

In this paper, the oxidation behaviour of new 9-12 wt.% Cr steels in environments containing water vapour (test atmosphere for simulation was mainly Ar-50vol.% H_2O) has been studied in the temperature range 550-650°C. Specimens were examined after exposure using optical microscopy, electron microscopy (SEM with EDX and WDX), X-ray diffraction (XRD) and secondary ion mass spectroscopy (SIMS).

In steam oxidation tests, it has been demonstrated that Cr contents above 11% are necessary for the formation of thin and protective oxide scales at 600 to 650°C. The temperature limits imposed by steam oxidation depend on the component wall thickness and on the steam oxidation induced reduction of the load-bearing cross section. However, increasing the Cr content to 11% or more may lead to problems in obtaining the full martensitic structure that is necessary for good creep properties.

The potential for further development of the martensitic steels toward application temperatures as high as 700°C is limited. New classes of material e.g. Ni-base superalloys must be evaluated for the desired long term application.

Production and Properties of Nano-Scale Oxide Dispersion Strengthened (ODS) Martensitic Steel Claddings

S.Ukai[1], T.Kaito[1], S.Ohtsuka[1]
M.Fujiwara[2] and T.Kobayashi[3]

1) O-arai Engineering Center,
Japan Nuclear Cycle Development Institute, Japan
2) Kobelco Research Institute Inc., Japan
3) Sumitomo Metal Technology Ltd., Japan

1.Introduction

To achieve higher plant operation temperature for improved thermal efficiency, efforts have being made to improve high temperature properties in the field of the power-generation industry. The oxide dispersion strengthened (ODS) ferritic-martensitic steels are the most promising materials with a potential to be significantly improved in the high temperatures strength over 650℃. Leading technology development of ODS ferritic-martensitic steels has being conducted in Japan Nuclear Cycle Development Institute (JNC), particularly emphasizing fuel cladding application for fast reactors [1]. In order to control the extended grain morphology along rolling direction in ODS ferritic-martensitic steels, α / γ phase transformation was developed as a capable method for controlling grain morphology[2]. In this study, cladding production is executed using the cold-rolling process. The high temperature mechanical properties of the produced claddings are investigated, focusing on varying heat-treatment and oxygen content in 9Cr-ODS martensitic steels.

2. Cladding production

The mother tubes were produced by the hot-extrusion of the mechanically milled 9Cr-ODS martensitic steel powder at 1150℃, and claddings were produced into the dimension of 8.5 mm outer diameter, 0.5 mm thickness and 3 m length through four times cold-rolling and intermediate heat-treatment, where cold-rolling was conducted under the softened ferritic phase by slow cooling rate at 150℃ per hour from austenitic phase at intermediate heat-treatment. At the final heat-treatment, normalizing and tempering were undertaken, which is designated M11. The ferritic structure claddings were also produced by utilizing significantly reduced cooling rate of 5℃ per hour at the final heat-treatment, which is designated MS11. The basic composition of both M11 and MS11 is Fe-9Cr-0.13C-1.95W-0.20Ti-0.35Y_2O_3-0.06Ex.O (mass %), where excessive oxygen (Ex.O) is defined as the oxygen content by subtracting oxygen coupled with Y_2O_3 from the total amount of oxygen. In addition, the extruded bar of 0.15 mass % of Ex.O. was produced, keeping exactly same chemical composition as M11 and MS11 for other elements, which is designated T3.

3. Mechanical properties

Fig.1 represents the results of analyses of the internal creep rupture curves of M11 cladding at 650℃, 700℃ and 750℃ by solid symbols and solid lines, as compared with both ferritic-martensitic PNC-FMS and austenitic PNC316. The strength level of M11 cladding is considerably superior to PNC-FMS, and is improved over even those of PNC316

at the time longer than 10,000 hr for 700℃ and 1,000 hr for 750℃. A significantly improved strength of M11 cladding is attributed to extreme reduction of oxide particle size to the nano-scale of 3 nm by complex Y-Ti-O oxide formation and resultantly shortened inter-particle spacing between oxide particles.

The internal creep rupture strength of MS11 having ferritic-structure, shown by open circles, represents similar strength level to those of normalized-tempered M11, however, it tends to be improved at longer time to rupture at 700℃. This improvement in the internal creep rupture strength could be owing to slightly coarsened ferritic grains in MS11. On the other hand, internal creep rupture strength of T3 is abruptly decreased at 700℃, where the oxide particles are not reduced and their size is around 10 nm. The large amount of excessive oxygen and thus high oxygen potential leads to separate formation of titania. The complex Y-Ti-O oxide formation is prevented in T3.

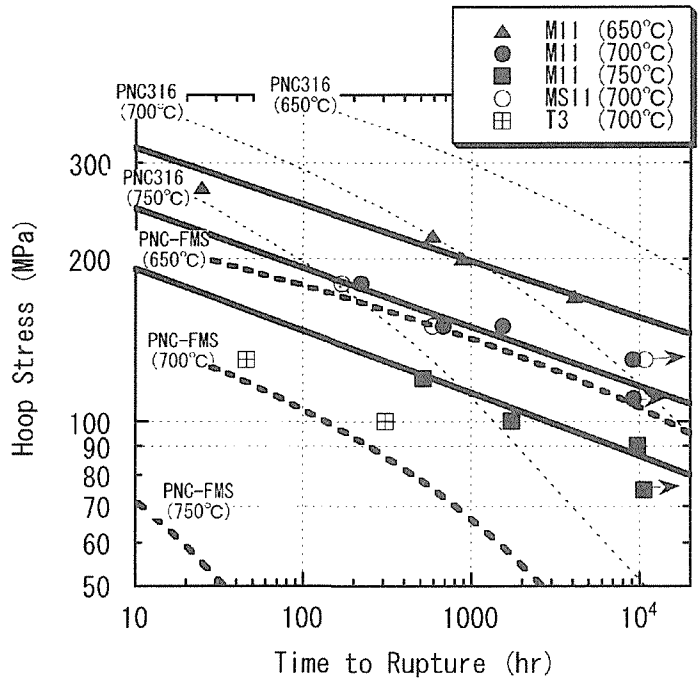

Fig.1 Creep rupture properties of 9Cr-ODS martensitic steel claddings, comparing with conventional austenitic and ferritic-martensitic steels

4. Conclusion

9Cr-ODS martensitic steel claddings were produced by cold-rolling under the softened ferritic phase induced by slow cooling at 150℃ per hours from austenite phase. The produced claddings attained the noticeable improvement in tensile and internal creep rupture strength by making homogeneous grains by means of normalized-tempered martensitic structure and ferritic structure induced by significantly slow cooling rate of 5℃ per hour at the final heat-treatment. The excessive oxygen control is indispensable in the course of cladding production process to maintain superior high temperature strength.

[1] Ukai,S., Mizuta,S., Yoshitake,T., Okuda,T., Fujiwara,M., Hagi,S. and Kobayashi,T.: J.Nucl.Mater.,283-287(2000)702

[2] Ukai,S., Nishida,T., Okuda,T. and Yoshitake,T., J.Nucl.Scie. and Technol.,Vol.35,No.4,(1998) 294,

Creep Properties of Precipitation Hardened Carbon Free New Martensitic Alloys

S.Muneki, H.Okada, K.Yamada, H.Okubo, M.Igarashi and F.Abe
Materials Research Group, NIMS, Japan

1. Introduction

Creep behavior of precipitation hardened carbon free new martensitic alloys was found to be completely different from that of the conventional high-Cr ferritic steels. The alloys exhibited gradual change in the creep rate with strain both in the transition and acceleration creep regions, and gave a larger strain for the minimum creep rate.

In this study creep properties of the carbon free (C-free) alloy has been investigated. The fine precipitates of the C-free alloy were found stable even at 973K, and effectively decreased the minimum creep rate much lower than that of the 9Cr ferritic steel.

2. Experimental Procedure

Chemical compositions of materials used in this study are given in Table 1. C-free alloy was solution treated at 1273K for 0.5h. 9Cr ferritic steel was also prepared as the reference and was tempered at 1043K for 4h after normalization at 1373K for 1h.

Table 1 Chemical composition of materials used (mass %).

	C	Si	Mn	Cr	W	V	Nb	B	N	Ni	Co	Ti	Al	Fe
C-free alloy	0.0005	0.02	0.46	5.0	9.9			0.0052	0.0005	12.1	9.0	0.12	0.06	Bal.
9Cr steel	0.087	0.32	0.52	9.2	3.3	0.2	0.048	0.0046	0.061		3.0			Bal.

3. Results and Discussion

Fig.1 shows creep properties of the 9Cr steel and the C-free alloy crept at 923K with 200 and 100MPa. Creep rate of the C-free alloy was much lower than that of the 9Cr steel both in transition creep and minimum creep. The C-free alloy showed the prolongation of transition strain from minimum to acceleration creep comparing with the 9Cr steel, indicating the homogeneous creep deformation.

Fig.2 shows creep properties of both materials crept at 973K with 120 and 80MPa. The C-free alloy also exhibited superior creep property to the 9Cr steel at 973K. For example time to rupture of the C-free alloy crept with 120MPa was more than 300 times longer than that of the 9Cr steel.

Fig.3 shows typical SEM microstructures of the C-free alloy after crept at 923K and at 973K. A large amount of fine 100nm under precipitates distributed at grain boundaries and inside the grain and was considered one of the causes of these excellent creep properties.

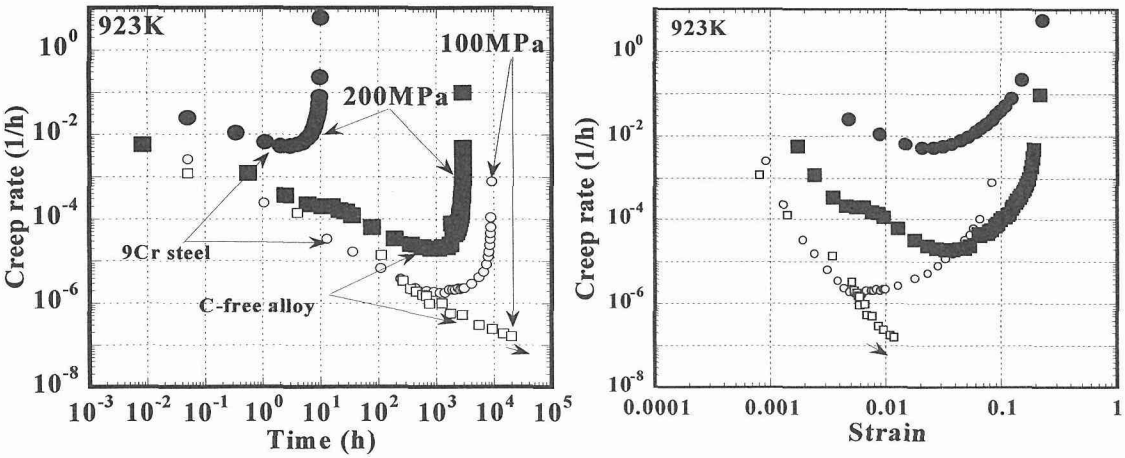

Fig.1 Creep properties of the 9Cr steel and the C-free alloy crept at 923K with 200 and 100MPa.

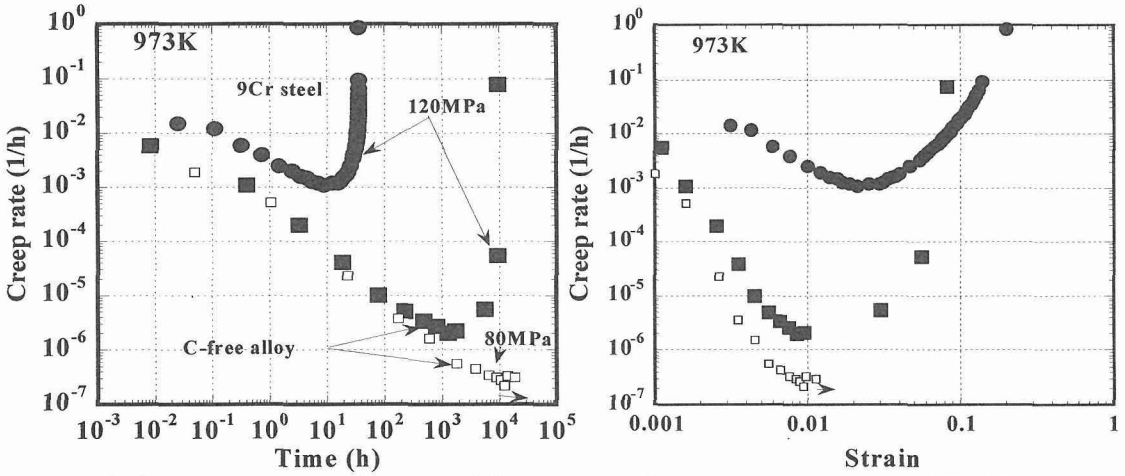

Fig.3 Creep properties of the 9Cr steel and the C-free alloy crept at 973K.

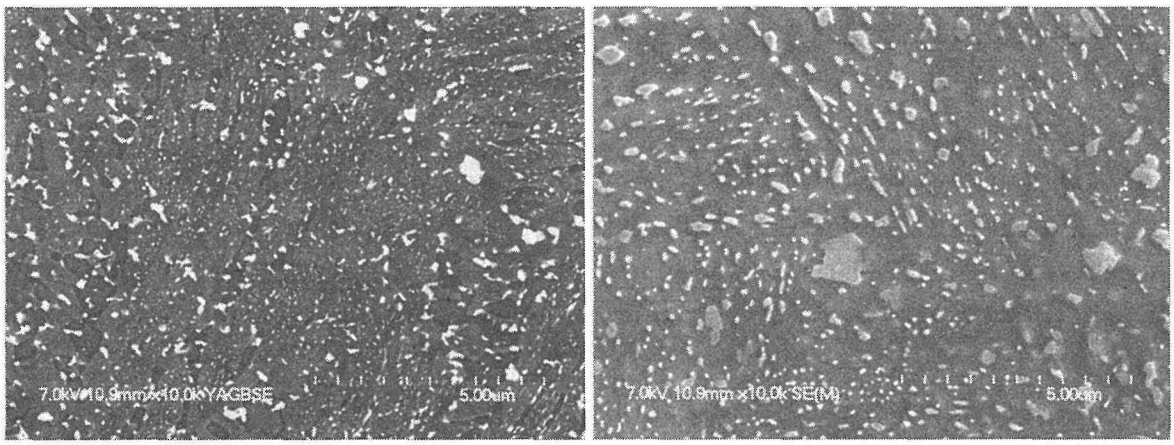

923K, 200MPa : Rt=2810h, Strain=0.242 973K,120MPa : Rt=3577h, Strain=0.015

Fig.2 SEM micrographs showing homogeneous precipitation of μ and Laves phases of the carbon-free allov.

Design Principle for Improvement of Toughness of Precipitation Strengthened 15Cr Steels

Y. Toda[(a)], H. Tohyama[(b)], K. Kimura[(a)] and F. Abe[(c)]
[(a)]Materials Creation Research Group, NIMS, Japan
[(b)]Interdisciplinary Graduate School of Science and Engineering, Tokyo Institute of Technology, Japan
[(c)]Strength and Life Evaluation Research Group, NIMS, Japan

1. Introduction

Creep strength of fully annealed and precipitation strengthened 15Cr ferritic steels has been studied, in order to replace conventional ferritic creep resistant steels which based on a tempered martensite microstructure. It has been found that increase in W and Co contents and optimization of C and N concentrations could improve long-term creep strength of fully annealed ferrite base 15Cr steel beyond the strength level of conventional one [1-3]. Higher Cr content of the 15Cr steel than those of the conventional one is suitable for better oxidation resistance [1-3]. However, toughness of the fully annealed 15Cr steel is very poor, and it must be improved to ensure formability and reliability. Therefore, the aim of the present study is to discuss a possibility of improvement in toughness of the fully annealed 15Cr ferritic steels, the effects of heat treatment and addition of Ni on toughness have been investigated.

2. Experimental Procedure

Chemical compositions of the steels used in the present study are shown in **Table 1**. Base composition is C and N free 15Cr-1Mo-0.2V-0.05Nb-6W-3Co-0.003B steel and the other four steels contain various concentrations of C and N [3]. In addition to the above steels, influence of Ni content on impact toughness have been investigated on 0C-7N and 5C-3N steels. These steels were prepared in a vacuum induction furnace, hot forged into bars and annealed for 30min at 1473K followed by furnace cooling or water quenching. Charpy impact tests were conducted on V-notch type specimens at room temperature and about 370K. Microstructure of the steels in the as-annealed condition was examined under an optical microscope (OM) and a scanning electron microscope (SEM).

Table 1 Chemical compositions (mass%) of the present studied steels.

	C	Cr	Mo	W	V	Nb	Co	N	B
base	**0.001**	14.91	1.01	6.03	0.19	0.045	2.96	**0.0018**	0.0031
0C-7N	**0.003**	14.91	1.01	6.00	0.19	0.045	2.96	**0.066**	0.0028
10C-0N	**0.10**	14.88	1.01	6.01	0.19	0.045	2.96	**0.0019**	0.0028
5C-3N	**0.046**	15.00	1.00	6.07	0.19	0.043	2.97	**0.033**	0.0030
10C-8N	**0.096**	15.10	0.99	5.94	0.18	0.064	3.00	**0.082**	0.0027

3. Results and Discussion

Fig. 1 shows Charpy impact values of the Ni free five steels in the as furnace cooling or water quenching conditions at room temperature and 370K. The differences in toughness between water quenched steels and furnace cooled ones are little in 0C-7N, 10C-0N and 5C-3N steels. However, the impact values of the water quenched base and 10C-8N steels are higher than those of the furnace cooled ones. Especially, the impact value of 224J/cm^2 at 370K for the water quenched base steel is very excellent. So, it can be said that increase in a cooling rate after annealing improve a toughness of the fully annealed 15Cr ferritic steels, though the effects of increase in cooling rate depend on the C and N contents strongly.

Fig.2 shows influence of Ni concentration on the Charpy impact value of the water quenched 0C-7N and 5C-3N steels at room temperature and 370K. The Charpy impact toughness of 0C-7N steels at room temperature is lower than 10J/cm^2 independent of Ni concentration.

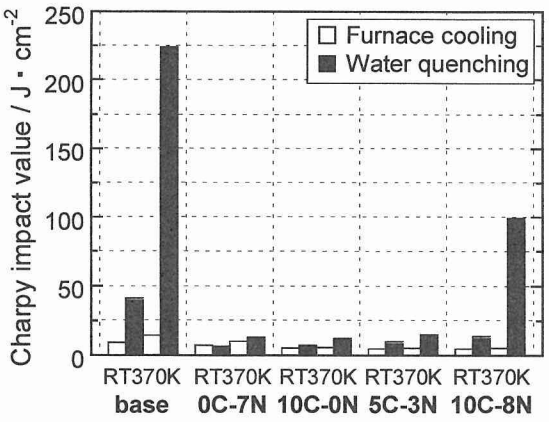

Fig. 1 Charpy impact values of the furnace cooled and water quenched steels tested at room temperature (RT) and 370K.

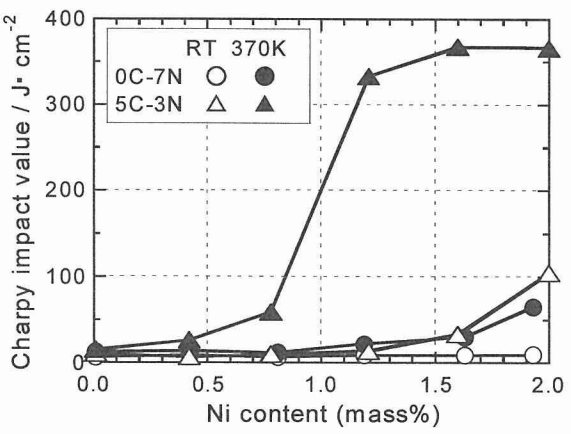

Fig. 2 Ni content dependence of Charpy impact value of the water quenched 0C-7N and 5C-3N steels tested at room temperature (RT) and 370K.

However, the addition of 1.5mass%Ni and more improves the impact value of 0C-7N steel at 370K. On the other hand, the impact value of 5C-3N steel increases drastically with the increase in Ni content. The impact value of the 5C-3N steel contains 2mass%Ni is about 100J/cm^2 at room temperature, and those of the steels contain 1mass% of Ni and more are higher than 300J/cm^2 at 370K. So, the Charpy impact values of the present studied steels, especially 5C-3N, are drastically improved by the addition of Ni.

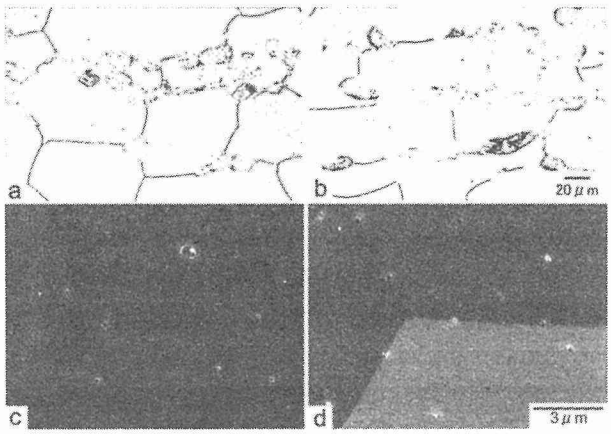

Fig. 3 Optical micrographs of (a) 5C-3N-0.4Ni and (b) 5C-3N-1.2Ni, and SEM micrographs of (c) 5C-3N-0.4Ni and (d) 5C-3N-1.2Ni. Both steels are in the as water quenched condition.

Fig. 3 shows optical micrographs of (a) 5C-3N-0.4Ni and (b) 5C-3N-1.2Ni, and SEM micrographs of (c) 5C-3N-0.4Ni and (d) 5C-3N-1.2Ni. Both steels are in the as water quenched condition. Volume fractions of martensite phase, which is observed as dark gray contrast on the grain boundary of ferrite matrix in the OM micrographs, and grain sizes are almost the same each other. Furthermore, a few precipitates are observed on the grain boundary in the both steels, and SEM micrographs show that some particles with size of hundreds μm are precipitated within the grain. However, the Charpy impact values of 5C-3N-0.4Ni and 5C-3N-1.2Ni are 26J/cm^2 and 330J/cm^2, respectively, and the impact values are improved drastically with increase in Ni concentration. Consequently, it has been supposed that the increase in Charpy impact value of the steel with increase in cooling rate and concentration of Ni is attained by the improvement of toughness of ferrite matrix itself.

References

[1] K. Kimura, K. Seki, Y. Toda, H. Kushima and F. Abe, ISIJ Int., 41(2001), Supplement, pp.S121-S125.

[2] Y. Toda, K. Seki, K. Kimura and F. Abe, JSME Int. J., A45(2002), No.1, pp.25-29.

[3] K. Kimura, H. Tohyama, Y. Toda, H. Kushima and F. Abe, Report of 123rd Committee on Heat Resistant Metals and Alloys, Japan Soc. for the Promotion of Sci., 43(2002), No.1, pp.33-42, (in Japanese).

Properties of Advanced Austenitic Stainless Steel (TEMPALOY AA-1:18Cr-10Ni-3Cu-Ti-Nb) for Power Plant Application

A.Tohyama[1)], H.Hayakawa[1)] and Y.Minami[2)]
1) Product Design and Quality Control, NKKTUBES, Japan
2) Materials and Processing Research Center, NKK CORPORATION, Japan

1. Introduction

Recently, the design of thermal power plants has tended towards higher thermal efficiency, prompted largely by concerns over global environmental problems. For coal-fired thermal power plants, in particular, ultra super critical (USC) boilers, which use steam at very high temperatures and pressures, are under construction. Such boilers require the use of steel having superior high temperature strength greater than that of conventional 18-8 stainless steels.

The effects of various alloying elements on the creep rupture strength of 18-8 stainless steels were examined. As a result, the new heat resisting steel(TEMPALOY AA-1:18Cr-10Ni-3Cu-Ti-Nb) has been developed. This paper describes various properties of this newly developed steel and the results of 2 years field service in thermal power plant as a superheater tube.

2. Properties of TEMPALOY AA-1 tube

Precipitation strengthening is mainly possible method for improving the creep rupture strength of austenitic stainless steel. 18Cr-10Ni steel was selected as the base metal. Nb and Ti were added to produce MC carbides precipitation strengthening, and 3wt.% Cu was added to provide precipitation strengthening of Cu-rich phase. In addition, a small amount of B was added in order to aim at the reinforcement of the grain boundary. The chemical composition of TEMPALOY AA-1 is determined as shown in Table 1.

Table 1 Chemical composition of newly developed steel TEMPALOY AA-1 (mass %)

	C	Si	Mn	P	S	Cu	Ni	Cr	Ti	Nb	B
Sample	0.10	0.29	1.57	0.025	0.004	2.87	10.37	17.92	0.19	0.27	0.0024
Range	0.07 ~ 0.14	≦1.00	≦2.00	≦ 0.040	≦ 0.010	2.50 ~ 3.50	9.00 ~ 12.00	17.50 ~ 19.50	0.10 ~ 0.25	0.10 ~ 0.40	0.0010 ~ 0.0040

Several size of boiler tubes were manufactured, and various properties were evaluated.

In the case of boiler tube used for super critical conditions, as for countermeasures against steam oxidation, both internal shot-blasted treatment and internal fine grained treatment can be considered applicable to TEMPALOY AA-1 steel tube as well.

The allowable stress of TEMPALOY AA-1 more than 600℃ is shown in Fig.1 compared with conventional 18-8 stainless steels. The allowable stress of this steel at 675℃ is 66N/mm^2, which is fully sufficient to a development aim that this tube can be used in the severe steam conditions exceeding 630℃ and 30MPa that are forecast for the near future.

3.Results of field test

The field service test was performed in the boiler for industrial power generation in NKK Keihin Works. The steam pressure and temperature are 13.2/2.86MPa and 541℃, respectively. The dimension of the tube is an outer diameter 57.1mm, the wall thickness 11.9mm.The chemical composition of the test tube is shown in Table 1. The tube was installed in the secondary superheater of the boiler, and the field test duration is 2 years.

After the field test, there is no dimension change in the outer diameter and wall thickness of the tested tube. And either partial corrosion of the surface of the inside and outside is not admitted. The high temperature tensile test and the creep rupture test were examined. The results of creep rupture test at 650 and 700℃ are shown in Fig.2 comparing with the average creep rupture strength of the unused tube. It is thought that material quality deterioration is hardly caused at the use temperature of 600℃ or less for the use time of less than 100,000 hours.

4. Discussion

The high temperature strength of this new steel is excellent as described above. It is possible thought to use the precipitation strengthening of $M_{23}C_6$, MC and Cu-rich phase. The transmission electron microscope (TEM) observation results of the tested tube are shown in Photo 1. In the grain, fine precipitated NbC and TiC of about 0.02 μm were observed. Moreover, the precipitation of $M_{23}C_6$ of about 0.20 μm was observed in the grain boundary. The results of the TEM observation by the high magnification , the strain according to fine precipitation of Cu-rich phase was observed. The creep rupture strength of TEMPALOY AA-1 steel tube has improved by these fine dispersion precipitates.

5. Conclusion

This report has introduced the newly developed boiler tube which named TEMPALOY AA-1 (18Cr-10Ni-3Cu-Ti-Nb). The cost performance , which is the balancing of the high temperature strength and the content of alloy element, of this steel is excellent. This tube can be used as superheater tubes in USC boilers at a pressure of 30 MPa and temperature of 630℃.

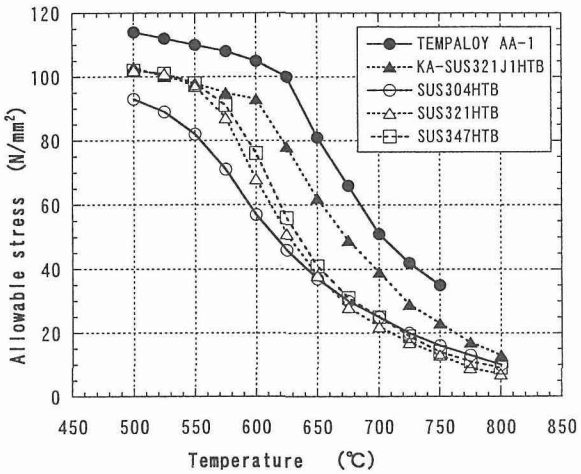

Fig.1 Comparison of allowable stress

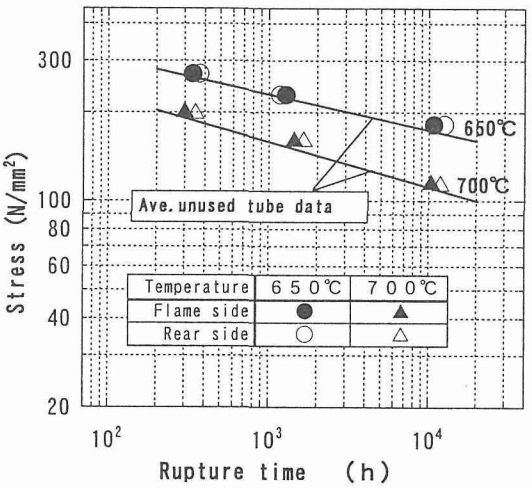

Fig.2 Creep rupture strength of the tested tubes.

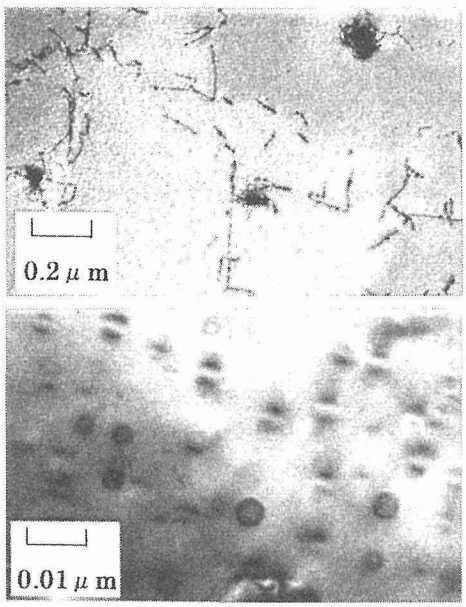

Photo 1 Transmission electron microscope (TEM) observation result of the tested tube. (upper: carbides, lower: Cu-rich phase)

HIGH TEMPERATURE DEFORMATION BEHAVIOR OF DISSIMILAR METAL JOINTS BETWEEN MODIFIED 9Cr-1Mo STEEL AND ALLOY 800

M. Sireesha, J. Swaminathan*, Shaju K. Albert**, M. Kamaraj and S. Sundaresan

Department of Metallurgical Engineering, Indian Institute of Technology Madras, Madras-600 036, INDIA

**National Metallurgical Laboratory, Council of Scientific and Industrial Research, Jamshedpur-831 007, INDIA*

***Materials Technology Division, Indira Gandhi Center for Atomic Research, Kalpakkam-603 102, INDIA*

Transition joints in power plants between ferritic steels and austenitic stainless steels suffer from a mismatch in coefficients of thermal expansion (CTE) and the migration of carbon during service from the ferritic to the austenitic stainless steel [1]. To overcome these, nickel-base consumables are commonly used. The use of a trimetallic combination with an insert piece of intermediate CTE provides for a more effective lowering of thermal stresses [2]. The heterogeneous microstructures present in such transition welds exhibit different creep strengths. Thus, under conditions encountered in power generating plants, viz., temperatures of about 550°C, the austenitic base metal and nickel-base weld metal have significantly greater creep strength than the ferritic steel and failures occur by cavitation developed along the weld metal / ferritic steel interface [3]. The current work envisages a trimetallic joint involving modified 9Cr-1Mo steel and 316LN austenitic stainless steel as the base materials and Alloy 800 as the intermediate piece. Two joints are thus involved: one between 316LN austenitic stainless steel and Alloy 800, and the other between Alloy 800 and modified 9Cr-1Mo steel. For the joint between Alloy 800 and modified 9Cr-1Mo steel, Inconel 82/182 is the established filler material. This paper examines the effect of stress and temperature on fracture of the joints between Alloy 800 and modified 9Cr-1Mo steel. Creep studies have been carried out in air on these joints at 550, 590 and 630° C, under constant load condition at stress levels ranging between 50 and 285 MPa.

In general the strain versus time plots took the form of conventional creep curves with primary, secondary and tertiary stages, with rupture time ranging from 100 to 8000 hours. The steady state creep rate increased systematically with increasing temperatures in the applied stress regimes. The relation obtained in the temperature range of 550-630°C is a straight line which is governed by the power law equation given by $\dot{e}_{min}=A_1\sigma^{n}$, where A_1 is the temperature dependent constant and n the creep exponent. In the current study, the values of n are found to lie in the range 9-20.

The temperature dependence of the rupture data can be described by a set of parallel straight lines linking results at each stress level so that the overall stress and temperature

dependence can be described by the expression $t_r=A_2\ \sigma^{-n}\exp(-Q/RT)$ where T is the absolute temperature, R and A_2 are constants. For the current joint under study, a value of the activation energy for creep, Q of about 645 kJ/mole provides a reasonable description of the results. This value is in good agreement with the published value for self-diffusion in modified 9Cr-1Mo steel [4]. This agreement supports the view that failure in these weldments is controlled by self-diffusion in the modified 9Cr-1Mo steel.

The rupture data for all tests are plotted as stress versus rupture time for each temperature and the data are correlated, using the Larson-Miller equation with a C value equal to 31.

The Monkman-Grant relation on a log-log plot with least squares fitting (regression coefficient=0.89) to the data yielded a slope of –1.6 and C_{MG}=0.021 for the joint. On normalizing the minimum creep rate data with fracture strain, there was a marginal reduction in the data scatter. Log-log least square fitting of the data values was carried out and the slope of the line was found to be -1 and the constant C_{MMG} is equal to 0.19. Thus, both Monkman-Grant as well as the modified Monkman-Grant relation is found to be valid for the joint under study and can be used to predict the rupture life for a specified creep rate.

The time to onset of tertiary creep t_{23} is generally related to rupture life by a factor f: $t_{23}=ft_r$ Thus from the rupture time, t_r, the time up to the secondary stage can be computed and t_{23} thus obtained, can be used for design life of components which are not supposed to enter into the tertiary stage during their service life. The joint between alloy 800-modified 9Cr-1Mo steel exhibited $t_{23}=0.5t_r$.

Detailed examination of the fracture behavior has shown that failure develops as a consequence of metallurgical degradation in the modified 9Cr-1Mo steel. No cavities were observed in the creep-tested samples. The fracture behavior of the welds varied with applied stress levels exhibiting the following pattern:
1. At the highest applied stresses of 270 and 285 MPa, failure occurred as a consequence of geometric instability in the modified 9Cr-1Mo steel parent material, with significant necking that resulted in high ductility failures with reductions in area of the order of 85%.
2. At all other lower stress levels (<270MPa), the samples failed in a relatively low ductility manner in the HAZ close to the fusion boundary. Post-test optical metallographic examination on longitudinally sectioned creep tested specimens showed absence of intergranular damage of the form of r-type cavities and wedge cracks.

References:

1. Slaughter, G.M. and T.R. Housley (1964) Welding Journal, 43, 454s-460s
2. King, J.F., M. D. Sullivan and G. M. Slaughter (1977)Welding Journal, 56, 354s - 358s
3. Nicholson, R.D (1982) Metals Technology, 9, 305-311.
4. Foldyna, V., J. Purmensky and Z. Kubon (2001) ISIJ International, Supplement, s81-s85

Microstructural Degradation of the HAZ in 11Cr-0.4Mo-2W-V-Nb-Cu Steel (P122) During Creep

N. Komai and F. Masuyama
Mitsubishi Heavy Industries, Ltd., Japan

1. Introduction

11Cr-0.4Mo-2W-V-Nb-Cu steel(P122)[1] has excellent corrosion resistance and approximately 1.3 times higher creep strength than Mod.9Cr-1Mo steel (P91). This steel has already been used for main steam pipes, high temperature reheat pipes and headers, as well as SH/RH tubes in modern large capacity fossil power plants. It is well known that weldments are weaker in creep strength than base metal under higher temperature and lower stress conditions[2]. Weldments usually fracture at the intercritical HAZ adjacent to base metal, known as Type IV failure. However the failure mechanism has not yet been elucidated. In this study the microstructual degradation of the HAZ of this steel during creep was investigated in order to better understand the mechanism of Type IV failure.

2. Experimental Procedure

Table 1 shows the chemical composition of the steel tested. Weldments were fabricated by means of GTAW process welding using steel plates with 34mm thickness. Post-weld heat treatment was applied to the weldment at 750°C. Fig. 1 shows a large creep specimen taken from the weldments. The specimens were subjected to creep testing and interrupted at specified times prior to rupture. Microstructual changes in the HAZ were investigated using OM, SEM, TEM and the extraction replica technique.

3. Results

1) The creep test specimen ruptured in the fine-grained HAZ as shown in Fig. 2. Weldments were weaker in creep strength than base metal in tests conducted at higher temperature and lower stress.
2) Fig. 3 shows the hardness traverse for the weldment during creep. The hardness of the weld metal, coarse-grained HAZ and base metal decreased with increases in the creep damage rate, while hardness changed only slightly in the fine-grained zone.
3) Fig. 4 shows TEM micrographs at fine-grained HAZ. The fine-grained HAZ consisted of recovered martensite with low dislocation densities, and the microstructure changed to subgrains during creep.
4) Creep cavities were detected at grain boundaries in the fine-grained HAZ. As shown in Fig. 5, the densities of creep cavities increased with the creep damage rate. Fig. 6 shows the linked cavities observed in the fine-grained HAZ after creep.
5) $M_{23}C_6$, M_7C_3 and MX type carbides had already precipitated in the HAZ before the creep test. A Laves phase arose at the grain boundary of the coarse- and fine-grained zones of the HAZ during the creep test.

References

[1] Y. Sawaragi, A. Iseda, K. Ogawa, F. Masuyama and T. Yokoyama : E. Metcalf (ed.), New Steels for Advanced Plant up to 620°C, PicA Publishing, London, UK, (1995), p45.
[2] F. Masuyama, M. Matsui and N. Komai : Key Engineering Materials, 171-174(2000), p99.

Table 1 Chemical composition of steel tested (mass%)

C	Si	Mn	Cr	Ni	P	S	Mo	W	Cu	V	Nb	B	N
0.12	0.28	0.61	10.50	0.34	0.018	0.001	0.36	2.05	0.97	0.21	0.06	0.0029	0.069

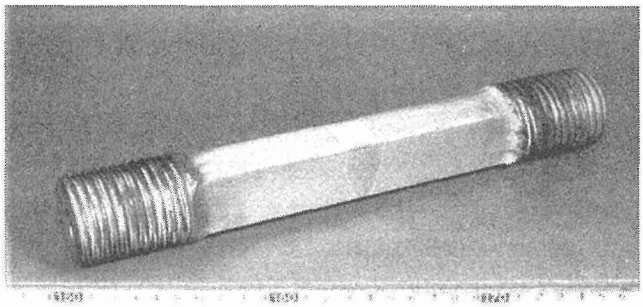

Fig. 1 Appearance of large size creep specimen

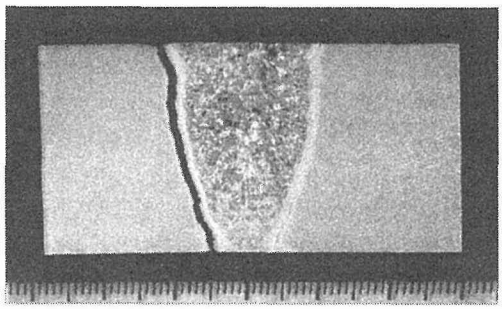

Fig. 2 Macrostructure of creep ruptured specimen

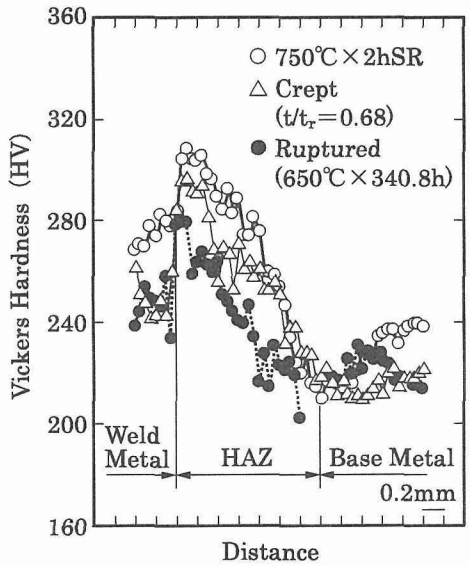

Fig. 3 Changes in hardness distribution in weldment during creep

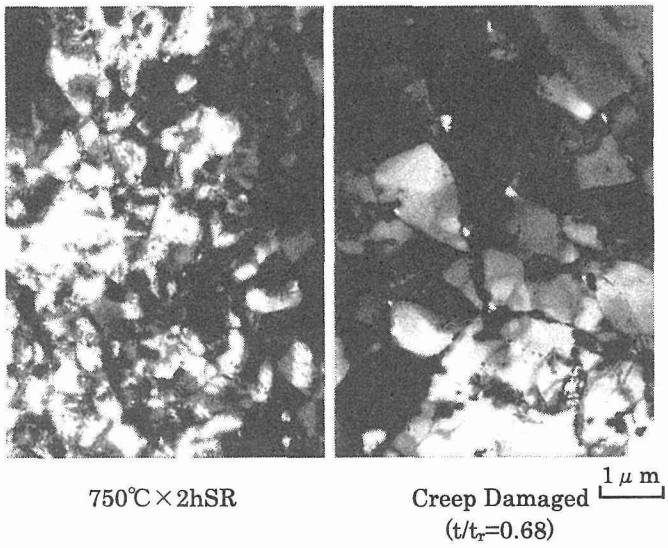

Fig. 4 TEM micrographs at fine-grained HAZ

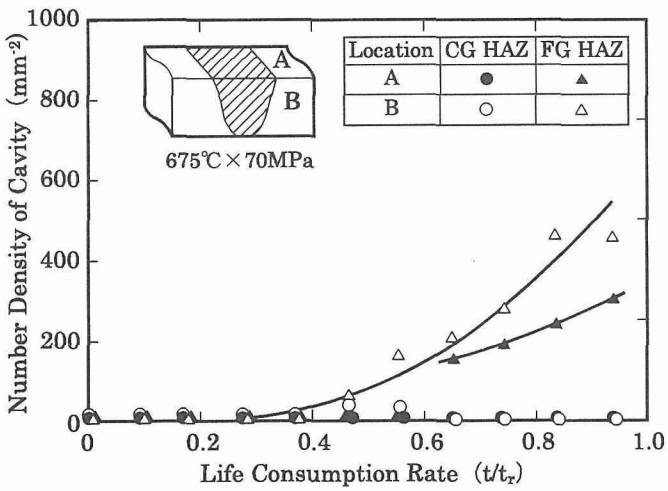

Fig. 5 Relationship between number density of cavity and life consumption rate

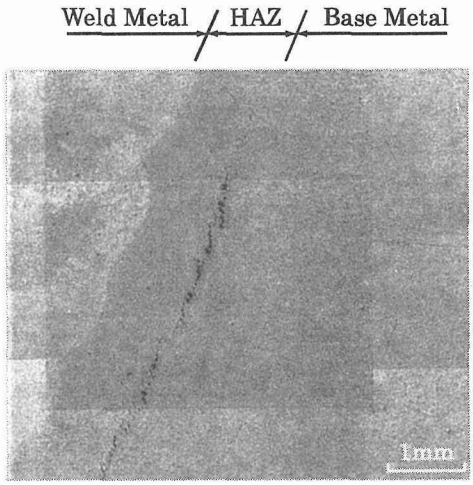

Fig. 6 Microstructure of creep damaged HAZ observed by replica

MICROSTRUCTURAL INVESTIGATIONS ON TYPE IV CRACKING IN A HIGH Cr STEEL

S.K. Albert*, M. Matsui and M. Tabuchi
National Institute for Materials Science
1-2-1 Sengen, Tsukuba, Ibaraki 305-0047, Japan
**Indira Gandhi Centre for Atomic Research, Kalpakkam-603102, India*

High Cr steels with higher creep strength and ductility than the conventional Cr-Mo steels are being developed worldwide. One of the limitations in this class of steels to achieve the desired high temperature properties is the problem of cracking in the heat affected zone (HAZ) of their welds during service or creep tests, often referred to as Type IV cracking. The creep life of the weldments of these steels can be as low as 20% of the base metals and cracking almost always occurs in the HAZ close to the base metal [1]. This zone is heated to a temperature between Ac_1 and Ac_3 temperatures (intercritical HAZ or ICHAZ) or just above Ac_3 (fine-grained HAZ or FGHAZ) during welding, and is characterized by fine grain size. In the present study, microstructural changes that lead to Type IV cracking in HCM12A (12Cr-0.4Mo-2WCuVNb) steel HAZ have been studied systematically in the as-welded condition, after post weld heat treatment (PWHT) for different duration and after creep test. Studies were also carried out on specimens with simulated HAZ structures. Microstructural simulation was carried out both by furnace heat treatment and by weld simulator (Gleeble weld simulator).

SEM micrographs of the coarse grained HAZ (CGHAZ) and FGHAZ after a PWHT of 1013K/15 minutes are shown in Fig. 1. A comparison of the microstructures reveals that the precipitates in FGHAZ are much larger than that present in the CGHAZ. Figure 2 shows the hardness profiles in the HAZ in the as-welded condition and after PWHT for 15 and 240 minutes respectively at 1013K. Hardness of the ICHAZ has come down from 250 VHN to 220 VHN even after 15 minutes of PWHT. No further reduction in the hardness of this zone was noticed with increase in time, though hardness of the HAZ close to weld metal reduced with increase in time. Hardness values clearly indicate the tempering kinetics of the ICHAZ is much faster than that of the rest of the HAZ and this zone has the minimum strength after the PWHT.

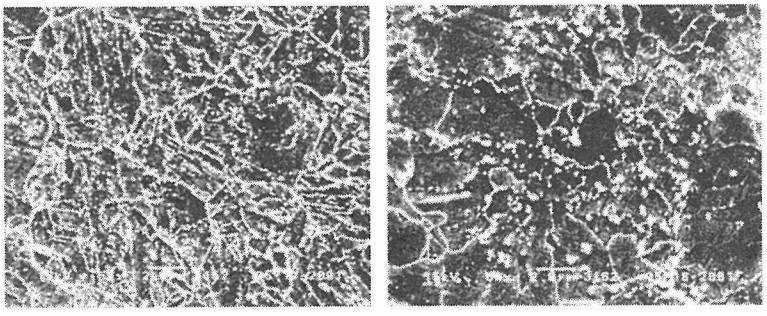

a) b)

Fig.1 Microstructure of a) HAZ close to fusion line and b) FGHAZ after PWHT of 1013K/15 min.

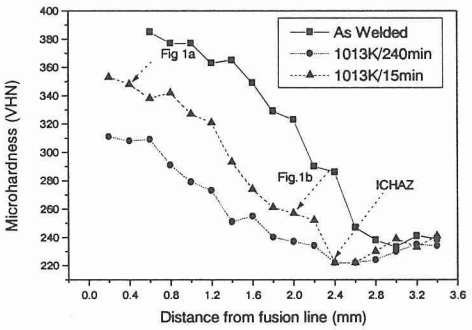

Fig.2 Microhardness profile in the HAZ. Location of microstructures in Fig.1 is indicated in the graph.

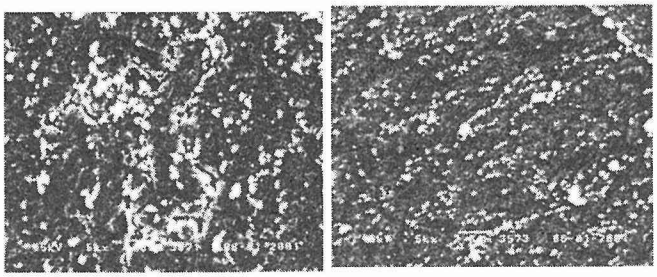

a) b)

Fig.3 Microstructure of creep tested weld joint a) HAZ close to base metal with creep cavities formed around large particles b) base metal with small precipitates and without cavities

Figure 3 shows microstructures of the weld joint after creep test (923K, 40MPa rupture time 11273h) from the HAZ where fracture eventually took place (Fig. 3a) during testing and the base metal (Fig.3b). Precipitates in the location of fracture are larger than those in the base metal and the creep cavities appear to have nucleated around large precipitates.

Results of the creep tests of specimens with HAZ microstructure simulated by heat treatment also confirmed that creep life of ICHAZ and FGHAZ is lower than that of base metal and rest of the HAZ. However, in weld joint, creep cavitation was the predominant mode of fracture while in the HAZ simulated specimens this was not so. HAZ microstructure was also simulated by a weld simulator in which cooling rate and peak temperature experienced by ICHAZ and FGHAZ in the actual weld were employed. A comparison of this simulated microstructure with that of the actual weld joint and also with that simulated by heat treatment (Fig.4) shows that HAZ microstructure simulated by weld simulator matches more closely with that of the actual weld. During heating part of the thermal cycle, transformation to austenite begins initially along the prior austenite and lath boundaries. The precipitates (predominantly carbides) in these regions dissolve in the austenite while those within the lath interiors remain without dissolving. During cooling part of the thermal cycle, austenite transforms to martensite and the net result of the weld thermal cycle in these parts of HAZ is a microstructure as shown in Fig. 4a; with partial transformation of matrix and partial dissolution of precipitates. Due to relatively high concentration of carbon (due to dissolved carbides) in the transformed martensite and the availability of pre-existing carbides, tempering kinetics of the martensite formed in the FGHAZ and ICHAZ would be faster than rest of the HAZ where complete transformation has taken place. This in turn leads to reduction in hardness, increase in the size of the precipitates and destruction of the lath structure in the FGHAZ and ICHAZ after PWHT. As a result of all these changes, high temperature strength of these zones comes down which eventually leads to Type IV cracking during creep test or in service. Creep tests using specimens with ICHAZ and FGHAZ simulated by weld simulator is expected to provide more information on the mechanism of type IV cracking and probable methods to overcome it.

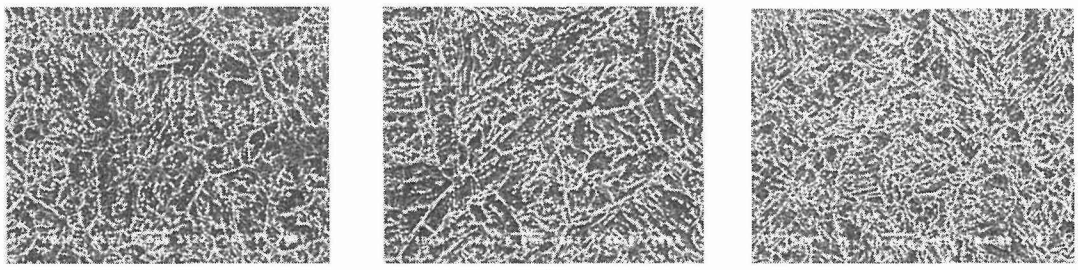

a) b) c)

Fig. 4 Microstructures of a) HAZ of actual weld (1.6mm from fusion line) b) HAZ simulated by weld simulator and c) HAZ simulated by heat treatment (peak temp. of simulation 1123K)

References

[1] Ellis, F.V and Viswanathan, R., Review of Type IV Cracking in Piping Welds, Integrity of High Temperature welds Professional Engineering Publishing Ltd. UK. 1998 PP 125-134

Stress/Strain Analysis Concerning Deterioration of Creep Property at HAZ of High Cr Heat-Resisting Steel

Li Dejun, Shinozaki K., Kuroki H.
Graduate School of Engineering, Hiroshima University, Japan

1. Introduction

Previous report[1] has discussed the role of precipitate in creep void initiation by using 2-D model. However it is impossible to introduce triaxial stresses in welded joint because of 2-D model limitation. Therefore a 3-D precipitate and matrix model is performed to do microscopic stress analysis in this study. At the same time stress analysis in the welded joint is also carried out and its computed result is introduced into the 3-D model as applied stress. Based on macro and micro models, the effects of precipitate and the width of fine-grained heat affected zone (FGHAZ) on creep void occurrence are discussed.

2. Model

2.1 Macro model of one pass welded joint

The prototype of macro model is an actual one pass welded joint specimen used in the creep test. The diameter of specimen is 5mm. The widths of weld metal (WM), coarse -grained heat affected zone (CGHAZ), FGHAZ and base metal (BM) are determined to be 8, 1.9, 1.3 and 6.8 mm respectively by measuring the specimen. Figure 1 shows the axial symmetric model, which is 1/4 of the actual specimen. Creep temperature is 923 K. Applied stress are 90 and 100 MPa respectively. Creep process is assumed to follow Norton's creep law, described as $\dot{\varepsilon} = A\sigma^n$. The values of A and n used are shown in Table 1[2]. The simulation is carried out by the FEM code ANSYS 5.5.

2.2 3-D micro model of precipitate and matrix

The precipitate and matrix model is assumed to be an isolated precipitate embedded in matrix. The matrix creeps but the precipitate does not. The radius of precipitate is 0.2 μ m and the matrix is $4\times4\times4$ μ m^3. Figure 2 shows the micro symmetric model, which is 1/8 of the physical model. The computed result of the welded joint model is introduced into this 3-D micro model as applied stress.

3. Results and Discussions

Figure 3 shows contour map of equivalent strain after 600h creep at stress 100MPa. The largest equivalent strain appears at FGHAZ. Figure 4 shows the comparison in distribution between creep void number and calculated equivalent strain. The peak positions of creep void number and equivalent strain almost correspond. This phenomenon suggests the critical role of equivalent strain on creep void occurrence. Figure 5 shows the effect of width of FGHAZ on equivalent strain. The largest equivalent strain decreases from 0.054 to 0.023 with a decrease in width of FGHAZ from 1.8 mm to 0.8 mm. This result implies that narrow FGHAZ has beneficial effect on prolonging creep lifetime of welded joint.

The computed result of one pass welded joint model is introduced into 3-D micro model. The result of 3-D model is similar as 2-D model. Their largest equivalent strains appear at precipitate/matrix interface and it is used in the following discussion. Figure 6 shows the equivalent strain as a function of creep time under the conditions of precipitate existing and not. It can be seen that equivalent strain rate under the condition of precipitate existing is much higher than that without precipitate. Figure 7 shows the equivalent strain as a function of creep time when precipitate is located at the largest equivalent strain mesh in FGHAZ, CGHAZ and BM respectively. It can be seen that FGHAZ still has the highest strain concentration. At the same time, CGHAZ and BM have high strain rates too. However, it should be noted that the equivalent strain of most area for CGHAZ and BM is still much lower than that of FGHAZ.

The results indicate that precipitate aggravates the strain concentration at precipitate/matrix interface and is easy to lead to creep void occurrence, and narrow width of FGHAZ can decreases the tendency of occurrence of creep void.

References:

[1] Shinozaki K. et al., Preprints of the national meeting of J.W.S. (2001), No.68, pp.288
[2] Tabuchi M. et al., Report of ISIJ meeting 13 (2000), No. 3, pp.257

Table 1 Creep properties used in simulation

Temperature 923 (K)	A ($MPa^{-n}h^{-1}$)	N
Weld metal (WM)	$3.37x10^{-57}$	24.0
Coarse grained HAZ (CGHAZ)	$6.97x10^{-26}$	10.2
Fine grained HAZ (FGHAZ)	$2.80x10^{-24}$	9.8
Base metal (BM)	$3.76x10^{-33}$	13.6

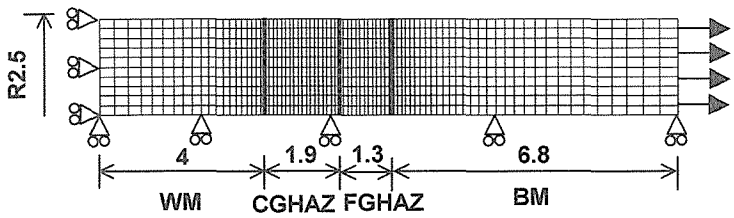

Fig. 1 Welded joint model (mm)

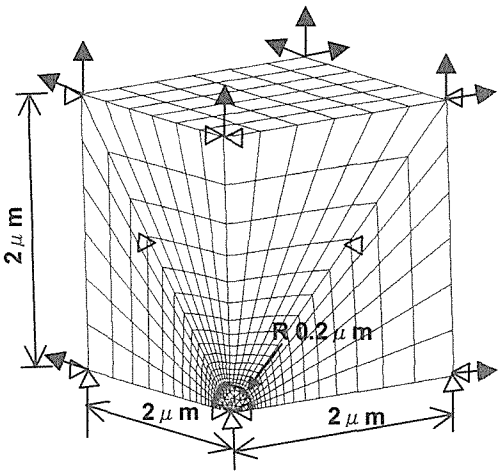

Fig. 2 3-D precipitate and matrix model

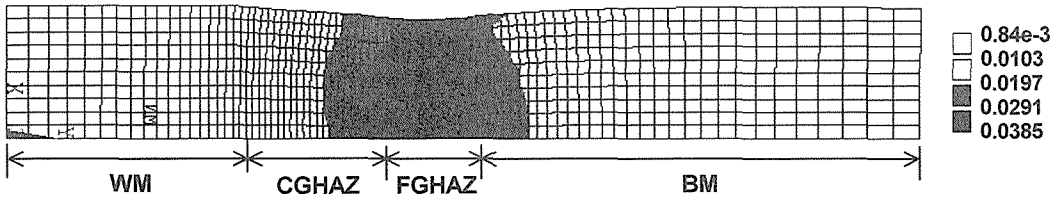

Fig. 3 Equivalent strain contour of welded joint after 600h (100MPa)

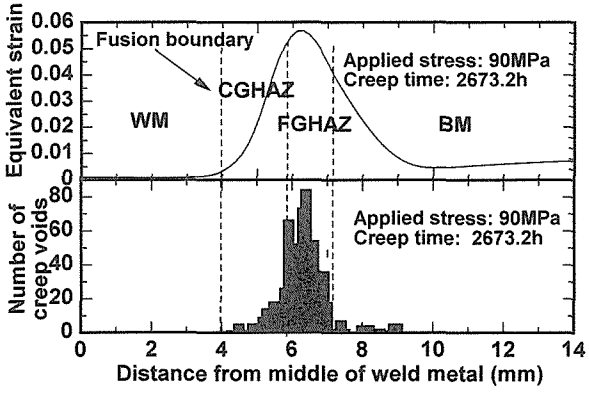

Fig. 4 Comparison between equivalent strain and creep void distribution along specimen length

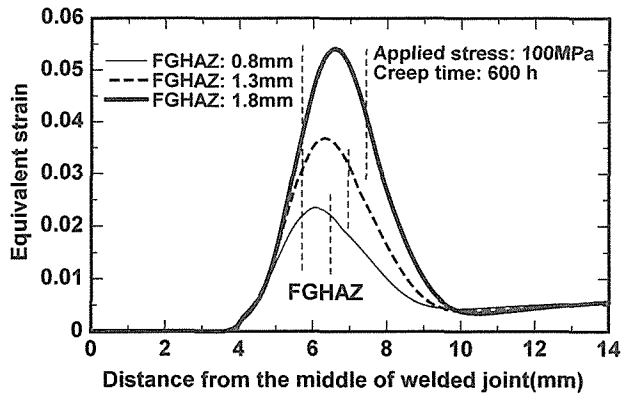

Fig. 5 Equivalent strain distributions along specimen length under different FGHAZ widths

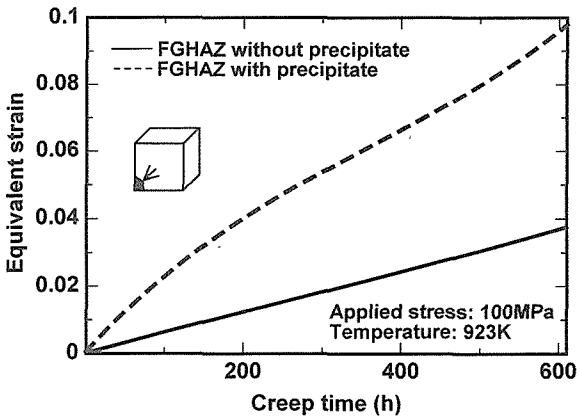

Fig. 6 Equivalent strains vs. creep time at largest equivalent strain mesh of FGHAZ under conditions of precipitate existing and not

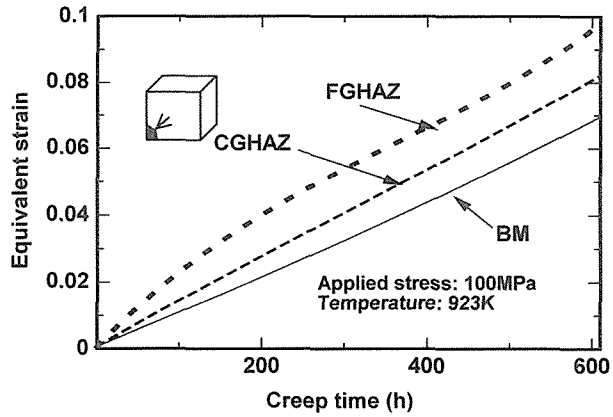

Fig. 7 Equivalent strains vs. creep time when precipitate is located at largest equivalent strain mesh of FGHAZ, CGHAZ and BM

Comparative Evaluation of Creep Behaviour of Plain and Modified 9Cr-1Mo Weld Joints

K.Laha, K.S.Chandravathi, K.Bhanu Sankara Rao and S.L.Mannan
Materials Development Group, Indira Gandhi Centre for Atomic Research,
Kalpakkam – 603 102, India

1. Introduction

9Cr-1Mo steels are being widely used in the construction of power generation and petrochemical plants. Joining by fusion welding is commonly employed in such large-scale plants. Weld joints of these steels are prone to premature creep failure [1]. In this work, creep deformation and fracture behaviour of weld joints of plain (T9) and modified (T91) 9Cr-1Mo steels have been studied. Relative failure susceptibility of the weld joints compared to their respective base metals has been assessed. The results have been explained on the basis of different microstructures developed in the heat-affected zones (HAZ) of the weld joints.

2. Experimental Details

Similar weld joints of T9 and T91 steels were fabricated by fusion welding. The joints were post-weld heat-treated at 973 K (for T9) and 1033 K (for T91) for 1 hour. Microhardness measurement and optical and electron microcopy of the microstructures across the weld joints were carried out. Creep tests on both the base metals and weld joints were conducted at 823-923 K in the stress range of 50-250 MPa. The creep strain accumulation in the different microstructures across the weld joints was determined by interrupting the creep test and measuring the distances between the marker points made on the specimen prior to the commencement of creep test. SEM was used to investigate the creep cavity accumulation in the different microstructures of the joints. Different HAZ structures of both the steel weld joints were simulated and tensile properties were evaluated to identify the weak link in the HAZ.

3. Results and Discussion

HAZ of both weld joints is composed of coarse prior-austenitic grain martensite, fine prior-austenitic grain martensite and intercritical structure adjoining the unaffected base metal. A hardness trough was observed in the intercritical region of HAZ of both the weld joints. T91 showed higher creep rupture strength than the T9 steel. Weld joints of both the steels showed lower rupture life than their respective base metals; the reduction was more at higher test temperatures and lower applied stresses. At a given test temperature and applied stress, the reduction was more in T91 steel than in T9 steel. T91 weld joint exhibited higher creep strength than the T9 steel. The creep failure in both the steel weld joints occurred in the intercritical region of the HAZ by type IV mode. Creep failure location in the intercritical HAZ of both the

joints agreed well with the lower hardness in the intercritical region of HAZ of the joints as well as with the lower tensile strength of the steels subjected to intercritical heat treatment. The characteristic features of the type IV failure in T9 and T91 weld joints differed considerably. The creep strain accumulation (Fig.1) with no indication of creep cavitation in the intercritical region of HAZ led to the premature failure of the T9 joint. In T91 joint, both creep strain accumulation and creep cavitation occurred in the intercritical HAZ (Fig.2). Creep cavitation was predominant at higher test temperatures and lower applied stresses. Higher reduction in creep strength of T91 joint compared to its base metal than that in T9 joint was associated with the occurrence of creep cavitation damage in the intercritical HAZ. TEM investigations revealed that fine lath structure with high dislocation density of both steels, had been replaced by equiaxed subgrains with low dislocation density in the intercritical region [2]. Coarser carbides were observed in the steels subjected to intercritical heating compared to those in the base metals. These microstructural changes led to lower hardness in the intercritical HAZ of the joints contributing to lower creep strength.

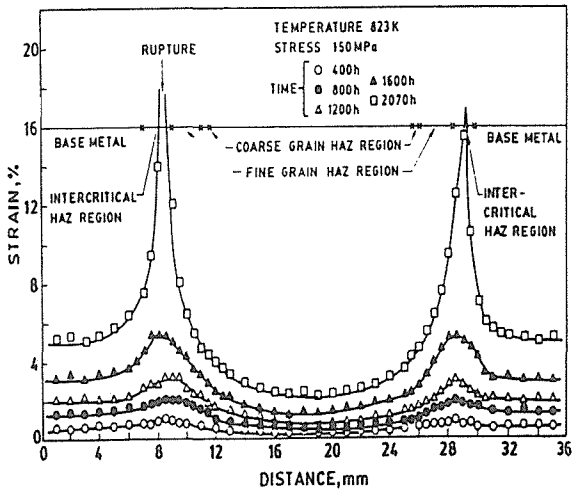

Fig.1 Strain distribution profile across T9 weld joint (823K, 150 MPa, t_r-2070 h).

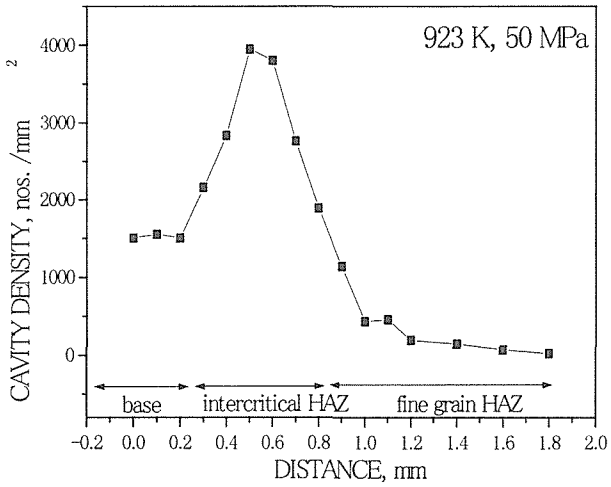

Fig.2 Creep cavity distribution across T91 weld joint (923K, 50 MPa, t_r-12723 h).

3. Conclusions

Both the T9 and T91 joints possessed lower creep strength than their respective base metals. Failure occurred in the intercritical region of HAZ. T91 steel weld joint was found more susceptible to strength reduction than the T9 weld joint.

4. References

[1] Eggeler,G., Ramteke, A., Coleman,M., Chew, B., Peter, G., Burblies, A., Hald, J., Jefferey, C., Rantala, J., deWhite, M. and Mohrmann, R., Int.J.Pres.Ves&Piping, 69(1994) 237-257.

[2] M. DeWitte, M. and Coussement, C., Mat., High Temp., 9 (1991), pp.178-184.

Evolution of Microstructure in Creep-Resistant Steels

H. K. D. H. Bhadeshia
University of Cambridge
Department of Materials Science and Metallurgy,
Pembroke Street, Cambridge CB2 3QZ, U.K.

1. Introduction

There are contradictory requirements in the design of creep-resistant alloys [1-3]. The alloys are designed to resist deformation by incorporating a large number density of barriers to dislocation motion. The resulting fine dispersions of particles gives the material a stored energy which in turn reduces the stability of the microstructure as the system tends towards a state of minimum free energy. This paper deals with local and long-range factors which contribute to the stored energy of creep-resistant steels, and the new methodologies which may in the future help in deducing the roles of alloying elements in controlling the stability of the overall microstructure.

2. Stored Energy

Energy can be stored in a material in a large variety of ways [4]. The table below compares the calculated stored energies of some elementary microstructures relative to an equilibrium mixture of ferrite, cementite and graphite. The phases in cases 1 and 2 involve the partitioning of all elements so as to minimise free energy. In cases 3-5, the iron and substitutional solutes are configurationally frozen (for martensite even the interstitial elements are frozen). Case 6 refers to an iron-base mechanically alloyed oxide-dispersion strengthened sample which to my knowledge, has the highest reported stored energy prior to recrystallisaton [5]. The magnitudes of the free energy changes as the sytem approaches equilibrium are seen to be very small, but creep-resistant steels have to last for very long time periods, so even these small changes are of importance. Thus, Abe a co-workers have adopted a novel approach in which they design steels where the initial grain structure and precipitate size is very coarse, and have shown that this can lead to creep rupture lives comparable to microstructures where the initial scale is very fine [6,7]

Table 1: Calculated stored energies of a variety of microstructures [4]

Phase Mixture in Fe–0.2C–1.5Mn wt.% at 300 K	Stored Energy / J mol^{-1}
1. Ferrite, graphite & cementite	0
2. Ferrite & cementite	70
3. Paraequilibrium ferrite & paraequilibrium cementite	385
4. Bainite and paraequilibrium cementite	785
5. Martensite	1214
6. Mechanically alloyed ODS metal	55

The rate at which a microstructure changes will naturally be greater when the stored energy is large, but account must also be taken of the barriers to achieving equilibrium Kinetics plays an important role and there has been considerable recent research on understanding the

interactions between complicated precipitation reactions. Thus, it has been demonstrated that the precipitation of $M_{23}C_6$ can be accelerated by many orders of magnitude, by a subtle change in the overall chemical composition [8,9]. Both the precipitation and dissolution of metastable precipitates is crucial in predicting these changes [8,9].

A major part of this paper will therefore deal with the following kinetic phenomena:

(i) Simultaneous precipitation reactions, their control and the evolution of undesirable phases. This will also cover multiphase coarsening phenomena.
(ii) The role of multicomponent diffusion in controlling precipitation and coarsening phenomena. It will be demonstrated that the binary diffusion equations do not reveal the essential trends in coarsening reactions.
(iii) There are major approximations used in many kinetic models, particularly in the treatment of multicomponent capillarity effects, which can be seminal in the discovery of which alloying elements are best at suppressing coarsening reactions.

References

[1] Bendersky, L., Rosen, A., Mukherjee, A. K., Creep and dislocation substructure, International Metals Reviews, 30 (1985) 1-15.
[2] Fujita, T., Heat resistant steels for advanced power plant, Advanced Materials and Processes, 4 (1992) 42-47.
[3] Cerjak, H., Hofer, P. and Schaffernak, B., Microstructural aspects and the service behaviour of advanced power plant steels, ISIJ International 39 (1999) 874-888
[4] Bhadeshia, H. K. D. H., Alternatives to the Ferrite-Pearlite Microstructures, Materials Science Form, 284-286 (1998) 39-50.
[5] Bhadeshia, H. K. D. H., Mechanically Alloyed Metals, Materials Science and Technology, 16 (2000) 1404--1411
[6] Igarashi, M., Muneki, S. and Abe, F., Creep properties of advanced heat-resistant martensitic steels strengthened using ordered intermetallic phase, Key Engineering Materials 171-175 (2000) 505-512
[7] Kimura, K., Kazuhiro, S., Toda, Y. and Abe, F., Development of high strength 15Cr ferritic creep resistant steel with addition of tungsten and cobalt, ISIJ International, 41 (2001) S121-S125.
[8] Bhadeshia, H. K. D. H., ISIJ International, Design of Ferritic Creep-Resistant Steels, 41 (2001) 626-640.
[9] Robson, J. D. and Bhadeshia, H. K. D. H., Modelling Precipitation Reactions in Power Plant Steels, Materials Science and Technology, 13 (1997) 631-644.

Precipitate stability in Creep Resistant Ferritic Steels - Experimental Investigations and Modelling

J. Hald, L. Korcakova
IPL-MPT, Technical University of Denmark, Lyngby Denmark

1. Introduction

Alloy development in the last 25 years of 9-12%Cr ferritic creep resistant steels for critical components in steam power plants like steam lines, turbine rotors and casings, has led to a doubling of the 10^5h creep rupture strength at 600°C. This has been achieved through apparently minor alloy compositional changes to well established steels like the 9Cr1Mo and 12CrMoV. Newly developed alloys like the modified 9Cr1Mo steel P91 and the tungsten alloyed 9Cr and 11Cr steels P92 and P122 have recently been used in full scale in new power plants, which operate at advanced steam conditions in Japan and Europe. The decision to introduce the new alloys in power plant was mainly based on results from long-term creep rupture tests lasting up to app. 60.000 hours. However, power plants are expected to operate for up to 200.000-300.000 hours, so considerations about the long term creep stability of the new alloys are necessary to support the decision to introduce them. Such considerations about long term creep stability must rely on studies of the microstructure stability.

Numerous investigations of the tempered martensite microstructure of the new 9-12%Cr steels indicate that the precipitate particles play a crucial role for the microstructure stability under creep conditions. It has been found that the apparently minor changes to chemical composition in the new steels introduce new precipitates in the microstructure, which contribute to particle strengthening. In order to make predictions about the long-term stability of the precipitates it is therefore necessary to develop new advanced characterisation techniques, which allow on-line discrimination between various precipitate types, and new models to predict precipitate growth and coarsening based on thermodynamic and kinetic principles.

2. Precipitate characterisation

The new 9-12%Cr steels contain several precipitate types, which form at different time and temperature either during the final normalising and tempering heat treatment of the steels or during creep exposure. Table 1 shows an overview of the most common precipitates in tungsten alloyed 9Cr steels like the P92.

Precipitate particles in the 9CrW steel P92			
Precipitate	**Elements**	**Mean size**	**Remark**
$M_{23}C_6$	Cr, W, Mo, Fe, C	≈100 nm	Precipitate during tempering
MX	Nb, V, C, N	≈100 nm	Undissolved during austenitization
MX	V, N	≈ 35 nm	Precipitate during tempering
Laves phase	$(Fe,Cr)_2(Mo,W)$	≈ 250-300 nm	Precipitate during creep (T<720°C)

Table 1.

In order to make statements about the influence of the precipitates on creep strength it is necessary to determine volume fraction and mean particle size of the individual precipitate types, and the development of these as a function of time and temperature. As seen from Table 1 the various precipitates have distinct chemical compositions, which means that it is possible to discriminate between them by means of newly developed electron microscopy methods like Energy Filtered Transmission Electron Microscopy (EFTEM). This technique is

based on high resolution mapping of information from electron energy loss spectra (EELS), and it allows accurate measurements of particle sizes down to a few nm [1]. However, there is a lower limit to the useable magnification in EFTEM microscopes, which means that statistically sound determination of mean particle sizes larger than app. 200 nm become unpractical with the EFTEM method. For the larger particles it is now possible to make particle size measurements in Scanning Electron Microscopes (SEM), as the resolution power has been improved in recent years by the introduction of new high intensity electron sources. For the Tungsten containing Laves phase particles in 9CrW steels discrimination from other particles can be obtained in the SEM based on the atomic number contrast in backscattered electron images [2].

Particle size measurements on steel P92 in the as-received condition as well as after exposure up to 60.000 hours at 600°C show that VN particles are very stable and coarsen from app. 35 nm to app. 40 nm diameter. $M_{23}C_6$ carbides coarsen slowly from app. 80 nm to app.100 nm diameter. Laves phase particles precpitate and grow during the first app. 10.000 hours to a size of app. 200 nm diameter, and then they coarsen to app. 250 nm diameter after 60.000 hours of exposure.

3. Modelling of precipitate stability

Modelling of precipitate stability focus on growth and coarsening processes. Recent developments of databases and software to predict thermodynamic equilibria in multicomponent systems (e.g. Thermocalc), and development of multicomponent diffusion databases and associated software like the DICTRA has allowed significant progress in the modelling of precipitate stability. Based on the assumption of local equilibrium at the precipitate/matrix interface the problem of particle growth can be treated as a moving boundary problem [3]. The problem of particle coarsening can be treated similarly by incorporating a contribuition from the interfacial energy to the Gibbs energy of the particle. This leaves the interfacial energy as the only fit parameter in the coarsening model [4].

The paper will give examples of calculations of growth and coarsening compared with experimental measurements of particle sizes as well as considerations on the influence of chemical composition on particle stability.

4. Referances

[1] Hättestrand, M. and Andrén, H-O, Evaluation of particle size distributions of precipitates in a 9% chromium steel using energy filtered transmission electron microscopy. Micron 32 (2001) 789-797

[2] Korcakova, L. Hald, J. and Somers, M. A. J, Quantification of Laves phase particle size in 9CrW steel. Materials Characterization 47 (2001) 111-117

[3] Bjärbo, A. and Hättestrand, M, Complex Carbide Growth, Dissolution and Coarsening in a Modified 12 Pct Chromium Steel – an Experimental and Theoretical Study. Metallurgical and Materials Transactions A, 32A (2001) 19-28

[4] Gustafson, Å and Hättestrand, M, Coarsening of precipitates in an advanced creep resistant 9% chromium steel – quantitative microscopy and simulations. Submitted to Metallurgical and Materials Transactions A.

TTT DIAGRAM FOR THE PRECIPITATION OF LAVES PHASE IN Fe-Cr-W-C QUATERNARY STEEL CONSTRUCTED BY SYSTEM FREE ENERGY THEORY

Y. Murata[(1)], T. Koyama[(2)], M. Morinaga[(1)], T. Miyazaki[(3)] and M. Doi[(2)]

(1) Department of Materials Science and Engineering, Graduate School of Engineering, Nagoya University, Japan, E-mail : murata@numse.nagoya-u.ac.jp
(2) Nagoya Institute of Technology, Japan.
(3) Emeritus Professor of Nagoya Institute of Technology, Japan.

INTRODUCTION

In advanced heat resistant ferritic steels, the Laves phase is believed to precipitate in a granular shape and to exist in the boundaries of martensite lath, block, packet and some prior austenite grains. However, a number of fine Laves-phase precipitates are found to exist even inside the martensite lath in the tempered steels containing 10mass%Cr and 4.6mass%W [1]. There is a room to debate on the contribution of the Laves phase to creep strength, but the fine Laves phase must contribute to the creep strength. Then it is important to make it clear the morphological change of the Laves phase for understanding the creep strength of those steels.

The objective is to elucidate the microstructural evolution of the Laves phase in advanced high Cr heat resistant ferritic steels following the system free energy theory.

SYSTEM FREE ENERGY THEORY

The total free energy of the microstructure is estimated by the sum of a chemical free energy, G_0, an elastic strain energy, E_{str}, and an interfacial energy, E_{surf}, and then a possibility of predicting the microstructure development is treatable on the basis of the total free energy [2]. The total free energy is called as system free energy, G_{system} $(=G_0+E_{str}+E_{surf})$.

In this study, the Fe-Cr-W-C quaternary system is employed for simulating the advanced heat resisting steels, and special attention is directed towards the morphological evolution of the Laves phase. The existence of $M_{23}C_6$ carbide is also being considered in this simulation. Each energy in the system free energy is estimated by the following equations;

$$G_0 = (1-f)G_c^{\alpha} + fG_c^{Laves},$$

$$E_{str} = (AE/(1-\nu))\varepsilon_0^2 V_m f(1-f),$$

$$E_{surf} = \gamma_S V_m S_p / V_p .$$

Here, G_c^{α} and G_c^{Laves} are calculated by using the Thermo-Calc data, and f is the volume fraction of the Laves phase. E and ν are the Young's modulus and the Poisson ratio, respectively, and the values of pure iron are used in this study. A is a constant, and ε_0 is the elastic strain. γ_S is the interfacial energy density [3] between the ferrite phase (α) and the Laves phase, and it is 0.150J/m^2 for the coherent state and 0.468J/m^2 for the incoherent state. V_m and V_p are the molar volumes for the ferrite phase and the Laves phase, respectively. Also, S_p is the surface area of the Laves phase.

If the temperature, steel composition and microstructural morphology such as the shape and size of the precipitate are fixed, then the system free energy G_{system} can be calculated. The calculated system free energies are compared among various sizes of the Laves phase in both coherent and incoherent states, and a stable microstructure with the lowest G_{system} is obtained at a given temperature and a given composition.

RESULTS AND DISCUSSION

Figure 1 shows the calculated results exhibiting the stable morphology of the Laves phase which changes with the W content, the size and the temperature in Fe-10Cr-W-0.11C

(mass%) alloy (notice: W coordinate shown in Fig.1 is represented in mol%). Three bottom figures show stable regions for the coherent and the granular Laves phases at 900, 1000 and 1100K. The size scale corresponds to the time scale due to the equation, $r^m = kt$, where k is a constant. On the basis of similar figures calculated at various temperatures, a quasi-binary phase diagram for the Laves phase is obtained as shown in the upper figures of Fig.1. It is found that the critical W concentration at which the Laves phase changes the shape from fine to granular one increases with increasing temperature. The fine coherent Laves phase exists in the region of the higher W contents and the lower temperatures in this quasi-binary phase diagram.

In the upper figures, experimental data are also plotted using square and triangle marks, which are obtained at 923K in Fe-10Cr-0.1C-W-Co-V-Mo (mass%) ferritic steels [4]. The square marks show the solid-solubility for the Laves phase. On the other hand, the open triangle and solid triangles show the positions, where the granular Laves phase and the fine coherent Laves phase are observed, respectively. By comparing these experimental data with the calculated phase boundaries, it is found that the prediction from the system free energy agrees well with the experimental results.

CONCLUSION

It is found that the critical W concentration for the transition from coherent-to-incoherent Laves phase in the Fe-Cr-W-C system is predicted based on the system free energy.

ACKNOWLEDGEMENT

This work is supported in part by the Grant-in-Aid for Scientific Research of Japan Society for the Promotion of Science (JSPS), Japan.

REFERENCES

[1] Y.Murata, K.Takami, M.Kamiya, M.Morinaga, R.Hashizume. K.Miki, T.Azuma and T.Ishiguro: Tetsu-to-Hagane, 88(2002) pp.214-221.
[2] T.Miyazaki and T.Koyama: Materials Sci. and Eng., A136 (1991) pp.151-159.
[3] L.E.Murr: *Interfacial Phenomena in Metals and Alloys*, Addison-Wesley, Reading, MA, 1975, p.82.
[4] Y.Murata, M.Kamiya, M.Morinaga, R.Hashizume. K.Miki, T.Azuma and T.Ishiguro: to be published.

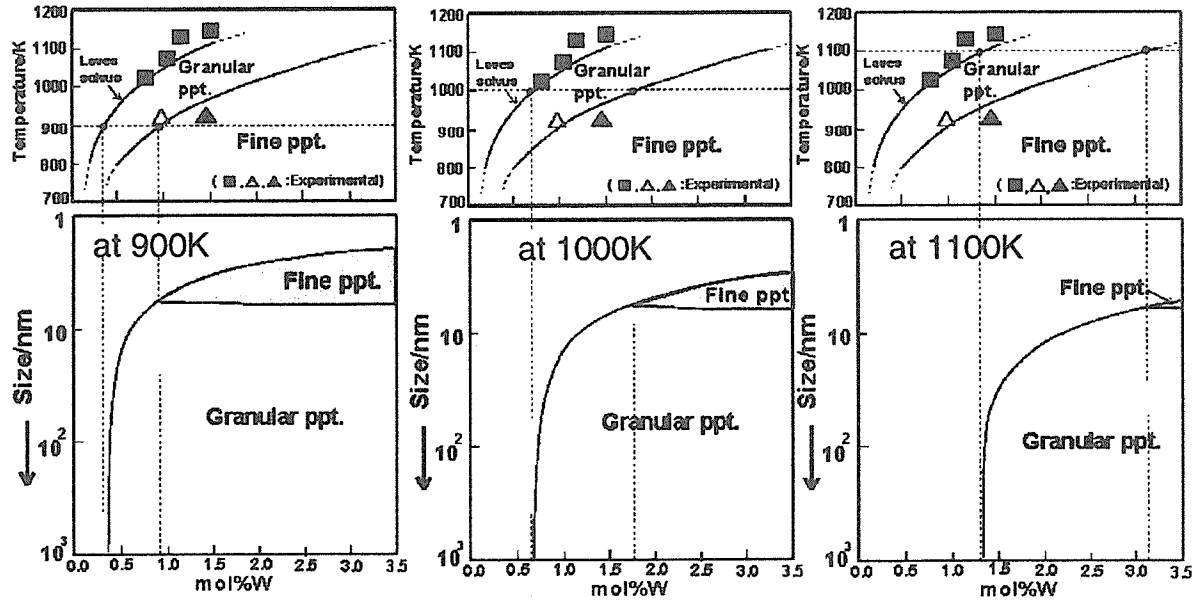

Fig.1 Stable morphology of the Laves phase depending on the W content, precipitate size and temperature in the Fe-Cr-W-C system.

In-situ observation of dislocation motion and its mobility in Fe-Mo and Fe-W solid solutions at high temperature

D. Terada, F. Yoshida[†], H. Nakashima[†], H. Abe[†] and Y. Kadoya[‡]
Graduate student, Kyushu University, Japan
[†]Interdisciplinary Graduate School of Engineering Sciences, Kyushu University, Japan
[‡]Mitsubishi Heavy industries, ltd., Japan

1. Introduction

Recently in development for high-strength heat resistant steels, it has become clear that the creep strength increases by replacing a part of Mo with W. W and Mo atoms are recognized to have effect on solid solution hardening. It is know that the size misfit parameter of W (9.97% [1]) is larger than that of Mo (8.43% [1]). However, solid solution hardening cannot be evaluated by only the size misfit parameter. To estimate solid solution hardening exactly, it is necessary to evaluate mobility of edge dislocation. Therefore, in order to estimate amount of solid solution hardening caused by W and Mo, dislocations motion was observed *in-situ* by TEM, and the mobilities of edge dislocations were evaluated in Fe-W and Fe-Mo solid solution alloys. Furthermore, their mobilities were estimated by a simulation using the interaction energy between an edge dislocation and solute atoms in imaginary lattice[2]. The results from TEM observation were compared with the results from simulation.

2. Experimental

The specimens used in this study are ferritic steels with 0.7at%W and 0.7at%Mo respectively. The *in-situ* TEM observation was carried out with a JEM-1000 and a heating holder with a two-axes tilt goniometer at HVEM laboratory of Kyushu University. The foil specimens were heated up to maximum 1023K. The thermal stress which is caused by the difference between the holder and the specimen moves the dislocations. The behaviors of dislocations were continuously recorded with VTR.

3. Results and discussions

Figure 1 and figure 2 show the *in-situ* TEM micrographs of successive movements of dislocation of Fe-W alloy at 993K and Fe-Mo alloy at 1011K, recorded by VTR. The dislocations indicated by arrows moved to right and to left, respectively. Figure 3 and figure 4 show the relationships between distance of dislocation movement and time in Fig. 1 and Fig. 2. It is found that moving distance is proportional to time in Fig.3 and Fig.4. From these results, it is found that dislocation velocities are constant. It is consider that movements of dislocations are viscous and dislocations drag the atmosphere of W and Mo respectively.

The dislocation velocities were calculated by slopes of Fig.3 and Fig.4, while the driving force of the dislocation is regarded as the stress acting on the dislocation, and the stress τ was given by $\tau = Gb/2r$ (where G is shear modulus, b Burgers vector and r curvature radius of the dislocation). The dislocation velocities v and driving forces τ were 2.2×10^{-8}ms^{-1} and 3.8MPa in Fe-W alloy and 2.3×10^{-8}ms^{-1} and 5.3MPa in Fe-Mo alloy, respectively. From these results, it is possible to estimate the dislocations mobilities B by $B = v/\tau$. The dislocation mobilities B were 5.7×10^{-15}mPa^{-1}s^{-1} in Fe-W alloy and 4.3×10^{-15}mPa^{-1}s^{-1} in Fe-Mo alloy. The mobility in Fe-W alloy is similar to that in Fe-Mo alloy. It means that the amount of solid solution hardening of W is similar to that of Mo.

Figure 5 shows the relationship between dislocation mobilities and reciprocal temperature from simulation. The values measured from TEM observation are also ploted in the figure. It is found that the dislocation mobility in Fe-W alloy is lower than that in Fe-Mo alloy in simulation. This result does not agree with the results from TEM observation. The value measured in Fe-Mo alloy is almost same as the simulated value while the value measured in

Fe-W alloy is different from the simulated value. The simulated values strongly depend on diffusion coefficient. Therefore, it is expected that inexactness of diffusion coefficient in Fe-W caused the difference between the measured value and the simulated value.

The results that the amount of solid solution hardening of W is similar to that of Mo suggest that the increase of creep strength by addition of W cannot be explained by solid solution hardening. Thus, increase in creep strength is not caused by solid solution hardening, but is caused by other hardening mechanism such as delay of recovery by solid solution atoms or precipitation strengthen.

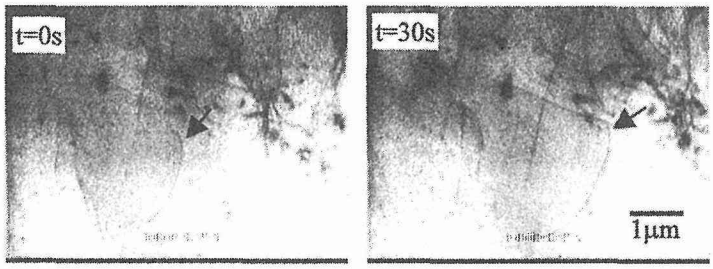

Fig.1 TEM micrograph of Fe-W at 993K

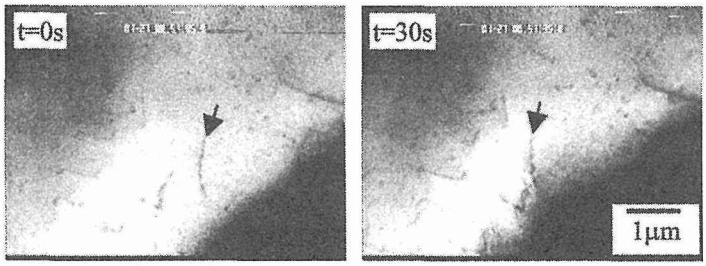

Fig.2 TEM micrograph of Fe-Mo at 1011K

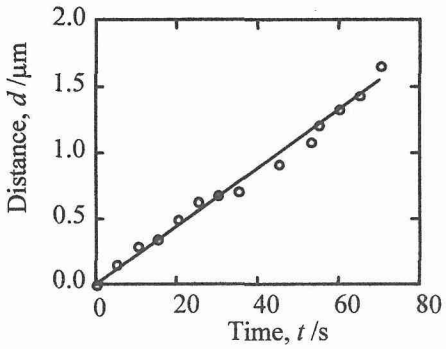

Fig.3 Relationship between distance of dislocation movement and time in Fe-W at 993K

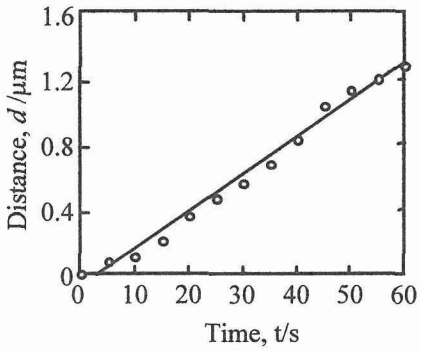

Fig.4 Relationship between distance of dislocation movement and time in Fe-Mo at 1011K

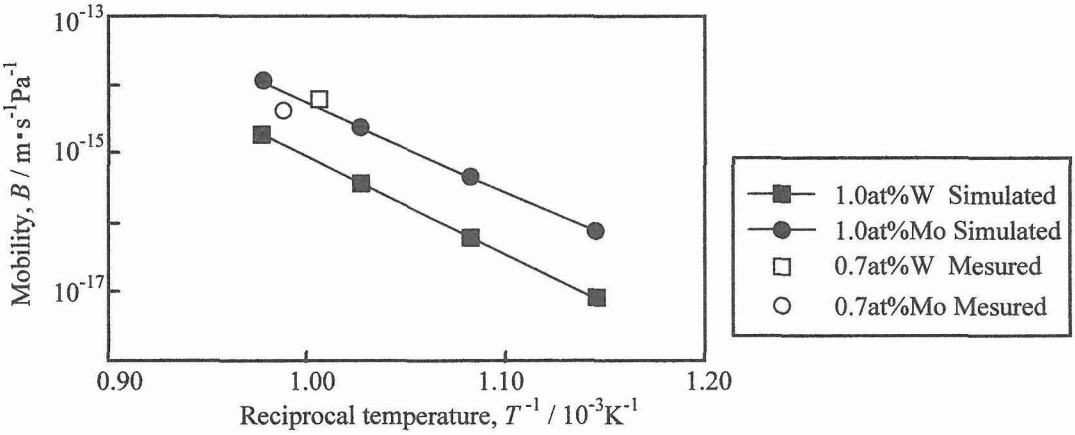

Fig.5 Relationship between dislocation mobilities and reciprocal temperature

References

[1] T. Motoyoshi, H. Sato and H. Oikawa, J. Japan Inst. Metals, **57**(1993), 890

[2] H. Yoshinaga and S. Morozumi, Phi. Mag. , **23**(1971), 1367

Interaction between Dislocation and Copper Particles in Fe-Cu Alloys

K. Nakashima, Y. Futamura, T. Tsuchiyama and S. Takaki
Dept. of Materials Science and Engineering, Kyushu University, Japan

1. Introduction

Upon aging treatment of copper (Cu) bearing steels, Cu precipitates within ferrite matrix finely as a simple substance and this leads to a marked precipitation strengthening[1]. Therefore, the Cu bearing steels are expected to be used for high strength structural materials such as steel sheets for vehicle[2] or heat resistant martensitic steels[3]. However, the mechanism of precipitation strengthening by Cu could not be explained by the conventional Orowan mechanism, because the Cu particle is softer than the iron matrix and its interaction with dislocation would be essentially different from that with hard particles. For the application of the high strength Cu bearing steels to practical uses, it is important to clarify the strengthening mechanisms and control its microstructure so as to obtain the required property. In this study, the precipitation strengthening behaviors at room temperature and elevated temperature (873K) were investigated in terms of the interactions between Cu particle and dislocation in the aged Fe-Cu binary alloys.

2. Experimental Procedure

Fe-(1～3)%Cu alloys were used in this study. Specimens were subjected to solution treatment at 1273K or 1473K for 1.8ks, followed by water quenching, and then aged at 773K or 873K for various times. Microstructures were observed with transmission electron microscope (TEM). Tensile tests were carried out with an Instron-type testing machine at room temperature or 873K with a initial strain rate of $1.67\times10^{-3}(s^{-1})$.

3. Results and Discussions

When a moving dislocation is pinned by dispersed particles in steels, the stress ($\Delta\sigma$) required for bowing the dislocation with angle θ is expressed by the following equation as a function of mean particle spacing (λ) and the bowing angle (θ).

$$\Delta\sigma = (2.8Gb/\lambda)\sin\theta \quad \cdots (1)$$

where G is the shear modulus of matrix and b is the magnitude of the Burgers vector. The coefficient of 2.8 was determined from the relation between λ and $\Delta\sigma$ in a carbon steel with carbide particles using $\theta=\pi/2$ for the equation (1).

Fig. 1 shows relations between mean Cu particle spacing (λ) and increment of yield stress by

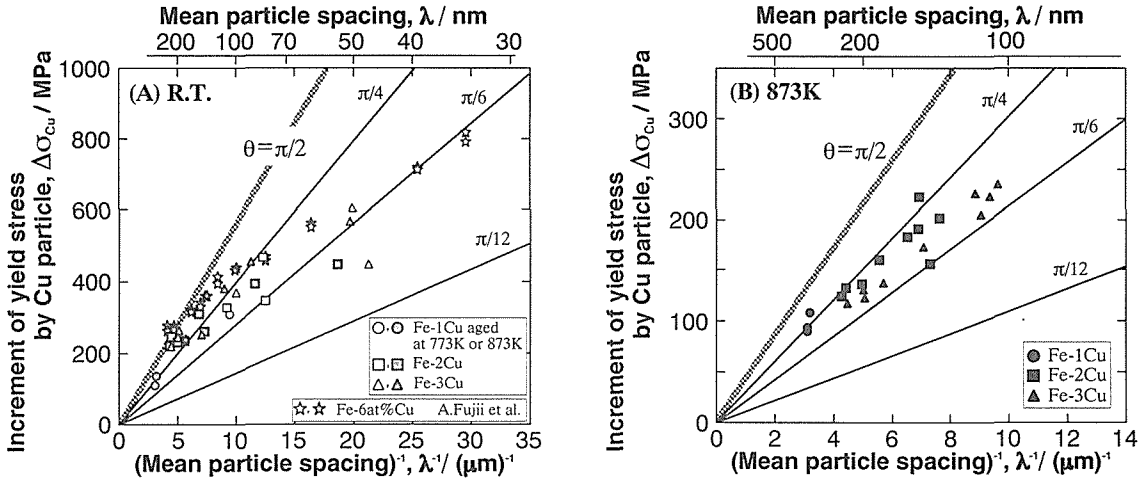

Fig. 1 Relations between mean particle spacing and increment of yield stress by Cu particles at R.T. (A) and 873K (B) in Fe-Cu binary alloys. Specimens were aged at 773K or 873K after the solution treatment. Straight lines are theoretical precipitation strengthening given by the equation(1) on various θ.

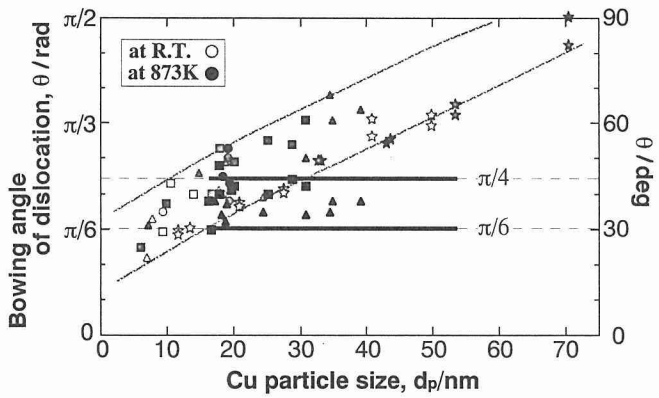

Fig. 2 Relation between bowing angle of dislocation and Cu particle size at R.T. and 873K. The angles were estimated from the results in Fig. 1 with equation (1).

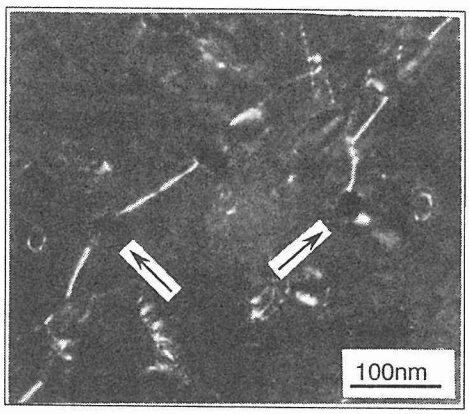

Fig. 3 Weak-beam TEM micrograph of Fe-3%Cu alloy tensile-deformed by 1.9% at 873K.

Cu particles ($\Delta\sigma_{Cu}$) at room temperature (A) and 873K (B) in the Fe-Cu binary alloys. The straight lines denote theoretical precipitation strengthening given by the equation (1) using various θ. The $\Delta\sigma_{Cu}$ at both temperatures tend to increase with decreasing λ, but the values of $\Delta\sigma_{Cu}$ are smaller than the Orowan stress (θ=π/2). **Fig. 2** shows the effect of Cu particle size on the bowing angle of dislocation (θ). Each θ was estimated from the results of Fig. 1 with the equation (1). At room temperature, the θ constantly increases with enlarging the particle size and reaches π/2 when the Cu particle size becomes 70nm. This means that the moving dislocations can cut small Cu particles and pass through them, however, the stress required for the cutting increased with coarsing of Cu particles. The 70nm is minimum Cu particle size for obtaining Orowan stress. Therefore, $\Delta\sigma_{Cu}$ is dependent on not only λ but also the Cu particle size on condition that Cu particle size is less than 70nm. On the other hand, at 873K, the θ is a constant of π/5 regardless of the Cu particle size. Weak-beam TEM image of Fe-3%Cu alloy tensile-deformed by 1.9% at 873K revealed that the strain around dislocation has been almost relaxed at the particle/matrix interface as represented in **Fig. 3**. These are similar phenomena as confirmed in the precipitation strengthening with Srolovitz mechanism[4][5]. That is to say, dislocations attractively interact with the Cu particles and $\Delta\sigma_{Cu}$ is determined only by λ at the elevated temperature.

4. Conclusions

①Increment of yield stress of Fe-Cu alloys by precipitation strengthening is dependent on not only mean particle spacing but also the Cu particle size at room temperature on condition that Cu particle size is less than 70nm.

②The precipitation strengthening with large Cu particles (>70nm) can be estimated with the Orowan stress.

③At elevated temperature of 873K, dislocations attractively interact with Cu particles and the increment of yield stress is dependent on only by the mean particle spacing of the Cu particles.

References

[1]A.Fujii et al. Trans.Jpn.Inst.Met. **9**(1968), pp. S374-S380.
[2]R.Onodera et al. Iron & Steels **79**(1993), No.6, pp.671-677.
[3]Y.Futamura et al. ISIJ Int. **41**(2001), pp. S106-S110.
[4]R.O.Scattergood et al. Acta metall. **30**(1982), pp.1665-1677.
[5]H.Nakashima et al. Iron & Steels **77**(1991), pp.1399-1406.

Characterization of MX Distributions in P92 Steel by EF-TEM

K. Sawada, T. Hara, K. Kubo and F. Abe
Strength and Life Evaluation Research Group, NIMS, Japan

1. INTRODUCTION

Recent high chromium ferritic steels have a tempered martensitic lath structure and are strengthened by $M_{23}C_6$ carbides, MX carbonitrides((V(N,C), Nb(N,C)), Laves phase and dissolved atoms in the matrix. The strengthening mechanism of MX carbonitrides is not clear due to the uncertainty of precipitation sites, although the MX carbonitrides markedly improves creep rupture strength. In order to clarify the distribution of the MX carbonitrides and its effect on change in dislocation structure during creep deformation, conventional TEM and energy filtered TEM(EF-TEM) method[1] were used for thin foil observations.

2. EXPERIMENTAL PROCEDURE

The steel studied is P92(9Cr-0.5Mo-1.8W-VNb) steel. Normalizing and tempering condition is 1070℃ · 2h (A.C.) and 780℃ · 2h (A.C.), respectively. Uniaxial creep tests were performed under constant loads at 550℃ to 750℃ in air. The sites of the MX carbonitrides in thin foil are characterized by TEM (200kV, JEOL2010F with energy filter) observations for as tempered and ruptured specimens. Specimens for TEM observations were prepared by the electro-polishing method.

3. RESULTS

A bright field image and energy filtered images of chromium and vanadium in the as tempered specimen are shown in Fig. 1. The dislocation density is not so high because a relatively thin area was selected for EF-TEM observations, although a tempered martensitic lath structure is seen. The chromium map and vanadium map show the distributions of Cr-rich ($M_{23}C_6$ carbides) and V-rich (MX carbonitrides) particles, respectively. Comparison of the three micrographs indicates the $M_{23}C_6$ carbides and MX carbonitrides are distributed mainly on lath boundaries. However, the fine MX carbonitirdes are assumed to interact with free dislocations inside lath grain during creep. The MX carbonitrides observed in this study are relatively larger than reported value(20-30nm), indicating the fine MX carbonitrides were not detected inside lath grains in this study.

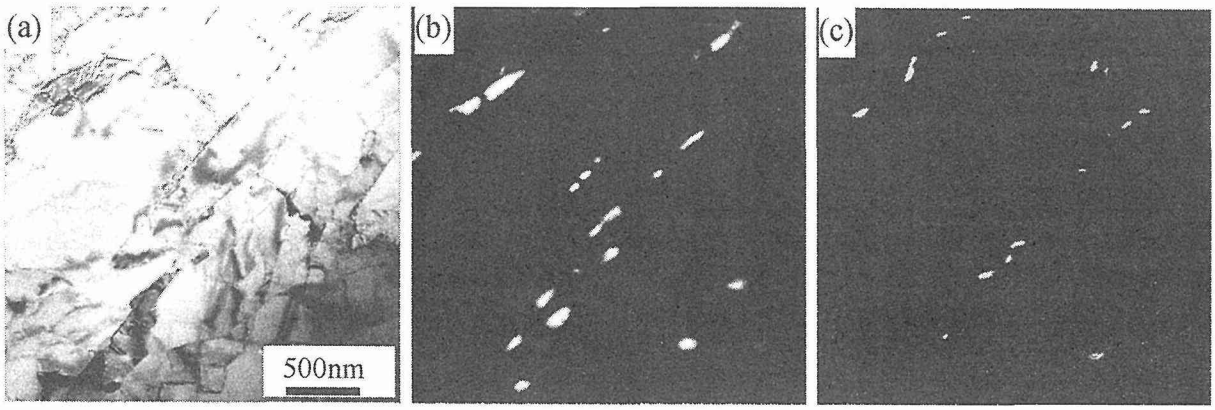

Figure 1 Bright field image (a) and elemental mappings of Cr (b) and V (c) in as tempered specimen.

Figure 2 shows the MX carbonitrides distribution in another area. A block boundary is located on center of the micrograph. $M_{23}C_6$(Cr-rich) and MX(V-rich) particles are also distributed on the block boundary.

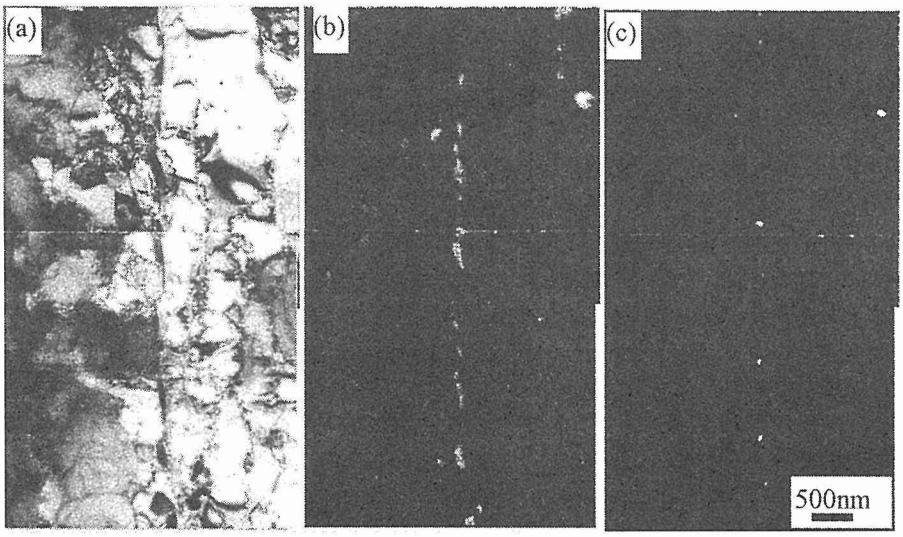

Figure 2 Distributions of $M_{23}C_6$ carbides and MX carbonitrides on block boundary.
(a) bright field image, (b) Cr map, (c) V map

Consequently, it is expected that the MX carbonitrides stabilize lath and block boundaries during creep. The interaction between a lath boundary and the MX carbonitrides during creep is demonstrated in Fig. 3. The particles with arrows were identified as the MX carbonitrides by EDS analysis. Lath grains grow during creep by lath boundary migration and the growth of lath grains leads to decrease in creep strength. The MX carbonitrides pin lath boundary migration during creep shown in Fig. 3.

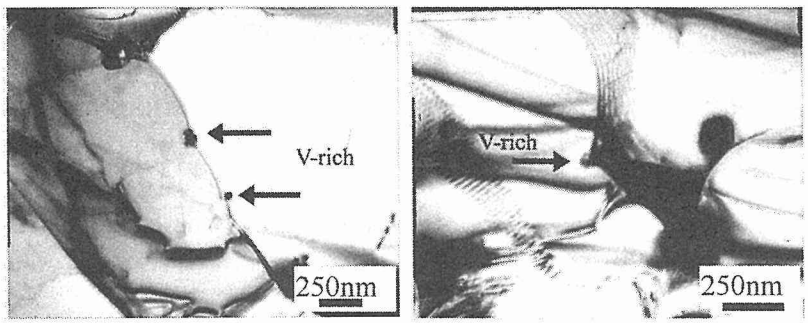

Figure 3 Interaction between the MX carbonitrides and lath boundary during creep.
750℃ · 20MPa t_r = 5713 h

4. CONCLUSIONS

The distributions of the MX carbonitrides were investigated in the as tempered specimen by using EF-TEM method. The MX carbonitrides are precipitated not only inside lath grain but also on lath and block boundaries. The MX carbonitrides pin lath boundaries during creep deformation, contributing to improvement of creep strength in the P92 steel.

REFERENCES

[1] Hofer P., Cerjak H., Schaffernak B. and Warbichler P., Steel Res., 69(1998), No.8, pp.343-347.

Structure Change in Creep Deformation of Ferritic Steel

Hideharu Nakashima
Department of Molecular and Material Sciences, Kyushu University, Japan

1. Introduction

Mod. 9Cr-1Mo steel has been used for the heat resisting steel as fossil power plants. As Mod. 9Cr-1Mo steel has used to parts in high temperature and high pressure, it was important to clarify the structure change during creep deformation. It is well-known that Mod. 9Cr-1Mo steel has any kinds of boundary, that is, Lath, Block and Packet boundaries due to matrensitic transformation. In this work, from the viewpoint of grain boundary it was clarified the structure change of Mod. 9Cr-1Mo steel during creep deformation. The structure change was observed by mainly SEM-OIM. And, analysing the crystal orientation in each grain, the grain boundary distribution was estimated.

2. Experimental Procedure

Mod. 9Cr-1Mo steel was annealed at 1045℃ for 10min, and and quenched in a water. After then, the steel was tempered at 780℃ for 1hr, and air-cooled. The creep test was conducted at a stress 72MPa and a temperature 940K in an air by using a conventional creep machine. In this condition, time to fracture was 1466hr. In order to reveal the structure change deformed at high temperature, TEM and SEM-OIM were conducted with interrupt creep specimens. Scanning step is 0.5 μm in SEM-OIM observation. In this work, boundary type was analysed from the orientation of scanning point by using computer program.

3. Results and Discussion

Figure 1(a) shows an OIM image of initial structure. Here, in Fig.1(a), colour is correspond to the orientation shown in Fig.1(b). Similar colour regions mean as close orientations. Then, these regions were correspond to Block in the martensitic structure. In Fig.1(a), there are black regions. In these regions, clear Kikuchi lines could not be obtained, then the orientation could not decided.

Figure 2 shows the relative frequency of the grain boundary with <110> common axis against the rotation angle. The boundary with <110> common axis is correspond to Block boundary in the martensitic structure. It was geometrically predicted that in Block boundary $\Sigma 3$(rotation angle 70.5°), near $\Sigma 11$(rotation

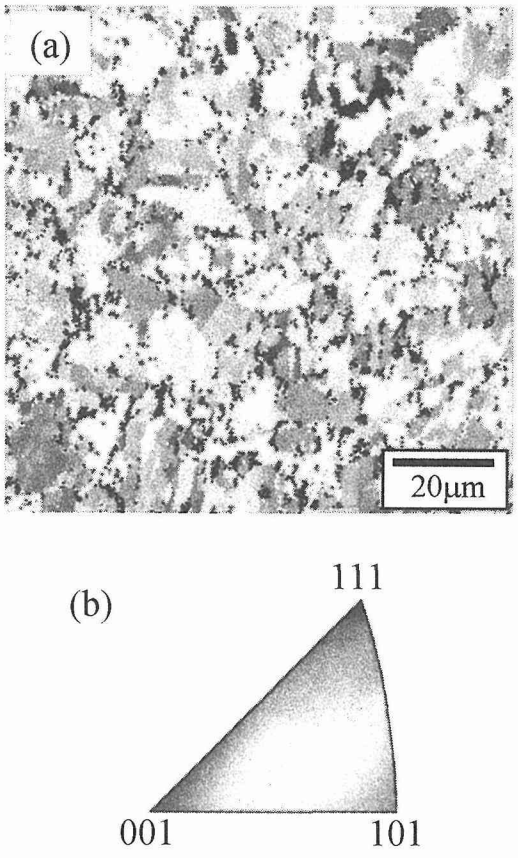

Fig.1 (a) OIM image of initial mod. 9Cr-1Mo steel
(b) Orientation map[1]

angle 50.5°) and small angle(rotation angle 10°) boundaries existed in the martensite. This result agrees with the result predicted with K-S orientation relationship. But, it was found that the density of $\Sigma 3$ boundary decreased, and that of near $\Sigma 11$ and small angle boundaries increased during the high temperature deformation. These facts show that the structure change comes from the migration of some special boundaries during the high temperature deformation. If the migration of $\Sigma 3$ or near $\Sigma 11$ boundary can be restricted, it is thought that the thermal stability of the martensitic structure may improves.

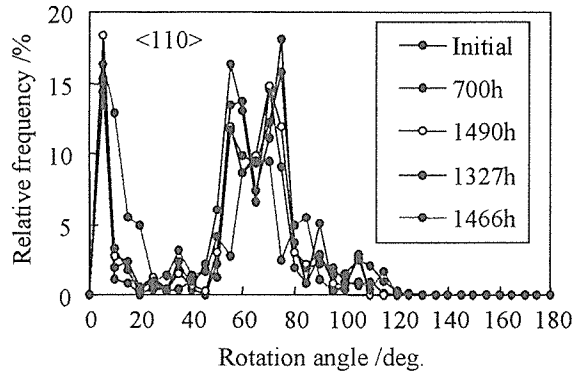

Fig. 2 Relationship between rotation angle and relative frequency of boundaries with <110> common axis[1]

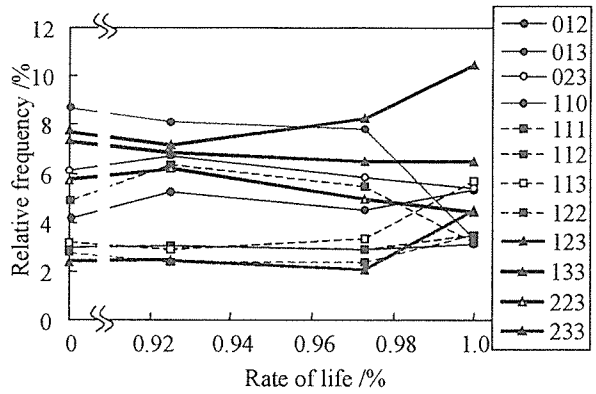

Fig. 3 Relationship between rate of life and relative frequency [1]

Figure 3 shows the relation between common axis and life fraction expended. In initial structure, relative frequency of <110> common axis(Block boundary) is largest to compare with other axes. But, just before the rupture, the frequency of <110> suddenly decreased and <123> and <233>(not Block or Packet boundaries) increased. New Block grain was never observed in sample fractured. Therefore, during creep deformation, dynamic recrystallization was not considered to occur. From this finding, it is considered that the Block boundary changed to random boundary during creep deformation.

4. Conclusion

In order to clarify the structure change during creep deformation in Mod. 9Cr-1Mo steel, the structures were observed by TEM and SEM-OIM. And, analysing the crystal orientation at each grain, following conclusion was obtained.

From the analysis of EBSP data, it was found that the density of $\Sigma 3$ boundary was decreased, and near $\Sigma 11$ and small angle boundary were increased during high temperature deformation. Therefore, it was considered that the structure change comes from the migration of some special boundaries.

References

[1]H. Nakashima, D. Terada, F. Yoshida, H. Hayakawa and H. Abe:ISIJ International, **41**(2001), S97-S199.

Inhomogeneous Change in Microstructure and Degradation in Long-term Creep Strength of Ferritic Steels

K. Kimura[1], H. Kushima[2] and F. Abe[2]

[1] Materials Creation Research Group, NIMS, Japan
[2] Strength and Life Evaluation Research Group, NIMS, Japan

1. Introduction

High strength 9-12Cr ferritic creep resistant steels have been investigated and developed for high temperature structural components of modern thermal power plant, in order to improve energy efficiency. To ensure a reliability of power plant and procure higher creep strength than the present materials, microstructural stability of high temperature materials at the elevated temperatures should be understood. In this paper, degradation mechanism in the long-term and a prediction method of long-term creep strength has been described on high Cr ferritic creep resistant steels.

2. Inhomogeneous progress in recovery

During creep exposure at the elevated temperatures, creep strength of 9-12Cr ferritic creep resistant steels decrease as a result of changes in tempered martensite microstructure, such as increases in lath width and/or subgrain size and decrease in dislocation density. Recovery of tempered martensite microstructure progress with increase in creep exposure time, as shown in Figure 1 (a)-(c), however, inhomogeneous microstructural change is observed in the specimen creep ruptured after 34,141.0h at 873K, Figure 1 (d) [1]. Significantly recovered region is recognized along the prior austenite grain boundary.

Such preferential recovery is supposed to be caused by larger diffusion coefficient of grain boundary than that of lattice diffusion, faster coalescence and coarsening of grain boundary precipitates and higher concentration at the grain boundary of local internal strain introduced by martensitic transformation. Moreover, precipitation of Z-phase may also contribute on the preferential recovery, since it tends to precipitates at the vicinity of prior austenite grain boundary and very rapid coarsening of it dissolve a lot of fine MX particles [2].

Preferential recovery at the vicinity of prior austenite grain boundary promotes the onset of accelerating creep stage and results in decreases in creep rupture life and creep rupture ductility. That is the origin of degradation in the long-term and an inflection of the relation between stress and time to rupture [1].

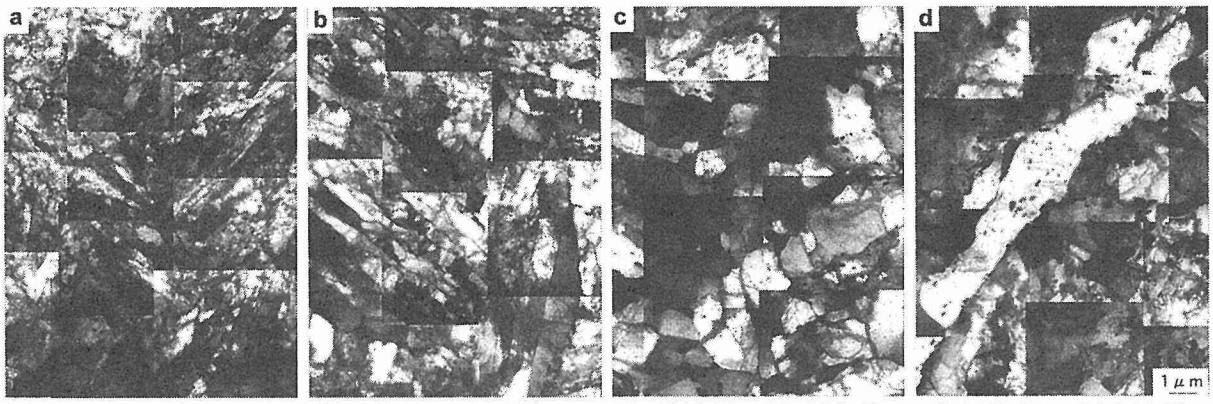

a) as tempered b) 160MPa, 971.2h c) 120MPa, 12,858.6h d) 100MPa, 34,141.0h

Figure 1 Bright field TEM images of the Mod.9Cr-1Mo steels (a) in the as tempered condition and (b)-(d) the specimens creep ruptured at 873K and 160, 120 and 100MPa.

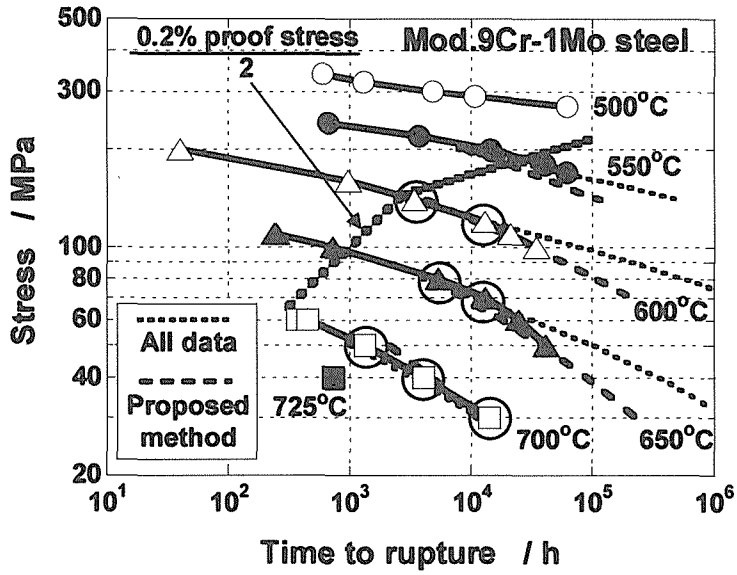

Figure 2 Creep rupture strength of a Mod.9Cr-1Mo steel and the predicted creep rupture lives by a conventional method and proposed new one based on range partitioning.

3. Long-term creep strength prediction

It is difficult to predict long-term creep strength of high Cr ferritic creep resistant steel accurately, because of inflection of relation between stress and creep rupture life. Good correspondence between stress condition where an inflection of the stress vs. time to rupture curve is observed and a half of the 0.2% proof stress at the temperature has been observed.

By considering a half of the 0.2% proof stress at the temperature as a boundary condition, much better result of long-term creep strength prediction has been obtained from the creep rupture data under the stresses lower than the above boundary condition, as shown in Figure 2 [3]. It has been supposed that the reason of such good correspondence between a half of the 0.2% proof stress and inflection of the curve is an occurrence of local plastic deformation as a result of micro scale yielding under a half of the 0.2% proof stress at the temperature.

4. Conclusions

Inhomogeneous microstructural change as a result of preferential recovery at the vicinity of prior austenite grain boundary is though to be an important degradation mechanism in the long-term of high Cr ferritic creep resistant steels. Preferential recovery at the vicinity of prior austenite grain boundary should be taken into account for assessment of long-term creep strength and development of high strength ferritic creep resistant steels. By considering the stress dependence of such inhomogeneous microstructural change, an accuracy of long-term creep strength prediction of high chromium creep resistant steels can be improved.

References

[1] Kimura, K., Kushima, H. and Abe, F., Heterogeneous Changes in Microstructure and Degradation Behaviour of 9Cr-1Mo-V-Nb Steel During Long Term Creep, Key Engineering Materials, 171-174(2000), No.8, pp.483-490.

[2] Kimura, K., Suzuki, K., Kumai, S., Kushima, H. and Abe, F., Precipitation of Z-phase and its effect on creep strength of Mod.9Cr-1Mo steel, Proc. Creep Resistant Metallic Materials, Prague, April, 2001, (2001), pp.186-195.

[3] Kimura, K., Kushima, H. and Abe, F., Degradation and Assessment of Long-term Creep Strength of High Cr Ferritic Creep Resistant Steels, Proc. Int. Conf. on Advances in Life Assessment and Optimization of Fossil Power Plant, Orland, March, 2002, (2002).

Creep Modelling of 9-12%Cr Martensitic Heat Resistant Steels Based on Quantitative Analysis of Microstructural Degradation

H. Semba*, B.F. Dyson** and M.McLean**
*Sumitomo Metal Industries, Ltd., Japan
**Imperial College of Science, Technology and Medicine, UK

A Physically-based Continuum Creep Damage Mechanics (CDM) approach to creep modelling [1][2] has been extended to a multi-state variable formulation for creep rates which can quantitatively incorporate the effects of microstructural degradation. In this paper, physically-based CDM is applied to modelling the shapes of creep curves and estimating lifetimes in 9-12%Cr martensitic heat resistant steels such as P91 (9Cr-1Mo-V-Nb), in which microstructures are thermodynamically unstable. In these steels, martensite lath structures recover during creep deformation and result in coarsened subgrain structures. Furthermore, fine carbides working as obstacles to dislocation movement coarsen and solid-solution elements are depleted as a result of Laves-phase precipitation. Each tape of damage — subgrain coarsening; carbide coarsening; and depletion of solid-solution elements — is coupled with the creep rate equation as a dimensionless variable whose evolution is described by a separate rate equation. The coupled differential equation sets constituting the creep rate equation and evolution equations for the variables can completely describe creep behaviour.

The physically-based CDM methodology employs the hyperbolic sine function to describe creep rates of particle hardened alloys [2][3].

$$\dot{\varepsilon} = \dot{\varepsilon}_0 \, sinh\left(\sigma(1-H)/\sigma_0\right) \tag{1}$$

where $\dot{\varepsilon}_0$ and σ_0 are microstructural parameters. $\dot{\varepsilon}_0$ is dependent on temperature and independent of stress. σ_0 is dependent on the Orowan stress for particle bypass. H is defined as $H=\sigma_i/\sigma$ where σ is an applied stress and σ_i is an internal back stress; then, $\sigma(1-H)$ $(=\sigma-\sigma_i)$ gives the stress acting in the matrix phase. The internal back stress arises during stress redistribution within 'hard' regions of microstructure, which are particles, subgrains etc [3]. H can vary from zero to H^*, which is a saturation value depending on microstructures. H^* is a function of a volume fraction for plastically 'hard' regions. The evolution rate of H is given by equation (6) [3]. Here, it is assumed that the matrix is physically homogeneous, but subgrain (lath) boundaries are plastically hard. Then, the effects of subgrain coarsening are incorporated into the model as a decrease in the volume fraction of subgrain (lath) boundaries, that is, H^* in equation (6) is not a constant but is a variable. The evolution rate of H^* is derived as equation (7) based on a relationship between creep strain and subgrain size that has been obtained experimentally [4]. D_d in equation (7) is a dimensionless variable defined in terms of the current (ρ) and the initial (ρ_i) dislocation densities in the matrix.

$$D_d = (\rho/\rho_i) - 1 \tag{2}$$

D_d takes a value of zero when no softening occurs ($\rho=\rho_i$), and approaches -1 with decreasing the dislocation density. The evolution rate of D_d is theoretically derived as equation (8); then, the coupled differential-equations (5)-(8) (k', C_i and ρ_s are constants) are the constitutive creep model incorporating the damage due to subgrain coarsening. Carbide coarsening is a thermally-induced damage; hence, it is more significant at higher temperatures. It is taken into the dimensionless damage parameter, D_p, through the particle spacing.

$$D_p = 1 - (P_i / P) \tag{3}$$

where P_i is the initial particle spacing and P is the current particle spacing. The evolution rate of D_p is derived based on Ostwald ripening theory. It is described as equation (9) if volume diffusion controls the coarsening behaviour. Solid-solution depletion caused by precipitation of Laves-phase is also a thermally-induced damage. The damage parameter D_s is defined in terms of the current (c_t) and the initial (c_0) concentrations of solutes in the matrix.

$$D_s = 1 - (c_t / c_0) \tag{4}$$

The damage evolution rate, equation (10), is given by Wert and Zener growth kinetics. Equation (11) is the evolution rate of stress under constant-load conditions. Fig.1 shows experimental data for P91 and the computed creep curve with this equation-set at 500°C, 284MPa. In this calculation the effect of carbide coarsening is not considered because it is likely to be negligible at 500°C. It can be seen that this model well describes the creep curve of P91 at the lower temperature. Fig.2 shows the computed creep curve and experimental data of P91 at 650°C, 78MPa. Laves-phase does not precipitate at this temperature; therefore the creep curve was calculated with $\dot{D}_s = 0$. These results indicate that the developed model using physically-based CDM well describes the creep curves of microstructurally unstable martensitic steels.

$$\dot{\varepsilon} = \dot{\varepsilon}_0 \frac{(1+D_d)}{(1-D_s)} \sinh\left(\frac{\sigma(1-H)}{\sigma_0(1-D_p)}\right) \tag{5}$$

$$\dot{H} = \frac{h'}{\sigma}\left(1 - \frac{H}{H^*}\right)\dot{\varepsilon} \tag{6}$$

$$\dot{H}^* = k'\left(1 - (1+D_d)^{1/2}\left(\frac{\rho_i}{\rho_s}\right)^{1/2}\right)H^*\,\dot{\varepsilon} \tag{7}$$

$$\dot{D}_d = C_i(1+D_d)^{1/2}\left(1 - (1+D_d)^{1/2}\left(\frac{\rho_i}{\rho_s}\right)^{1/2}\right)\dot{\varepsilon} \tag{8}$$

$$\dot{D}_p = \frac{K_p}{3}(1-D_p)^4 \tag{9}$$

$$\dot{D}_s = K_s D_s^{1/3}(1-D_s) \tag{10}$$

$$\dot{\sigma} = \sigma\dot{\varepsilon} \tag{11}$$

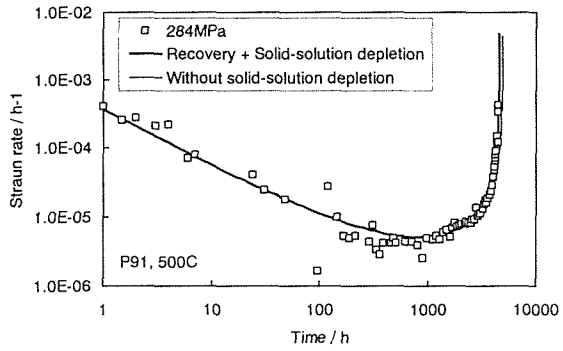

Fig.1: The computed creep curve and experimental data. (500°C, 284MPa)

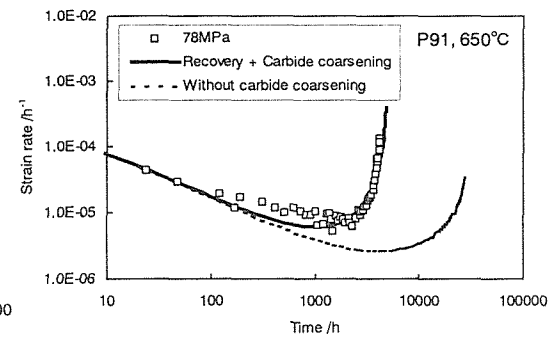

Fig.2: The computed creep curve and experimental data. (650°C, 78MPa)

References

[1] M.F. Ashby and B.F. Dyson: *Advances in Fracture Research*, edited by S.R. Valluri *et al*, Pergamon Press, 1(1984), pp.3.

[2]B.F. Dyson and M. McLean: Microstructural Stability of Creep Resistant Alloys, IOM(1998), pp.371.

[3] B.F. Dyson and S. Osgerby: NPL Report DMM A116(1993).

[4]P. Polcik, S. Straub, D. Henes and W. Blum: *Microstructural Stability of Creep Resistant Alloys for High Temperature Plant Applications*, edited by A. Strang, J. Cawley and G.W. Greenwood, IOM(1998), pp.405.

Creep deformation mechanism of advanced ferritic steels for USC power plant

M. Igarashi[1)], S. Muneki[2)], K. Yamada[2)], H. Okada[2)], F. Abe[2)] and Y. Shirai[3)]
[1)] Sumitomo Metal Industries, Ltd.
1-8 Fuso-cho, Amagasaki, Hyogo, 660-0891, JAPAN.
[2)] National Institute for Materials Science (NIMS)
1-2-1 Sengen, Tsukuba, Ibaraki, 305-0047,JAPAN.
[3)] Graduate School of Osaka University
1-1 Yamadaoka, Suita, Osaka, 565-0871, JAPAN.

PURPOSE

Ultra super critical (USC) power plant requires new steels with improved creep strength at elevated temperatures over 600°C. This paper describes a new technique to understand the creep deformation and strengthening mechanism of the advanced ferritic steels for the USC plant. We find the microstructural evolution of the steel during creep deformation can be characterized well by change in the positron annihilation lifetime of the steel in question.

EXPERIMENTAL

Model steels with different initial microstructures consisting of α, α'+$M_{23}C_6$ and γ were vacuum induction melted and processed to 15 mm thick plates. The chemical compositions of the steels used are given in Table 1. The α and α'+$M_{23}C_6$ steels were normalized for 4 h at 1100°C followed by air-cooling, and tempered for 4 h at 770°C (hereafter *NT*) for creep testing. The γ steel was solutionized for 4 h at 1100°C followed by air-cooling. Creep testing was performed at 650°C with stresses of 60, 70 and 150 MPa for the α, α'+$M_{23}C_6$ and γ steel, respectively. Positron annihilation lifetime was measured for the specimens crept and interrupted using a γ-γ coincidence measurement system. The Microstructures of the specimens were examined using a transmission electron microscopy (JEOL 2000EX) operated at 200kV.

RESULTS AND DISCUSSION

Fig.1 shows creep rate vs. time curves of the steels. The steel with the α phase matrix and no precipitation has exhibited a very low initial creep rate which has been decreased much during the transient creep region and has been increased in turn rapidly in the acceleration creep region, resulting in a shorter creep life. The steel with α '+$M_{23}C_6$, on the other hand, has shown higher creep rates during the transient creep region but the longer creep life, which has been achieved by homogeneous creep deformation.

Fig.2 shows positron annihilation mean lifetime measured for the specimens taken from the steels crept and interrupted at 650°C. It is seen that the positron lifetime of the α and γ steels increase during the creep deformation but it decreases in case of the α'+$M_{23}C_6$ steel.

It is found that the microstructural evolution of the steel during creep deformation can be characterized well by change in the positron annihilation lifetime of the steel in question. **Fig.3** shows the positron lifetime and the corresponding creep curve and TEM micrographs of the α'+$M_{23}C_6$ steel. In the transient creep region, dislocation density is clearly reduced inside individual lath grains. At the off-set to the acceleration creep, lath- and block-boundaries seem to start migration followed by the sub-grain formation in the acceleration creep region. The positron lifetime is rapidly decreased in the transient creep region but is slowly decreased in the acceleration creep region. The creep deformation mechanism based on the interraction between the dislocations and precipitates will be discussed in detail at the Conference.

Table 1 The Chemical compositions of the steels used (mass%, Bal.Fe)

	C	Si	Mn	Ni	Cr	Mo	V	Nb	B	N
M1(α)	0.002	0.3	0.5	–	9.0	1.0	0.2	0.05	0.005	0.002
M3(α'+M23C6)	0.100	0.3	0.5	–	9.0	1.0	–	–	0.005	0.050
M5(γ)	0.080	0.6	1.8	10.3	18.7	0.1	–	–	–	0.040

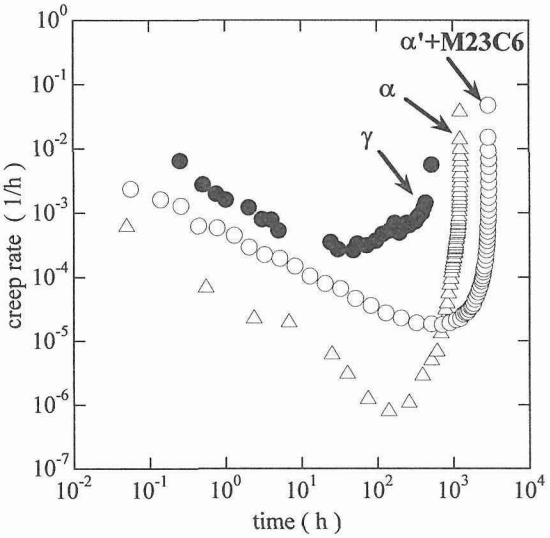

Fig. 1 Creep rate vs. time curves of the steels.

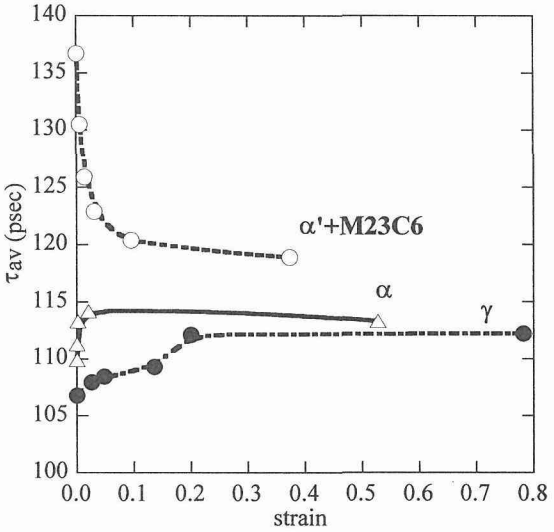

Fig.2 Positron mean lifetime measured for the steels shown in Fig.1.

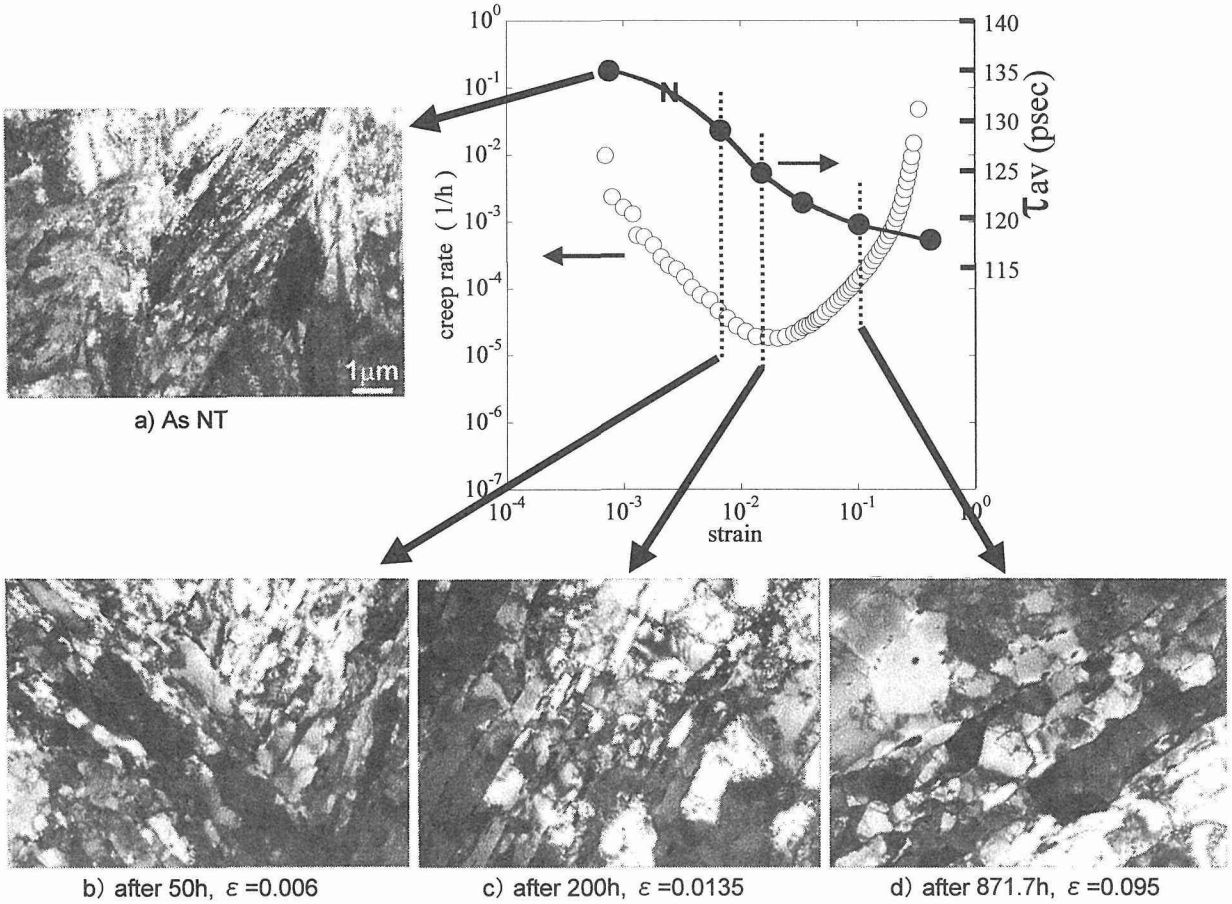

Fig. 3 Positron mean lifetime measured and the corresponding creep curve and TEM micrographs of the specimens from the α'+$M_{23}C_6$ steel crept and interrupted.

Improvement of creep strength of a tempered martensitic 9Cr steel by nano-scale MX nitrides along lath and grain boundaries

M.Taneike, K.Sawada and F.Abe
Strength & Life Evaluation R.G., NIMS, Japan

1. Introduction

Ferritic heat resistant steels have attracted strong interest in applications for boilers and turbines of ultra super critical power plants. These steels are used for a long period over ten years and hence the improvement of the more long-term creep strength is strongly demanded. In order to maintain a high level of creep strength for up to long times at high temperature, it is required to stabilize the microstructure for up to long times. Especially, coarsening of precipitation strengthening particles promotes the microstructure evolution, which causes a significant decrease of creep strength [1]. In conventional 9 - 12 Cr steel, both $M_{23}C_6$ and MX particles precipitate during tempering and intermetallic compounds such as Laves phase precipitate during creep. $M_{23}C_6$ carbides act as obstacles for migrating boundaries, but they tend to coarsen easily during creep. The MX carbonitrides of niobium and vanadium precipitate as fine particles of about 2 - 20 nm mainly on dislocations in the matrix. The MX is more stable during creep than the $M_{23}C_6$, because it precipitates coherently with the matrix and the solubility of constituents, niobium and vanadium, is quite low [2]. Many researches for using both particles effectively have been carried out until now. However, no attempt has been examined for 9 - 12 Cr steels to eliminate the $M_{23}C_6$ carbides and to stabilize the microstructure only by the MX nitrides.

The purpose of the present research is to investigate the distribution of MX nitrides consisting of vanadium and niobium in a 9Cr steel containing extremely low carbon and its effect on creep strength at 923K.

2. Experimental procedure

Chemical compositions of steels studied are Fe-9Cr-3W-0.06Nb-0.2V-0.05N with carbon of 0.002 and 0.08 mass%. The steels is named 0C steel and 008C steel, accordingly to the carbon concentration. These steels were normalized at 1373K for 1h, cooled in air, and tempered at 1073K for 1h. Vickers hardness of the tempered steels were almost the same, about 230. The microstructures of the steels were observed to be tempered martensite. Creep tests were carried out at 923K under stress conditions between 140 and 180MPa. Microstructure of the steels was observed by optical and transmission electron microscopes. The precipitates were observed by using carbon extraction replicas and were identified by EDS analysis. The concentration of alloying elements contained in the precipitates was measured by ICP analysis of electrolytically extracted residues.

3. Results

Figure 1 shows stress vs. time to rupture curves at 923K. The results of 9Cr-0.5Mo-2W-V-Nb (ASME P92) are also shown by the dotted line for comparison. The creep life of the 0C steel is about ten times as long as that of the 008C steel and about one hundred times as long as that of the P92 steel. It should be emphasized that the creep strength of the 0C steel is excellent from a short time to a long time about 10^4h. Figure 2 shows the results of TEM observations of the steels after tempering. In conventional 9Cr steel, the $M_{23}C_6$ carbides precipitate on block boundaries and prior austenite grain boundaries, and the MX carbonitrides precipitate within lath mainly. As shown in Fig.2, the microstructure of the 008C steel is similar to that of the conventional steel. On the other hand, in the 0C steel, almost no $M_{23}C_6$ particle

precipitates and the fine precipitates having a size of 2 - 20 nm are densely distributed along prior austenite grain boundaries and lath boundaries. The fine precipitates are identified as MX nitrides consisting of vanadium and niobium. The higher creep rupture strength of the 0C steel at a short time of 1000h than the others (Fig.1) results from a fine dispersion of the MX nitrides. The maintain of a high level of creep rupture strength of the 0C steel for up to long times suggests that the fine MX nitrides are stable during long-term creep and that the recovery of lath martensitic microstructure is effectively suppressed during creep. The present results suggest that the fine distribution of the MX nitrides alone along lath boundaries is preferable for the stabilization of lath martensitic microstructure during creep than the distribution of both the $M_{23}C_6$ carbides and the MX carbonitrides. Then, it is considered that to stabilize the microstructure near the boundary is most important in order to increase resistance for creep deformation.

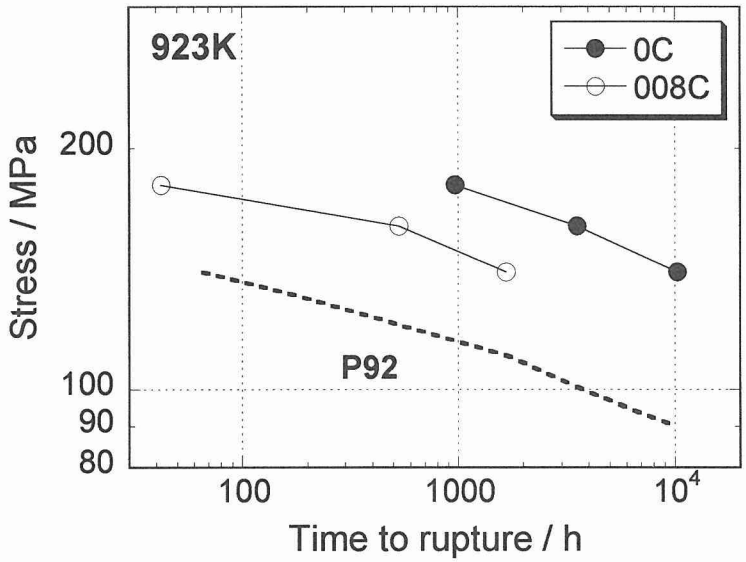

Figure 1. Stress vs. time to rupture curves of the present studied steels and the conventional steel P92 at 923 K

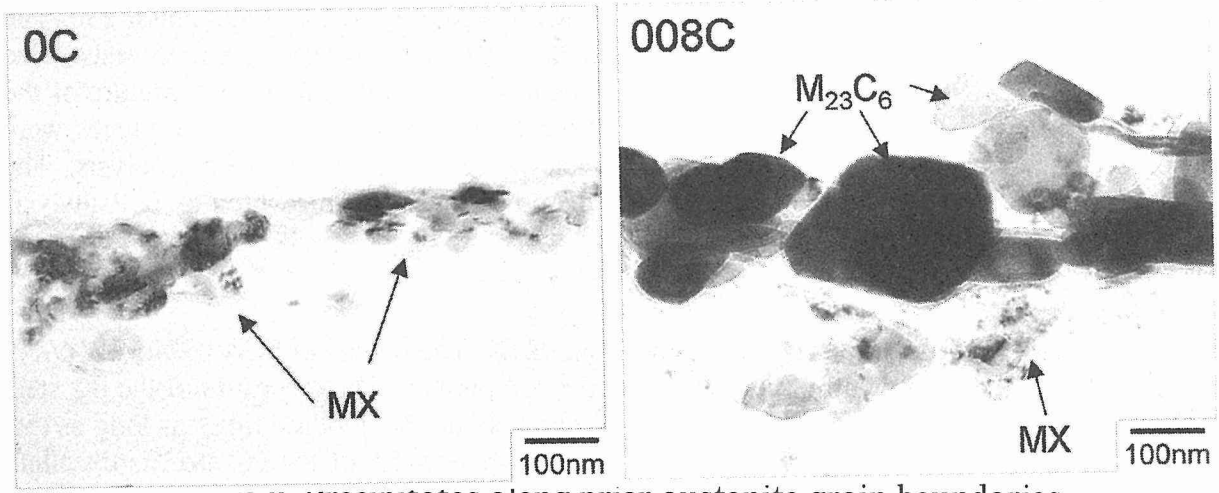

Figure 2. Precipitates along prior austenite grain boundaries in the 0C and 008C steels after tempering

References

[1] K.Kimura: Materia, 35(1996), 535
[2] A.Iseda, Y.Teranishi, F.Masuyama: Tetsu-to-Hagane, 76(1990), 1076

Effect of B addition on creep strengthening through precipitation behavior in high Cr ferritic heat resistant steel

T. Azuma, K. Miki
Muroran Research Laboratory, The Japan Steel Works, Japan

1. Introduction

The addition of B increases the creep strength in high Cr ferritic heat resistant steel [1][2]. It was reported by Takahashi et al. that the addition of B affected to suppress the growth of $M_{23}C_6$ precipitate [1]. Authors reported the effect of adding B on precipitation behavior of MX [3]. However the mechanism of creep strengthening by adding B is not clear yet.

In this research, in order to investigate the effect of B addition on the creep strengthening mechanism, precipitation behavior such as $M_{23}C_6$, MX and Laves phase during creep deformation and aging treatment was examined.

2. Experimental procedure

Table 1 shows the chemical composition of laboratory heats. These were cast into 50kg ingot by using VIM and then these were forged to 35mm thickness plates. After forging, preliminary heat treatment and quality heat treatment were performed. At quality heat treatment, 100°C/h control cooling was performed from austenitizing temperature of 1075°C. This cooling rate was the simulation in the center portion of rotor forging. Double tempering was performed at 570°C and 680°C. Creep interruption test was performed at 650°C, 157MPa. The growth behavior of precipitates was evaluated by using carbon extraction replica and thin foil made from gauge portion of the creep specimen.

Table 1 Chemical composition of laboratory heats (mass%)

	C	Si	Mn	P	S	Ni	Cr	Mo	V	Nb	W	Co	B	N
B free	.13	.02	.08	.009	.0015	.23	10.29	.69	.20	.06	1.77	3.12	-	.0237
140 ppm B	.11	.03	.07	.008	.0012	.24	10.35	.71	.20	.07	1.81	3.00	.0140	.0225

3. Test result

(1) Figure 1 shows the creep strain versus time curves of B free steel and 140ppm B containing steel. Rupture time of 140ppm B containing steel is two times longer than that of B free steel. In figure 1, the arrows show the interruption time of creep test.

(2) Figure 2 shows the growth rate of precipitates of $M_{23}C_6$ and Laves phase during creep deformation. From this measurement result of growth rate in precipitate, it was confirmed that the addition of B suppressed the growth of $M_{23}C_6$ and Laves phase.

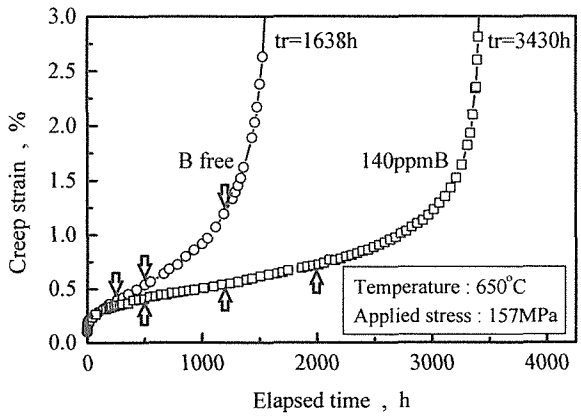

Fig.1 Effect of B addition on creep strain v.s. time curve of high Cr steel at 650°C

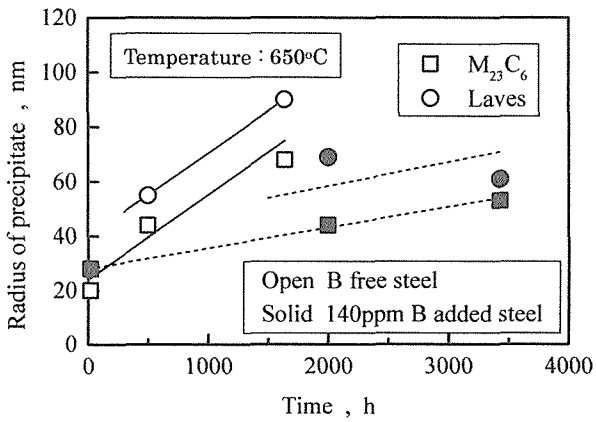

Fig.2 Growth behavior of precipitates in gauge portion during creep deformation.

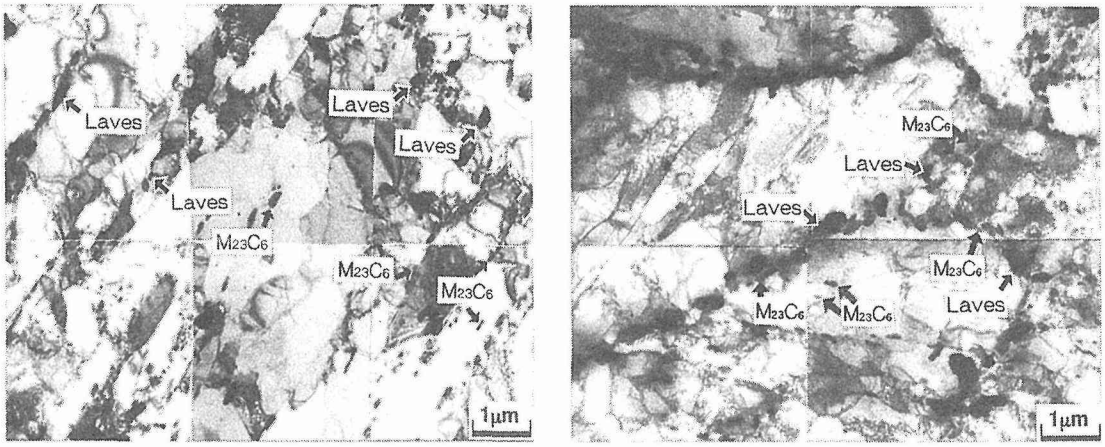

(a) B free (tr=1638h) (b) 140ppm B (tr=3430h)

Fig.3 TEM micrographs of the crept specimen at 650°C

(3) Figure 3 shows the microstructure of crept specimen. Lath structure was kept in 140ppm B containing steel, and lath structure became to subgrain in B free steel. It was confirmed that the fine precipitates suppressed the recovery of lath structure during creep deformation.

(4) Analyzing result of extracted residue during aging treatment is shown in figure 4. It was obtained that the amount of V in precipitate only decreased with adding B. V is one of the main constituent elements of MX which remarkably contributes to the improvement of creep strength. Lundin et al. [4] and Murayama et al. [5] indicated by using AP-FIM that there was the ultra very fine precipitate bearing V in B containing high Cr steel. From this analyzing result, it is evaluated that the amount of MX didn't reduce, but the size of MX became small and the precipitation strengthening ability increased by adding B.

(5) Thus the addition of B increases the creep strength in high Cr ferritic steel, through improving the high temperature stability of microstructure by suppressing the growth of $M_{23}C_6$ and Laves phase, and decreasing the size of MX.

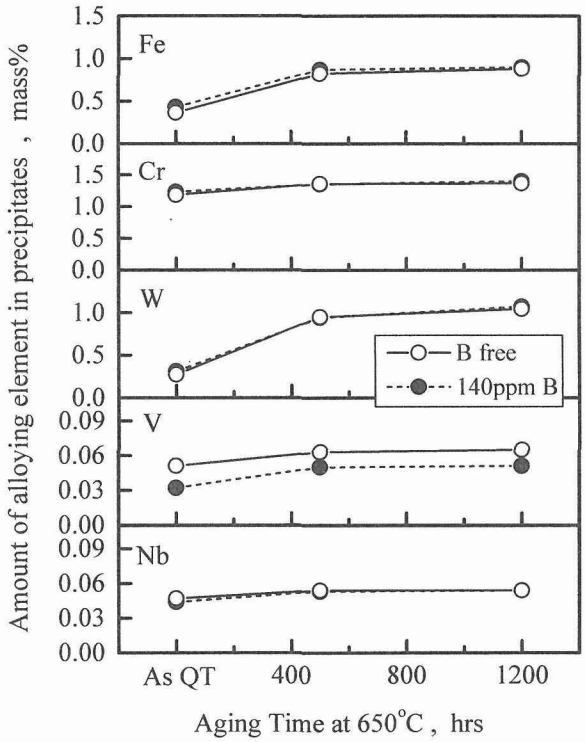

Fig.4 Chemical analysis of extracted residue from grid portion of interrupted creep specimen at 650°C

4. Reference

[1] N.Takahashi, T.Fujita and T.Yamada : Tetsu-to-Hagane, 61(1975), p.2263

[2] T.Fujita : Proceedings of the 3rd conference on Advances in Material Technology for Fossil Power Pants, April 5-6 2001, Swansea, UK, p.33

[3] T.Azuma, K.Miki, Y.Tanaka and T.Ishiguro : Tetsu-to-Hagane, 86(2000), p.667

[4] L.Lundin, S.Fällman and H.-O.Andrén: Materials Science and Technology, 13(1997), p.233

[5] M.Murayama, K.Houno, M.Igarashi and F.Abe : CAMP ISIJ, 13(2000), p.572